ERRATUM

Title of ETD:

TARGETED DELIVERY OF ANTICANCER AGENTS TO CANCER

Name of Author:

Lu, Jianqin

Description of Correction(s):

In the original dissertation, the TEM image for FA-PEG_{5K}-EB_2/DOX micelles in Figure 25D on page 91 was wrongly used. (Corrected image inserted in PDF and included for comparison in accompanying document.)

In the original dissertation, the confocal images for FA-PEG_{5K}-EB_2/DOX with 100 μM free folate in Figure 30B on page 99 was wrongly used. (Corrected images inserted in PDF and included for comparison in accompanying document.)

In conclusion, we regret the non-intentional errors, but the corrections made to the dissertation will not affect the conclusion in it.

	November 11, 2020
Graduating School Approval	Date Initialed
AJG	November 19, 2020
Office of the Provost Approval	Date Initialed

University of Pittsburgh

TARGETED DELIVERY OF ANTICANCER AGENTS TO CANCER

by

Jianqin Lu

B.S. of Pharmacy, Hunan University of Chinese Medicine, Changsha, China, 2010

Submitted to the Graduate Faculty of

Pharmacy in partial fulfillment

of the requirements for the degree of

Doctor of Philosophy

University of Pittsburgh

2014

UNIVERSITY OF PITTSBURGH

SCHOOL OF PHARMACY

This dissertation was presented

by

Jianqin Lu

It was defended on

November 19th, 2014

and approved by

Wen Xie, M.D., Ph.D., Professor
Director of the Center for Pharmacogenetics, Department of Pharmaceutical Sciences
Joseph Koslow Endowed Chair in Pharmaceutical Sciences, School of Pharmacy
Department of Pharmacology, School of Medicine, University of Pittsburgh

Raman Venkataramanan, Ph.D, Professor
Director of the Clinical Pharmacokinetics Laboratory, Department of Pharmaceutical Sciences, School of Pharmacy
Director of Therapy Drug Monitoring, Department of Pathology, School of Medicine
University of Pittsburgh

Lisa C. Rohan, Ph.D, Associate Professor
Department of Pharmaceutical Sciences, School of Pharmacy
Department of Obstetrics, Gynecology, and Reproductive Sciences, School of Medicine
Clinical Translational Science Institute, University of Pittsburgh
Magee Womens Research Institute, University of Pittsburgh Medical Center

Pradeep Tyagi, Ph.D, Associate Professor
Department of Urology, School of Medicine, University of Pittsburgh

Dissertation Advisor: Song Li, M.D., Ph.D., Professor
Department of Pharmaceutical Sciences, School of Pharmacy
University of Pittsburgh Cancer institute
University of Pittsburgh

TARGETED DELIVERY OF ANTICANCER AGENTS TO CANCER

Jianqin Lu, Ph.D.

University of Pittsburgh, 2014

Our research focuses on developing dual functional polymeric micelles for the targeted delivery of anticancer agents to tumors.

We first developed a poly(ethylene) glycol (PEG)-derivatized anticancer agent-Embelin (EB) (PEG-EB_2) as an effective nanomicellar carrier for the delivery of Paclitaxel (PTX) to tumors. Our data demonstrated that PEG-EB_2 retained similar biological effect as EB. Surprisingly, it can self-assemble into micelles (~20 nm) in aqueous solution and was also efficient in delivering the Paclitaxel (PTX) to cancers with enhanced antitumor activity. Further, folate (FA), a tumor specific ligand, was anchored into PEG_{5K}-EB_2 micelles (FA-PEG_{5K}-EB_2) to realize the active tumor targeting. The intracellular uptake of Doxorubicin (DOX) was markedly improved when incorporated into FA-PEG_{5K}-EB_2 over the one without FA, resulting in the significant higher level in inhibiting tumor growth.

Moreover, structure activity relationship (SAR) study was performed in PEG-derivatized Vitamin E (PEG-VE), in which our data has shown that PEG-VE with longer PEG length (5K) and double VE chains (PEG_{5K}-VE_2) garnered significant better PTX loading, stability and improved antitumor efficacy. Additionally, aiming to improve the DOX loading and stability, a drug-interactive motif-Fmoc was placed in the interfacial region of the PEG_{5K}-VE_2 (PEG_{5K}-Fmoc-VE_2). The data suggested that introduction of Fmoc to PEG_{5K}-VE_2 brought about dramatic augmentation in DOX loading and formulation stability, which consequently led to an enhanced inhibition on tumor development. Another finding in my research is to formulate Camptothecin

(CPT), a highly lipophilic antineoplastic drug, in an innovative fashion. CPT was conjugated with VE at its hydroxyl group via carbonate ester bond (CPT-VE) or disulfide linkage (CPT-S-S-VE), which can self-assemble into nanofiber upon stabilized by PEG_{5K}-Fmoc-VE_2. VE-derivatized CPT prodrugs significantly buttressed the stability of CPT due to the additional steric hindrance to the lactone ring on CPT. Meanwhile, compared to CPT-VE, CPT-S-S-VE can more readily liberate CPT at tumors in a controlled manner (high GSH conc. in tumor), leading to the superior tumor growth suppression *in vivo*.

To reiterate, our data demonstrated that PEG-derivatized anticancer agents can serve as effective nanocarriers for the targeted delivery of chemotherapeutics. Additionally, incorporation of Fmoc into the interfacial region of dual functional carriers led to significantly increased drug loading and formulation stability, resulting in improved antitumor activity. Furthermore, coupling of VE to anticancer drugs may represent a novel platform in ameliorating their compatibility with utilized carrier.

TABLE OF CONTENTS

LIST OF TABLES

LIST OF FIGURES

PREFACE

This Ph.D. dissertation described herein is comprised of the research undertaken at the Center for Pharmacogenetics, Department of Pharmaceutical Sciences, in University of Pittsburgh under the immediate supervision of my mentor, Dr. Song Li.

It has been a fairly challenging journey this past four years, with a multitude of ups and downs. Luckily, there were always critical guidance and enlightenment to me through those rough dips. This work would never be accomplished without the help, support, and encouragement from all those important people in my life. For this, I would like to kindly thank them.

First and foremost, I am extremely indebted to my advisor, Dr. Song Li, a dedicated scientist and superb mentor. I could still remember clearly four and half years ago when I was lying on the bed, I first received the call from Dr. Li, and nervously preparing what to talk with him. Despite my weak performance in that phone interview, he still kindly provided me a M.S. student position in his laboratory, which was a huge surprise to me, given my bachelor background and the prominence of the School of Pharmacy of University of Pittsburgh. Two years later, I successfully transferred to the Ph.D. program under his belief and confidence in me. Throughout these years, Dr. Li, has extended me a variety of opportunities working on different projects ranging from biology, chemistry to pharmaceutics, which have greatly broadened my academic vision and enriched my professional expertise. Owing to the inter-disciplinary nature of the research in his laboratory, not only I learned how to design and develop novel nanocarriers for

drug delivery, but also I gained the insight and ability to take advantage of chemical synthesis and molecular biology. It is his enormous direction and unconditional support that made me where I am.

Meanwhile, I am really grateful to my committee members, Dr. Wen Xie, Dr. Raman Venkataramanan, Dr. Lisa Rohan, and Dr. Pradeep Tyagi, for their valuable suggestions and comments along the way. In Li's lab, many thanks go to Dr. Jiang Li for his kind instruction on my biology-related studies; to Dr. Xiang Gao for teaching me how to make my first ever micellar formulation; to Dr. Yixian Huang for his direction on the organic chemistry synthesis; and other labmates (Yifei Zhang, Mohammed Ghazwani, Peng Zhang, Jilong Li, Xiaolan Zhang, Yichao Chen, Jieni Xu). Without the accompanying of them, the research would be much less enjoyable.

Further, I intend to express my gratitude to Dr. Lisa Rohan, Dr. Sean Xie, Dr. Donna B Stolz and Ming Sun, Dr. Peijun Zhang and Dr. Chuang Liu, Dr. Liang Xu, Dr. Rebecca Marquez, and Hao Liu, for the friendly collaboration and lab equipment. Besides, I owe appreciation to Dr. Patricia Dowley Kroboth, Dr. Randall B. Smith, Dr. Barry Gold, Dr. Robert B Gibbs, Dr. Maggie Folan, Lori Schmotzer, William C Smith and Douglas E. Nelson for their generous help and support over these years, who are from Center for Pharmacogenetics and the School of Pharmacy at the University of Pittsburgh.

This dissertation is dedicated to my mother, Zhangyun Liu and my father, Xing Lu, for their endless love and thoughtful care ever since I was born; and to my grandfather, Genyuan Liu and grandmother Mantao Li for their unselfish loving care, who always encouraged me to be a scientist; and to my Uncle, Yuxing Liu, for being a role model for me since my childhood; and all my other beloved relatives. Finally, I would like to express my deep gratitude to my girlfriend

Xinyu Cao, for her cordial love and thoughtful care. They have been a driving force for me to study fearlessly and conquer the difficulties ahead of me.

1.0 INTRODUCTION

1.1 AN OVERVIEW OF CANCER

Cancer, involving abnormal cell proliferation, is able to invade or spread to other parts of the body, resulting in a variety of disorders and eventually death (Portales, Thezenas et al. 2011). Cancer is a leading cause of death world-wide and is responsible for approximately 13% of all deaths, according to the World Health Organization (Shaha, Pandian et al. 2011). In males, lung cancer, prostate cancer, colorectal cancer, and stomach cancer are the most common types of cancer, and in females, the most common types are breast cancer, lung cancer, cervical cancer and colorectal cancer (Kuper, Boffetta et al. 2002).

There are a range of different facts that give rise to cancer development. It has been reported that tobacco is responsible use for 22% of cancer deaths (Wang, Jiang et al. 2012). Also, 10% of the cancer population is attributed to obesity, rising from inadequate amount of physical activity, unhealthy diet, as well as drinking alcohol (Luo, Morrison et al. 2007). Besides, exposure to environmental pollutants, and ionizing radiation can also contribute significantly to cancer (Burns, Uddin et al. 2004). Almost 20% of cancers are caused by infections such as hepatitis B, hepatitis C, and human papillomavirus, in developing countries . Another 5-10% cases of cancers are closely related to genetic disorder inherited from the parents (Giovannucci, Liu et al. 2006). It takes time for the normal cells to progress to cells with observable mass to

eventual utter tumor (Hanahan and Weinberg 2000) (Hanahan and Weinberg 2011). Once the tumor is developed, it becomes insensitive to anti-growth signals and can escape from apoptosis (Hanahan and Weinberg 2000). Moreover, cancer will be endowed with endless replicative potential to grow in an uncontrolled manner. Further, in order to acquire sufficient nutrients and discharge the waste during the tumor development, a multitude of neovaculature will be generated (Hanahan and Weinberg 2000). Finally, cancer is capable of spreading and invading the other tissues of the body, a process known as metastasis (Hanahan and Weinberg 2000). The underlying mechanism of carcinogenesis is intricate. Studies from the past a few decades showed that development of cancer is mainly ascribed to the failure of regulating tissue growth, when the genes modulating cell growth and differentiation are mutated (Croce 2008). Meanwhile, it has been clarified that these genes alterations could be arisen from mutation of DNA sequence in both oncogenes and tumor suppressor genes, as well as epigenetic alterations (Baylin and Ohm 2006). Recent investigations on epigenetic deficiencies in expression of DNA repair genes demonstrated the enhanced incidence of mutations, subsequently, part of which appear in tumor suppressor genes and oncogenes, resulting in the carcinogenesis (O'Hagan, Mohammad et al. 2008).

A variety of approaches have been taken to fight against cancer, including, chemotherapy, radiaton therapy, surgery, as well as immunotherapy, among which chemotherapeutics has been increasingly paid attention to due to its high tumor cell-killing efficacy (Rekers, Troost et al. 2014) (Lang-Lazdunski 2014) (Baylin and Ohm 2006). However, administration of conventional anti-neoplastic drugs cannot only kill the cancer cells, but also poison the normal tissue, leading to the severe adverse effects because their non-specific targeting (Patil, Gada et al. 2013). Moreover, the effectiveness of anticancer agents oftentimes

was restrained by their poor water solubility (Shen, Song et al. 2014). Further, non-protected free chemotherapeutics injected *in vivo* can rapidly be eliminated from the blood stream by the reticuloendothelial system (RES), which results in insufficient antitumor efficacy (Yao, Zhang et al. 2013). To solve these issues, tumor targeted therapy via employing nanotechnology-based anticancer drug formulations has been emerging as an important therapeutic platform for the treatment of various cancers (Akhtar, Ahamed et al. 2014). In the last several decades, emphasis have been placed on the development of nanomedicine therapeutics by using liposome, dendrimer, polymeric micelle, as nanocarriers for the tumor targeted delivery of anticancer agents, among which polymeric drug delivery system are of high interest (Mei, Zhang et al. 2013) (Kakizawa and Kataoka 2002). A systemic discussion of polymeric micellar system as effective nanocarrier for the delivery of anti-neoplastic agents is presented in the following sections.

1.2 TARGETED DELIVERY OF CHEMOTHERAPEUTICS BY POLYMERIC MICELLES FOR THE TREATMENT OF CANCER

Typical polymeric micelles are comprised of hydrophobic tail and hydrophilic polymer shell, in which PEG is commonly utilized (Cheng and Cao 2009) (Zhang, Huang et al. 2014). In aqueous solution, they can self-assemble into nanosized particles (10-100 nm) with hydrophilic segment protruding outside, confining the hydrophobic regions in the micelle core, where poorly water soluble drugs can be incorporated. Owing to the protection from the PEG corona and the small size, extended blood circulation time, preferred tumor accumulation, as well as decreased side effects have been inevitably garnered in polymeric micellar formulations (Zhang, Huang et al.

2014). In this chapter, the discussion is focused on the current progress regarding the development of novel PEG-anticancer drugs as functional nanocarriers. Besides, the significance of using active targeting ligand in chemotherapy is also highlighted. Additionally, special emphasis is placed on the discovery of approaches to improve the carrier/drug interactions so as to achieve desirable nanoformulations with enhanced stability and drug loading. Furthermore, tocopherol-conjugated anticancer agents' prodrugs as an effective method of formulating chemotherapeutics is summarized as well.

1.2.1 INTRODUCTION

The efficacy of the hydrophobic chemotherapeutics is often greatly limited by their poorly water solubility (Shen, Song et al. 2014). Concurrently, not only can the free anticancer agents get to the tumoral sites, but can also be taken up by normal tissues, resulting in toxicity, after the *in vivo* administration (Shen, Yin et al. 2013). Hence, selectively delivering the therapeutic agents to tumors while without adversely affecting the innocent tissues is of crucial importance. In the past years, nanocarriers including, liposomes, dendrimers, as well as polymeric micelles have been researched widely for the targeted delivery of drugs to the pathological sites (tumor), among which polymeric micelles have been paid intensive attention due to its technical ease and the relatively smaller size, which allows them to passively target to tumors more readily (Mei, Zhang et al. 2013) (Kakizawa and Kataoka 2002), compared to its counterparts.

Polymeric micelles are generally composed by the amphiphilic block copolymers (Cheng and Cao 2009). In aqueous solution, above the critical micelle concentration (CMC), the amphiphilic block copolymers are able to spontaneously self-assemble into supramolecular core/shell nanoaggregates (Adak, Kumar et al. 2012). The hydrophobic inner core serves as a

reservoir for storing the hydrophobic bioactive compounds, which can either be physically loaded or conjugated covalently. Meanwhile, the hydrophilic corona contribute greatly to the overall colloidal stability of polymeric micelles, as they prevents the recognition by opsonin and blood proteins *in vivo*, leading to prolonged circulation period (Miller, Hill et al. 2012). Moreover, the small sizes of polymeric micelles (10-100 nm), along with the extended blood circulation times, renders the preferential accumulation at the solid tumor, based on the enhanced permeability and retention (EPR) effect featuring leaky vasculature and impaired lymphatic drainage (Matsumura and Maeda 1986). Further, the preferred accumulation of micelles in tumor is also likely to reduce systemic toxicity. Therefore, in recent decades, polymeric micelles have been under intensive investigation as drug carrier for the targeted delivery of anticancer agents. Conventionally, amphiphilic polymer micelles tend to aggregate into spheres, however, recently, micelles with varying shapes have also been reported including nanorods, nanotubules, as well as lamellae (Yu, Zhang et al. 1998, Shen, Zhang et al. 1999, Choucair and Eisenberg 2003). More importantly, it has been established that the *in vivo* pharmacokinetics is closely related to the spatial arrangement of the micelles (Geng, Dalhaimer et al. 2007). Geng et al. found that worm-like filomicelles exhibited significantly prolonged blood circulation time, in comparison to its analogue with components (Geng, Dalhaimer et al. 2007). In addition to the hydrophobic interactions in forming the self-assembled micelles, there are also some other interactions that can trigger the formation of micelles. Polymeric micelles formed due to the complexion of intermolecular hydrogen bonding was also described in literature. Besides, it was reported that electrostatic interactions can also lead to the generation of polyion complex (PIC) micelles in an aqueous milieu, employing a pair of oppositely-charged block copolymers with poly(ethylene glycol) segments (Gaucher, Dufresne et al. 2005).

Among the hydrophilic polymers in forming the polymeric micelles, Poly(ethylene glycol)(PEG) is the most widely used due to its non-toxicity, neutralized charge, highly water-miscible property, low degree of immunogenicity and antigenicity, availability of the terminal primary hydroxyl groups for derivatization. Moreover, as a "golden standard" of hydrophilic coating for a myriad of drug carriers, a number of PEGylated products have already been approved by the FDA. In the polymeric micelles, PEG acts as the protecting hydrophilic corona, minimizing the non-specific binding to the blood proteins, thereby, contributing to the extended circulation times, which favorably alters the pharmacokinetics of the loaded drugs. Aside from PEG, the applications of other polymers such as, poly(N-(2-hydroxypropyl) methacrylamide) (pHPMA) (Lu, Kopeckova et al. 1998), poly(vinyl alcohol) (PVA) (Francisco, da Silva et al. 2010), as well as polyethylenimine (PEI) (Vinogradov, Batrakova et al. 1999), as hydrohphilic shell-forming block of polymeric micelles, have also been reported in the literature. With respect to the core, a multitude of hydrophobic polymers have been investigated, such as poly (ε-caprolactone) (Shuai, Ai et al. 2004), poly(propylene oxide) (PPO)(Ha, Kim et al. 1999), poly(lactic acid) (PLA), as well as poly(L-lysine) (PLL). Traditionally, core-forming components of micelle are made of polymers, however, recently, lipids have been brought into attention for the application as hydrophobic core-forming material. It has been found that PEG conjugated phosphatidylethanolamine (PEG-PE) can self-assemble into micelles with significantly lower CMC compared to conventional surfactants (Lukyanov and Torchilin 2004, Musacchio, Laquintana et al. 2009). Moreover, PEG-PE micelles were able to effectively solubilize a variety of hydrophobic anticancer drugs and achieved enhanced antitumor activity (Wang, Mongayt et al. 2004). In addition to the aliphatic lipids, cholic acid (CA), an insoluble bile acid, was also employed to function as hydrophobic portion in micelles (Luo, Xiao et al.

2010, Xiao, Li et al. 2011, Xiao, Luo et al. 2011). The PEG-CA conjugates formed very small sized micelles (20-60 nm) with low CMC and high drug loading (Luo, Xiao et al. 2010). Besides, the PEG-CA micelles-delivered PTX or DOX presented significantly improved tumor growth inhibition effect in a number of murine tumor models (Xiao, Luo et al. 2011) (Luo, Xiao et al. 2010).

In addition to targeted delivery, controlled drug release has also been given heavy attention so as to create optimal drug delivery systems. It is expected that the micelles shall be able to maintain their physical integrity during circulation in the blood or in normal tissues, but need to be dissociated and effectively release their payloads in pathological site such as in tumor, upon unique environmental stimuli. Disulfide bond, a glutathione (GSH)-responsive linkage, is stable under normal physiological condition with low glutathione (GSH) level (2-20 μM). However, the reducing environment with high GSH concentration (~10 mM) in tumor cells can readily lead to the breakage of the disulfide linker (Wu, Fang et al. 2004). Hence, the micelles containing disulfide bond sensitive linker have been widely studied and garnered compelling improvement in the controlled release of anticancer drugs in tumurol sites (Cui, Xue et al. 2013, Song, Ding et al. 2013). In addition to the reducing condition, tumors are also characterized with mildly acidic milieu. Therefore, pH-triggered drug release in acidic tumors have become another promising strategy to achieve triggered release of chemotherapeutics on target. Acid-cleavable linkers such as hydrazones, orthoestes, as well as acetals have been intensively investigated in polymeric micelles for the controlled release of the encapsulated anticancer agents (Bae, Fukushima et al. 2003, Toncheva, Schacht et al. 2003, Torchilin 2009).

Thanks to the considerable efforts dedicated to the development of polymeric micelle drug delivery system, many micelles-delivered anticancer agents' nanoformulations have

advanced into clinical trials. NK911, a DOX-loaded micellar formulation, has passed Phase I clinical trial with acceptable toxicity profile in patients and is currently under Phase II trials (Nakanishi, Fukushima et al. 2001). The carrier was composed of PEG-b-poly(α,β-aspartic acid) copolymer conjugated with DOX via amide bonds. After loading DOX, the strong π-π stacking effect between the physically entrapped DOX and the core-forming DOX can significantly augment the stability of the micelles. Likewise, PTX-loaded polymeric micelles (NK105) and SN-38-loaded polymeric micelles (NK012) have already been in the Phase III and Phase II trials, respectively (Matsumura and Kataoka 2009, Hamaguchi, Doi et al. 2010). Besides, micelles consisting of PEG-b-poly(D,L-lactide) copolymer encapsulating PTX in the inner core (Genexol-PM) have already been on the market in Bulgaria, Hungary and South Korea, and are currently being evaluated in U.S. in Phase II trials (Nehate, Jain et al. 2014).

Although significant advances have been obtained in developing novel polymeric micelle drug delivery systems during the past decade, the achievements are still far from meeting the needs of effectively treating diseases including cancer. Therefore, improvement is invariably needed. In the following sections, discussion will be focused on the progress regarding the rational design of the biologically functional carriers for the delivery of hydrophobic anticancer agents for synergistic chemotherapy. Additionally, approaches of active targeting to tumor are also summarized. Further, emphasis is placed on how to improve drug loading and the formulation stability via enhancing drug/carrier interactions. Finally, VE-derivatized anticancer agents' prodrugs as a novel way to formulate highly lipophilic chemotherapeutics is also discussed.

1.2.2 PEG-DERIVATIZED ANTICANCER AGENTS AS FUNCTIONAL NANOMICELLES FOR THE DELIVERY OF ANTITUMOR DRUGS

1.2.2.1 Foundations in developing drug-conjugated polymeric micelles

For a long time, the materials forming the micelles in drug delivery were "inert" and were of no therapeutic activity. The large amount of carrier materials used in the drug formulation also posed safe concerns. Hence, development of bioactive carriers for the tumor targeting delivery of the chemotherapeutics is of high interest. Hydrophobic drugs can be conjugated to hydrophilic polymers (PEG) to yield amphiphiles, which can self-assemble into micelles based on the strong hydrophobic interactions between the hydrophobic drugs. The therapeutically active micelles have many advantages over the conventional non-functional carriers. First, drug-formulated in bioactive micelles warrant the delivery of multiple therapeutics to the same target simultaneously, which may give rise to the enhanced therapeutic outcome via modulating different signaling pathways. Additionally, the dual functional carrier can not only synergize with the payload, but also is likely to offset the systemic toxicity arising from the loaded antitumor drugs (Lu, Zhao et al. 2014). More importantly, functional carriers might be also capable of facilitating the loaded drugs to reverse the multidrug resistance (Lu, Zhao et al. 2014).

Nonetheless, to date, scarcely have hydrophobic anticancer drugs been entrapped and delivered by micelles consisting of the polymer-drug conjugates. To this end, the following discussion is focused on the progress of the delivery of chemotherapeutics by the functional polymeric micelles derived from the PEG-drug conjugates from our group and others.

1.2.2.2 PEG-DERIVATIZED EMBELIN AS A DUAL FUNCTIONAL NANOMICELLAR SYSTEM FOR PACLITAXEL DELIVERY TO TUMOR.

Embelin (EB), a naturally occurring alkyl substituted hydroxyl benzoquinone compound and a major constituent of *Embelia ribes* BURM, has been demonstrated to show a range of different biological activities, such as antidiabetic, anti-inflammatory, and hepatoprotective activities (Chitra, Sukumar et al. 1994, Bhandari, Jain et al. 2007, Singh, Singh et al. 2009). Besides, EB also exhibits significant antitumor activity in various types of cancers including colon, prostate, pancreatic, and breast (Chitra, Sukumar et al. 1994, Sreepriya and Bali 2005, Dai, Qiao et al. 2009). Based on computational structure, EB was originally discovered via computer screening in Wang et al.'s group (Nikolovska-Coleska, Xu et al. 2004), in which it was found to inhibit the X chromosome-linked inhibitor of apoptosis protein (XIAP). XIAP plays a negligible role in the growth of normal cells, however, the function of which has been overly relied on in promoting the tumor cells proliferation (Tamm, Kornblau et al. 2000), where it was overexpressed, expecially in apoptosis-resistant cancer cells (Berezovskaya, Schimmer et al. 2005). XIAP targeting has been deemed as a new approach in the development of anticancer agents to enhance the overall outcome of the chemotherapeutics and radiation therapy. EB is able to target the BIR3 domain of XIAP, which leads to the suppression on the activity of caspase 9 and caspase 3, eventually resulting in the apoptotic cell death (Nikolovska-Coleska, Xu et al. 2004). Additionally, EB is also capable of downregulating the expression of IAP1/2, TRAF1, cFLIP, survivin, Bcl-2, and Bcl-x_L via the inhibition on NF-κB activation (Ahn, Sethi et al. 2007).

Owing to its long lipophilic chain and benzene ring, EB is invariably hydrophobic with poor water solubility. In an attempt to improve the solubility of EB, PEGylated approach was employed (Lu, Huang et al. 2013, Lu, Zhao et al. 2014). Interestingly, it was found that after

conjugating PEG to EB_2 (PEG-EB_2), the PEG-EB_2 can self-assemble into spherical micelles with very small size (20 nm) in aqueous solution (Lu, Huang et al. 2013, Lu, Zhao et al. 2014). This result did not happen by chance, given the structural similarity of EB and PE. The PEG-derivatized EB still retained considerable bioactivity of EB. Meanwhile, $PEG_{3.5K}$-EB_2 can be also used as a nanocarrier to effectively solubilize PTX, in which the potent synergism between PTX and EB in PTX-loaded $PEG_{3.5K}$-EB_2 has been demonstrated in a number of cancer cell lines (Lu, Huang et al. 2013, Lu, Zhao et al. 2014). Structure activity relationship studies demonstrated that the conjugate with two EB chain worked significantly better in PTX loading in comparison to the one with only one EB chain (Lu, Zhao et al. 2014). This could be attributed to the stronger hydrophobic interaction endowed by the close proximity of the two EB chains in contrast to the relatively loose spatial arrangement in single EB chain conjugate. Further, increasing the length of PEG from 3.5K to 5K in doubled EB chains conjugates (PEG_{5K}-EB_2) led to significant improvement with respect to PTX loading and formulation stability (Lu, Huang et al. 2013). The PEG_{5K}-EB_2 exhibited extremely low CMC (0.35 μM), which compares favorably to most of the reported micellar system (Lu, Huang et al. 2013). In addition, the minimal hemolytic effect from PEG-derivatized EB warranted that it can be a safe and reliable nanocarrier without triggering any systemic toxicity in delivering chemotherapeutics (Lu, Huang et al. 2013). Moreover, in the maximum tolerated dose study (MTD), we found that PTX-formulated in PEG_{5K}-EB_2 (>100 mg/kg) gave almost 7-fold higher MTD than PTX in its clinical formulation-Taxol (15 mg/kg) (Lu, Huang et al. 2013). Furthermore, *in vivo* near infrared fluorescence imaging study performed in PC-3 xenograft tumor model demonstrated superior passive tumor targeting ability using PEG_{5K}-EB_2 as a nanomicellar carrier (Lu, Huang et al. 2013). Paramountly, delivery of

PTX employing PEG_{5K}-EB_2 contributed to drastically improved antitumor efficacy compared to Taxol in both breast and prostate tumor models (Lu, Huang et al. 2013).

1.2.2.3 PEG-DERIVATIZED VITAMIN E AS A NANOMICELLAR FORMULATION FOR TUMOR TARGETED DELIVERY OF CHEMOTHERAPEUTICS.

Vitamin E (VE), a nontoxic and biocompatible hydrophobic lipid, acts by hindering the production of reactive oxygen species (ROS) generated when fat undergoes oxidation (Zhu, Cromie et al. 2014). Also, recent studies showed that VE can also inhibit cancer cell growth (Cheng, Zielonka et al. 2013, Hodul, Dong et al. 2013). Based on the pharmacological advantages and the hydrophobic nature, VE has been extensively utilized in the development of functional drug delivery system (Danhier, Kouhe et al. 2014, Laouini, Andrieu et al. 2014, Zhang, Huang et al. 2014). D-a-tocopheryl polyethylene glycol succinate 1000 (TPGS), a FDA approved pharmaceutical adjuvant in drug formulation, is a water-soluble PEG_{1K}-derivatized natural VE, produced through the esterification of VE-succinate with PEG_{1K} (Ma, Zheng et al. 2010). In the past decades, TPGS has been widely exploited in forming a great number of nanocarriers for the delivery of the therapeutic agents, such as being a penetration enhancer (Aggarwal, Goindi et al. 2012), emulsifier in Poly (lactic-co-glycolic acid) (PLGA) nanoparticles (Mu and Feng 2002), TPGS-based liposomes (Vijayakumar, Muthu et al. 2013), solubilizer and stabilizer (Yu, Bridgers et al. 1999), as well as copolymers (Zhang and Feng 2006). Recently, it has also been found that TPGS can function as excipient for the reversing of multidrug resistance due to its inhibition of the activity of ATPase in P-gp mediated efflux pump, resulting in improved effectiveness and efficacy of anticancer drugs (Dintaman and Silverman 1999). Further, TPGS can also be combined with other polymers such as Pluronic P105 (Gao, Li et al. 2008) and

Pluronic P123 (Zhao, Shi et al. 2011), to produce micelles for the delivery of anticancer drugs, in which increased cell-killing activity was obtained.

Nonetheless, delivery of chemotherapeutic agents by nanocarriers composed solely of TPGS has been shown to be ineffective due to its high CMC (Mi, Liu et al. 2011). Therefore, a series of efforts have been placed on modifying TPGS so as to exploit its potential as the only component in forming the micelles for effective delivery of anticancer agents. Under this condition, no shared surfactants will be employed, which could result in decreased systemic toxicity caused by large amount of carriers used. To this end, first, longer PEG (2K) chain was used to substitute the original PEG (1K) and coupled with one VE-succinate to yield $TPGS_{2K}$ (Mi, Liu et al. 2011). $TPGS_{2K}$ had much lower CMC (0.0219 mg/mL) compared the traditional micelles with TPGS involved (0.2 mg/mL), which provided the foundation to form stable micelles by sole $TPGS_{2K}$. Indeed, $TPGS_{2K}$ can efficiently incorporate hydrophobic anticancer agent-docetaxel and exhibited potential synergistic effect (Mi, Liu et al. 2011). This modification has led to the successful formation of stable drug TPGS nanomicellar formulation without additional stabilization from other polymers or lipids. It has been established that in micelles, longer PEG chain can offer better steric hindrance protection, compared to the one with shorter PEG length, which can further reduce the non-specific internalization of micellar formulation by RES (Lu, Huang et al. 2013). Secondly, in addition to prolong the PEG length to improve the performance of TPGS in drug loading and stability, increasing the number of VE chains has also been investigated. Wang et al. found that $TPGS_{2K}$ with doubled VE chains (PLV_{2K}) presented significantly improved formulation stability with CMC as low as 1.14 μg/mL, which is drastically lower than that for $TPGS_{2K}$ (21.9 μg/mL) and TPGS (200 μg/mL) (Wang, Sun et al. 2012). In addition, PLV_{2K} retained similar P-gp inhibitory effect as TPGS, which enabled it to

overcome the multidrug resistance when delivering chemotherapeutics to tumors (Wang, Sun et al. 2012). More importantly, PLV_{2K}-delivered DOX exhibited improved antitumor activity compared to DOX-loaded TPGS (Wang, Sun et al. 2012). More recently, our group developed four PEG-derivatized VE conjugates with varying PEG length (PEG_{2K} vs PEG_{5K}) and the molar ratio of PEG/Vitamin E (1/1 vs 1/2) in the conjugates (PEG_{2K}-VE, PEG_{2K}-VE_2, PEG_{5K}-VE, and PEG_{5K}-VE_2) (Lu, Huang et al. 2013). Our data suggested that PEG_{5K}-VE_2 was most effective in formulating DOX with respect to drug loading capacity and formulation stability (Lu, Huang et al. 2013). Moreover, the four PEG-derivatized VE conjugates well maintained the suppression of P-gp function (Lu, Huang et al. 2013). Greatly, PTX-loaded PEG_{5K}-VE_2 nanomicelles gave rise to the highest level of delaying the tumor growth, compared to PTX formulated in PEG_{2K}-VE or PEG_{2K}-VE_2, as well as Cremophor EL (Taxol) in a mouse model bearing 4T1.2 breast cancer (Lu, Huang et al. 2013).

1.2.2.4 PEG-DERIVATIZED FARNESYLTHIOSALICYLATE CONJUGATES AS POLYMERIC MICELLES FOR THE DELIVERY OF PACLITAXEL.

S-trans, trans-farnesylthiosalicylic acid (FTS), a nontoxic and synthetic small lipidic molecule, functions by antagonizing Ras proteins in cell membrane (Marom, Haklai et al. 1995, Haklai, Weisz et al. 1998). FTS is the first-in-class direct Ras antagonist developed to restrain the uncontrolled proliferation of cancer cells arising from oncogenically activated Ras or growth factor receptor-mediated Ras activation (Marom, Haklai et al. 1995, Haklai, Weisz et al. 1998). Significant reduction of Ras levels by the treatment of FTS has been demonstrated in a number of tumor models devoid of noticeable untoward effects (Gana-Weisz, Halaschek-Wiener et al. 2002). Prevailingly, one major mechanism of inhibiting Ras by FTS is to dislodge Ras protein

from its anchorage domains, which led to the degradation of Ras, subsequently leading to its inability to cue in the cell membrane (Paz, Haklai et al. 2001, Rotblat, Ehrlich et al. 2008).

However, being hydrophobic and water insoluble, the bioavailability of FTS was markedly limited (Kraitzer, Kloog et al. 2011). To address its solubility issue, PEG (5K) was conjugated with two FTS molecules to generate PEG_{5K}-FTS_2, which can self-aggregate into nanoscaled micelles and also effectively formulate other hydrophobic anticancer drugs such as PTX (Zhang, Lu et al. 2013). This is explainable considering the similar lipophilic chain of FTS with EB and VE. Moreover, strong synergy was shown in PEG_{5K}-FTS_2-delivered PTX micelles tested in various tumor cell lines (Zhang, Lu et al. 2013). Further, significantly enhanced tumor growth inhibition was achieved using PTX-loaded PEG_{5K}-FTS_2 over Taxol in murine breast tumor model (Zhang, Lu et al. 2013). Although PEG_{5K}-FTS_2 exhibited great promise in serving as a nanomicelles carrier, its biological potential needs to be further unleashed. Therefore, we moved on to develop PEG-derivatized FTS with disulfide linkage (PEG_{5K}-S-S-FTS_2) so that FTS can be released maximally from conjugates, and present its anti-Ras activity to the fullest extent (Zhang, Liu et al. 2014). Surprisingly, PEG_{5K}-S-S-FTS_2 formed micelles with 4-fold decrease in CMC compared to the one without disulfide bond (Zhang, Liu et al. 2014). Also, HPLC-MS study showed that FTS can be more readily liberated from PEG_{5K}-S-S-FTS_2 conjugate in tumor cells or tissues compared to PEG_{5K}-FTS_2 conjugate (Zhang, Liu et al. 2014). More importantly, delivery of PTX by PEG_{5K}-S-S-FTS_2 showed greater antitumor activity in comparison to that by PEG_{5K}-FTS_2 and Taxol (Zhang, Liu et al. 2014). In order to elucidate the structure activity relationship, four PEG-FTS conjugates that differed in the molecular weight of PEG (PEG_{2K} vs PEG_{5K}) and the molar ratio of PEG/FTS (1/2 vs 1/4) in the conjugates were developed (Zhang, Huang et al. 2014). Our data indicated that the PEG-FTS conjugates with four FTS molecules

were more effective over the conjugates with two molecules of FTS (Zhang, Huang et al. 2014). Besides, conjugates with PEG_{5K} were clearly more effective than the ones with PEG_{2K} in forming stable PTX-loaded micelles (Zhang, Huang et al. 2014). Finally, it has been implied that PEG_{5K}-FTS_4/PTX was the most efficacious PTX nanomicellar formulation referring to hindering the tumor growth *in vivo*, in contrast to the PTX formulated in PEG_{2K}-FTS_2, PEG_{2K}-FTS_4, PEG_{5K}-FTS_2 micelles (Zhang, Huang et al. 2014).

1.2.3 TUMOR-SPECIFIC TARGETING BY LIGAND-EQUIPPED POLYMERIC NANOCARRIERS.

Owing to the nature of herperpermeable vasculatures and compromised lymphatic drainage in tumors, nanocarriers-encapsulated drugs can be passively targeted to cancerous tissue based on EPR effect, after sufficient circulation time in the blood stream (Matsumura and Maeda 1986). Although the improved bioavailability of delivered anticancer drugs or diagnostic agents to tumors was achieved via the solubilization and protection from the nanocarriers, the internalization efficiency by tumor cells sometimes remains poor. In order to obtain adequate nutrients to support the overly proliferation, tumor cells overexpress a variety of receptors such as receptors of folate (Zhao, Li et al. 2008), transferrin (Elliott, Elliott et al. 1993), epidermal growth factor (EGF) (Zeng, Lee et al. 2006), α_2-glycoprotein (Yin, Litvinov et al. 2006), as well as luteinizing hormone-releasing hormone (LHRH) (Dharap, Qiu et al. 2003). Specific interactions between the ligands with receptors displayed on tumor cells leads to the selective accumulation of drugs in the tumor tissue with high affinity. Besides, active targeting can also significantly reduce the unwanted side effects in normal tissue, as drugs accumulates primarily in the tumor sites. Furthermore, ligand-conjugated nanocarriers will be taken up through specific

ligand/receptor-mediated endocytosis, which could potentially bypass the p-gp-modulated efflux pump, resulting in the reversal of multidrug resistance in tumors, especially, in drug resistant cancers.

It has been found that conjugation of α_2-glycoprotein to Pluronics micelles–incoporated fluorescein isothiocyanate (FITC) exhibited preferential accumulation of FITC in brain glial tumor and reduced clearance of FITC by lung in comparison to that of pluronics micelles without α_2-glycoprotein ligand (Yin, Litvinov et al. 2006). Zeng et al found that EGF-decorated PEG-b-poly (δ-valerolactone) micelle can specifically target the EGF receptors overexpressed by the MDA-MB-468 breast cancer cells, which subsequently, led to the accumulation of micelle in the nucleus and perinuclear region in the tumor cells, suggesting the potential of EGF conjugation as an effective approach for the selective nuclear delivery of anticancer agents (Zeng, Lee et al. 2006). Transferrin, an 80-kDa blood plasma glycoprotein with two specific high affinity Fe (III), binds to the endogenous iron in plasma so as to control the level of free iron in biological fluids. It has been reported that transferrin-bound PLGA nanoparticles containing PTX presented increased intracellular uptake and decreased exocytosis, resulting in enhanced tumor growth regression compared to free drug or the one without transferrin conjugation (Elliott, Elliott et al. 1993). Folate, a type of vitamin, is one of the most widely used ligand in drug delivery for the active tumor targeting due to its non-toxicity, supplemental effect, as well as non-immunogenicity (Zhao, Li et al. 2008). Being overexpressed on various tumor cells such as lung, colon, breast, ovarian, and brain, folate has a broad spectrum of targeting tumors (Zhao, Li et al. 2008). Therefore, folate-targeted nanomedicine has been extensively investigated in drug delivery field. Liu et al. developed a block copolymer, poly (N-isopropylacrylamide-co-N, N-dimethylacrylamide-co-2-aminoethyl methacrylate)-b-poly (10-undecenoic acid) (P (NIPAAm-

co-DMAAm-co-AMA)-b-PUA), in which folic acid was coupled with AMA (Liu, Wiradharma et al. 2007). The folate-targeted system led to much lower IC_{50} in 4T1 and KB cancer cells compared to the counterparts without folate (Liu, Wiradharma et al. 2007). Yoo et al. showed that conjugation of folate to PLGA-PEG polymeric micelles led to dramatic improvement in delivering DOX in nude mice bearing KB epidermal carcinoma with greater tumor growth inhibition, compared to the counterpart without folate (Yoo and Park 2004). Also, Lee et al. demonstrated that DOX-loaded pH-sensitive micelles decorated with folate (PHSM/f) showed significantly improved antitumor activity in comparison to free DOX or micelles without folate as targeting ligand in DOX resistant MCF-7 (MCF-7/DOX^R) murine tumor model, suggesting the potential of PHSM/f in bypassing the P-gp efflux pump, leading to the reversal of drug resistance (Lee, Na et al. 2005). Also, the accumulation of DOX from PHSM/f in solid tumors was 20 times or 3 times higher than free DOX group or PHSM group, respectively, which implied that folate-decorated micelles can be more efficiently internalized via folate/folate receptor-mediated endocytosis (Lee, Na et al. 2005).

Recently, our group further improved the PEG_{5K}-EB_2 dual function carrier by attaching a folate ligand onto the surface of the micelles (FA-PEG_{5K}-EB_2) (Lu, Zhao et al. 2014). Significant enhanced cytotoxicity was achieved in FA-PEG_{5K}-EB_2/DOX in cancer cells such as 4T1.2, MCF-7, as well as NCI/ADR-RES, a drug resistant cell line, compared to free DOX, Doxil (PEGylated DOX formulation), and the PEG_{5K}-EB_2/DOX (Lu, Zhao et al. 2014). More importantly, for the first time, we found that PEG_{5K}-EB_2 can significantly suppress the activity of P-gp by restraining the function of ATPase, which is of great importance in overcoming the P-gp-mediated multidrug resistance (Lu, Zhao et al. 2014). Besides, improved DOX uptake was also observed in the folate targeted system (Lu, Zhao et al. 2014). Finally, all of the advantages

from FA-PEG_{5K}-EB_2/DOX gave rise to significantly enhanced antitumor efficacy *in vivo* (Lu, Zhao et al. 2014).

1.2.4 IMPROVED PERFORMANCE OF MICELLES VIA INTRODUCTION OF DRUG-INTERACTIVE MOTIF.

Although the solubility of hydrophobic anticancer agents have been improved significantly after loading into nanocarriers including polymeric micelles, the drug loading capacity and formulation stability remains a challenge in the field of drug delivery. The poorly water soluble chemotherapeutic agents can be incorporated into the hydrophobic core of polymeric micelles during the self-aggregation process that is mainly driven through the hydrophobic interactions among the hydrophobic components of the micelles. Under this circumstance, the drug loading and formulation stability is mainly determined by the interactions between the hydrophobic domains of polymeric micelles and drugs with hydrophobicity. While working well to some degree, the satisfactory drug loading and formulation stability are still hard to be achieved to meet the therapeutic intent due to the lack of sufficient drug/carrier compatibility. Therefore, there is an urgent need to create nanocarriers that can load more drugs with acceptable stability. To this purpose, a wealth of approaches have been studied. One of them is to utilize disulfide cross-linker to enhance the stability of drug-loaded micelles. Li et al. found that the disulfide cross-linked micelles made of PEG and cholic acid (DCMs) was able to significantly enhance the stability of micelles with superior PTX loading (35.5%), which inevitably led to better antitumor effect in vivo (Li, Xiao et al. 2011).

Moreover, it has been reported that introduction of drug-interactive moieties into the conventional micellar systems can further increase the drug loading capacity and formulation

stability via offering additional interactions between carrier/drug or carrier/carrier (Huh, Lee et al. 2005, Kim, Kim et al. 2010, Han, Feng et al. 2011, Verma, Aswal et al. 2011). Hydrotropy refers to the improvement in water solubility arising from the introduction of suitable quantity of a second solute (Cloninger 2002). Most of hydrotropic molecules (hydrotrope) are composed of an aromatic ring which is substituted by moieties with anion or cation (Cloninger 2002). Owing to the small size of the amphiphilic hydrotropes, basically, it is impossible to promote the micellization. It is only exceeding the minimum hydrotropic concentration (MHC) that the hydrotropes can self-aggregate, during which the poor solubility of hydrophobic drugs can be increased via the complexation (Al-Jamal, Sakthivel et al. 2003). Notwithstanding the complete mechanism of how the hydrotropes solubilize the sparingly water soluble drug is not fully elucidated, the potential interactions such as π-π stacking, hydrophobic interaction, as well as hydrogen bonding have been proposed (Huh, Lee et al. 2005, Kim, Kim et al. 2010). The free hydrotropes worked well to some extent with respect to increasing the solubility of some hydrophobic therapeutics, but the effectiveness in solubilizing a wide spectrum of hydrophobic drugs remains inadequate. Another concern is the toxicity attributed by the cosolvents and surfactants used in the application of free hydrotropes as solubilizer for hydrophobic molecules (Huh, Lee et al. 2005). Further, in drug formulation, the freely dissolved hydrotropes can be readily absorbed systematically in the body, posing safety issue (Cheon Lee, Kim et al. 2003). Fortunately, being amenable to structure modifications, hydrotropes normally can be covalently linked polymers in which their solubilizing ability can be employed, while at the same time, minimizing concerns of systemic absorption (Huh, Lee et al. 2005). It is expected the addition of hydrotropes into the polymeric micelles can provide extra solubility power to better formulate poorly water soluble drugs. In Park's research, N,N-diethylnicotinamide (DENA), a typical

hytrotrope, was conjugated to the hydrophobic block of a copolymer to yield PDENA-PEG, which was able to formulate PTX with significantly improved loading and enhanced formulation stability, compared to the other polymer micelles without hydrotropes incorporation (PPA-PEG and PLA-PEG) (Huh, Lee et al. 2005). Recently, park et al. developed a novel hydrotropic polymer micelle system in which hydrotropic N,N-dimethylbenzamide (DMBA) was covalently linked to the hydrophobic polymer (Kim, Kim et al. 2011). The DMBA-based system can be exploited as a versatile carrier to increase the water solubility for 1~3 order of magnitude and enhanced formulation stability for a variety of hydrophobic drugs with diverse molecular structures with polymeric hydrotropes at the 1% (w/v) in comparison to its counterparts without hydrotropes incorporation (Kim, Kim et al. 2011). This strategy can provide a unique means of formulating various poorly soluble drugs without adding large amount of organic solvents. Furthermore, Kataoka's group has shown that conjugation of the poorly soluble drug (DOX, PTX, SN-38, and Epirubicin) into the hydrophobic core of a polymer micelles, can greatly facilitate the drug loading capacity and improve stability when formulating the same hydrophobic drugs (Cabral and Kataoka 2014). This could be due to the enhanced interactions between the physically entrapped drug and the hydrophobic core materials that were composed of the same drugs.

More recently, our group has found that introduction of a drug-interactive motif into the interfacial region of the lipid-core micelles or emulsion components can significantly strengthen the drug loading and formulation stability for a multitude of hydrophobic anticancer agents. Among a number of functional groups examined in PEGylated lipopepetides for formulating JP4-039, a synthetic antioxidant, fluorenylmethyloxycarbonyl (Fmoc), a commonly used amine protecting group in peptide chemistry, was found to be the most effective drug-interactive group

in enhancing carrier/drug interactions (Gao, Huang et al. 2013). Fmoc group embraces a bulky and fused fluorenylmethyl ring that is able to offer strong π-π stacking effect and hydrophobic interactions with other molecules containing aromatic moieties, including itself (Gao, Huang et al. 2013). In addition, the carbamoyl bond that bridges the lysine to benzene ring is of hydrogen bonding power (Gao, Huang et al. 2013). It has been reported that Fmoc played a pivotal role in forming elongated nanoasseblies by promoting parallel interactions of short peptides or lipopeptides with the same group (Zhang, Gu et al. 2003, Jayawarna, Smith et al. 2007). Our data exhibited that the drug-loaded emulsion containing Fmoc as drug-interactive motif resulted in marked improvement pertaining to formulation stability (Gao, Huang et al. 2013). Additionally, we developed another Fmoc-containing amphipilic polymers composed of PEG5K and two oleoyl molecules, which was able to readily form micelles with much lower CMC and enhanced PTX loading in contrast to the one without Fmoc (Zhang, Lu et al. 2014). Additionally, this system was also fairly effective in formulating another seven hydrophobic drug with diverse chemical structures, implying the versatility of this carrier as a drug carrier (Zhang, Lu et al. 2014). In an attempt to improve the performance of our dual functional carriers developed previously, Fmoc was conjugated to the interfacial area of the PEG_{5K}-VE_2 (PEG_{5K}-Fmoc-VE_2 (Lu, Zhao et al. 2014, Zhang, Huang et al. 2014). The PEG_{5K}-Fmoc-VE_2 conjugate also well reserved the intrinsic function of VE in inhibiting the activity of P-gp. Notably, PEG_{5K}-Fmoc-VE_2 presented dramatically improved DOX (39.95%) or PTX (20.8%) loading with enhanced formulation stability, compared to PEG_{5K}-VE_2 in formulating DOX (2.9%) or PTX (5.4 %) (Lu, Zhao et al. 2014, Zhang, Huang et al. 2014). In addition, pharmacokinetic (PK) and biodistribution studies exhibited an augmented half-life in circulation and more effective tumor accumulation for DOX formulated in PEG_{5K}-Fmoc-VE_2 micelles (Lu, Zhao et al. 2014). More

importantly, DOX-loaded PEG_{5K}-Fmoc-VE_2 micelles showed a MTD (~30 mg DOX/kg) that was about 3 times as much as that in free DOX (Lu, Zhao et al. 2014). Finally, drastically enhanced antitumor efficacy was achieved in 4T1.2 breast, PC-3 prostate, as well as drug resistant-KB 8-5 tumor models (Lu, Zhao et al. 2014). The underlying mechanism of the greatly ameliorated compatibility between PEG_{5K}-Fmoc-VE_2 and drugs was demonstrated to be ascribed to the additional π- π stacking, hydrophobic interactions, as well as hydrogen bonding effects arisen from addition of Fmoc through FT-IR, fluorescence quenching, UV absorbance, and NMR studies (Lu, Zhao et al. 2014). Similar results were also obtained in Fmoc-containing PEG-derivatized FTS (PEG_{5K}-Fmoc-VE_2) in comparison to its counterpart without Fmoc (Zhang, Huang et al. 2014).

1.2.5 A-TOCOPHEROL-CONJUGATED ANTICANCER DRUGS: AN EFFECTIVE APPROACH OF FORMULATING CHEMOTHERAPEUTICS.

The vitamin E (VE), nontoxic, nonimmunogenic, and biocompatible lipids, is composed of lipophilic tocopherols and tocotrienols, among which γ-tocopherol is the most widely used in the diet in North America (Brigelius-Flohe and Traber 1999). While, α-tocopherol exhibits the highest level of biological activity in VE (Bieri and Evarts 1974, Brigelius-Flohe and Traber 1999). Therapeutic potential of VE has also been extensively evaluated for a number of disorders including cancer, heart diseases, as well as Alzheimer's disorder (Lee, Tseng et al. 2013, Dysken, Sano et al. 2014, Li, Sen et al. 2014). In previous chapter, VE-derivatized polymeric micelles as effective nanocarriers for the delivery of anticancer agents have been elaborated. Herein, emphasis will be placed on derivatizing hydrophobic anticancer drugs with tocopherol as a promising novel platform to formulate sparingly water soluble chemotherapeutics. It was

reported that VE was able to synergize with other chemotherapeutics when treating cancer (Mi, Liu et al. 2011). Further, VE was also capable of overcoming the multidrug resistance (MDR) through inhibiting the p-gp efflux pump (Tang, Fu et al. 2013). Besides, VE-derivatives can significantly improve the solubility of hydrophobic drugs (Duhem, Danhier et al. 2014). Therefore, conjugation of VE to another anticancer drugs not only increase the compatibility of the parent drug, but also greatly enhance its therapeutic efficacy.

In Duhem et al's study, DOX was covalently coupled to D-α-tocopherol succinate via an amide linkage to yield N-DOX-TOS, which can self-aggregate into highly ordered lamellar inner structure with particle size around 250 nm upon stabilization by D-α-tocopherol PEG 2000 succinate (PEG-TOS) (Duhem, Danhier et al. 2014). Besides, great DOX loading and low *in vitro* drug release were both secured by using N-DOX-TOS system (Duhem, Danhier et al. 2014). More importantly, the VE-derivatized DOX nanoformulations was able to offer significantly enhanced ability of delaying the tumor growth *in vivo* compared to free DOX (Duhem, Danhier et al. 2014). Recently, Liu et al. ped a series of novel nanomaterials consisting of hydrophobic prodrugs that can self-assemble into nanoparticles by themselves, which was distinct from conventional amphipilic or ionic interactions (Wang, Liu et al. 2014). VE was conjugated to a number of anticancer agents (PTX, DOX, fluorouracil, and gemcitabine) or diagnostics (sulforhodamine B) via disulfide linker (Wang, Liu et al. 2014). The VE-based prodrugs can readily self-aggregate into stable nanomedicine with unimodal size distribution in aqueous solution. These nanoassemblies improved drug loading capacity significantly and mitigated safety issues concerning the shared application of excipient which may cause side effects. Finally the PEGylated VE-based prodrugs containing disulfide bond showed both favorable PK, enhanced inhibition on tumor growth, as well as considerable imaging ability in

tumor (Wang, Liu et al. 2014). The underlying mechanism addressing this unique self-assembly system was found to be the insertion of disulfide bond between VE and drugs, as the counterparts without disulfide bond linker was discerned as marked crystal aggregates instead of individual nanoparticles (Wang, Liu et al. 2014). It has been observed that disulfide bonds tend to exhibit dihedral angles to approach 90^{o}, which contributed dramatically to balancing intermolecular forces, and presented the favorable spatial configuration, in which high density of negative charge on the nanoparticles' surface was exposed, resulting in the disruption of crystallization (Wang, Liu et al. 2014).

Our improved dual functional vectors worked well for most of chemotherapeutics, but cannot accommodate campothecin (CPT), a potent antitumor drug by suppressing the activity of topoisomerase I. In order to ameliorate the compatibility of CPT, CPT was modified via conjugating to VE at its hydroxyl group through either carbonate ester bond (CPT-VE) or disulfide linkage (CPT-S-S-VE) (Lu, Liu et al. submitted). Our data showed that both VE-derivatized CPT prodrugs can effectively self-assemble into nanofibers with monodispersity upon stabilization of PEG_{5K}-Fmoc-VE_2 carrier (Lu, Liu et al. submitted). The CPT loading was improved remarkably in CPT-VE (6.6%) or CPT-S-S-VE (9.2%) prodrugs nanoparticles along with greater stability (CPT-VE system > 20 days, CPT-S-S-VE system > 30 days) over CPT formulated in PEG_{5K}-Fmoc-VE_2 (0.65%) (Stability≈8 days) (Lu, Liu et al. submitted). The improved CPT loading and stability in CPT prodrugs nanoassemblies, especially in CPT-S-S-VE system is highly likely due to the addition of VE molecule to CPT, in which the compatibility of CPT-VE or CPT-S-S-VE with carriers was significantly ameliorated. Meanwhile, the hydrophobic interactions between VE molecules from CPT prodrugs and carriers could act as the driving force to form nanoparticles during self-assembly process, leading to both increased CPT

loading and enhanced formulation stability. Besides, the additional hydrogen bonding could also be involved in the formation of the stable CPT prodrugs nanofibers based on our FT-IR study (Lu, Liu et al. submitted). Furthermore, the flexible CPT-S-S-VE could offer augmented degree of freedom of rotation, in contrast to relatively rigid CPT-VE, which could adjust the spatial arrangement of CPT-S-S-VE to the optimal position so as to be anchored into carriers in a more stabilized fashion, which was reflected by stronger hydrophobic interactions and π- π stacking in CPT-S-S-VE illustrated by the fluorescence quenching and UV absorbance study. Moreover, CPT prodrugs, particularly in CPT-S-S-VE system, were able to retain good biological activity of the parental CPT *in vitro* (Lu, Liu et al. submitted). Confocal imaging study demonstrated CPT prodrugs nanofibers were taken up via endocytosis, which was of great importance in overcoming drug resistance in drug resistant tumors through bypassing the P-gp-mediated efflux pump (Lu, Liu et al. submitted). Finally, CPT-S-S-VE nanoassemblies achieved significantly more CPT accumulation in tumor and superior antitumor efficacy in mice bearing 4T1.2 breast tumor (Lu, Liu et al. submitted). The better performance in CPT-S-S-VE over CPT-VE nanofibers concerning tumor CPT accumulation and tumor regression was attributed to the significantly easier release of CPT from CPT-S-S-VE in tumor as where high level of GSH can break down the disulfide bond, liberating CPT.

2.0 PEG-DERIVATIZED EMBELIN AS A DUAL FUNCTIONAL CARRIER FOR THE DELIVERY OF PACLITAXEL

2.1 BACKGROUND

Low water-solubility, high protein-binding and relatively short half-life are major problems in the clinical applications of many potent anti-cancer drugs such as paclitaxel (PTX) (Paal, Muller et al. 2001, Xie, Guan et al. 2007). Currently a variety of drug delivery systems such as liposomes, dendrimers, microcapsules and polymeric micelles have been developed to address these problems and further to promote sustained, controlled and targeted delivery of poorly water-soluble anti-cancer drugs (Torchilin 2007). Of all these delivery systems, polymeric micelles have gained considerable attention as a versatile nanomedicine platform due to their technical ease, high biocompatibility, and high efficiency in drug delivery (Sutton, Nasongkla et al. 2007, Mi, Liu et al. 2011). Polymer micelles have been demonstrated to improve the aqueous solubility of chemotherapeutic agents and prolong their *in vivo* half-lives, owing to the steric hindrance provided by a hydrophilic shell (Sutton, Nasongkla et al. 2007, Mi, Liu et al. 2011). Moreover, compared with other delivery systems, micelles show advantages in passive tumor targeting through the leaky vasculature via the enhanced permeability and retention (EPR) effect due to their small size ranging from 10-100 nm (Matsumura and Maeda 1986). Favorable drug biodistribution and improved therapeutic index can be achieved by using the micelle delivery

system (Sutton, Nasongkla et al. 2007, Torchilin 2007). However, most of the polymeric systems use "inert" excipients that lack therapeutic activity. The presence of large amounts of carrier materials not only adds to the cost but also imposes additional safety issue (Croy and Kwon 2006).

One of the most sophisticated designs of drug delivery systems is that the components forming the carriers can also be of therapeutic effects. The carrier materials may be capable of counteracting the side effects caused by the loaded anticancer drugs (Dong and Feng 2005). Also, it is possible that the carrier may collaborate with the loaded drug to achieve synergistic effects to better treat the tumor (Mi, Liu et al. 2011). However, the strategy of using highly water-insoluble drugs themselves as the hydrophobic region of polymeric micelle is rarely reported. One example is the pegylated vitamin E, D-α-tocopheryl polyethylene glycol succinate (Vitamin E TPGS or TPGS) (Zhang and Feng 2006, Zhang, Lee et al. 2008, Prashant, Dipak et al. 2010). Vitamin E shows antitumor activity against a number of types of cancers through various mechanisms such as induction of apoptosis, inhibition of tumor cell proliferation and differentiation, suppression of nuclear factor-kappa B (NF-κB) activation, and so forth (Husain, Francois et al. 2011, Ji, Wang et al. 2011). The pegylated vitamin E is a highly water soluble amphiphilic molecule comprising lipophilic alkyl tail and hydrophilic polar head portion. In addition to its antitumor activity, it is effective in solubilizing various hydrophobic drugs such as PTX. Synergistic actions between the TPGS-based carrier and delivered anticancer agents have been reported (Mi, Liu et al. 2011).

In this study, we report the development of PEG-derivatized embelin as another novel and dual-functional carrier for delivery of poorly water-soluble anticancer drugs. Embelin is a naturally occurring alkyl substituted hydroxyl benzoquinone compound and a major constituent

of *Embelia ribes* BURM. It has been shown to possess antidiabetic, anti-inflammatory, and hepatoprotective activities (Chitra, Sukumar et al. 1994, Bhandari, Jain et al. 2007, Singh, Singh et al. 2009). Embelin also shows antitumor activity in various types of cancers (Chitra, Sukumar et al. 1994, Sreepriya and Bali 2005, Dai, Qiao et al. 2009, Danquah, Li et al. 2009, Singh, Singh et al. 2009, Heo, Kim et al. 2011). One major mechanism involves the inhibition of the activity of X-linked inhibitor of apoptosis protein (XIAP) (Nikolovska-Coleska, Xu et al. 2004). XIAP is overexpressed in various types of cancers cells, particularly drug-resistant cancer cells and inhibition of XIAP has been explored as a new approach for the treatment of cancers (Tamm, Kornblau et al. 2000, Holcik, Gibson et al. 2001). XIAP plays a minimal role in normal cells and therefore embelin shows significantly less toxicity on normal cells. Embelin also downregulates the expression of survivin, XIAP, IAP1/2, TRAF1, cFLIP, Bcl-2, and Bcl-x_L through the inhibition of NF-κB activation (Ahn, Sethi et al. 2007). Embelin is poorly water soluble and PEG modification was originally explored by us as an approach to increase its solubility. Interestingly, PEG-derivatized embelin forms micelles that are highly efficient in solubilizing other compounds such as PTX. Preparation of PEG-derivatized embelin can be readily achieved with commercially available embelin. In addition, we have developed an efficient synthesis strategy to prepare PEG-embelin conjugate. Our *in vitro* studies showed that PEG-embelin has similar activity as free embelin with IC_{50} in the low μM range. More importantly, PEG-embelin synergizes with PTX at much lower doses (~nM) in a number of cancer cell lines tested.

2.2 METHODS

2.2.1 Materials

Paclitaxel (98%) was purchased from AK Scientific. Inc. (CA, USA). 2,5-dihydroxy-3-undecyl-1,4-benzoquinone (embelin 98%) was purchased from 3B Scientific Corporation (IL, USA). Dulbecco's phosphate buffered saline (DPBS) was purchased from Lonza (MD, USA). Methoxy-$PEG_{3,500}$-OH, dimethyl sulfoxide (DMSO), 3-(4,5-dimethylthiazol-2-yl)-2,5-diphenyl tetrazolium bromide (MTT), trypsin-EDTA solution, Triton X-100, and Dulbecco's Modified Eagle's Medium (DMEM) were all purchased from Sigma-Aldrich (MO, USA). Fetal bovine serum (FBS) was purchased from Gibco Life Technologies (AG, Switzerland). Penicillin-streptomycin solution was from Invitrogen (NY, USA). All solvents used in this study were HPLC grade.

2.2.2 Cell culture

DU145 and PC3 are two androgen-independent human prostate cancer cell lines. MDA-MB-231 is a human breast adenocarcinoma cell line. 4T1 is a mouse metastatic breast cancer cell line**.** All cell lines were cultured in DMEM containing 10% FBS and 1% penicillin-streptomycin in a humidified environment at 37 ℃ with 5% CO_2.

2.2.3 Synthesis of $PEG_{3.5K}$-Embelin$_2$ ($PEG_{3.5K}$-EB_2)

Figure 1 shows the synthesis sequence of $PEG_{3.5K}$-EB_2 conjugate. Synthesis of the intermediates and structural characterizations are detailed below.

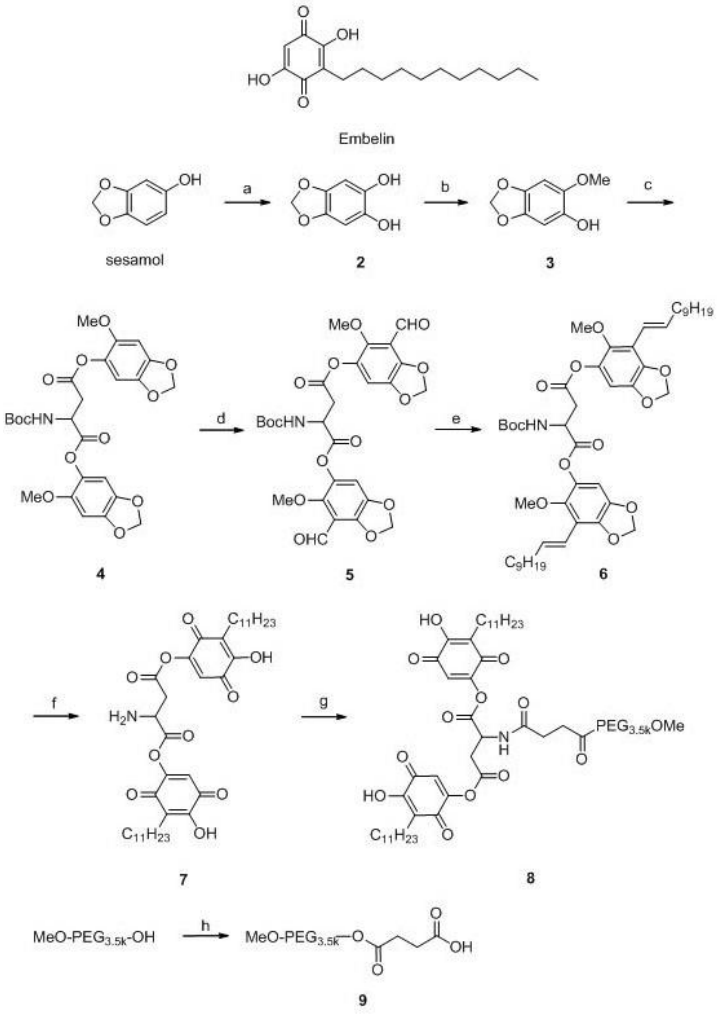

Figure 1 The synthetic route of $PEG_{3.5K}$-EB_2. Conditions: (a) water, Fremy's salt, KH_2PO_4, 5 min; NaS_2O_4, 30 min; (b) water, Mel, NaOH, 1 h; (c) Boc-Aspartic acid, DCC, DMAP, CH_2Cl_2, overnight; (d) MeCN, DMF, $POCl_3$; (e) THF, LiHMDS 2M in THF, decyltriphenylphosphonium bromide, 2 h; (f) 1) MeOH, H_2, Pd/C; 2) MeCN, CAN; 3) dioxane, HCl, 2 h; (g) CH_2Cl_2, DCC, DMAP, 9; overnight; (h) succinic anhydride, DMAP, CH_2Cl_2, 2 days.

Compound **2:** Sesamol (1.52 g, 24 mmol) in 30 mL of methanol was added to a rapidly stirred solution of Fremy's salt (7.96 g, 30 mmol) and 5.49 g (40 mmol) of KH_2PO_4 in 400 mL

water at 5 ℃. The color of the solution changed from light brown to bright yellow within 5 min. The mixture was stirred for another 30 min and then extracted with 4 × 40 mL of ethyl acetate. The ethyl acetate phase was treated with a solution of $Na_2S_2O_4$ (9.0 g, 52 mmol) in water (30 mL), and the yellow color changed to a colorless solution. The organic layer was acidified with HCl (1 N), extracted with ethyl acetate (3 × 30 mL), washed with water (20 mL), dried with anhydrous $MgSO_4$, and concentrated to give 1.1 g (65%) of **2** as a light pink solid. ^{1}H NMR($(CD_3)_2CO$): δ7.49 (s, 2H), 6.45 (s, 2H), 5.79 (s, 2H).

Compound **3:** A solution of **2** (1.54 g, 10 mmol) in water (30 mL) was treated with NaOH (0.4 g, 10 mmol) while the flask was kept in an ice bath. The reaction mixture was stirred for 15 min after which MeI (1.41 g, 10 mmol) was added dropwise. The reaction mixture was then heated under reflex for 1 h, allowed to cool down to room temperature and the solvent was removed via a rotary evaporator. The crude product was purified by flash chromatography with silica gel (ethyl acetate: petroleum ether, 1: 5) and pure **3** was obtained as an amber oil with a yield of 99% (1.68 g). ^{1}H NMR($CDCl_3$): δ 6.11 (m, 2H), 5.88 (s, 2H), 5.35 (s, 1H), 3.72 (s, 3H).

Compound **4:** To a solution of *N*-(*tert*-Butoxycarbonyl)-L-aspartic acid (Boc-Asp-OH) (2.33 g, 10 mmol) in CH_2Cl_2 (40 mL) was added dicyclohexylcarbodiimide (DCC) (6.2 g, 30 mmol), 4-dimethyamineopyridine (DMAP) (0.61 g, 5 mmol), and compound **3** (3.36 g, 20 mmol) at room temperature. The reaction mixture was stirred overnight at room temperature. After the reaction was completed, 100 mL Et_2O was added to the mixture. The mixture was filtered to remove the insoluble DCU byproduct and the organic phase of the filtrate was concentrated under vacuum. The resulting residue was purified by silica gel flash chromatography (MeOH: CH_2Cl_2, 1:10) to give pure **4** as an oil in 62% yield (3.31 g). ^{1}H NMR

($CDCl_3$): δ 6.11 (m, 4H), 5.88 (m, 4H), 5.40 (m, 1H), 4.65 (m, 1H), 3.74 (s, 3H), 3.72 (s, 3H), 2.88 (m, 1H), 2.64 (m, 1H), 1.42 (s, 9H). ESI-MS *m/z* 534.2 ($[M+H]^+$).

Compound **5**: To a solution of **4** (5.33 g, 10 mmol) in acetonitrile (MeCN, 10 mL) at 0-5℃, dry dimethylformamide (DMF) (0.73 g, 10 mmol) and $POCl_3$ (1.78 g, 11 mmol) were added with constant stirring over 0.5 h. The salt formed was filtered, washed with cold MeCN, dissolved in 20 mL of water, heated at 50 ℃ for 0.5 h, and then cooled. The mixture was extracted with 3 × 40 mL of CH_2Cl_2, the combined organic phase was washed with brine, dried over anhydrous Na_2SO_4, and concentrated in vacuum. The crude residue was purified by silica gel flash chromatography (MeOH: CH_2Cl_2, 1: 10) to give pure **5** as an oil in 80% yield (4.82 g). ^1H NMR ($CDCl_3$): δ 10.21 (s, 1H), 10.18 (s, 1H), 6.65 (m, 2H), 5.92 (m, 4H), 5.37 (m, 1H), 4.51 (m, 1H), 3.75 (s, 3H), 3.72 (s, 3H), 2.85 (m, 1H), 2.60 (m, 1H), 1.40 (s, 9H). ESI-MS *m/z* 590.5 ($[M+H]^+$).

Compound **6:** A solution of sodium bis(trimethylsilyl)amide (12 mL, 2 M solution in THF) was added dropwise to a stirred solution of decanyltriphenylphosphonium bromide (9.67g, 20 mmol) in 40 mL THF at room temperature. The resulting mixture was stirred for 30 min at room temperature and then cooled to -78℃. To this mixture was added compound **5** (6.03 g, 10 mmol). The reaction mixture was stirred for 2 h at -78℃ and then warmed up to room temperature. The reaction mixture was quenched with saturated solution of NH_4Cl, extracted with ethyl acetate. The combined organic layer was washed with brine, dried over anhydrous Na_2SO_4, and concentrated in vacuum. The crude residue was purified by silica gel flash chromatography (MeOH: CH_2Cl_2, 1: 10) to give pure **6** as an oil in 90% yield. ^1H NMR ($CDCl_3$): δ 6.48 (m, 2H), 6.39 (m, 2H), 6.02 (m, 2H), 5.86 (m, 4H), 5.35 (m, 1H), 4.53 (m, 1H), 3.75 (s,

3H), 3.72 (s, 3H), 2.83 (m, 1H), 2.61 (m, 1H), 2.15 (m, 4H), 1.40 (s, 9H), 1.29 (m, 28H), 0.91 (m, 6H). ESI-MS *m/z* 838.4 ($[M+H]^+$)

Compound **7**: The double bond in compound **6** (8.37 g, 10 mmol) was saturated by catalytic hydrogenolysis with Pd/C (10%, 500 mg) under H_2 (1 atm) in a methanol solution (50 mL) at room temperature for 2 h. The solution was filtered to remove Pd/C and concentrated under vacuum. The resulting product was then dissolved in the solution of 10 mL of water, 10 mL MeCN, and 20 mmol CAN (ammonium ceric nitrate) (10.96 g). The mixture was cooled to 0℃ and stirred for another 2 h. MeCN was then removed via evaporation under reduced pressure, 100 mL CH_2Cl_2 was added to the remaining aqueous solution. The organic phase was washed with brine and then concentrated under vacuum. 10 mL dioxane and 10 mL HCl were then added to the residue. The mixture was stirred at room temperature for 24 h. The reaction mixture was quenched with saturated solution of $NaHCO_3$, extracted with ethyl acetate. The organic layer was washed with brine, dried over anhydrous Na_2SO_4, and concentrated under vacuum. The crude product was purified by silica gel flash chromatography (MeOH: CH_2Cl_2, 1:10) to give pure **7** as an oil in 42% yield (2.89 g). ^{1}H NMR($CDCl_3$): δ 8.16 (m, 2H), 6.75 (m, 2H), 5.35 (m, 2H), 4.53 (m, 1H), 2.85 (m, 1H), 2.60 (m, 1H), 2.43 (m, 4H), 1.25 (m, 36H), 0.89 (m, 6H). ESI-HRMS calcd for $C_{38}H_{55}NO_{10}Na$ ($[M+Na]^+$) 708.4766, found 708.4747.

Compound **8:** A solution of MeO-$PEG_{3.5k}$-CO_2H (3.5 g, 1 mmol) in CH_2Cl_2 (5 mL) was treated with DCC (0.41 g, 2 mmol), DMAP (0.12 g, 1 mmol), and compound **7** (689 mg, 1 mmol) at room temperature. The reaction mixture was stirred overnight. After the reaction was completed, 100 mL of Et_2O was added and the mixture was filtered and concentrated under vacuum**.** The resulting residue was purified by silica gel flash chromatography (MeOH: CH_2Cl_2, 1:10) to give pure **8 (**$PEG_{3.5K}$-EB_2**)** as a wax solid in ~50% yield (2.1 g). ^{1}H NMR ($CDCl_3$): δ

8.14 (m, 2H), 6.72 (m, 2H), 5.57 (m, 1H), 4.98 (m, 1H), 3.35 (s, 3H), 2.60 (m, 10H), 1.25 (m, 36H), 0.89 (m, 6H).

2.2.4 Formation of micelles

PTX-solubilized micelles were prepared by the following method. PTX (10 mM in chloroform) was added to $PEG_{3.5K}$-EB_2 (10 mM in chloroform) with various carrier/drug ratios. The organic solvent was first removed by nitrogen flow to form a thin film of drug/carrier mixture. The film was further dried under high vacuum for 2 h to remove any traces of remaining solvent. Drug-loaded micelles were formed by suspending the film in DPBS. The drug-free micelles were similarly prepared as described above.

2.2.5 Measurement of size and zeta potential

Zetasizer (Zetasizer Nano ZS instrument, Malvern, Worcedtershire, UK) was used to measure the particle size and zeta potential of drug-free and drug-loaded micelles. Micelles were stored at 4 ℃, and the samples were tested for changes in particle size and size distribution.

2.2.6 Determination of PTX loading efficiency

PTX-solubilized micelles were prepared at an input PTX concentration of 1.07, 2.14, and 3.21 mg/mL respectively. Aliquots of samples were filtered through 0.45 μm PVDF syringe filter. PTX in the filtered and non-filtered micelles was extracted using methanol and measured by high performance liquid chromatography (HPLC, Waters). A reverse phase column (C18) was

employed. The detection was performed by using UV detector at 227 nm, 70% methanol as a mobile phase, flow rate at 1.0 mL/min. Drug loading capacity (DLC) and drug loading efficiency (DLE) were calculated according to the following formula:

DLC (%) = [weight of drug used/(weight of polymer + drug used)] ×100%

DLE (%) = (weight of loaded drug/weight of input drug) ×100%

2.2.7 Determination of the critical micelle concentration (CMC)

The CMC of $PEG_{3.5K}$-EB_2 was determined by employing pyrene as a fluorescence probe (La, Okano et al. 1996). A drug-free micelle solution in DPBS (2.5 mg/mL) was prepared via solvent evaporation method. A series of 2-fold dilutions was then made with $PEG_{3.5K}$-EB_2 concentrations ranging from 7.63×10^{-5} to 2.5mg/mL. At the same time, aliquots of 50 μL of 4.8×10^{-6} M pyrene in chloroform were added into 15 separate vials. The chloroform was first removed by nitrogen flow to form a thin film. The film was further dried under high vacuum for 2 h to remove any traces of remaining solvent. Then, the pre-prepared micelle solutions (400 μL in DPBS) of varying $PEG_{3.5K}$-EB_2 concentrations were added to the pyrene film to obtain a final pyrene concentration of 6×10^{-7} M for each vial. The solutions were kept on a shaker at 37 ℃ for 24 h to reach equilibrium before fluorescence measurement. The fluorescence intensity of samples was measured at the excitation wavelength of 334 nm and emission wavelength of 390 nm by Synergy H1 Hybrid Multi-Mode Microplate Reader (Winooski, VT). The CMC is determined from the threshold concentration, where the sharp increase in pyrene fluorescence intensity is observed.

2.2.8 Transmission electron microscope (TEM)

The morphology of micelles was observed on a Jeol 1011 transmission electron microscope (TEM). The aqueous micelle solution (1.0 mg/mL) was added onto copper grids coated with Formvar, and then stained with 1% uranyl acetate. The sample processing and imaging was performed at room temperature.

2.2.9 Hemolysis assay

Fresh blood samples were collected through cardiac puncture from rats. Ten mL blood was added with EDTA-Na_2 immediately to prevent coagulation. Red blood cells (RBCs) were separated from plasma by centrifugation at 1500 rpm for 10 min at 4 ℃. The RBCs were washed three times with 30 mL ice-cold DPBS. RBCs were then diluted to 2% w/v with ice-cold DPBS and utilized immediately for the hemolysis assay. One mL of diluted RBC suspension was treated with various concentrations (0.2 and 1.0 mg/mL) of $PEG_{3.5k}$-EB_2 and PEI, respectively, and then incubated at 37 ℃ in an incubator shaker for 4 h. The samples were centrifuged at 1500 rpm for 10 min at 4 ℃, and 100 μL of supernatant from each sample was transferred into a 96-well plate. The release of hemoglobin was determined by the absorbance at 540 nm using a microplate reader. RBCs treated with Triton X-100 (2%) and DPBS were considered as the positive and negative controls, respectively. Hemoglobin release was calculated as $(OD_{sample}-OD_{negative\ control})/(OD_{positive\ control}-OD_{negative\ control}) \times 100\%$

2.2.10 *In vitro* cell cytotoxicity

DU145 (2000 cells/well), PC-3 (5000 cells/well), MDA-MB-231 (2000 cells/well), or 4T1 (1000 cells/well) were seeded in 96-well plates followed by 24 h of incubation in DMEM with 10% FBS and 1% streptomycin-penicillin. Then various concentrations of PTX (dissolved in DMSO or formulated in $PEG_{3.5K}$-EB_2 micelles) were added in quadruplicate and cells were incubated for 72 h. Twenty μL of 3-(4, 5-dimethylthiazol-2-yl)-2,5-diphenyltetrazoliumbromide (MTT) in PBS (5mg/mL) was added and cells were further incubated for 4 h. The medium in the plates was removed and MTT formazan was solubilized by DMSO. The absorbance was measured by microplate reader with wavelength at 550 nm and reference wavelength at 630 nm. Untreated groups were used as controls. Cell viability was calculated as $[(OD_{treat}-OD_{blank})/(OD_{control}-OD_{blank}) \times 100\%]$.

2.3 RESULTS

2.3.1 Synthesis of $PEG_{3.5K}$-EB_2 conjugates

We have developed a strategy to synthesize $PEG_{3.5K}$-EB_2 conjugate in which two molecules of embelin were coupled to one molecule of PEG via a linker of aspartic acid. This is modified from the scheme reported by Wang's group for the total synthesis of Embelin (Chen, Nikolovska-Coleska et al. 2006). This involves the synthesis of benzoquinone followed by coupling to carboxyl groups of aspartic acid. Undecyl side chains were then installed onto each of the two benzoquinone rings. Finally PEG was coupled to aspartic acid-EB_2 through the

deprotected amino group. HPLC shows that the purity of the final product ($PEG_{3.5K}$-EB_2) is 94% (**Figure 2**).

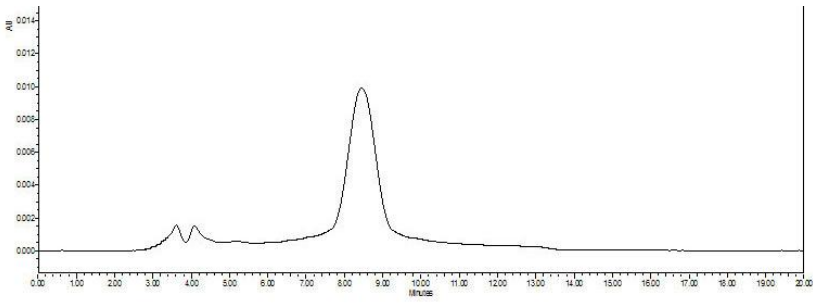

Peak	Migration Time	Area	% Area	Height
1	3.614	18750	3.05	1176
2	4.088	14191	2.31	911
3	8.454	581040	94.63	9433

Purity = 94.63 %

1. Column: Hibal®250-4 HPLC Column, Lichrospher® 100 RP-18(5 μm）
2. Solvent: 95% Methanol: 5% H_2O (Contain 10 mM H_3PO_4).
3. Wavelength: 254 nm
4. Flow: 1 mL/min
5. HPLC System: Waters 600-717-486 System
6. Software: Empower 2 TM.

Figure 2 HPLC trace of $PEG_{3.5K}$-EB_2.

^{1}H NMR spectrum of $PEG_{3.5K}$-EB_2 shows signals at 3.63 ppm attributable to the methylene protons of PEG, the embelin proton signals at 8.14 and 6.72 ppm and the carbon chain singles at 1.05-1.25 ppm. The aspartate signals were identified at 5.57, 4.98 and 2.60 ppm (**Figure 3**).

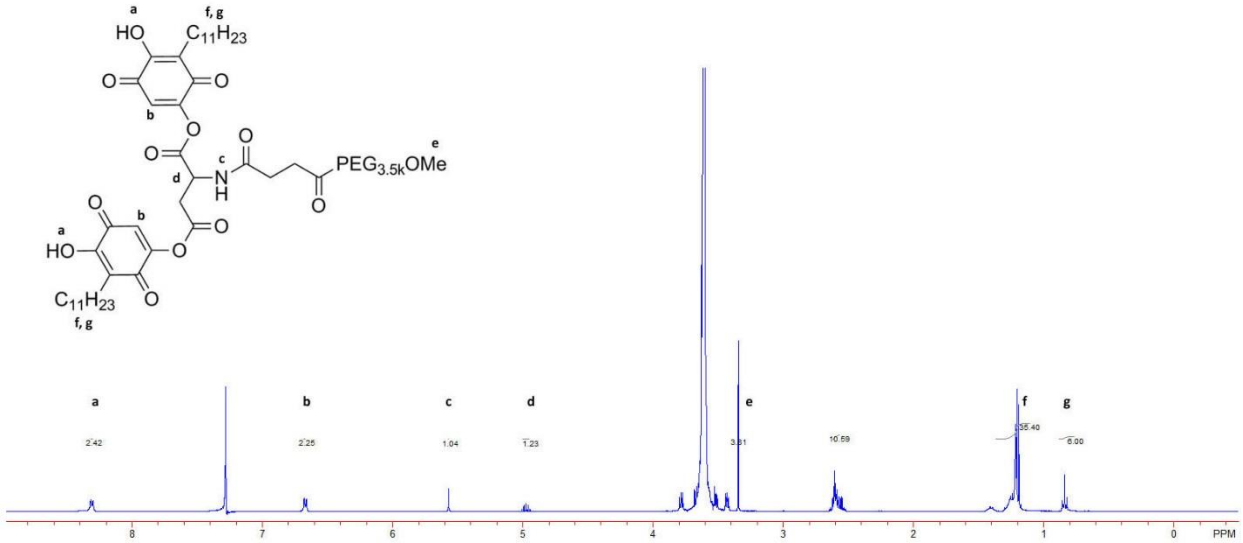

Figure 3 ^{1}H-NMR spectra (400 MHz) of $PEG_{3.5K}$-EB_2 in $CDCl_3$.

The molecular weight of the $PEG_{3.5K}$-EB_2 conjugate from MALDI-TOF MS (4197) is very similar to the theoretical value (4203) (**Figure 4**). These results suggest successful synthesis of $PEG_{3.5K}$-EB_2 conjugate.

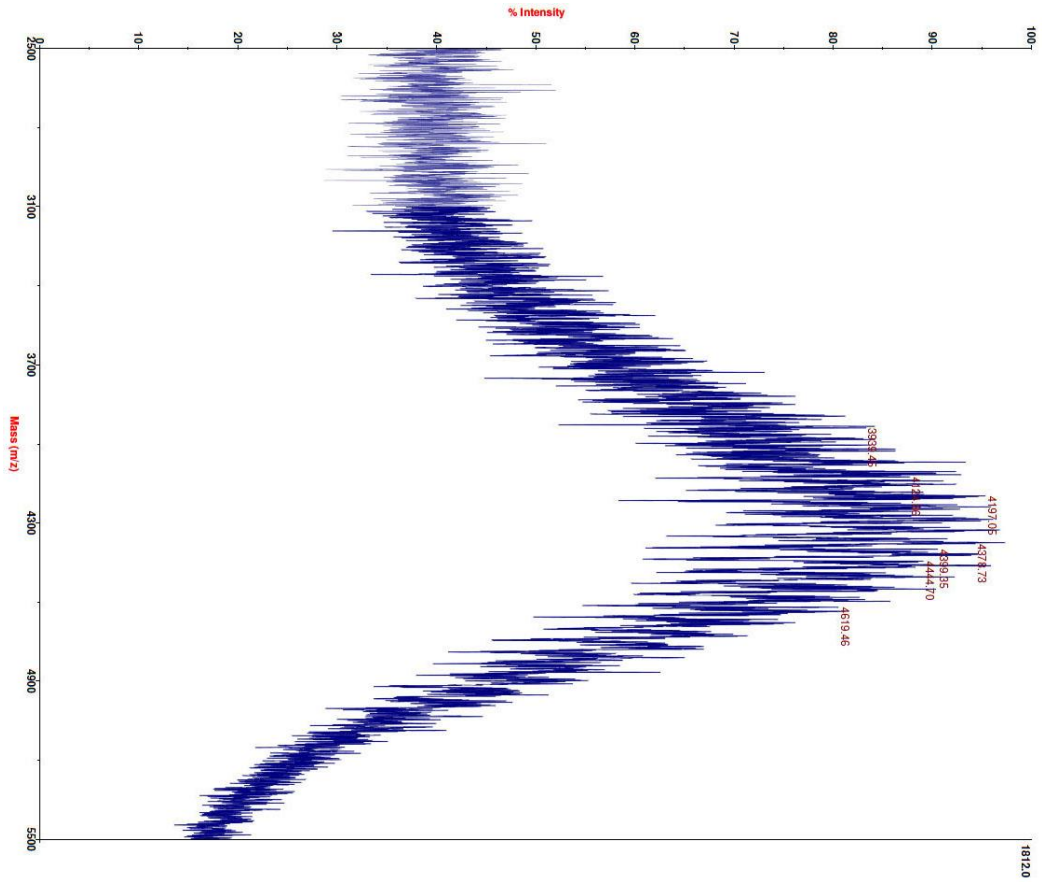

Figure 4 MALDI-TOF of $PEG_{3.5K}$-EB_2.

2.3.2 Biophysical characterization of micelles

Micelles were readily prepared from $PEG_{3.5K}$-EB_2 conjugate via solvent evaporation method. $PEG_{3.5K}$-EB_2 conjugate can be dissolved in water at concentration up to 750 mg/mL (data not shown). Dynamic light scattering (DLS) measurements showed that these micelles had

hydrodynamic sizes around 22 nm at the concentration of 20 mg/mL (**Figure 5A**), which shall ensure efficient passive targeting to the solid tumors.

PTX, a potent hydrophobic anticancer agent, was readily loaded into $PEG_{3.5K}$-EB_2 micelles. **Figure 5C** shows the DLS size measurement of PTX-loaded $PEG_{3.5K}$-EB_2 micelles at a drug concentration of 1 mg/mL. There were little changes in sizes when PTX was loaded into micelles at a carrier/drug ratio of 7.5/1 (m/m).

Figure 5B&D show the TEM images of drug-free and PTX-loaded micelles after staining with 1% uranyl acetate. Spherical particles of uniform size were observed for both drug-free and PTX-loaded micelles. The sizes of the micelles observed under TEM are consistent with those measured by DLS.

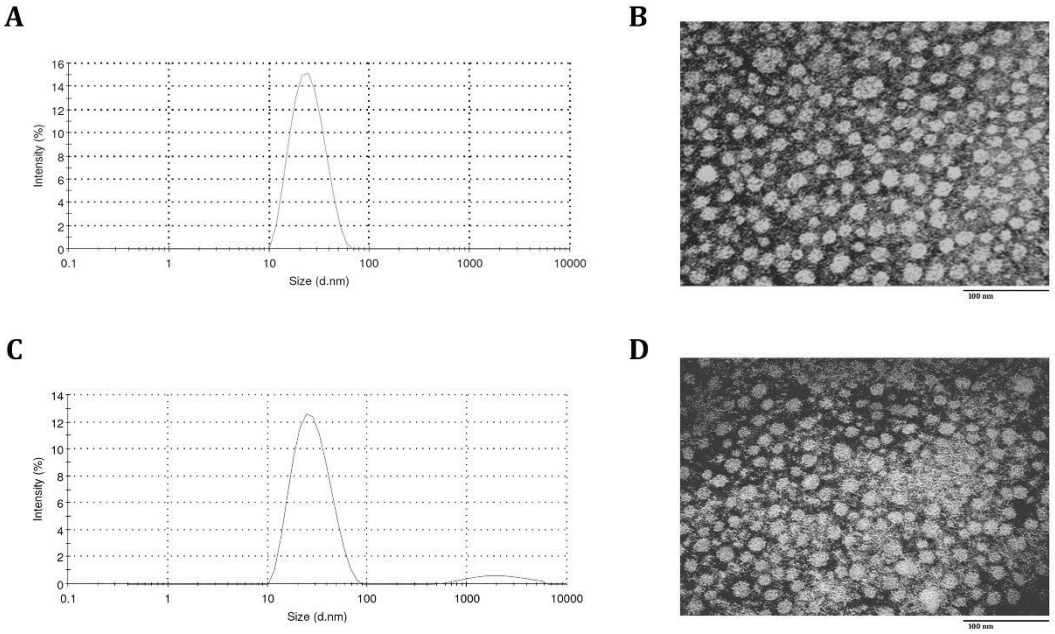

Figure 5 Particle size distribution of $PEG_{3.5K}$-EB_2 (A) and PTX-loaded $PEG_{3.5K}$-EB_2 (C); TEM images of self-assembled micelles of $PEG_{3.5K}$-EB_2 (B) and PTX-loaded $PEG_{3.5K}$-EB_2 (D). The spherical micelles with the diameter of around 20 nm were observed. The drug loading level was 1 mg/mL (PTX) in $PEG_{3.5K}$-EB_2.

Table 1 shows the sizes of PTX-loaded micelles at different carrier/drug molar ratios. PTX-loaded $PEG_{3.5K}$-EB_2 micelles had relatively large size (~143 nm) at a carrier/drug ratio of 2.5: 1 (m/m) and the particles were stable for less than 1 day. Increasing the input molar ratio of

$PEG_{3.5K}$-EB_2/PTX led to gradual decrease in the size of PTX-loaded micelles. At the molar ratio of 7.5/1, the size of the PTX-loaded micelles was similar to that of drug-free micelles.

Table 1 DLS analysis of the sizes of free and drug-loaded $PEG_{3.5K}$-EB_2 micelles

micelles	molar ratio	size (nm)[a]	PDI[b]
$PEG_{3.5K}$-EB_2	——	22.8±0.3	0.09
$PEG_{3.5K}$-EB_2:PTX[c]	2.5:1	143±17	0.23
$PEG_{3.5K}$-EB_2:PTX	5:1	58.7±0.5	0.32
$PEG_{3.5K}$-EB_2:PTX	7.5:1	27.5±0.2	0.23

[a]Measured by dynamic light scattering particle sizer (Zetasizer)
[b]PDI = polydispersity index
[c]PTX = paclitaxel
PTX concentration in micelle was kept at 1 mg/mL. Blank micelle concentration was 20 mg/mL
Values reported are the means ± SD for triplicate samples

2.3.3. Drug loading efficiency (DLE)

DLE of PTX-loaded micelles were determined by HPLC and the results are shown in **Table. 2**.

Table 2 Physicochemical characterization of PTX-loaded $PEG_{3.5K}$-EB_2 micelles.

$PEG_{3.5K}$-EB_2:PTX (m/m)	concentration of PTX in micelles (mg/mL)	DLC[a] (%)	DLE[b] (%)	zeta[c] (mV)
2.5:1	1.07	7.51	79.9	1.58±0.37
5:1	1.07	3.90	96.7	1.89±0.08
7.5:1	1.07	2.63	98.6	-1.52±0.20
	2.14	2.63	97.5	-1.29±0.19
	3.21	2.63	81.3	-2.64±0.43

[a]DLC = drug loading capacity
[b]DLE = drug loading efficiency
[c]Measured by dynamic light scattering particle sizer (Zetasizer)
Values reported are the means ± SD for triplicate samples.

DLE was as high as 79.89% when PTX was formulated in $PEG_{3.5K}$-EB_2 micelles at a carrier/PTX input ratio of 2.5/1 (m/m) and PTX concentration of 1.07 mg/mL. Increasing the carrier/PTX input ratios led to further increase in DLE. $PEG_{3.5K}$-EB_2/PTX formed the most stable particles at a carrier/drug ratio of 7.5/1. At this ratio, PTX was quantitatively formulated in the $PEG_{3.5K}$-EB_2 micelles when the PTX concentration was less than 2.14 mg/mL. Increasing the PTX

concentration to 3.21 mg/mL led to a slight decrease in DLE (81.3%). The surface charges of PTX-loaded $PEG_{3.5K}$-EB_2 micelles were close to neutral (+1.89 ~ -2.64) for all particles examined.

2.3.4 CMC measurements

Figure 6 shows the results of CMC measurements using pyrene as a fluorescence probe. Upon incorporation into the micelles, the fluorescence intensity of pyrene increases substantially at the concentration of micelles above the CMC (La, Okano et al. 1996). Based on the partition of the pyrene, the CMC of $PEG_{3.5K}$-EB_2 could be obtained by plotting the fluorescence intensity versus logarithm concentration of the polymer. The CMC of $PEG_{3.5K}$-EB_2 was determined from the crossover point at the low concentration range. The CMC of the $PEG_{3.5K}$-EB_2 conjugate is 4.9 μM, which is similar to most reported micellar delivery systems.

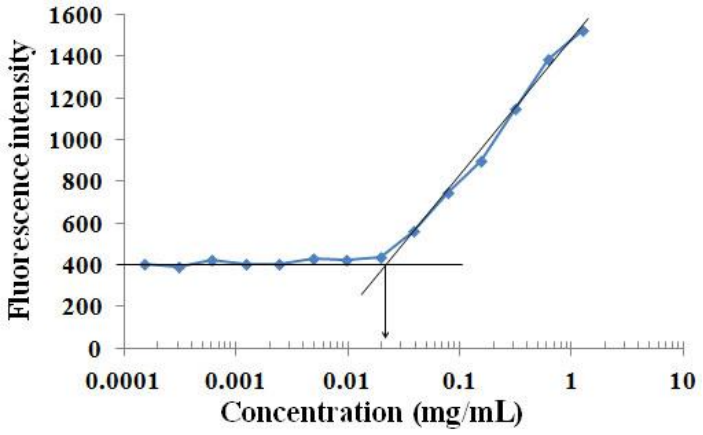

Figure 6 CMC measurement of the $PEG_{3.5K}$-EB_2 micelles using pyrene as a hydrophobic fluorescence probe.

2.3.5 Hemolysis study

One of the safety concerns for polymeric micelle systems is the hemolytic activity. To address this issue, the hemolytic activity of drug-free $PEG_{3.5K}$-EB_2 micelles was examined and compared to a strong detergent Triton X-100 and polyethylenimine (PEI), a cationic polymer known to have significant hemolytic effect (Reul, Nguyen et al. 2009). As shown in **Figure 7**, PEI induced hemolysis in a dose-dependent manner. In contrast, no observable hemolytic activities (< 5%) were found for $PEG_{3.5K}$-EB_2 micelles, suggesting the excellent safety of our new delivery system.

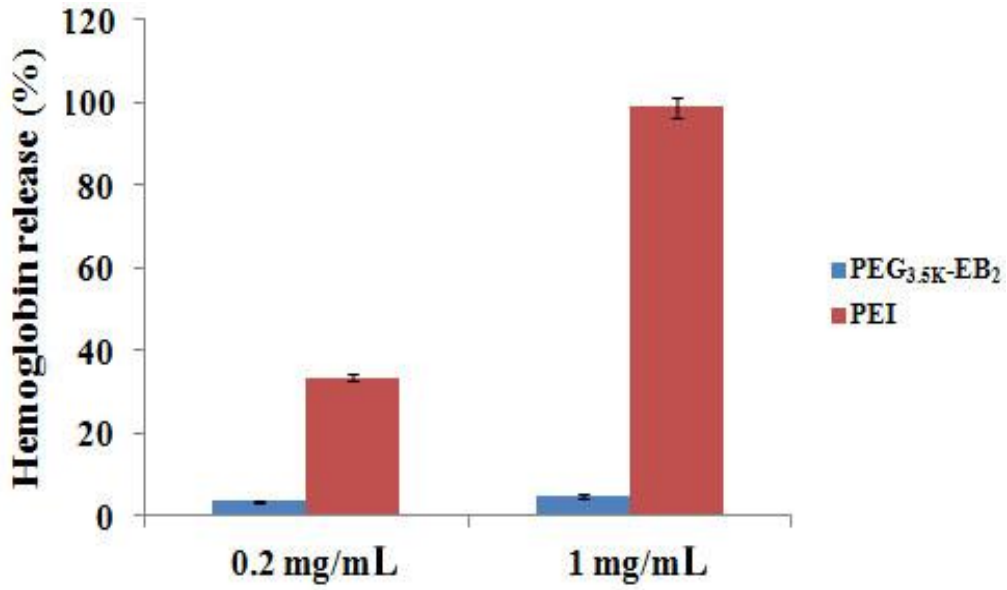

Figure 7 *In vitro* hemolysis assay of $PEG_{3.5K}$-EB_2 compared with PEI.

2.3.6 *In vitro* cytotoxicity

Figure 8 shows the cytotoxicity of $PEG_{3.5K}$-EB_2 in comparison with free embelin (dissolved in DMSO) in 4 cancer cell lines tested including human breast cancer cells MDA-MB-231, murine

breast cancer cells 4T1, and two human prostate cancer cell lines PC3 and DU145. $PEG_{3.5K}$-EB_2 was comparable to free embelin in antitumor activity in all 4 cancer cell lines with IC_{50} in the low μM range.

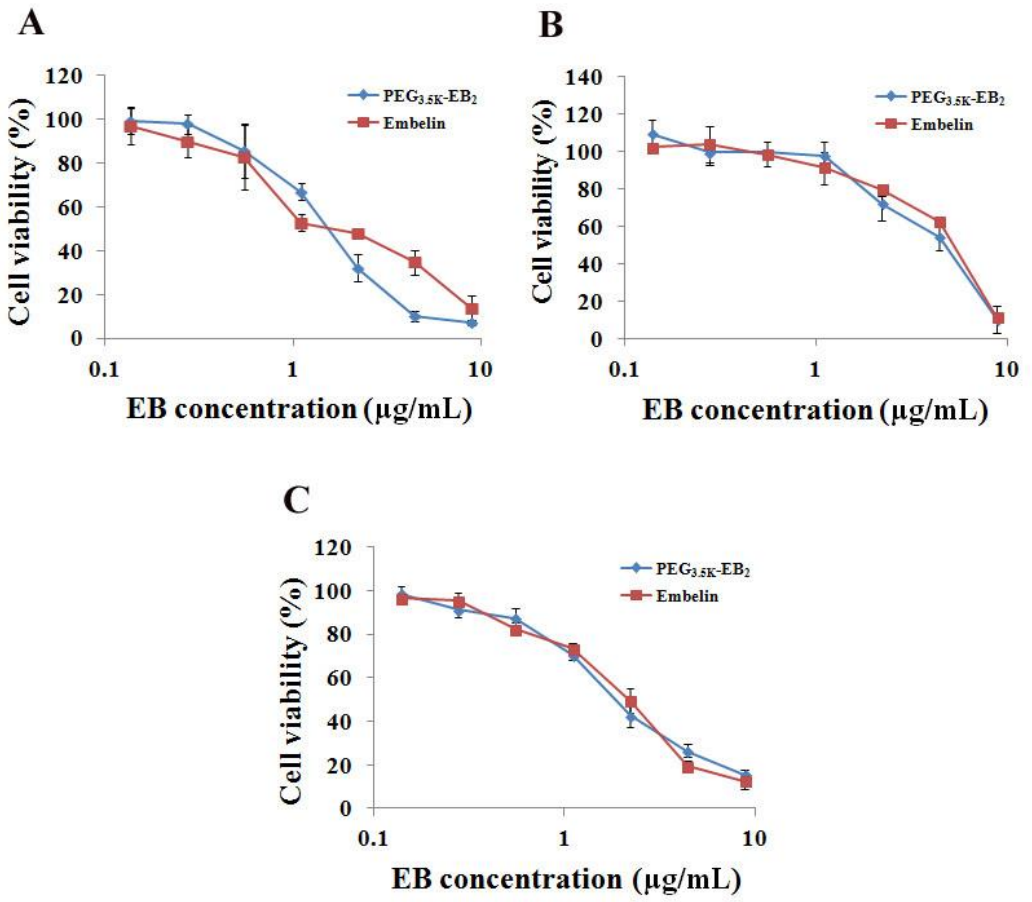

Figure 8 Cytotoxicity of free EB and $PEG_{3.5K}$-EB_2 against 4T1 mouse breast cancer cells (A) and two androgen-independent human prostate cancer cells PC-3 (B) and DU145 (C).

Figure 9A compares the cytotoxicity of free PTX (in DMSO) to that of $PEG_{3.5K}$-EB_2-formulated PTX (5/1, m/m) in MDA-MB-231 cells. Drug-free $PEG_{3.5K}$-EB_2 did not cause any cytotoxicity to MDA-MB-231 cells due to its relatively low concentrations used in this study. Free PTX exhibited cytotoxicity on MDA-MB-231 cells in a dose-dependent manner. However, formulation of PTX in $PEG_{3.5K}$-EB_2 micelles resulted in a significant increase in the cytotoxicity. Similar results were found with three other cancer cell lines (**Figure 9B-D**).

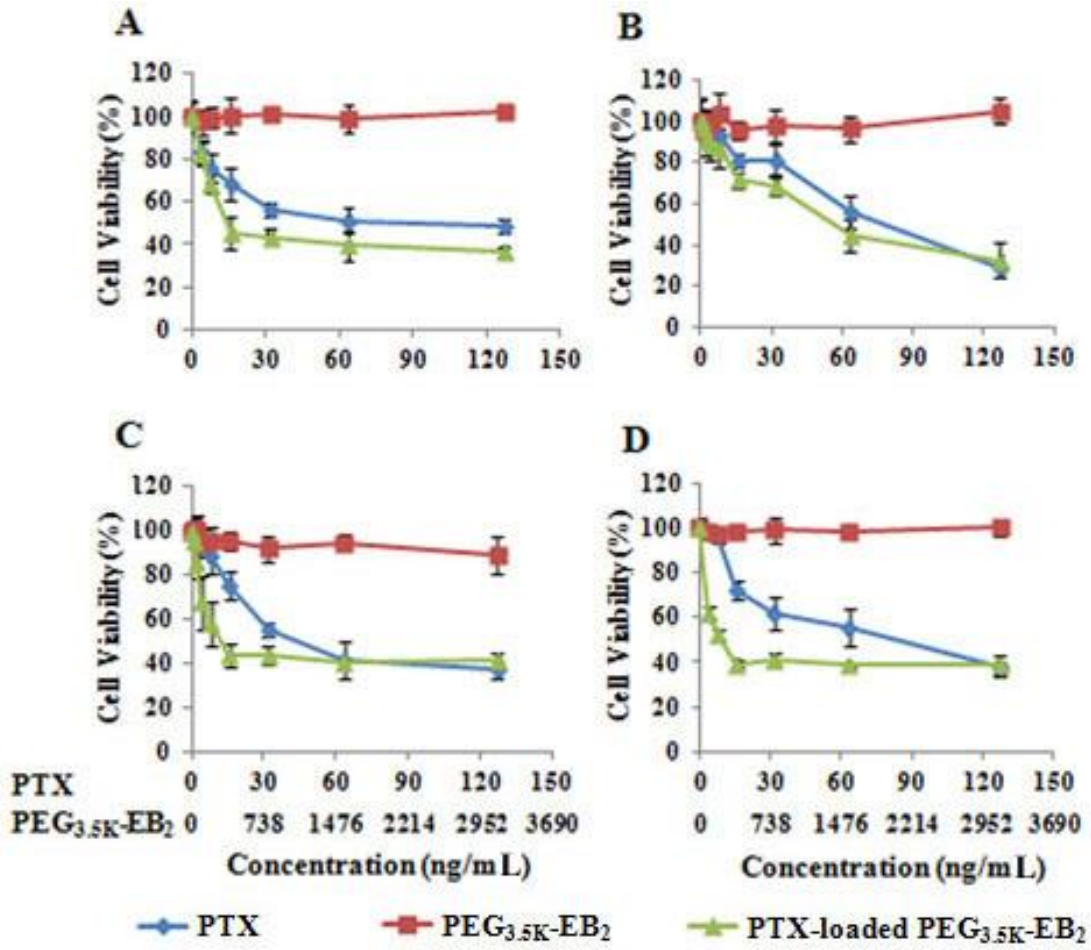

Figure 9 Cell-killing effect of free PTX, free $PEG_{3.5K}$-EB_2, and PTX-loaded $PEG_{3.5K}$-EB_2 in MDA-MB-231 human breast cancer cells (A), the 4T1 mouse breast cancer cells (B), human prostate cancer cells PC-3 (C) and DU145 (D).

Table 3 summarizes the IC_{50} of free PTX and $PEG_{3.5K}$-EB_2-formulated PTX in the four different cancer cell lines. Dependent on the cell lines, the IC_{50} was decreased by 1.5- to 8.7-fold when PTX was formulated in $PEG_{3.5K}$-EB_2 micelles.

Table 3 IC_{50} of PTX and PTX-loaded $PEG_{3.5K}$-EB_2 in different cancer cell lines.

	IC_{50}[a] (ng/mL)			
	MDA-MB-231	4T1	PC-3	DU145
PTX-loaded $PEG_{3.5K}$-EB_2	13.5	51	12.7	8.9
PTX	65	73	42.3	78

[a] The concentration of a drug that is required for 50% inhibition *in vitro*.

2.4 DISCUSSION

We have developed a new delivery system that consists of an embelin-based hydrophobic domain and a PEG hydrophilic segment. The $PEG_{3.5K}$-EB_2 conjugate readily forms micelles in aqueous solutions. More importantly, hydrophobic drugs such as PTX can be loaded into $PEG_{3.5K}$-EB_2 micelles.

Various polymeric micelle systems have been reported. Most micellar systems consist of a hydrophobic core that does not have any potential therapeutic effect (Li, Liu et al. 2011). In addition, the metabolites of the hydrophobic segments might contribute to some undesired effects, such as inflammation and systemic toxicity (Tang, Du et al. 2007, Li, Liu et al. 2011). The $PEG_{3.5K}$-EB_2 conjugate developed in this study represents a dual-functional delivery system that may overcome these limitations. Embelin is a natural product that demonstrates various biological effects including antitumor activity (Chitra, Sukumar et al. 1994). Embelin also shows excellent safety profiles in animals (Kumar, Dhamotharan et al. 2011). Thus, PEG-derivatized embelin may be an attractive delivery system to achieve synergistic activity with anticancer agents while minimizing the carrier-associated toxicity. PEG-embelin conjugates can be synthesized via direct coupling of embelin to PEG via an ester linkage. However, such synthesis is likely to yield a mixture of products with PEG randomly linked to the different hydroxyl groups in the benzene ring. We have developed a strategy to generate $PEG_{3.5K}$-EB_2 conjugate via total synthesis (**Figure 1**). This method was modified from a scheme reported by Wang's group for total synthesis of Embelin (Chen, Nikolovska-Coleska et al. 2006). Our synthesis ensures generation of structurally well-defined conjugate in which PEG is attached to 1-OH group in the quinone ring. Most of the steps give good yields and the synthesis of PEG-embelin conjugate

involves similar number of steps and cost as that of embelin alone (Chen, Nikolovska-Coleska et al. 2006).

$PEG_{3.5K}$-EB_2 conjugate forms small-sized micelles (20 ~ 30 nm) and loading of PTX did not significantly affect the size of the micelles. It was generally believed that particles in the size of 100 ~ 200 nm can effectively penetrate solid tumors via an EPR effect (Matsumura and Maeda 1986). A recent study from Lam's group compared the passive targeting of nanoparticles of different sizes in a subcutaneous model of human ovarian cancer xenograft. It was shown that particles with a size of 154 nm were significantly taken up by liver and lungs with limited accumulation at tumor sites. In contrast, particles with respective size of 17 and 64 nm were much more effective in passive targeting to the solid tumor (Luo, Xiao et al. 2010). Cabral and colleagues compared the targeting efficiency of polymeric micelles of different sizes (30, 50, 70 and 100 nm) in both highly and poorly permeable tumors. While all of the tested polymer micelles penetrated highly permeable tumors in mice, only the 30 nm micelles could penetrate poorly permeable pancreatic tumors to achieve an antitumor effect (Cabral, Matsumoto et al. 2011). The small size of our new micelle system suggests its potential for effective tumor targeting *in vivo*, which is currently being evaluated in our laboratory.

In vitro cytotoxicity with several cancer cell lines showed that $PEG_{3.5K}$-EB_2 is comparable to free embelin in antitumor activity with IC_{50} in the low μM range. More importantly, $PEG_{3.5K}$-EB_2 synergizes with PTX in antitumor activity at much lower concentrations (~nM) in all 4 cancer cell lines tested. The $PEG_{3.5K}$-EB_2-mediated cytotoxicity is unlikely attributed to its surface activity as $PEG_{3.5K}$-EB_2 showed minimal hemolytic activity even at mM concentrations (**Figure 7**). Embelin is coupled to PEG via a cleavable ester linkage. It is likely that embelin is released from the conjugate following intracellular delivery and executes the antitumor effect by

itself or synergizes with PTX in antitumor activity. These data are consistent with the observation that free embelin synergizes with PTX at subeffective doses (Lu & Li, unpublished data). More studies are needed to better understand the mechanism by which the $PEG_{3.5K}$-EB_2-based delivery system synergizes with PTX *in vitro*.

It should be noted that $PEG_{3.5K}$-EB_2 conjugate only represents a model micelle to demonstrate the utility of PEG-derivatized embelin as a dual functional delivery system for hydrophobic anticancer drugs. Considering the flexibility of our synthesis scheme more studies on structure-activity relationship (SAR) can be designed to further improve this new delivery system. These include optimization of the molar ratio of PEG/embelin in the conjugates, the length and structure of the acyl chain in the embelin, and the molecular weight of PEG. Recently embelin derivatives with improved affinity towards XIAP have been developed (Chen, Nikolovska-Coleska et al. 2006). The utility of these new derivatives as drug carriers can also be examined and compared to native embelin. Finally, promising candidates identified from these studies need to be further evaluated *in vivo*. These studies are currently ongoing in our laboratory.

3.0. PEG-DERIVATIZED EMBELIN AS A NANOMICELLAR CARRIER FOR THE DELIVERY OF PACLITAXEL TO BREAST AND PROSTATE CANCERS

3.1 BACKGROUND

Paclitaxel (PTX) is one of the first-line chemotherapeutic agents that are effective for the treatment of a wide range of cancers, including lung, ovarian, breast, prostate, head and neck cancer, and advanced forms of Kaposi's sarcoma. It works through interfering with normal breakdown of microtubules during cell division. The main challenge with PTX therapy is its poor solubility in aqueous solutions. Therefore, it is of tremendous incentive to develop effective delivery systems for PTX to enhance its accumulation at tumor site to maximize its therapeutic efficacy while minimizing the side effects. Taxol® and Abraxane® are two FDA approved PTX formulations. Taxol® is an alcohol/Cremophor formulation of PTX, which is irritating and can cause hyperactivity reactions. Abraxane® is PTX-loaded human albumin nanoparticles that have a size around 130 nm, which is within the range that can penetrate well-vascularized solid tumors via an enhanced permeability and retention (EPR) effect (Matsumura and Maeda 1986). It is now known that for less vascularized tumors, particles with smaller size (≤ 64 nm) were needed for effective penetration through neovasculatures to reach tumor cells (Luo, Xiao et al. 2010). There have been continuous efforts to develop various types of new formulations to improve targeted delivery of PTX to different types of tumors. Among all drug delivery systems being

investigated, polymeric micelles have gained considerable attention and are rapidly becoming a powerful nanomedicine platform for cancer therapeutics applications due to their simplicity, small sizes (10-100nm), ability to solubilize water insoluble anticancer drugs, and prolonged drug retention time (Sutton, Nasongkla et al. 2007, Torchilin 2007, Mi, Liu et al. 2011). However, most of the carrier materials in lipidic or polymeric drug delivery systems utilize "inert" excipients that lack therapeutic effect. The presence of large amount of carrier materials not only adds to the cost, but also imposes additional safety concerns (Croy and Kwon 2006).

One interesting strategy in formulation design is that components of carriers have therapeutic effects and can be freed from the delivery systems following intracellular delivery to achieve synergistic or additive effect with co-delivered drugs. One example is pegylated vitamin E, D-α-tocopheryl polyethylene glycol succinate (Vitamin E TPGS or TPGS) (Zhang and Feng 2006, Zhang, Lee et al. 2008, Prashant, Dipak et al. 2010). Vitamin E is linked to PEG via a biodegradable ester linkage and forms a hydrophobic core in this micellar system to solubilize other water-insoluble drugs. Vitamin E itself shows antitumor effect against different types of cancers through a variety of mechanisms (Husain, Francois et al. 2011, Ji, Wang et al. 2011). Synergistic antitumor activity has been demonstrated in a number of *in vitro* and *in vivo* studies for TPGS-based formulations of PTX and other anticancer agents (Liu, Huang et al. 2010, Mi, Liu et al. 2011).

Our group has previously developed PEG-derivatized embelin as another dual-functional carrier for the delivery of poorly water-soluble anti-cancer drugs (Huang, Lu et al. 2012). This system was constructed by coupling two embelin molecules to polyethylene glycol PEG 3500 ($PEG_{3.5K}$) through an ester linkage ($PEG_{3.5K}$-EB_2). Embelin is a naturally occurring alkyl substituted hydroxyl benzoquinone compound and a major constituent of *Embelia ribes* BURM.

It exhibits various biological effects including antidiabetic, anti-inflammatory, and hepatoprotective activities (Chitra, Sukumar et al. 1994, Bhandari, Jain et al. 2007, Singh, Singh et al. 2009). Embelin also shows antitumor activity in various types of cancers via inhibiting the activity of X-linked inhibitor of apoptosis protein (XIAP) (Chitra, Sukumar et al. 1994, Nikolovska-Coleska, Xu et al. 2004, Sreepriya and Bali 2005, Dai, Qiao et al. 2009, Danquah, Li et al. 2009, Heo, Kim et al. 2011). XIAP is overexpressed in various types of cancers cells, particularly drug-resistant cancer cells and inhibition of XIAP has been employed as a new strategy for the treatment of cancers (Tamm, Kornblau et al. 2000, Holcik, Gibson et al. 2001). We demonstrated that $PEG_{3.5K}$-EB_2 formed small-sized micelles (20-30 nm) and solubilized various hydrophobic agents including PTX (Huang, Lu et al. 2012). Preliminary study showed that the antitumor activity of embelin was well retained following coupling to $PEG_{3.5K}$. More importantly, $PEG_{3.5K}$-EB_2 synergized with PTX in antitumor activity in several cancer cell lines *in vitro*. In this study, we showed that a similar PEG derivative of embelin with a longer PEG, PEG_{5K}-$embelin_2$ formed stable micelles with PTX at lower carrier/PTX molar ratios. We further characterized the biophysical properties of the improved micellar system including size, loading capacity, and drug release kinetics. The *in vitro* cytotoxicity of PTX-loaded PEG_{5K}-$embelin_2$ was also studied in several cancer cell lines. Finally, the *in vivo* antitumor activity of PTX-loaded PEG_{5K}-$embelin_2$ was investigated in both breast cancer and prostate cancer models.

3.2 METHODS

3.2.1 Materials

Paclitaxel (98%) was purchased from AK Scientific Inc. (CA, USA). 2,5-dihydroxy-3-undecyl-1,4-benzoquinone (embelin 98%) was purchased from 3B Scientific Corporation (IL, USA). Dulbecco's phosphate buffered saline (DPBS) was purchased from Lonza (MD, USA). Methoxy-$PEG_{5,000}$-OH, dimethyl sulfoxide (DMSO), 3-(4,5-dimethylthiazol-2-yl)-2,5-diphenyl tetrazolium bromide (MTT), trypsin-EDTA solution, Triton X-100, and Dulbecco's Modified Eagle's Medium (DMEM) were all purchased from Sigma-Aldrich (MO, USA). Fetal bovine serum (FBS), penicillin-streptomycin solution, and DiD (1,1'-dioctadecyl-3,3,3',3'-tetramethylindodicarbocyanine perchlorate, D-307) were from Invitrogen (NY, USA). All solvents used in this study were HPLC grade.

3.2.3. Synthesis of PEG_{5K}-EB_2

PEG_{5k}-EB_2 was similarly synthesized according to our reported method for $PEG_{3.5k}$-EB_2 (Huang, Lu et al. 2012). This involves the synthesis of benzoquinone followed by coupling to Boc-aspartic acid. Undecyl side chains were then installed onto each of the two benzoquinone rings. Finally, PEG was coupled to aspartic acid-EB_2 through the deprotected amino group. The final product was analyzed by ^{1}NMR and MALDI-TOF.

3.2.4 Preparation and characterization of PTX- and DiD-loaded PEG_{5K}-EB_2 micelles

PTX-solubilized micelles were prepared by the following method. PTX (10 mM in chloroform) was added to PEG_{5K}-EB_2 (10 mM in chloroform) with various carrier/drug ratios. The organic solvent was first removed by nitrogen flow to form a thin dry film of drug/carrier mixture. The film was further dried under high vacuum for 2 h to remove any traces of remaining solvent. Drug-loaded micelles were formed by suspending the film in DPBS. The drug-free micelles and DiD-loaded micelles were similarly prepared as described above. The mean diameter of PEG_{5K}-EB_2 micelles with or without loaded drug was assessed by dynamic light scattering (DLS). The morphology and size distribution of drug-free or PTX-loaded PEG_{5K}-EB_2 micelles were observed using transmission electron microscopy (TEM) after negative staining. The CMC of PEG_{5K}-EB_2 was determined by employing pyrene as a fluorescence probe as described before (Huang, Lu et al. 2012). The concentration of PTX loaded in PEG_{5K}-EB_2 micelles was evaluated by HPLC as described previously (Huang, Lu et al. 2012). The drug loading capacity (DLC) and drug loading efficiency (DLE) were calculated according to the following formula:

$$\text{DLC (\%)} = [\text{weight of drug used}/(\text{weight of polymer} + \text{drug used})] \times 100\%$$

$$\text{DLE (\%)} = (\text{weight of loaded drug}/\text{weight of input drug}) \times 100\%$$

3.2.5 *In vitro* drug release study

An *in vitro* drug release study was carried out by dialysis using DPBS (PH = 7.4) containing 0.5% (w/v) Tween 80 as the release medium. Taxol formulation was employed as a control. Two mL of PTX-loaded PEG_{5K}-EB_2 micelles or Taxol (1 mg PTX/mL) were sealed in dialysis tubes (MWCO = 12 KDa, Spectrum Laboratories) which were then immersed in 200 mL release

medium in a beaker covered with parafilm. The beakers were placed in an incubator shaker at 100 rpm and 37°C. The concentration of PTX remaining in the dialysis tubes at various time points was measured by HPLC with the detector set at 227 nm. Values were reported as the means from triplicate samples.

3.2.6 Cell culture

DU145 and PC-3 are two androgen-independent human prostate cancer cell lines. 4T1.2 is a mouse metastatic breast cancer cell line. All cell lines were cultured in DMEM containing 10% FBS and 1% penicillin-streptomycin in a humidified environment at 37 ℃ with 5% CO_2.

3.2.7 Cellular uptake of Nile red-loaded PEG_{5K}-EB_2 micelles

The cellular uptake study was conducted with Nile red as a hydrophobic fluorescence probe (Greenspan, Mayer et al. 1985). Nile red-loaded PEG_{5K}-EB_2 micelles (7.5:1, m/m, PEG5K-EB2: Nile red) were prepared via a solvent evaporation method as described above. PC-3 cells were seeded in 24-well plates at 2×10^4 cells per well in 1 mL complete DMEM and cultured for 24 h, followed by removal of culture medium and addition of Nile red-loaded PEG_{5K}-EB_2 micelles at the Nile red concentration of 1μg/mL. The cells were incubated at 37℃ with 5% CO_2 for 2 h. Subsequently, the nuclei of cells were stained with Hoechst33342 for 5 min. Cells were then washed with DPBS three times and fixed with 4% paraformaldehyde for 30 min at room temperature. Finally, the slides were rinsed with DPBS three times and mounted with cover slips and observed under a fluorescence microscope (Eclipse TE300 Microscope).

3.2.8 *In vitro* cytotoxicity study

The cytotoxicity of PTX formulated in PEG_{5K}-EB_2 micelles was assessed with three cancer cell lines (DU145, PC-3, and 4T1.2) and compared to Taxol formulation. Briefly, DU145, PC-3 or 4T1.2 cells were seeded in 96-well plates followed by 24 h of incubation in DMEM with 10% FBS and 1% streptomycin-penicillin. Various dilutions of PTX-loaded PEG_{5K}-EB_2 and Taxol (at the equivalent concentrations of PTX) were added to cells. Controls include PEG_{5K}-EB_2 and Cremophor/ethanol and they were added to cells at concentrations equivalent to those of carriers in the corresponding PTX formulation groups. Cells were incubated for 72 h and cell viability was assessed by MTT assay as described previously (Huang, Lu et al. 2012).

3.2.9 Hemolytic effect of PEG_{5K}-EB_2 micelles

Fresh blood samples were collected through cardiac puncture from rats. EDTA-Na_2 was immediately added into 10 mL of blood to prevent coagulation. Red blood cells (RBCs) were separated from plasma by centrifugation at 1500 rpm for 10 min at 4℃. The RBCs were washed three times with 30 mL ice-cold DPBS. RBCs were then diluted to 2% w/v with ice-cold DPBS and utilized immediately for the hemolysis assay. One mL of diluted RBC suspension was treated with various concentrations (0.2 and 1.0 mg/mL) of PEG_{5k}-EB_2 and PEI, respectively, and then incubated at 37 ℃ in an incubator shaker for 4 h. The samples were centrifuged at 1500 rpm for 10 min at 4 ℃, and 100 μL of supernatant from each sample was transferred into a 96-well plate. The release of hemoglobin was determined by the absorbance at 540 nm using a microplate reader. RBCs treated with Triton X-100 (2%) and DPBS were considered as the

positive and negative controls, respectively. Hemoglobin release was calculated as (OD_{sample}-$OD_{negative\ control}$)/($OD_{positive\ control}$-$OD_{negative\ control}$) × 100%

3.2.10 Animals

Female BALB/c mice, 10-12 weeks were purchased from Charles River (Davis, CA). Male nude mice, 6-8 weeks ages, were purchased from Harlan (Livermore, CA). All animals were housed under pathogen-free conditions according to AAALAC guidelines. All animal-related experiments were performed in full compliance with institutional guidelines and approved by the Animal Use and Care Administrative Advisory Committee at the University of Pittsburgh.

3.2.11 Maximum tolerated dose (MTD)

Groups of 4 BALB/c mice were administered intravenously with Taxol (15, 20, 25 mg PTX/kg body weight), or PTX-loaded PEG_{5K}-EB_2 micelles (30, 50, 75, 100, 120 mg PTX/kg body weight), respectively. Changes in body weight and survival of mice were followed daily for two weeks. The MTD was defined as the dose that causes neither mouse death due to the toxicity nor greater than 15% of body weight loss or other remarkable changes in the general appearance within the entire period of the experiments.

3.2.12 Biodistribution of PEG_{5K}-EB_2 micelles via NIRF optical imaging

The *in vivo* biodistribution and tumor targeting efficiency of PEG_{5K}-EB_2 micelles were investigated by using a near infrared fluorescence dye, DiD. Two nude mice bearing bilateral s.c.

PC-3 xenografts were used in this study. Two-hundred μL of DiD-loaded PEG_{5K}-EB_2 micelles were i.v. injected into each mouse and the concentration of DiD in the formulation was 0.4mg/mL. At indicated times, the two mice were scanned using a Carestream Molecular Imaging System, In-Vivo Multispectral FX PRO, with the excitation at 630 nm and the emission at 700 nm using a 30 second exposure time. Prior to and during each imaging, the mice were anesthetized by isoflurane inhalation. X-ray images were also taken for tumor location and overlaid with corresponding NIR images. After imaging, the mice were euthanized by CO_2 overdose.

3.2.13 *In vivo* therapeutic study

Two mouse tumor models were used to examine the therapeutic effect of PTX formulated in PEG_{5K}-EB_2 micelles: a syngeneic murine breast cancer model (4T1.2) and a human prostate cancer (PC-3) xenograft model.

For the breast cancer model, 2 x 10^5 4T1.2 cells in 200 μL PBS were inoculated s.c. at the right flank of female BALB/c mice. Treatments were initiated when tumors in the mice reached a tumor volume around 50 mm^3 and this day was designated as day 1. On day 1, mice were randomly divided into six groups (n=5) and received i.v. administration of free PEG_{5K}-EB_2 micelles, Taxol (10 mg PTX/kg), PTX-loaded PEG_{5K}-EB_2, and saline, respectively on days 1, 4, 7, 10, and 13. PTX-loaded PEG_{5K}-EB_2 micelles were given at two different dosages, 10 mg/kg and 20 mg PTX/kg, respectively. Free PEG_{5K}-EB_2 micelles were given at the equivalent dosage of the carrier in the group of PTX-loaded PEG_{5K}-EB_2 micelles (20 mg PTX/kg). Tumor sizes were measured with digital caliper twice a week and calculated according to the following formula: $(L \times W^2)/2$, where L is the longest and W is the shortest in tumor diameters (mm). To

compare between groups, relative tumor volume (RTV) was calculated at each measurement time point (where RTV equals the tumor volume at a given time point divided by the tumor volume prior to first treatment). Mice were sacrificed when tumor reached 2000 mm^3 or developed ulceration.

To monitor the potential toxicity, the body weights of all mice from different groups were measured every three days. In addition, serum level of transaminases (AST, ALT) in the mice treated with PTX/PEG_{5K}-EB_2 (20 mg PTX/kg) and PBS groups was investigated at the completion of the study.

For establishment of PC-3 xenograft tumor model, 2×10^6 PC-3 cells in 200 μL PBS were inoculated s.c. at the right flank in male nude mice. Treatments were started when tumors in the mice reached a volume around 50 mm^3 and different groups (n = 6) were similarly treated as described above on days 1, 3, 7, 10, 13, 24, and 28. Tumor size and body weight were monitored as described above.

3.2.14 Statistical analysis

In all statistical analysis, the significance level was set at a probability of $P < 0.05$. All results were reported as the mean ± standard error (SEM) unless otherwise indicated. Statistical analysis was performed by Student's t-test for two groups, and one-way ANOVA for multiple groups, followed by Newman-Keuls test if $P < 0.05$.

3.3 RESULTS AND DISCUSSION

3.3.1 Preparation and characterization of PTX-loaded PEG_{5K}-EB_2 micelles

We previously developed a $PEG_{3.5K}$-EB_2 conjugate and preliminary *in vitro* study suggested that it functioned as a dual delivery system and showed synergistic activity with co-delivered PTX against several cancer cell lines (Huang, Lu et al. 2012). In this report we developed a similar PEG-derivatized embelin conjugate with a PEG of higher MW (PEG_{5K}) as parts of our efforts to improve the stability and loading capacity of this micellar system. The chemical structure of PEG_{5K}-EB_2 conjugate, in which two embelin molecules were linked to one molecule of PEG_{5K} through a bridge of aspartic acid, is shown in **Figure 10A**.

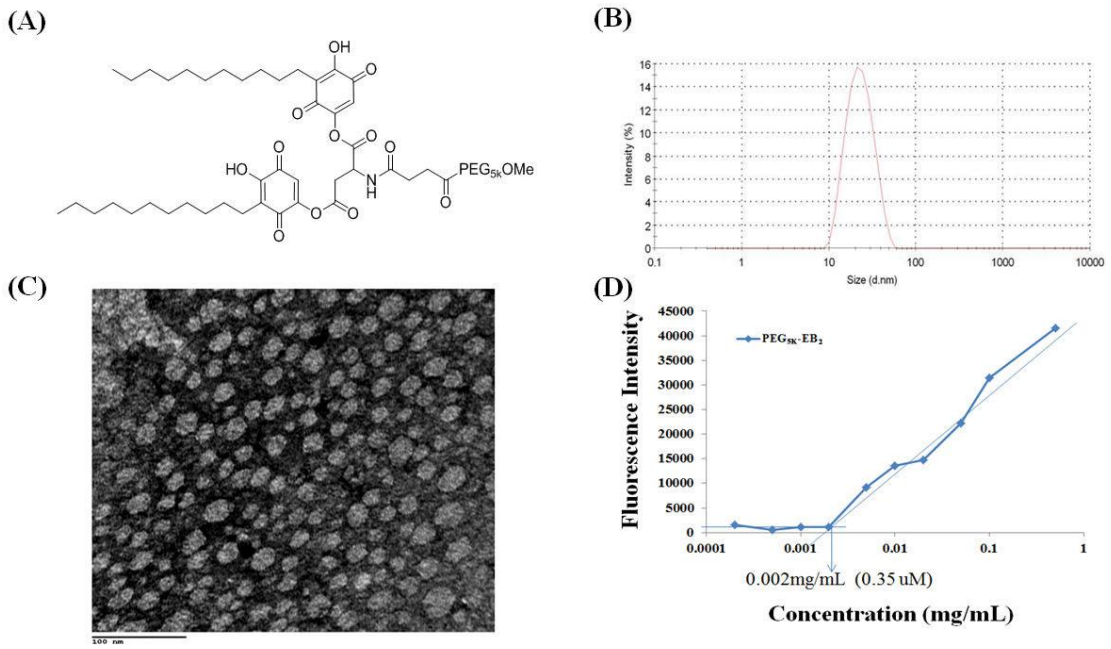

Figure 10 The chemical structure of PEG_{5K}-EB_2, (B) The size distribution of free PEG_{5K}-EB_2 nanoparticles in PBS measured by dynamic light scanning (DLS), (C) Transmission electron microscopy of PEG_{5K}-EB_2 micelles, and (D) critical micelle concentration (CMC) using pyrene as a fluorescence probe.

The PEG_{5K}-EB_2 conjugate was synthesized via stepwise solution-phase condensation reactions using MeO-PEG-OH, succinic anhydride, Boc-aspartic acid and embelin as building blocks. HPLC shows that the final product (PEG_{5K}-EB_2) is at least 95.57% pure (**Figure 11**).

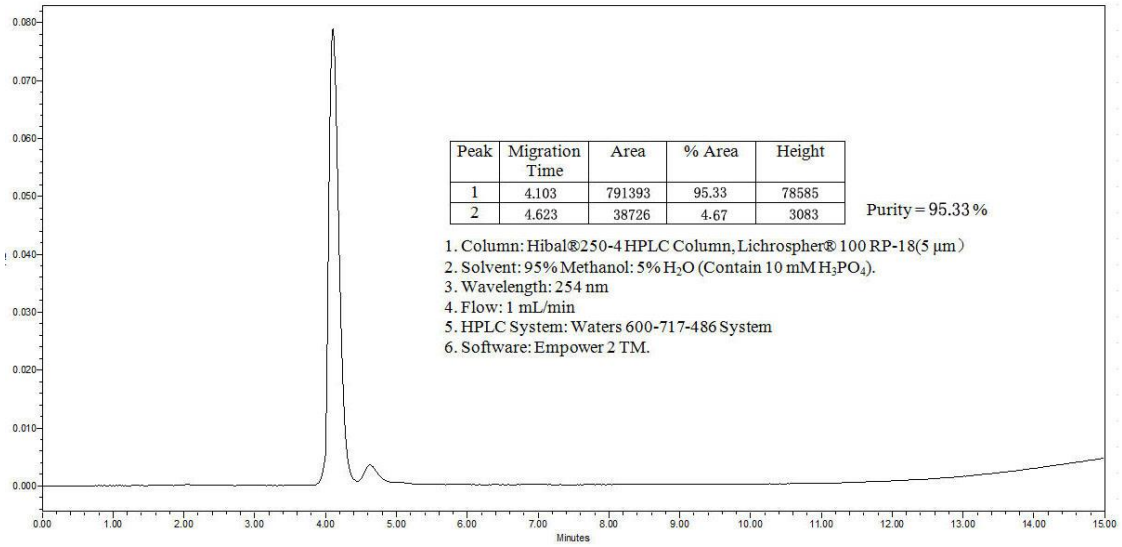

Figure 11 HPLC trace of PEG_{5K}-EB_2.

^{1}H NMR spectrum of PEG_{5K}-EB_2 shows signals at 3.63 ppm attributed to the methylene protons of PEG, the embelin proton signals at 8.14 and 6.72 ppm and the carbon chain signals at 1.05—1.25 ppm. The aspartate signals were identified at 5.57, 4.98 and 2.60 ppm (**Figure 12**).

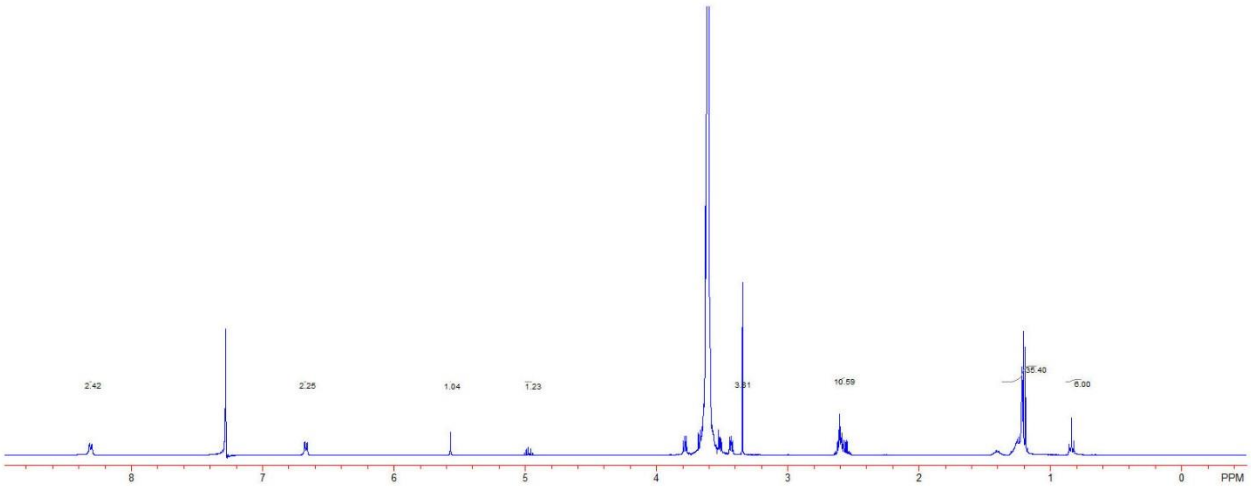

Figure 12 ^{1}H-NMR spectra (400 MHz) of PEG_{5K}-EB_2 in $CDCl_3$.

The molecular weight of the PEG_{5K}-EB_2 conjugate from MALDI-TOF MS (5701) is similar to the theoretical value (5703) (**Figure 13**), indicating the successful synthesis of PEG_{5K}-EB_2 conjugate.

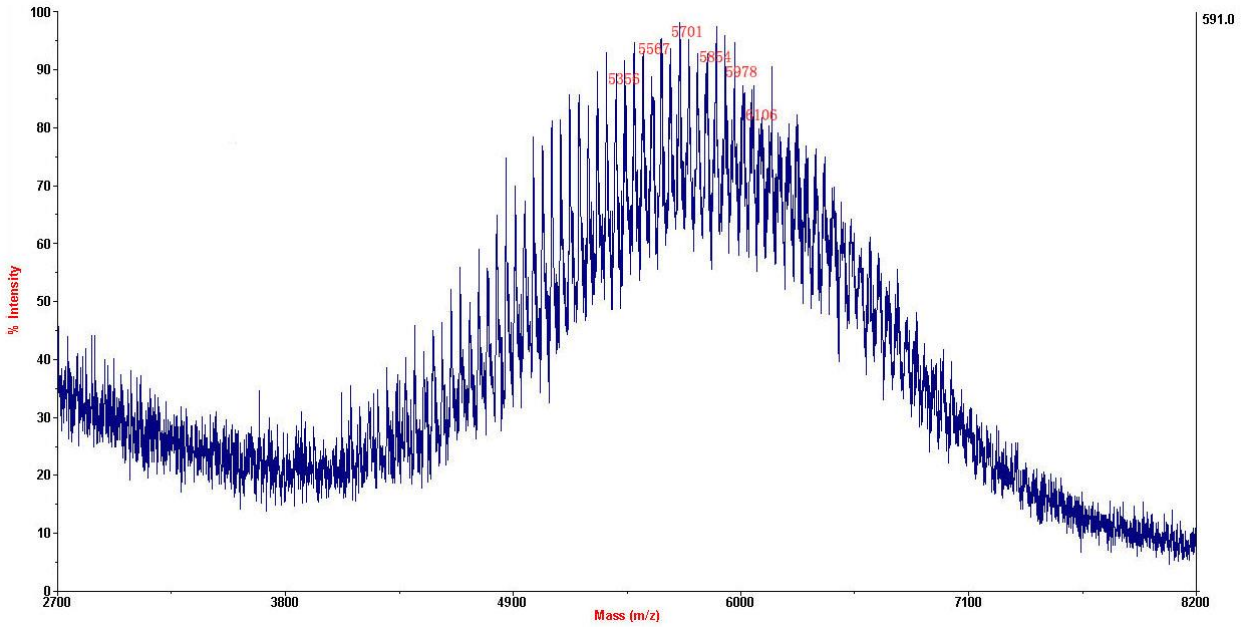

Figure 13 MALDI-TOF of PEG_{5K}-EB_2.

In aqueous solution, PEG_{5K}-EB_2 readily self-assembles to form micellar nanoparticles with the particle size of around 20 nm as determined by DLS analysis (**Figure 10B**). **Figure 10C** shows the TEM images of PEG_{5K}-EB_2 micelles after staining with 1% uranyl acetate. Spherical particles of uniform size were observed and the sizes of the micelles observed under TEM were consistent with those measured by DLS.

Figure 10D shows the CMC of PEG_{5K}-EB_2 micelles using pyrene as a fluorescence probe. Upon incorporation into the micelles, the fluorescence intensity of pyrene increases substantially at the concentration of micelles above the CMC (La, Okano et al. 1996). Based on the partition of the pyrene, the CMC of PEG_{5K}-EB_2 was obtained by plotting the fluorescence intensity versus logarithm concentration of the polymer. The CMC of PEG_{5K}-EB_2 was

determined from the crossover point at the low concentration range. The CMC of the PEG_{5K}-EB_2 conjugate is 0.35 μM, which is much lower than most single chain micelle surfactants used in drug delivery systems (mM). The relatively low CMC may render the micelles stable even upon dilution *in vivo*, which is important for effective delivery to tumors.

PEG_{5K}-EB_2 effectively solubilized PTX in aqueous solution. **Table 4** compares PEG_{5K}-EB_2 with $PEG_{3.5K}$-EB_2 with respect to the sizes of PTX-loaded micelles, the drug loading capacity (DLC), and the drug loading efficiency (DLE) under various drug/carrier molar ratios.

Table 4 Biophysical characterization of free and drug-loaded PEG-Embelin micelles.

Micelles	Molar ratio	Size(nm)	PDI	Conc. of PTX in micelles (mg/ml)	DLC (%)	DLE (%)
$PEG_{3.5K}$-EB_2	——	22.8±0.3	0.09	——	——	——
$PEG_{3.5K}$-EB_2:PTX	2.5:1	143±17	0.23	1	7.5	79.9
	5:1	58.7±0.5	0.32	1	3.9	96.7
	7.5:1	27.5±0.2	0.23	1	2.6	98.6
PEG_{5K}-EB_2	——	20.6±0.1	0.05	——	——	——
PEG_{5K}-EB_2:PTX	0.75:1	25.5±1.0	0.06	1	16.6	63.7
	1:1	21.7±0.4	0.25	1	13.0	70.8
				2	13.0	62.4
	2.5:1	22.0±0.28	0.04	1	5.6	93.1
				2	5.6	90.8
	5:1	21.9±0.32	0.01	1	2.9	98.6
				2	2.9	94.9
	7.5:1	22.2±0.14	0.11	1	2.0	96.6
				2	2.0	94.9
				3	2.0	84.4

PDI = polydispersity index. DLC = drug loading capacity. DLE = drug loading efficiency.
$PEG_{3.5K}$-EB_2 = $PEG_{3.5K}$-$Embelin_2$. PEG_{5K}-EB_2 = PEG_{5K}-$Embelin_2$. PTX = paclitaxel.
PTX concentrations in micelles were kept at 1 mg/mL.
Blank micelle concentration was 20 mg/mL.
Values reported are the means ± SD for triplicate samples.

For $PEG_{3.5K}$-EB_2 micelles, a minimal 2.5/1 of carrier/PTX molar ratio was required to form stable PTX-loaded micelles. Under this ratio, the size of the drug-loaded micelles was around 143 nm, which was significantly larger than the size of drug-free micelles. Increasing the carrier/PTX ratios resulted in a decrease in the sizes of PTX-formulated micelles. At a carrier/PTX ratio of 7.5/1, the size of PTX-loaded $PEG_{3.5K}$-EB_2 micelles was similar to that of drug-free micelles.

Compared to $PEG_{3.5K}$-EB_2, PEG_{5K}-EB_2 conjugate requires much lower carrier/PTX ratios to form stable and small-sized PTX-loaded micelles. PTX-loaded PEG_{5K}-EB_2 micelles still maintained the small size (25 nm) even at the carrier/PTX ratio of 0.75:1 and PTX concentration of 1 mg/mL. Further increase in carrier/drug ratios was associated with an increase in the drug loading efficiency and the PTX concentrations at which PTX-loaded PEG_{5K}-EB_2 micelles remained stable. The improved stability and loading capacity for PEG_{5K}-EB_2 micelles compared to $PEG_{3.5K}$-EB_2 micelles is likely due to longer PEG brushes capable of providing better steric hindrance and stabilizing effect for micelle nanoparticles.

The size of drug carriers plays a key role in effective targeted delivery to tumors. It has been long known that particles in the size range of 100–200 nm can effectively penetrate solid tumors via an EPR effect (Matsumura and Maeda 1986). However, a recent study reported that particles with a size of 154 nm were significantly taken up by liver and lungs with limited accumulation at tumor sites (Luo, Xiao et al. 2010). In contrast, particles with respective size of 17 and 64 nm were much more effective in passive targeting to the solid tumor in a subcutaneous model of human ovarian cancer xenograft (Luo, Xiao et al. 2010). The small size of PEG_{5K}-EB_2 micelles (20 ~ 30 nm) may explain their effective *in vivo* targeting as discussed later.

3.3.2 Release kinetics of PTX-loaded micelles

A dialysis method was used to assess the kinetics of release of PTX from PEG_{5K}-EB_2 micelles with DPBS (pH = 7.4) containing 0.5% Tween 80 (w/v) as the release medium. Taxol, a clinically used PTX formulation was included as a control. As shown in **Figure 14**, PTX

formulated PEG_{5K}-EB_2 exhibited significantly better stability than Taxol formulation.

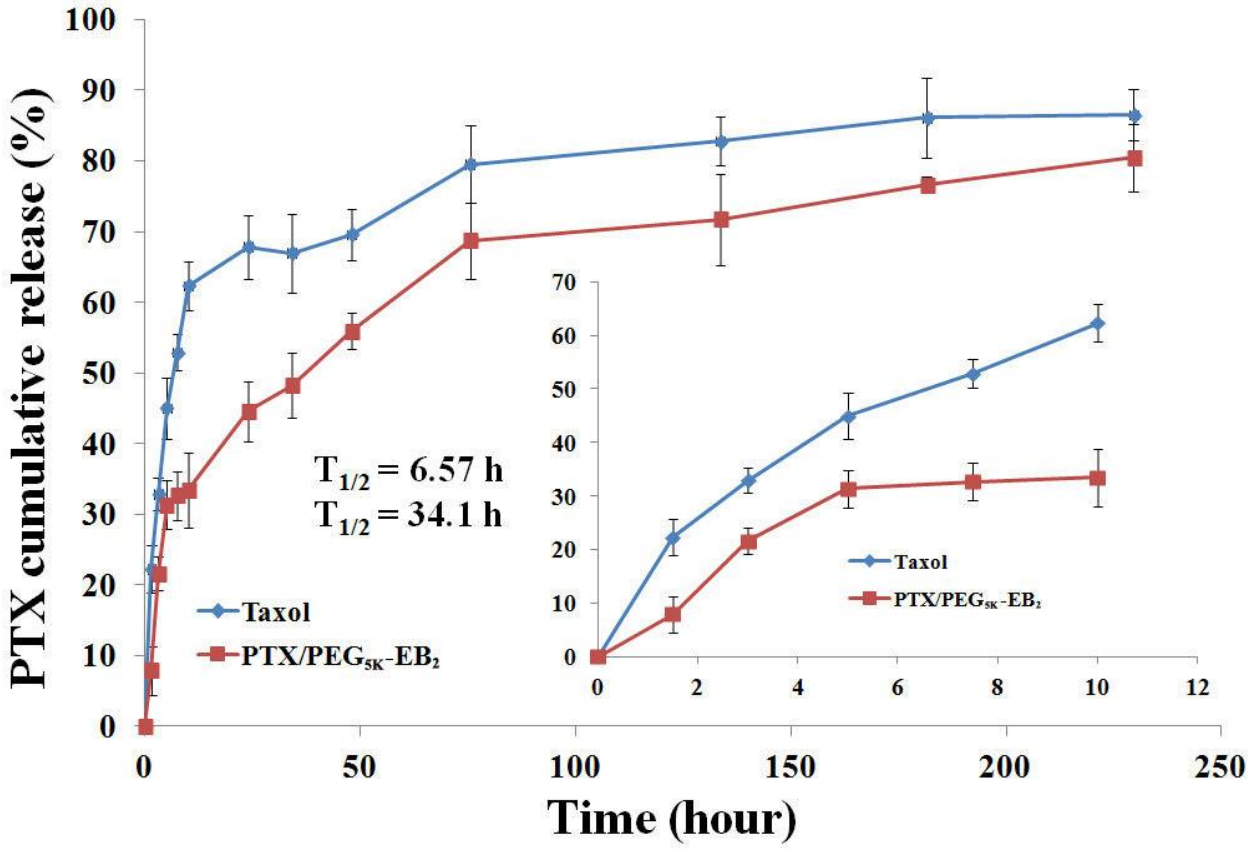

Figure 14 Cumulative PTX release profile from PTX-loaded PEG_{5K}-EB_2 micelles and Taxol.

For the first 10 h, there was only 33.42% of PTX released from the PEG_{5K}-EB_2 micellar formulation in comparison to the 62.32% release in Taxol formulation. PTX-loaded PEG_{5K}-EB_2 micellar formulation displayed a much slower PTX release compared to Taxol formulation during the entire experimental period. The $T_{1/2}$ of PTX release is 34.1 h for PEG_{5K}-EB_2 micelles, which is significantly longer than that for Taxol formulation (6.57 h). The relatively slower and sustained release in PTX-loaded PEG_{5K}-EB_2 micelle formulation may be ascribed to the strong interaction between the carriers and PTX. Embelin has a benzoquinone ring and a long alkyl chain. In addition to hydrophobic interaction with PTX, the π-π stacking and the hydrogen bonding also contribute to the overall carrier/PTX interaction. The close proximity of two

embelins in PEG_{5K}-EB_2 conjugate is likely to facilitate the interaction of the carrier with PTX. Indeed, PEG-embelin conjugates of 1:1 molar ratio were much weaker solubilizer for hydrophobic drugs including PTX (data not shown). More studies on the structure-activity relationship (SAR) may lead to the development of an improved carrier for *in vivo* applications.

3.3.3 Hemolysis assay

A major concern for micelle systems is whether or not the surface activity of the surfactant molecules affects cell membrane integrity. Therefore, we examined the hemolytic activity of drug-free PEG_{5K}-EB_2 micelles and compared to polyethylenimine (PEI), a cationic polymer with potent cell surface activity (Reul, Nguyen et al. 2009). As shown in **Figure 15**, treatment of RBCs with PEI resulted in significant hemolysis in a dose-dependent manner.

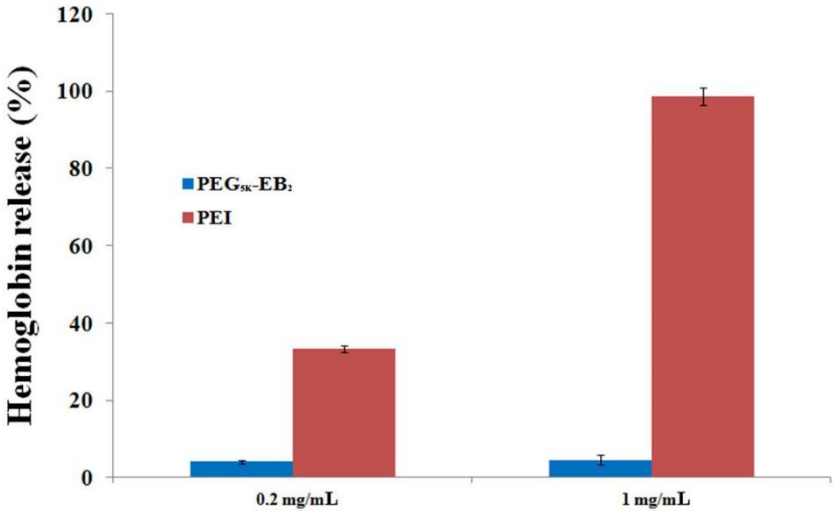

Figure 15 *In vitro* hemolysis assay of PEG_{5K}-EB_2 compared with PEI.

In contrast, no significant hemolysis was observed for blank PEG_{5K}-EB_2 micelles. The negligible hemolytic activity suggests that PEG_{5K}-EB_2 conjugate is a mild surfactant that is suitable for *in vivo* drug delivery.

3.3.4 Cellular uptake study

The cellular uptake of Nile red-loaded PEG_{5K}-EB_2 micelles in prostate cancer cell line PC-3 was investigated by fluorescence microscopy. PC-3 cells were cultured with Nile red-loaded PEG_{5K}-EB_2 micelles (equivalent concentration of Nile red at 1 μg/mL) at 37 ℃ for 2 h. The nucleus was then stained with Hochest 33342 for 5 mins prior to observation under a fluorescence microscope. As shown in **Figure 16**, fluorescence was observed both on the cell membrane and inside the cells with most of the signals located intracellularly.

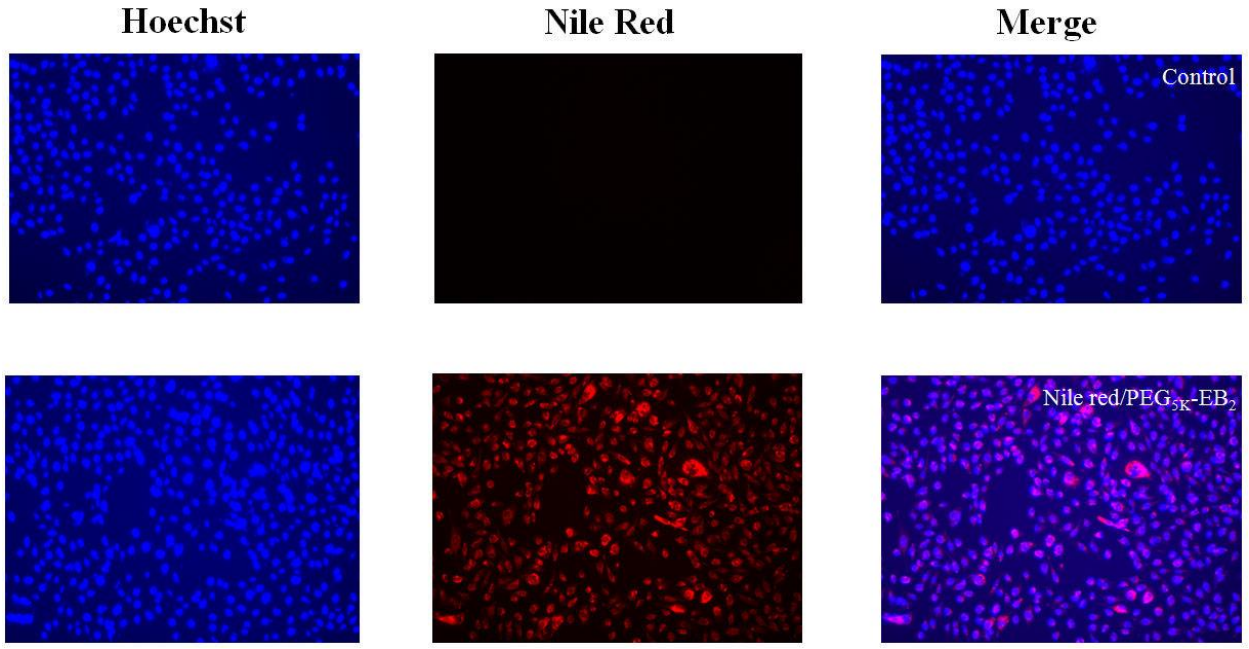

Figure 16 Fluorescence microscope images of PC-3 cells that incubated with Nile red-loaded PEG_{5K}-EB_2 for 2 h.

Both perinuclear punctuate and diffuse distribution was observed, suggesting that Nile red-loaded PEG_{5K}-EB_2 was largely taken up by cells via endocytosis and partially released into cytoplasm. Escape of the delivered cargos from endosome into cytoplasm is important as this is where the drug target(s) is located. Although more studies are needed to understand the

intracellular trafficking and the underlying mechanism, our data did suggest that PEG_{5K}-EB_2 micelles were capable of effectively mediating intracellular delivery of formulated drugs.

3.3.5. *In vitro* cytotoxicity of PTX-loaded PEG_{5K}-EB_2 micelles

In vitro cytotoxicity of PTX formulated in PEG_{5K}-EB_2 micelles was examined with three cancer cell lines (DU145, PC-3, and 4T1.2) and compared to Taxol formulation. PEG_{5K}-EB_2 alone showed minimal cytotoxic effect to human prostate cancer cells DU145 at the concentrations used to deliver PTX (**Figure 17A**). It is also apparent from **Figure 17A** that PTX formulated in PEG_{5K}-EB_2 micelles showed higher levels of cytotoxicity to DU145 cells compared to Taxol formulation, particularly at low PTX concentrations. Similar results were obtained in PC-3 (**Figure 17B**) and 4T1.2 (**Figure 17C**) tumor cells.

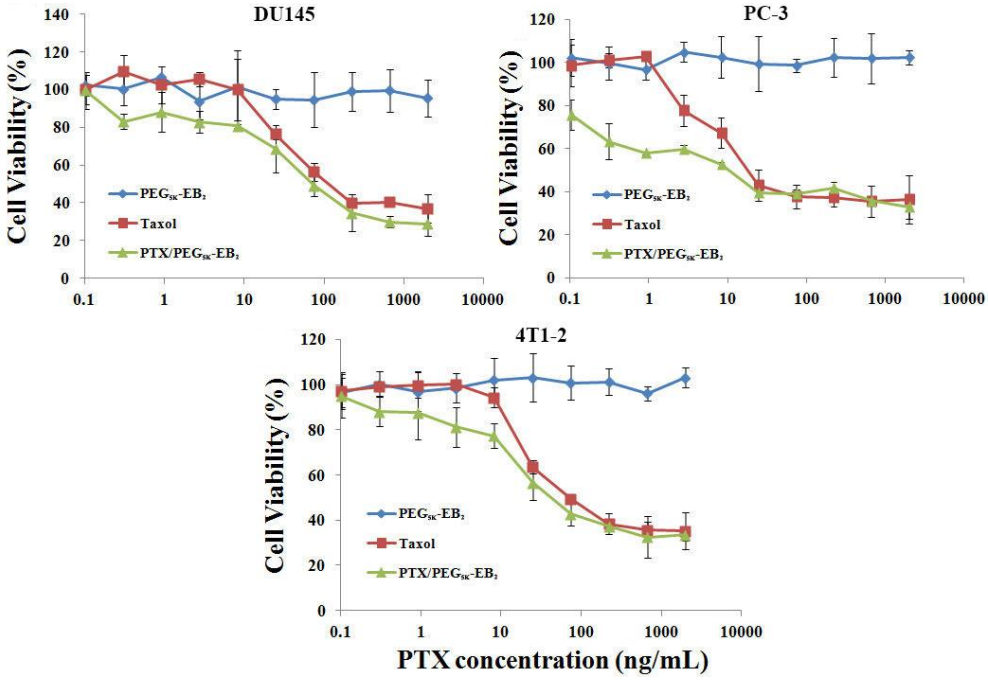

Figure 17 Cytotoxicity of Taxol, free PEG_{5K}-EB_2, and PTX-loaded PEG_{5K}-EB_2 nanoparticles in different tumor cell lines.

Most of the reported PTX micellar formulations showed lower or similar levels of cytotoxicity compared to Taxol (Li, Xiao et al. 2010, Luo, Xiao et al. 2010, Li, Xiao et al. 2011, Zhang, He et al. 2012). The improved *in vitro* cytotoxicity of PTX formulated in PEG_{5K}-EB_2 micelles may be due to the improved bioavailability of PTX inside the tumor cells. It remains to be tested whether there is also a synergistic effect between PEG_{5K}-EB_2 micelles and the co-delivered PTX. It has been reported that under the subeffective doses, embelin sensitized tumor cells to various types of therapies including chemotherapy and radiotherapy (Dai, Qiao et al. 2009, Danquah, Duke et al. 2012, Huang, Lu et al. 2012). Embelin is coupled to PEG via a cleavable ester linkage, embelin may be freed from the conjugate following intracellular delivery and synergizes with co-delivered PTX in antitumor activity. It should be noted that PEG_{5K}-EB_2 itself is less active in antitumor activity than $PEG_{3.5K}$-EB_2 (Huang, Lu et al. 2012). This might be due to less effective release of embelin from PEG_{5K}-EB_2 due to a more pronounced steric hindrance imposed by PEG_{5K}. More studies are needed to better understand the mechanism involved in the antitumor effect of PTX-loaded PEG_{5K}-EB_2 micelles.

3.3.6. Maximum tolerated dose study

The maximum tolerated dose for a single i.v. administration of PTX-loaded PEG_{5K}-EB_2 micelles was assessed in tumor-free mice and compared to Taxol. The mice were injected i.v. with different doses of PTX-loaded PEG_{5K}-EB_2 or Taxol followed by daily body weight measurement and observation of general signs of toxicity. As shown in **Table 5**, Taxol was well tolerated at the dose of 15 mg PTX/kg.

Table 5 Animal deaths and weight loss in the MTD study.

Formulations	Does (mg/kg)	Animal death	Weight loss (%)
Taxol	15	0/4	5.4
	20	2/4	N/A
	25	4/4	N/A
PTX-loaded PEG_{5K}-EB_2 micelles	30	0/4	-1.2
	50	0/4	1.6
	75	0/4	6.5
	100	0/4	8.7
	120	2/4	N/A

However, increasing the PTX dosage to 20 mg/kg resulted in the death of 2 mice among the 4 treated mice. For the mice treated with PTX-loaded PEG_{5K}-EB_2 micelles, there were only 8.7% weight loss and no noticeable changes in normal activity at a PTX dosage as high as 100 mg/kg. At the dosage of 120 mg PTX/kg, two out of 4 treated mice died of toxicity. Based on these data it was estimated that the single i.v. MTD for Taxol was 15~20 mg PTX/kg while that for PTX-loaded PEG_{5K}-EB_2 micelles was 100~120 mg PTX/kg. The MTD for PTX-loaded PEG_{5K}-EB_2 micelles is higher than most of the reported PTX formulations (Danhier, Magotteaux et al. 2009, Xiao, Luo et al. 2009, Wang, Wang et al. 2011). The high MTD for PTX/PEG_{5K}-EB_2 is likely due to the slow release kinetics for PTX (**Figure 14**), low levels of nonselective uptake by major organs (see later), and the excellent safety profile of embelin. Embelin has antiinflammatory and hepatoprotective activity (Chitra, Sukumar et al. 1994, Singh, Singh et al. 2009). In addition, normal tissues are less sensitive to embelin compared to tumor cells due to the significantly lower levels of XIAP expression in normal tissues. The significantly improved safety of our delivery system over Taxol formulation will allow high dosage of PTX to be given to achieve maximal therapeutic effect.

3.3.7. Biodistribution of PEG_{5K}-EB_2 micelles via NIRF optical imaging

Biodistribution and tumor targeting efficiency of PEG_{5K}-EB_2 micelles were evaluated in a mouse xenograft model of human prostate cancer (PC-3), using a hydrophobic near infrared fluorescence (NIRF) dye, DiD. Two hundred μL of micelles co-loaded with PTX and DiD was intravenously injected into two mice bearing bilateral PC-3 tumors, respectively. The two mice were then followed over time by the scanning with Carestream Molecular Imaging System. **Figure 18** shows the imaging of the tumor-bearing mice at 2, 24, 48 h following i.v. injection of PTX/PEG_{5K}-EB_2 mixed micelles carrying DiD.

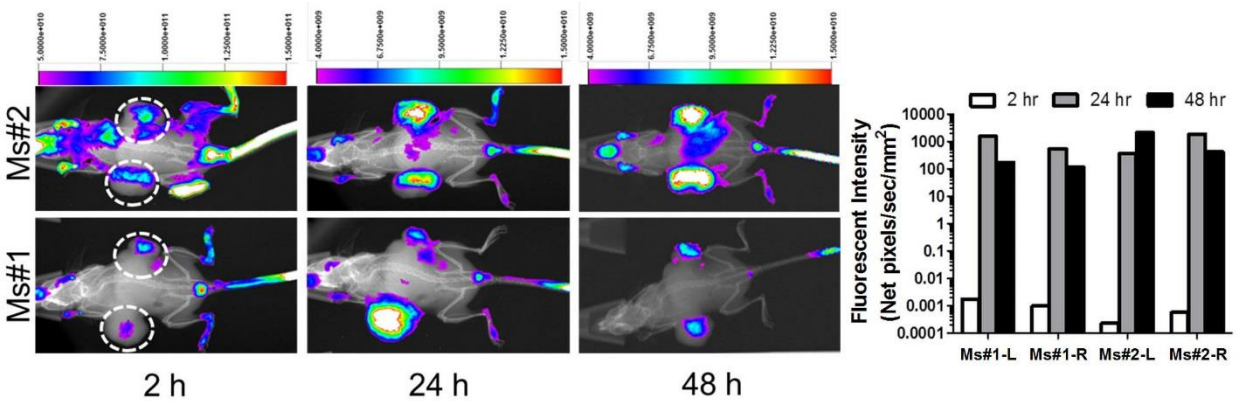

Figure 18 ***In vivo*** **NIRF imaging over time as indicated in prostate cancer PC-3-xenograft-bearing mice at 2, 24, 48 h following i.v. injection of PEG_{5K}-EB_2 micelles co-loaded with PTX and DiD.**

A noticeable signal in tumor was observed as early as 2 h post injection; the signal peaked around 24 h and remained clearly visible 48 h after injection. Interestingly, little fluorescence signal was observed in liver and spleen, the two major internal organs that are involved in the nonspecific clearance of nanoparticles by the reticuloendothelial system (RES). The effective targeting of PEG_{5K}-EB_2 micelles to the tumors and the minimal uptake by RES system are largely due to the very small-sized particles, excellent PEG shielding effect, and a likely excellent stability in the blood circulation. Our results were consistent with the studies with other

micellar systems of similar particle sizes (Xiao, Luo et al. 2009, Luo, Xiao et al. 2010, Zheng, Dai et al. 2012).

3.3.8 *In vivo* therapeutic study

The *in vivo* therapeutic activity of PTX formulated in PEG_{5K}-EB_2 micelles was investigated in two mouse tumor models: a syngeneic murine breast cancer model (4T1.2) and a human prostate cancer xenograft model (PC-3).

4T1.2 is a highly metastatic breast cancer cell line and was chosen in this study to stringently assess the therapeutic efficacy of our new delivery system. As shown in **Figure 19A**, PEG_{5K}-EB_2 alone showed no effect in inhibiting the tumor growth. This is likely due to a low concentration of embelin in this group. Taxol formulation showed a modest effect in inhibiting the tumor growth at a dose of 10 mg PTX/kg. In contrast, PTX formulated in PEG_{5K}-EB_2 micelles showed a much more pronounced antitumor activity at the same dosage.

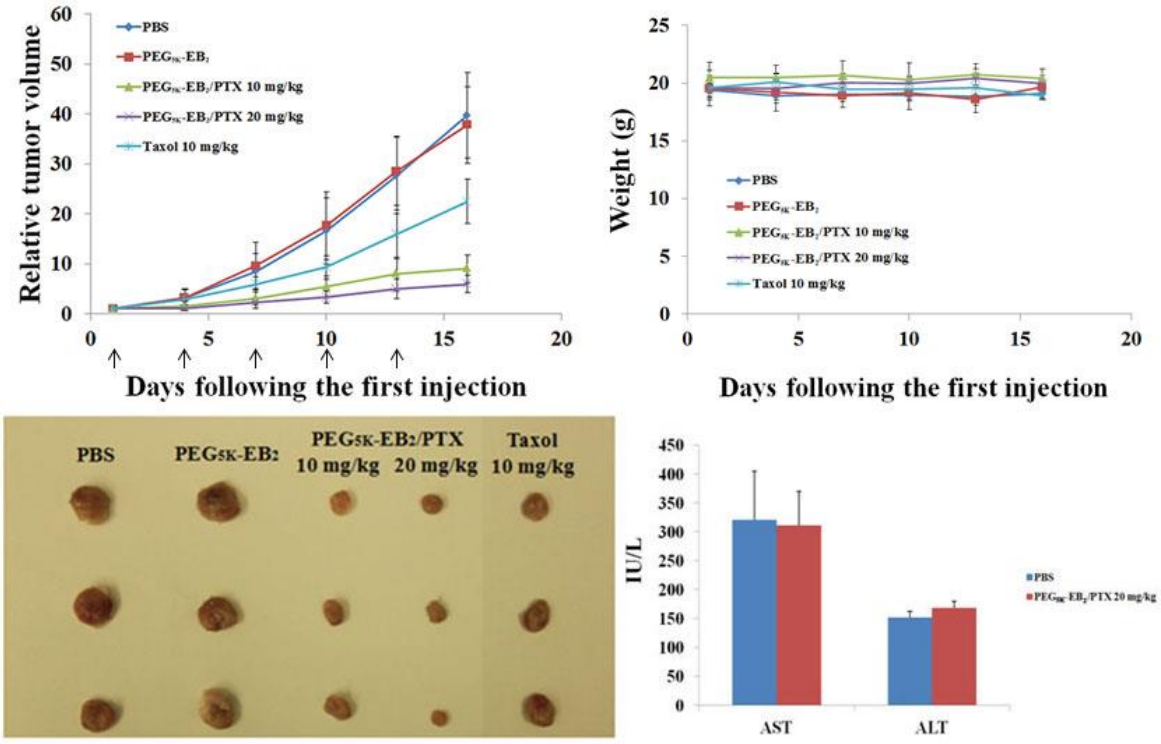

Figure 19 (A) Enhanced antitumor activity of PTX formulated in PEG_{5K}-EB_2 micelles in 4T1.2 tumor bearing mice. (B) Changes of body weight in mice receiving different treatments (C): Serum level of transaminase in the mice treated with PTX/PEG_{5K}-EB_2 (20 mg PTX/kg) at the end of the study.

Increasing the PTX dosage to 20 mg/kg resulted in a further improvement in the therapeutic effect. No significant changes in body weight were noticed in all treatment groups compared to PBS control group (**Figure 19B**). In addition, serum levels of transaminases in the mice treated with the high dose of PTX-loaded PEG_{5K}-EB_2 micelles were comparable to those in PBS control group (**Figure 19C**), suggesting that significant therapeutic effect can be achieved with minimal toxicity using our new delivery system.

Following the demonstration of effective antitumor activity in the syngeneic murine breast cancer model, the *in vivo* therapeutic effect of PTX-loaded PEG_{5K}-EB_2 micelles was further investigated in a human prostate cancer xenograft model (PC-3). PC-3 tumor-bearing

mice were similarly treated as described in the study with the 4T1.2 tumor model and the data are shown in **Figure 20A**.

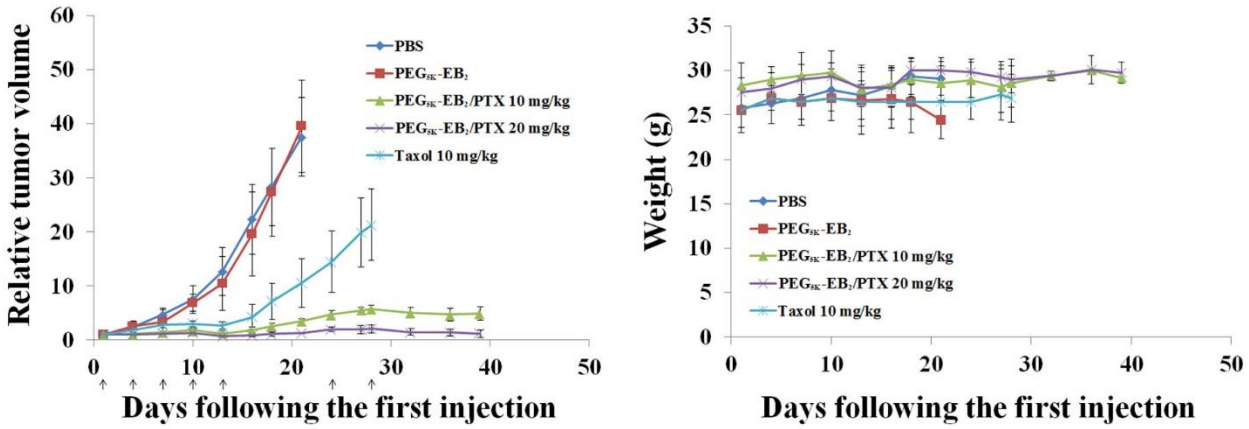

Figure 20 (A) Enhanced antitumor activity of PTX formulated in PEG_{5K}-EB_2 micelles in PC-3 tumor bearing nude mice. (B) Changes of body weight in mice.

It is apparent that tumor growth was more effectively controlled by PTX/PEG_{5K}-EB_2 micelles in PC-3 model compared to 4T1.2 tumor model. By day 16 after the first treatment, the tumor growth was completely suppressed with a RTV of 0.84 in the group treated with a high dose (20 mg PTX/kg) of PTX-loaded PEG_{5K}-EB_2 micelles. Tumor growth was also significantly slowed in the group treated with a low dose (10 mg PTX/kg), in which the tumors only reached a RTV of 1.75. This compared very favorably to Taxol group, in which RTV reached 4.24. Although the tumors started to recover slightly after day 24 in the two groups treated with PTX/PEG_{5K}-EB_2 mixed micelles, RTV was reduced back to 1.15 at day 39 in the high dose group following two additional treatments at days 24 and 28. In fact, two out of 6 mice in this group became tumor-free after day 32 without further treatment. The growth of tumor in the low dose group also became static after two additional treatments. In contrast, tumors in Taxol group continued to grow at a steady and fast rate. No noticeable changes in weight were shown from direct measurement of tumor-bearing mice in all groups (**Figure 20B**). The superior anti-tumor efficacy along with the minimal toxicity of PTX/PEG_{5K}-EB_2 micelles could be ascribed to their

high efficiency in tumor-targeting and minimal nonspecific uptake by RES (**Figure 18**). The slow release kinetics of PTX/PEG_{5K}-EB_2 micelles may also contribute to the enhanced antitumor activity (**Figure 14**). More studies are needed to better understand the mechanism for the antitumor activity of PTX-loaded PEG_{5K}-EB_2 micelles.

4.0. TARGETED DELIVERY OF DOXORUBICIN BY FOLIC ACID-DECORATED DUAL FUNCTIONAL NANOCARRIER

4.1 BACKGOUND

Doxorubicin, an anthracycline antibiotic, is one of the most commonly used anticancer agents for the treatment of various types of cancers, including breast, ovarian, prostate, brain, cervix and lung cancers. It intercalates between base pairs of the DNA helix, thereby preventing DNA replication and ultimately inhibiting protein synthesis. Additionally, doxorubicin inhibits topoisomerase II, leading to an increased level of stabilized drug-enzyme-DNA cleavable complex during DNA replication and impaired DNA repair. However, the clinical application of DOX has been limited by serious adverse effects (Minotti, Menna et al. 2004, Takemura and Fujiwara 2007). Therefore, there is a need for development of strategies to selectively deliver DOX to tumors to improve the therapeutic effect and minimize the untoward toxicity.

Recently, nanomedicine-based platforms have been actively pursued to improve the diagnosis and therapy for a wide range of diseases, including cancer. In order to reduce the adverse effects associated with many antineoplastic agents such as DOX and paclitaxel (PTX), a myriad of nanocarriers have been developed including liposomes, dendrimers, and polymeric micelles. These nano-drug carriers are selectively and passively targeted to tumors through the enhanced permeability and retention effect (EPR) (Matsumura and Maeda 1986). In addition, these formulations are capable of evading clearance by the reticuloendothelial system (RES) and

thereby circulating in the blood for a prolonged period of time (Woodle, Engbers et al. 1994, Li and Huang 2009). Doxil®, PEGylated liposomal DOX, is the first clinically used nanoformulation of DOX approved by the FDA for the treatment of leukemia, breast cancer, lung cancer, brain cancer and bone cancer. Although the DOX-related toxicity has been reduced to some degree, its anticancer efficacy has been shown to be only marginally improved (O'Brien, Wigler et al. 2004). Furthermore, Doxil has been shown to cause hand-foot syndrome and mucositis in recent clinical studies (Al-Batran, Meerpohl et al. 2006, Lorusso, Di Stefano et al. 2007, von Gruenigen, Frasure et al. 2010). Hence, there is need to develop improved formulations for *in vivo* applications of DOX.

During the past two decades, polymeric micelles have gained considerable attention as an attractive nanomedicine platform due to their technical ease, high biocompatibility, and high biodegradability (Sutton, Nasongkla et al. 2007, Huang, Lu et al. 2012, Gao, Huang et al. 2013, Lu, Huang et al. 2013, Zhang, Lu et al. 2013, Lu, Zhao et al. 2014). More importantly, the size of micelles (20-100 nm) is significantly smaller than liposomes (100~200 nm) which renders micelles more effective in passive targeting to solid tumors (Li, Xiao et al. 2010, Luo, Xiao et al. 2010). In addition, a targeting ligand can be introduced into the micellar system to further improve the active targeting to tumors and minimize the nonspecific uptake by normal tissues (Cheng, Wei et al. 2008, Bedi, Gillespie et al. 2013, Song, Ding et al. 2013). Different targeting systems have been studied, among which the folate-targeting system has been extensively investigated due to its simplicity and effectiveness (Li, Piao et al. 2011, Yan, Chen et al. 2013, Lachelt, Wittmann et al. 2014, van Dongen, Silpe et al. 2014).

We recently developed a dual functional drug delivery system that is based on PEG-derivatized embelin (Huang, Lu et al. 2012, Lu, Huang et al. 2013). Embelin is a naturally

occurring alkyl substituted hydroxyl benzoquinone compound and a major constituent of *Embelia ribes* BURM. It has been shown that embelin exhibits antitumor activity in various types of cancers via several different mechanisms (Nikolovska-Coleska, Xu et al. 2004, Sreepriya and Bali 2005, Dai, Qiao et al. 2009, Danquah, Li et al. 2009, Heo, Kim et al. 2011). Embelin is poorly water soluble and also has limited oral bioavailability (Li, Danquah et al. 2010). We showed that modification of embelin with PEG led to a significant increase in its water solubility. Interestingly, PEG-embelin self-assembles to form micelles that are capable of delivering other hydrophobic drugs. Delivery of paclitaxel via one such PEG-embelin conjugate, PEG_{5K}-EB_2, led to significantly improved antitumor activity in both breast and prostate cancer models (Lu, Huang et al. 2013). In this study, we examine the potential application of PEG_{5K}-EB_2 in delivery of DOX. Our data showed that DOX could be effectively formulated in PEG_{5K}-EB_2 micelles. Delivery of DOX via PEG_{5K}-EB_2 micelles led to improved antitumor activity over free DOX or Doxil *in vitro* and *in vivo*. In addition, we show for the 1st time that PEG_{5K}-EB_2 can significantly inhibit the activity of P-gp. Finally, the antitumor activity of DOX-loaded PEG_{5K}-EB_2 micelles was further improved via incorporation of folate.

4.2 METHODS

4.2.1 Materials

Doxorubicin hydrochloride (98%) (DOX.HCl) was purchased from AK Scientific Inc. (CA, USA). Doxil was purchased from Avanti® Polar Lipids (AL, USA). Boc amine PEG NHS ester (BocNH-PEG-NHS, MW 7500) was purchased from JenKem Technology USA, Inc. (Allen,

TX). 2,5-dihydroxy-3-undecyl-1,4-benzoquinone (embelin, 98%) was purchased from 3B Scientific Corporation (IL, USA). Folic acid NHS ester, methoxy-$PEG_{5,000}$-OH, dimethyl sulfoxide (DMSO), 3-(4,5-dimethylthiazol-2-yl)-2,5-diphenyl tetrazolium bromide (MTT), aspartic acid, trypsin-EDTA solution, Triton X-100, and Dulbecco's Modified Eagle's Medium (DMEM) were all purchased from Sigma-Aldrich (MO, USA). Fetal bovine serum (FBS) and penicillin-streptomycin solution were from Invitrogen (NY, USA). RPMI-1640 medium was purchased from Life Technologies (NY, USA). All solvents used in this study were HPLC grade.

4.2.2 Synthesis of PEG_{5K}-EB_2

PEG_{5K}-EB_2 was synthesized according to the methods described previously (Huang, Lu et al. 2012, Lu, Huang et al. 2013). Briefly, benzoquinone was first synthesized followed by coupling to Boc-aspartic acid. Then, undecyl side chains were conjugated to each of the two benzoquinone rings to form aspartic acid-EB_2. Finally, methoxy-PEG_{5K}-OH was coupled to aspartic acid-EB_2 to generate PEG_{5K}-EB_2 via the deprotected amino group. The final product was analyzed by ^{1}NMR and MALDI-TOF.

4.2.3 Synthesis of folic acid-$PEG_{7.5K}$-DOA (dioleyl amido aspartic acid)

Folate-$PEG_{7.5K}$-DOA was constructed based on the method reported by Zhang et el. with slight modification (Zhang, Huang et al. 2012). Briefly, Boc-aspartic acid was linked to oleyl amine in the presence of DCC and DMAP in anhydrous CH_2Cl_2. After the reaction was completed, the mixture was filtered and evaporated under reduced pressure, and the residue was purified by flash column chromatography to obtain Boc-Di-oleyl amine (Boc-DOA). Then, trifluoroacetic

acid (TFA) was added to remove Boc group in Boc-DOA to expose the active NH_2 followed by reaction with BocNH-$PEG_{7.5K}$-NHS to form BocNH-$PEG_{7.5K}$-DOA. After purification via precipitation with cold diethyl ether and ethanol, Boc group in BocNH-$PEG_{7.5K}$-DOA was removed by TFA. Finally, NH_2-$PEG_{7.5K}$-DOA was reacted with folic acid (FA) NHS ester to yield FA-$PEG_{7.5K}$-DOA.

4.2.4 Preparation and physiochemical characterization of DOX-loaded PEG_{5K}-EB_2 and FA-PEG_{5K}-EB_2 micelles

DOX·HCl was first neutralized by 3 molar equivalent of triethylamine in $CHCl_3$/MeOH (1:1. v:v) to remove HCl from the parent compound. DOX-loaded PEG_{5K}-EB_2 was prepared as reported previously (Lu, Huang et al. 2013). Briefly, DOX (10 mM in $CHCl_3$/MeOH) was added to PEG_{5K}-EB_2 (10 mM in chloroform) with different carrier/drug molar ratios. The organic solvent was first removed by nitrogen flow to form a thin dry film of drug/carrier mixture. The dry film was further dried under high vacuum for 2 h to remove any traces of remaining solvent. The film was then reconstituted in saline without further sonication. The FA-PEG_{5K}-EB_2 was composed of PEG_{5K}-EB_2/FA-$PEG_{7.5K}$-DOA at molar ratios of 99.5:0.5 according to the literature (van Dongen, Silpe et al. 2014). The DOX-formulated FA-PEG_{5K}-EB_2 micelles were prepared similarly as mentioned above. The mean diameter, size distribution, and zeta potential of micelles with or without loaded drug were evaluated by dynamic light scattering (DLS). The morphology of DOX-free or loaded micelles was observed under TEM. The concentration of DOX in DOX-loaded micelles was examined by HPLC with the detector set at 233 nm. The drug loading capacity (DLC) and drug loading efficiency (DLE) were calculated according to the following formula:

DLC (%) = [weight of drug used/(weight of polymer + drug used)] ×100%

DLE (%) = (weight of loaded drug/weight of input drug) ×100%

4.2.5 Release kinetics of DOX formulated in micelles

The *in vitro* release kinetics of DOX was carried out by dialysis method using DPBS (PH = 7.4) containing 0.5% (w/v) Tween 80 as the release medium. Free DOX was employed as a control. Two mL of DOX-loaded PEG_{5K}-EB_2 or FA-PEG_{5K}-EB_2 micelles (1 mg DOX/mL) were sealed in dialysis tubes (MWCO = 12 KDa, Spectrum Laboratories). The dialysis tubes were immersed in 500 mL release medium in a beaker covered with parafilm. The beakers were kept in an incubator shaker at 100 rpm and 37°C. At different time points, the concentration of DOX retained in the dialysis tubes was measured by HPLC with the detector set at 233 nm. Values were reported as the means from triplicate samples.

4.2.6 Cell culture

Mouse breast cancer cell line, 4T1.2, human breast cancer cell line, MCF-7, and drug-resistant cancer cell line, NCI/ADR-RES, were used in this study. All cell lines were cultured in RPMI-1640 medium (NY.USA) containing 10% fetal bovine serum (FBS) and 1% penicillin-streptomycin in a humidified incubator at 37 ℃ with 5% CO_2.

4.2.7 Animals

Female BALB/c mice, 8-10 weeks, were purchased from Charles River (Davis, CA). All animals were housed under pathogen-free conditions according to AAALAC (Association for Assessment and Accreditation of Laboratory Animal Care) guidelines. All animal-related experiments were performed in full compliance with institutional guidelines and approved by the Animal Use and Care Administrative Advisory Committee at the University of Pittsburgh.

4.2.8 *In vitro* cytotoxicity assay

The cytotoxicity of DOX formulated in micelles was assessed in different cancer cell lines (4T1.2, MCF-7, and NCI/ADR-RES) and compared to free DOX and Doxil. Briefly, cells were seeded in 96-well plates followed by 24 h incubation in RPMI-1640 medium with 10% FBS and 1% streptomycin-penicillin. Different DOX formulations with varying concentrations (at the equivalent concentrations of DOX) were added to cells. Controls including PEG_{5K}-EB_2 and FA-PEG_{5K}-EB_2 were added to cells at concentrations equivalent to those of carriers in the corresponding DOX formulation groups. In order to confirm the active targeting effect rendered by folate ligand attached to the PEG_{5K}-EB_2 micelles, free folate (100 μM), as a competitive inhibitor to folate receptor, was added along with the FA-PEG_{5K}-EB_2/DOX micelles (Paulos, Reddy et al. 2004). Cells were incubated for 72 h and cell viability was assessed by MTT assay as described previously (Huang, Lu et al. 2012, Lu, Huang et al. 2013).

4.2.9 Intracellular uptake study

3×10^5 4T1.2 and NCI/ADR-RES cells were seeded into each well of 6-well plates and were allowed to grow overnight. Then the medium was replaced by fresh medium containing free DOX, Doxil, and DOX-loaded PEG_{5K}-EB_2 and FA-PEG_{5K}-EB_2 micelles, respectively at an equivalent DOX concentration of 6 μg/mL. Following incubation for 30 min at 37 ℃, the cells were washed three times with cold PBS and fixed with 4% paraformaldehyde for 30 min. Afterwards, the nuclei were stained by Hoechst33342 for 5 min. Subsequently, cells were washed three times with cold saline. Finally, the intracellular uptake of DOX in various formulations was observed under confocal laser scanning microscopy (CLSM, FluoView 1000, Olympus, Japan).

Quantitative cellular uptake of various DOX formulations was evaluated by flow cytometry. Briefly, 4T1.2 and NCI/ADR-RES cells were seeded into the 6-well plates at a density of 3×10^5 cells/well. After overnight attachment, cells were treated with free DOX, Doxil, DOX-loaded PEG_{5K}-EB_2 and FA-PEG_{5K}-EB_2, and DOX-formulated in FA-PEG_{5K}-EB_2 micelles along with 100 μM free folic acid, respectively, at an equivalent DOX concentration of 6 μg/mL. Cells without treatment were used as a control. Following incubation at 37 ℃ for 30 min, cells were washed with cold PBS three times, and resuspended in 500 μL PBS for the flow cytometry analysis with CyAn™ ADP Analyzer (Beckman Coulter, Inc.). Cell-associated DOX was excited with an argon laser (480 nm), and fluorescence was detected at 570 nm. 20,000 events were collected for each sample.

4.2.10 P-gp ATPase assay

The effect of PEG_{5K}-EB_2 conjugate on P-gp was studied via examining its effect on a verapamil-stimulated ATPase activity as reported previously (Lu, Huang et al. 2013). TPGS was included as a positive control and sodium orthovanadate (Na_3VO_4) was used as a selective inhibitor of P-gp. Briefly, test samples containing verapamil (50μM) along with PEG_{5K}-EB_2 or TPGS (10 μM and 100 μM) or Na_3VO_4 were added to 96-well plates and incubated with P-gp membrane for 5 min at 37 ℃. Then, the reaction was initiated by the addition of MgATP followed by another 40 minutes' incubation at 37℃. The samples were then removed from 37℃ incubator and ATP detection reagent was added in order to develop the luminescence. Signals were measured 20 minutes later on a microplate luminometer (Victor^2 1420 multilabel counter). The changes of relative light unit (ΔRLU) were calculated as follows:

ΔRLU = (luminescence of Na_3VO_4-treated group) – (luminescence of the samples treated by the mixture of verapamil and PEG_{5K}-EB_2 or TPGS conjugate).

4.2.11 Maximum tolerated dose (MTD)

Groups of 3 female BALB/c mice were treated intravenously with free DOX (5, 10, 15 mg DOX/kg body weight) or DOX-loaded PEG_{5K}-EB_2 micelles (5, 10, 15, 20, 30 mg DOX/kg body weight), respectively. Changes in body weight and survival of mice were followed daily for two weeks. The MTD was defined as the maximal dose that causes neither mouse mortality owing to the systemic toxicity, nor greater than 15% loss in body weight as well as other noticeable changes in the general movement and signs within the entire period of the experiments.

4.2.12 *In vivo* near infrared fluorescence (*NIRF*) **optical imaging**

The *in vivo* tumor-targeting efficiency and biodistribution of PEG_{5K}-EB_2 micelles were studied by using a near infrared fluorescence dye, DiR. Two CL1 tumor-bearing nude mice were employed in this experiment. Briefly, 200 µL of DiR-loaded PEG_{5K}-EB_2 micelles (10 nmol DiR) was i.v. injected into one mouse and another mouse (as a control) was i.v. injected with 200 µl DiR in ethanol/water (1:4 v/v) solution. At different time points (4 h, 24 h, 48 h, 72 h and 96 h) post-injection, mice were scanned using a Carestream Molecular Imaging System (Carestream Health, Inc.) with excitation at 750 nm and emission at 780 nm using an exposure time of 60 s. After 96 h, mice were euthanized by CO_2 overdose. Tumors and major organs of mice were excised and imaged with Carestream Molecular Imaging System. The tissue distribution of DiR in tumors and other organs were quantified by measuring the signal intensity at the region of interest.

4.2.13 Pharmacokinetics and biodistribution of DOX *in vivo*

Free DOX and DOX-loaded micelles were administered via the tail vein with a dosage of 5 mg DOX/kg in 200 µL saline (n = 3). At predetermined time points (3 min, 8 min, 15 min, 30 min, 45 min, 1 h, 2 h, 4 h, 8 h and 12 h), blood samples were obtained from mice using a heparinized capillary tube. Plasma samples were isolated from the blood by centrifuging at 3000 rpm/min for 10 min. DOX in plasma was extracted by extraction buffer (10% Triton X-100, deionized water, and isopropanol at volumetric ratio of 1:2:15). The concentration of DOX at different time points was measured by HPLC with the detector set at 233 nm (Waters Alliance 2695 Separations Module combined with Waters 2998 Photodiode Array Detector, Waters Symmetry C18 5 µm

4.6*250 mm column, mobile phase: 80% MeOH:20% H_2O isocrate, flow rate: 0.6 mL/min). Pharmacokinetic parameters such as $t_{1/2}$, area under the curve (AUC), volume of distribution (V_d) and clearance (CL) were calculated by fitting the blood DOX concentrations to a non-compartment model using Phoenix WinNonlin.

In biodistribution study, free DOX, DOX-loaded PEG_{5K}-EB_2 and DOX-loaded FA-PEG_{5K}-EB_2 micelles were intravenously injected into 4T1.2 tumor bearing mice at the dose of 5 mg DOX/kg, respectively (n=3). At 24 h post-injection, tumor tissues, major organs (liver, spleen, lung, heart, and kidney) and blood were harvested from the mice. Tissues were homogenized using Power Gen 500 homogenizer (Fisher Scientific) with 100 mg tissues mixed with 900 μL extraction buffer, and DOX was extracted overnight at −20 °C using the same method mentioned above. The samples were centrifuged at 3000 rpm/min for 10 min, and the supernatant was then dried and dissolved in 400 μL 75%MeOH. Afterwards, the sample solutions were subjected to further centrifugation at 14500 rpm/min for 5 min to remove undissolved materials prior to HPLC measurement mentioned above. The percent injected dose and the percent injected dose per gram (tissue) values were calculated using the following equations:

% injected dose = (dose in blood or in tissue samples)/injected dose × 100%

% injected dose/g tissue = % injected dose/weight of tissue (g)

4.2.14 *In vivo* antitumor therapeutic study

A syngeneic murine breast cancer model (4T1.2) was used to evaluate the therapeutic efficacy of different DOX formulations. Briefly, 2 x 10^5 4T1.2 cells in 200 μL saline were inoculated subcutaneously at the right flank of female BALB/c mice. When tumors in the mice reached a

volume of 50 -100 mm^3, mice were randomly assigned to one of five groups (n = 5) and this day was designated as day 1. From day 1, mice were intravenously administered free DOX (5 mg/kg), Doxil (5 mg/kg), DOX-loaded PEG_{5K}-EB_2 or DOX-loaded FA-PEG_{5K}-EB_2 once every three days on days 1, 4, and 7, respectively. Tumor sizes were measured with a digital caliper on days 1, 4, 7, 10, 13, 16, 20, 24 and calculated according to the following formula: $(L \times W^2)/2$, where L and W are length and width of each tumor. To better compare between groups, relative tumor volume (RTV) was calculated at each measurement time point, where RTV = the tumor volume at a given time point/the tumor volume prior to first treatment. The tumor growth inhibition rate (IR) was assessed and defined as: IR % = (1 – relative tumor volume in the treated group/relative tumor volume in the saline group) × 100%. Toxicity also was monitored by following the body weights of all mice throughout the entire experiment. Mice were sacrificed when tumor reached 2000 mm^3 or developed ulceration. In addition, blood samples were collected from all mice at the completion of the study for the measurement of serum chemistry including aspartate aminotransferase (AST) and alanine aminotransferase (ALT).

4.2.15 Statistical analysis

In all statistical analyses, the significance level was set at a probability of $P < 0.05$. All results were reported as the mean ± standard deviation (SD) unless otherwise indicated. Statistical analysis was performed by using the Student's t-test for two groups, and one-way ANOVA for multiple groups, followed by Newman-Keuls test if $P < 0.05$.

4.3 RESULTS AND DISCUSSION

4.3.1 Synthesis and characterization of FA-$PEG_{7.5K}$-DOA and PEG_{5K}-EB_2

PEG_{5K}-EB_2 was synthesized and characterized as previously reported (Huang, Lu et al. 2012, Lu, Huang et al. 2013). FA-$PEG_{7.5K}$-DOA was also synthesized to mediate active targeted delivery of PEG_{5K}-EB_2 micelles to tumor cells that overexpress folate receptor (FR). A PEG of longer length ($PEG_{7.5K}$) was used as a spacer between FA and the lipid anchor (DOA) to improve the accessibility of FA on the surface of FA-decorated PEG_{5K}-EB_2 micelles for interaction with FR-overexpressing tumor cells. FA-$PEG_{7.5K}$-DOA conjugate was synthesized via stepwise solution-phase condensation reactions using BocNH-$PEG_{7.5K}$-NHS, Boc-aspartic acid, oleyl amine and FA NHS as building blocks. The complete synthetic route is described in **Figure 21**.

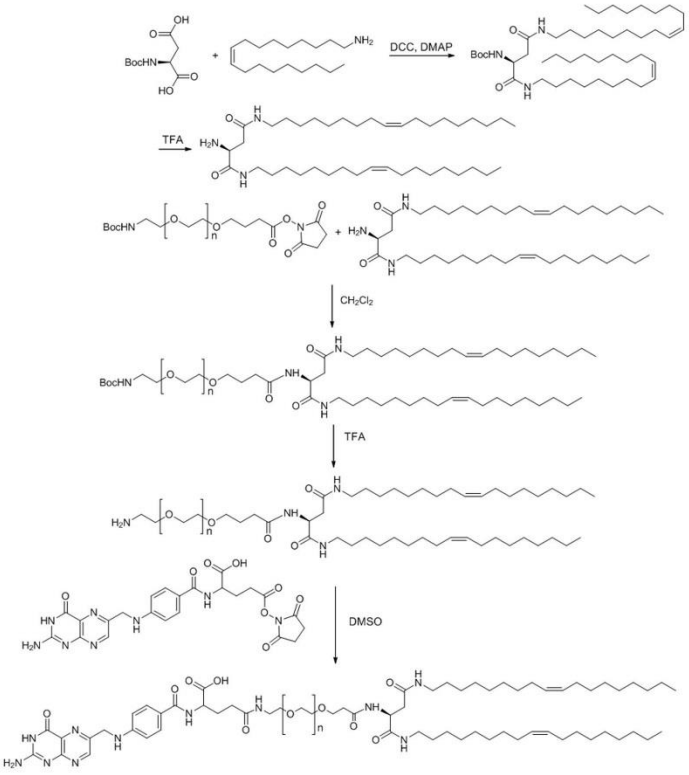

Figure 21 Synthetic route of FA-$PEG_{7.5K}$-DOA.

FA-PEG$_{7.5K}$-DOA was 95.03% pure as verified by HPLC (**Figure 22**).

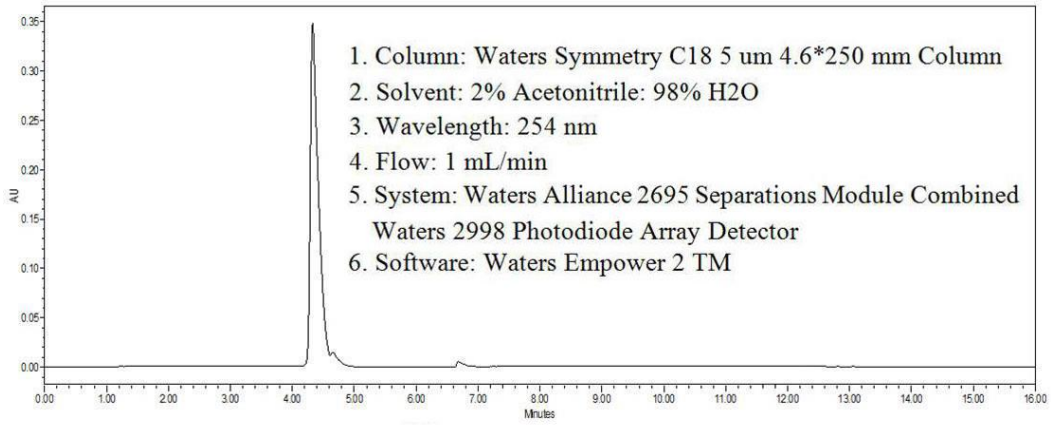

Peak	Migration Time	Area	% Area	Height
1	4.329	3170662	95.03	347718
2	4.649	126408	3.79	14406
3	6.681	39276	1.18	5475

Purity = 95.03 %

Figure 22 HPLC trace of FA-PEG$_{7.5K}$-DOA.

^{1}H NMR spectrum of FA-PEG$_{7.5K}$-DOA showed signals at 6.65 ppm, 7.65 ppm, and 8.65 ppm which are a typical spectrum of FA (**Figure 23)**.

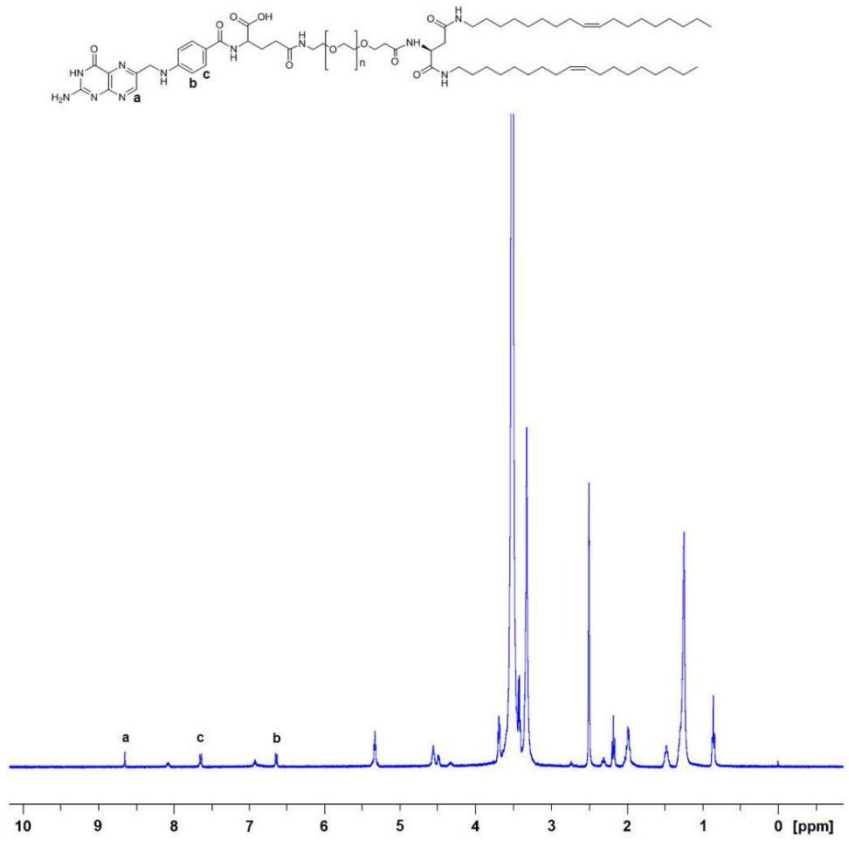

Figure 23 ^{1}H-NMR (400MHz) of FA-PEG$_{7.5K}$-DOA INDMSO.

MALDI-TOF further confirmed the identity of the compound (**Figure 24**). These data suggest successful synthesis of FA-PEG$_{7.5K}$-DOA conjugate.

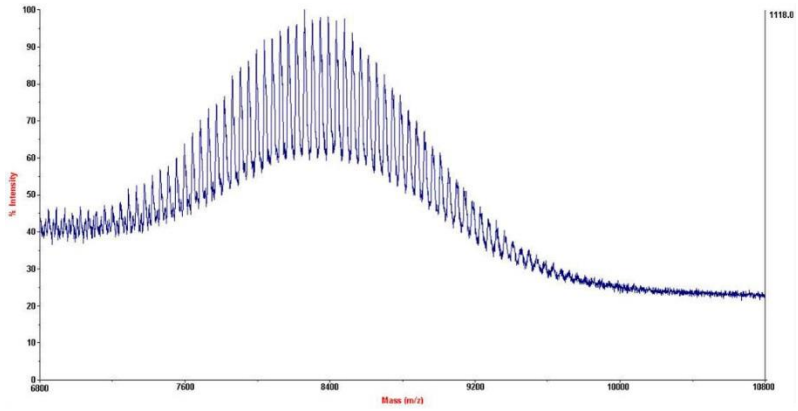

Figure 24 MALDI-TOF of FA-PEG$_{7.5K}$-DOA.

4.3.2 Physicochemical characterization of DOX-free and DOX-loaded micelles

In aqueous solution, both PEG_{5K}-EB_2 and FA-PEG_{5K}-EB_2 were able to readily self-assemble to form micelles with a particle diameter around 20 nm as measured by DLS analysis (**Table 6**).

Table 6 Physicochemical characterization of blank and DOX-loaded micelles.

Micelles	Molar ratios	Size (nm)	PDI	Zeta potential (mv)	DLC (%)	DLE (%)
PEG_{5K}-EB_2		20.6±0.1	0.05	0.68±0.13		
PEG_{5K}-EB_2:DOX	2:1	23.1±0.6	0.12	0.98±0.21	4.55	91.7
FA-PEG_{5K}-EB_2		21.3±0.5	0.09	-0.39±0.09		
FA-PEG_{5K}-EB_2:DOX	2:1	24.9±1.2	0.11	0.46±0.16	4.52	93.5

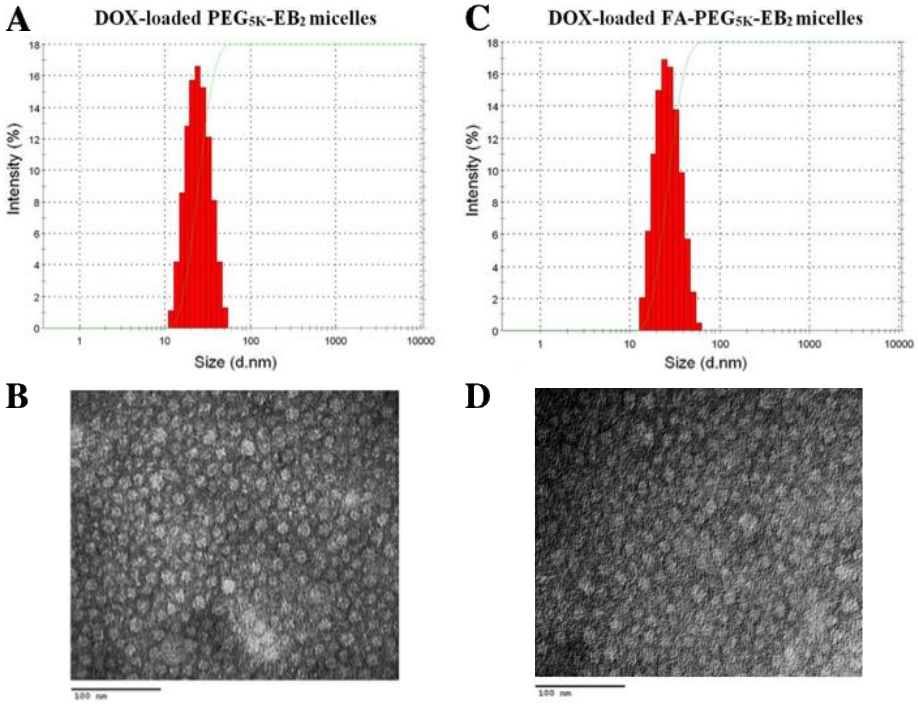

Figure 25 Size distribution of $PEG_{5K}EB_2$/DOX micelles (A) and FA-PEG_{5K}-EB_2/DOX micelles (C). Transmission electron microscopic (TEM) images of PEG_{5K}-EB_2/DOX micelles (B) and FA-PEG_{5K}-EB_2/DOX micelles (D). DOX concentration was kept at 1 mg/mL.

Figure 25A shows the size distribution of PEG_{5K}-EB_2 micelles following incorporation of DOX (1 mg/mL). The size of DOX-loaded micelles was similar to that of drug-free micelles. In addition, spherical particles of uniform size were observed under TEM (**Figure 25C**). The sizes

of the particles under TEM were consistent with those determined by DLS (**Figure 25A**). It is also apparent that attachment of FA to the surface of the micelles had no impact on their size and morphology (**Figure 25B & D**).

Table 6 shows that a DOX loading efficiency (DLE) of 91.7 and 93.5% was achieved for PEG_{5K}-EB_2 and FA-PEG_{5K}-EB_2 micelles, respectively, at a carrier/drug molar ratio of 2/1. To confirm that DOX was indeed incorporated into the interior hydrophobic core of PEG_{5K}-EB_2 micelles, we examined the ^{1}H NMR spectrum of DOX/PEG_{5K}-EB_2 in DMSO and deuterium oxide (D_2O), respectively.

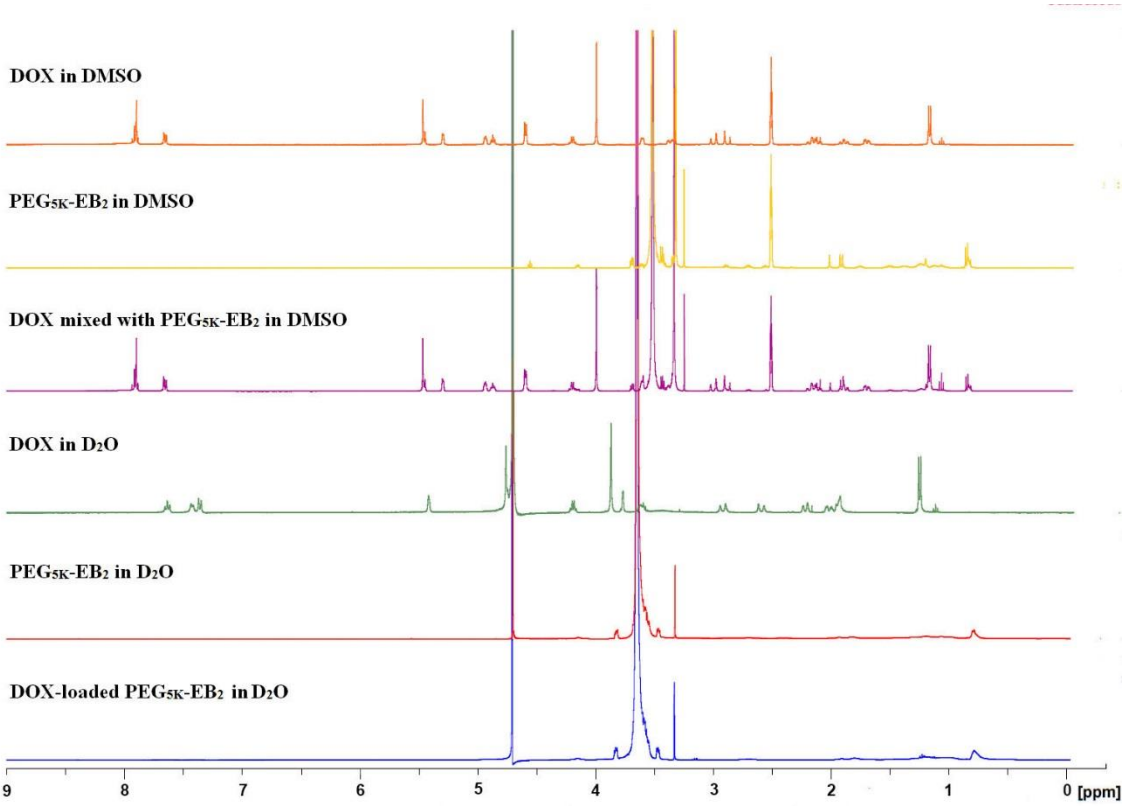

Figure 26 ^{1}H-NMR spectra of free DOX in D_2O, PEG_{5K}-EB_2 in D_2O or $CDCl_3$ and DOX-formulated in PEG_{5K}-EB_2 micelles in D_2O. Concentration of DOX was at 1 mg/mL.

As shown in **Figure 26**, free DOX showed a ^{1}H NMR spectrum in D_2O that was consistent with previous reports (Wang, Wang et al. 2010). A similar spectrum was collected when DOX was

examined in DMSO. PEG_{5K}-EB_2 in DMSO exhibited a ^1H NMR spectrum that was consistent with its structure (**Figure 26**). The signals for both DOX and PEG_{5K}-EB_2 were clearly visualized when DOX/PEG_{5K}-EB_2 was examined in DMSO (**Figure 26**). However, when the ^1H NMR spectrum of PEG_{5K}-EB_2 was collected in D_2O, the Embelin signals (0.5-3 ppm, 4-5 ppm) were nearly abolished (**Figure 26**). This is consistent with the notion that embelin molecules were tightly packed in the core of the micelles in aqueous solution and that embelin signals were shielded by PEG. A similar shielding of embelin signals was observed when DOX/PEG_{5K}-EB_2 was examined in D_2O. The typical peaks for DOX also were completely suppressed for DOX/PEG_{5K}-EB_2, suggesting that DOX was effectively incorporated into the interior core of DOX/PEG_{5K}-EB_2 micelles. A number of mechanisms are likely to be involved in the drug (DOX)/carrier (embelin) interactions including π-π stacking, hydrogen bonding, as well as hydrophobic/hydrophobic interactions.

4.3.3 Release kinetics of DOX formulated in micelles

The release profile of DOX formulated in PEG_{5K}-EB_2 and FA-PEG_{5K}-EB_2 micelles was evaluated using dialysis method in PBS (pH=7.4) to simulate physiologically relevant conditions. Free DOX was employed as a control.

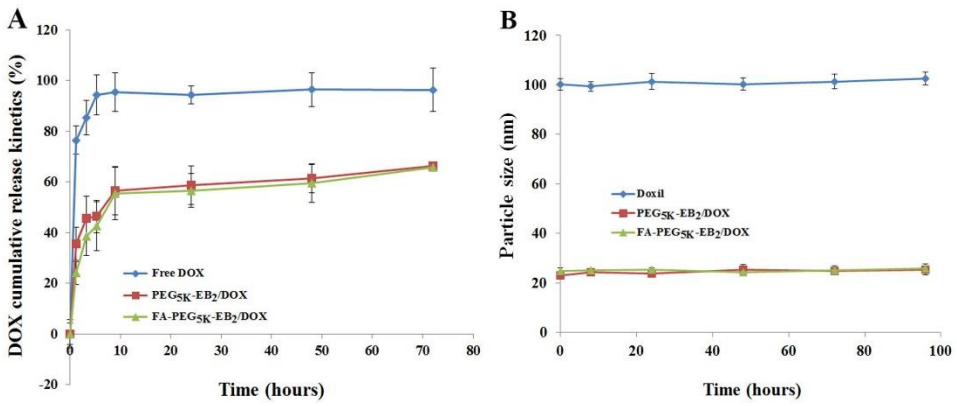

Figure 27 (A) Release kinetics of DOX from free DOX and DOX-loaded micelles determined by dialysis against DPBS (PH = 7.4) containing 0.5% (w/v) Tween 80. (B) Particle size change of DOX-loaded micelles, and Doxil® measured by DLS in aqueous solution over time at 37 °C.

As depicted in **Figure 27**, DOX formulated in PEG_{5K}-EB_2 micelles exhibited sustained release kinetics in comparison to free DOX. During the first 9 h, the amount of DOX released in the free DOX group reached 95.35%, which was substantially higher than that in PEG_{5K}-EB_2 micelles (17.45%). Strikingly, no initial burst release of DOX was observed for DOX-loaded PEG_{5K}-EB_2 micelles, indicating that an overall strong force was involved in the drug-carrier interaction. Additionally, DOX formulated in PEG_{5K}-EB_2 micelles displayed a much slower DOX release compared to free DOX during the entire experimental period. The $T_{1/2}$ of DOX release was 55.87 h for DOX/PEG_{5K}-EB_2 mixed micelles, which is significantly longer than that for free DOX (0.82 h). The significantly slower and controlled release in DOX-loaded PEG_{5K}-EB_2 micellar formulation may be attributed to the strong π-π stacking, hydrogen bonding, as well as hydrophobic interaction between the carrier and DOX as embelin has a benzoquinone ring and a long alkyl chain. Decoration of PEG_{5K}-EB_2 micelles with FA had negligible impact with respect to the DOX release kinetics (**Figure 27**).

4.3.4 *In vitro* cytotoxicity on cancer cells

Figure 28 shows the anti-proliferative effect of various DOX formulations on 4T1.2 mouse breast cancer cells. Cells were treated with different DOX formulations and the cytotoxicity was measured by MTT assay 72 h later. All of the DOX formulations showed time- and concentration-dependent cell-killing effect on 4T1.2 cells.

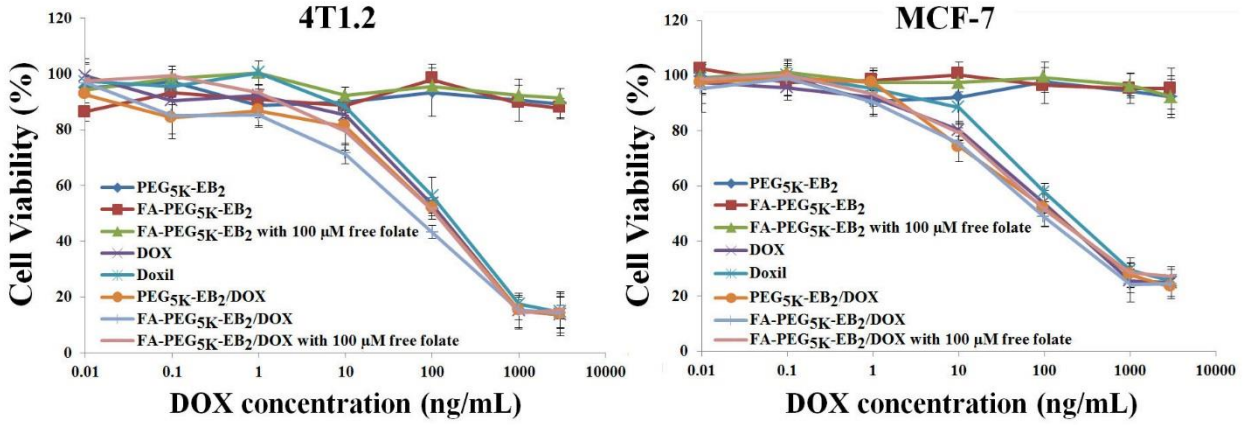

Figure 28 Cytotoxicity of DOX-loaded PEG_{5K}-EB_2 and FA-PEG_{5K}-EB_2 against a mouse breast cancer cell line-4T1.2 and human breast cancer cell line-MCF-7 in comparison to DOX and Doxil.

As summarized in **Table 7**, The IC_{50} was 176.13, 248.98, 138.93, and 78.53 ng/mL for DOX, Doxil, PEG_{5K}-EB_2/DOX, and FA-PEG_{5K}-EB_2/DOX micelles, respectively.

Table 7 IC_{50} of different formulations in 4T1.2 and MCF-7 cancer cells.

	IC_{50} (ng/mL)				
	DOX	Doxil	PEG_{5K}-EB_2/DOX	FA-PEG_{5K}-EB_2/DOX	FA-PEG_{5K}-EB_2/DOX with 100 μM free folate
4T1.2	176.13	248.98	138.93	78.53	130.13
MCF-7	211.53	345.16	173.19	95.18	148.76

DOX-loaded FA-PEG_{5K}-EB_2 is the most potent of all the DOX formulations with respect to cell growth inhibition. To determine whether this is due to folate-mediated active targeting, free folate (100 μM) was co-added to cells with the DOX-loaded FA-PEG_{5K}-EB_2 micelles. It has been reported that 100 μM free folate can block more than 99 % of the binding by folate receptor

(Paulos, Reddy et al. 2004). Indeed, the presence of excess free folate decreased the cytotoxicity of DOX-loaded FA-PEG_{5K}-EB_2 micelles to a level that was comparable to that for DOX-loaded PEG_{5K}-EB_2, suggesting that the greater *in vitro* cytotoxicity of DOX-loaded FA-PEG_{5K}-EB_2 micelles was attributed to the specific ligand-receptor interaction. On the other hand, the relatively high IC_{50} of Doxil might be ascribed to the insufficient intracellular internalization as confirmed in the later uptake study. The inadequate release of DOX from Doxil inside cells may also play a role. Similar results were obtained in MCF-7 human breast cancer cell line (**Figure 28**).

After demonstrating effective inhibition of proliferation of 4T1.2 and MCF-7 cells, we further studied the cytotoxicity of PEG_{5K}-EB_2/DOX in a drug-resistant cell line, NCI/ADR-RES. Drug resistance is a major factor involved in the failure of many types of cancer chemotherapy (Hu and Zhang 2009). Various mechanisms have been identified that are involved in the different types and/or stages of cancers (Gottesman 2002, Yuan, Li et al. 2008). One primary mechanism involves the overexpression of P-glycoprotein (P-gp), which plays a vital role in the development of multiple drug resistance (MDR) (Loo, Bartlett et al. 2004, Chavanpatil, Khdair et al. 2007, Collnot, Baldes et al. 2007, Sharma, Zhang et al. 2008, Zhang, Liu et al. 2013). P-gp, a member of ATP-binding cassette transporter, is one of the major drug efflux transporters and increased expression of P-gp leads to decreased drug accumulation in multidrug-resistant cells, and the development of resistance to anticancer drugs (Desai, Sawada et al. 2013). NCI/ADR-RES is one such MDR cell line and was extensively used for the investigation of multidrug resistance. As shown in **Figure 29**, the anti-proliferative effect of all of the DOX formulations was decreased significantly in this cell line. This is likely due to the increased P-gp activity and

therefore decreased DOX accumulation in NCI/ADR-RES cells, which was confirmed in later DOX cellular uptake studies.

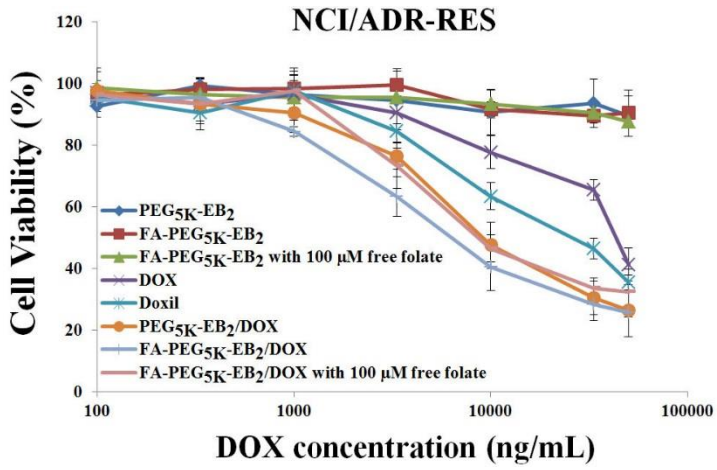

Figure 29 Cytotoxicity of free DOX, Doxil, DOX-loaded PEG_{5K}-EB_2 and DOX-loaded FA-PEG_{5K}-EB_2 micelles in NCI/ADR-RES cells.

In addition, unlike in 4T1.2 and MCF-7 cells, Doxil was more potent than free DOX in inhibiting the proliferation of NCI/ADR-RES cells. This is likely ascribed to the altered route of cellular uptake of Doxil, which decreases the availability of intracellularly delivered DOX to P-gp. These data are consistent with the previous work by Ogawara et al (Ogawara, Un et al. 2009). It is also apparent from **Figure 29** that DOX-loaded PEG_{5K}-EB_2 micelles exhibited enhanced anti-proliferative effect over DOX and Doxil in NCI/ADR-RES cells, with an improvement of efficacy by 3.67- and 2.02-folds, respectively (**Table 8**).

Table 8 IC_{50} of varied DOX formulations in NCI/ADR-RES cancer cell

	IC_{50} (μg/mL)				
	DOX	Doxil	PEG_{5K}-EB_2/DOX	FA-PEG_{5K}-EB_2/DOX	FA-PEG_{5K}-EB_2/DOX with 100 μM free folate
NCI/ADR-RES	43.97	28.43	9.42	7.19	9.11

In addition, coupling of folate to PEG_{5K}-EB_2/DOX micelles led to further improvement in the cytotoxicity towards NCI/ADR-RES cells (**Figure 29**). Again, addition of free folate was able to

reverse the improvement via inhibiting the specific binding of folate receptor to DOX-loaded FA-PEG_{5K}-EB_2 micelles.

4.3.5 *In vitro* cellular uptake

To investigate whether the enhanced cytotoxicity of our micellar systems was attributed to the improved intracellular DOX accumulation, the cellular uptake of DOX in different formulations was examined in 4T1.2 cells using confocal laser scanning microscopy (CLSM). **Figure 30A** shows the intracellular distribution of DOX at 30 min following treatment with different DOX formulations. DOX fluorescence signal was largely localized in the nucleus, suggesting that DOX was effectively translocated into the nucleus following delivery into the cytoplasm. It is also apparent that less fluorescence intensity was observed inside the cells treated with Doxil compared with all other formulations.

To better investigate the uptake efficiency, the intracellular accumulation of DOX was further examined quantitatively by flow cytometry. **Figure 31A** shows the data generated from 4T1.2 cells. In agreement with the confocal study, cells treated with Doxil showed the lowest mean fluorescence intensity. The level of cell-associated fluorescence intensity for PEG_{5K}-EB_2/DOX mixed micelles was similar to that for free DOX. However, surface decoration of PEG_{5K}-EB_2/DOX mixed micelles by FA significantly enhanced the DOX intracellular accumulation over free DOX and Doxil. The improvement in uptake of DOX-loaded FA-PEG_{5K}-EB_2 micelles was significantly abolished in the presence of excess free folate. These data, again, support the notion that the enhanced cellular uptake of DOX-loaded FA-PEG_{5K}-EB_2 micelles was specifically mediated by the folate receptor that is overexpressed on the tumor cells.

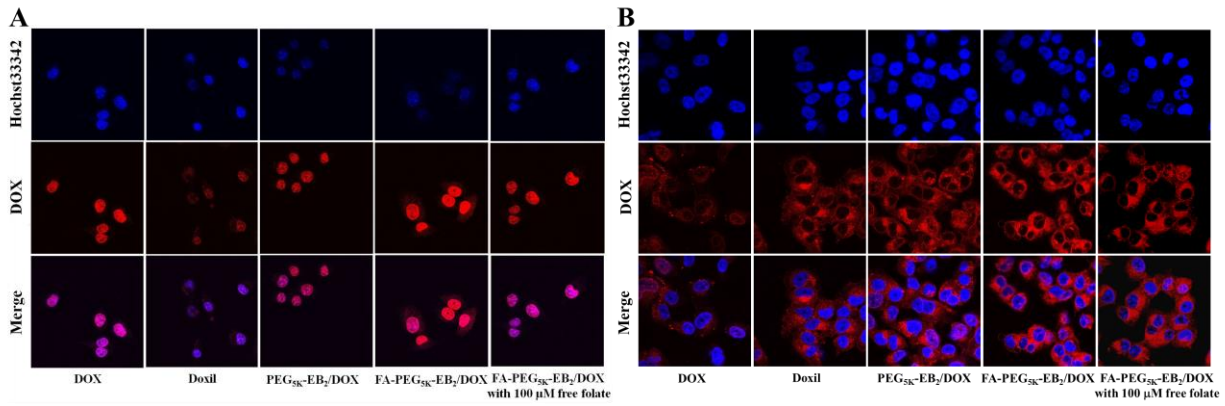

Figure 30 Confocal laser scanning microscopy (CLSM) images of 4T1.2 cells (A) and NCI/ADR-RES cells (B) after incubation with different DOX formulations for 30 min. DOX concentration was 6 µg/mL.

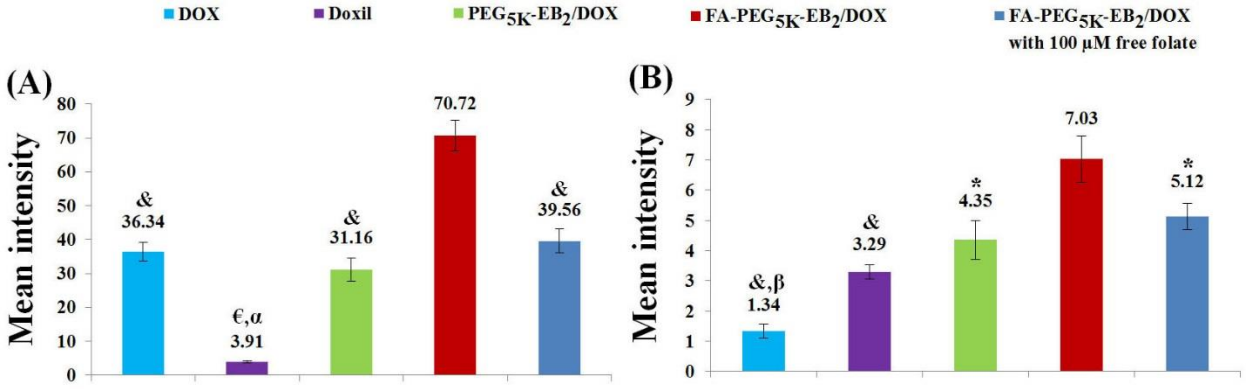

Figure 31 Cellular uptake of DOX in 4T1.2 (A) and NCI/ADR-RES (B) treated by DOX, Doxil, PEG_{5K}-EB_2/DOX, FA-PEG_{5K}-EB_2/DOX as well as FA-PEG_{5K}-EB_2/DOX with 100 µM free folate for 30 min. The numbers above each column are mean intensity values provided by the flow cytometry software, which represent the fluorescence intensity of the cells. Values are reported as the means ± SD for triplicate samples. DOX concentration was 6 µg/mL. *$p < 0.05$, $^{\&}p < 0.005$, $^{€}p < 0.0001$, compared to FA-PEG_{5K}-EB_2/DOX. $^{\alpha}p < 0.0001$, $^{\beta}p < 0.005$ compared to PEG_{5K}-EB_2/DOX.

We also examined the DOX uptake in NCI/ADR-RES cells treated with different DOX formulations (**Figure 30B**). Overall, the fluorescence signals were significantly weaker for all of the DOX formulations compared to the data generated from 4T1.2 cells (Figure 30A). In addition, most of the fluorescence signals were localized outside of the nucleus. This is consistent with the notion that P-gp activity is significantly increased in NCI/ADR-RES cells and significant amounts of "freely accessible" cytoplasmic DOX are effluxed out of the cells. It is

also apparent that NCI/ADR-RES cells treated with free DOX showed lowest level of fluorescence signals compared to cells treated with other formulations (**Figure 30B**).

Figure 31B shows the data of flow cytometry generated from NCI/ADR-RES cells. The data were consistent with confocal imaging. Cells treated with FA-PEG_{5K}-EB_2/DOX micelles gave the highest level of fluorescence intensity. Again, unlike the data generated from the drug-sensitive cells (**Figure 31A**), Doxil-treated-NCI/ADR-RES cells showed significantly higher levels of DOX fluorescence intensity compared to free DOX-treated-NCI/ADR-RES cells (**Figure 31B**). These data are consistent with the cytotoxicity data and suggest that DOX formulated in PEG_{5K}-EB_2 micelles could be effectively taken up by cells and exerted its cytotoxic activity against the tumor cells. More importantly, the data suggest that DOX/PEG_{5K}-EB_2 could overcome the P-gp-mediated DOX efflux and resensitize NCI/ADR-RES cells to DOX cytotoxicity.

4.3.6 Inhibitory effect of PEG_{5K}-EB_2 on P-gp ATPase

Despite the interesting observation that PEG_{5K}-EB_2 micelles were capable of reversing the DOX resistance in NCI/ADR-RES cells, the underlying mechanism remains unclear. It is possible that DOX formulated in PEG_{5K}-EB_2 micelles is taken up by an endocytosis pathway that renders the intracellularly delivered DOX less accessible to P-gp. We hypothesize that PEG_{5K}-EB_2 also overcomes the DOX resistance via directly inhibiting the activity of P-gp ATPase. It is well known that the activity of P-gp is energy-dependent. Thus, the hydrolysis of ATP by ATPase is a prerequisite to confer sufficient energy for the proper functionality of P-gp (Klaassen and Aleksunes 2010). To confirm that PEG_{5K}-EB_2 is, indeed, a P-gp inhibitor, the effect of PEG_{5K}-

EB_2 on P-gp activity was investigated via examining its inhibitory effect on verapamil-stimulated P-gp ATPase activity (**Figure 32**).

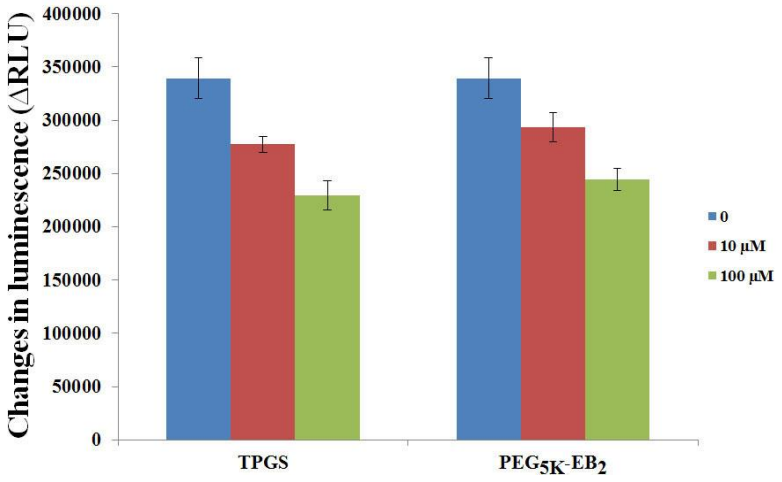

Figure 32 Inhibitory effect of PEG_{5K}-EB_2 and TPGS on verapamil-stimulated P-gp ATPase activity.

TPGS was utilized as a positive control due to its known inhibitory effect on P-gp activity (Dintaman and Silverman 1999). As shown in **Figure 32**, ΔRLU represents the consumption of ATP in the system. Consistent with previous reports, TPGS was able to significantly reduce the ΔRLU in a concentration dependent manner, suggesting the potent inhibition on verapamil-stimulated P-gp ATPase activity, which can lead to the decreased activity of P-gp efflux pump. Interestingly, the ΔRLU in PEG_{5K}-EB_2 group also was significantly reduced, indicating the significant inhibitory effect of PEG_{5K}-EB_2 on P-gp ATPase activity. These data support our hypothesis that PEG_{5K}-EB_2 is able to reverse the P-gp-mediated multidrug resistance through blocking the function of P-gp. There are two possible mechanisms that are involved in the inhibition of P-gp ATPase by PEG_{5K}-EB_2. First, PEG_{5K}-EB_2 may bind to the ATPase-substrate complex to hinder the activity of ATPase so that ATP will not be hydrolyzed. Second, PEG_{5K}-EB_2 may be a substrate of ATPase and directly compete with other substrates for the binding of ATPase. More studies are underway to unravel how PEG_{5K}-EB_2 inhibits P-gp activity. It should be noted that, other than DOX, there are many other potent chemotherapeutics that are the

substrates of P-gp, such as paclitaxel, camptothecin, and etoposide. Therefore, our system can potentially be extended to deliver these therapeutic agents to drug-resistant tumors.

4.3.7 Maximum tolerated dose (MTD) study

One of the potential advantages of drug delivery via nanocarriers is the reduced systemic toxicity of the formulated drugs, which allows for increased dosage to be administered to maximize the therapeutic effect. To evaluate whether our DOX-loaded PEG_{5K}-EB_2 micelles could similarly reduce the DOX-related systemic toxicity, the MTD following a single i.v. administration of PEG_{5K}-EB_2/DOX micelles was investigated in tumor-free mice and compared to free DOX (**Table 9**). The mice were treated with i.v. administration of different doses of DOX-loaded PEG_{5K}-EB_2 micelles or free DOX followed by observation of changes in body weight and other general signs of toxicity.

Table 9 MTD of DOX and DOX-loaded PEG_{5K}-EB_2 micelles.

Formulations	Dose (mg/kg)	Animal death	Weight loss (%)
Free DOX	5	0/3	2.2
	10	0/3	7.8
	15	2/3	N/A
DOX-loaded PEG_{5K}-EB_2 micelles	5	0/3	-2.5
	10	0/3	1.8
	15	0/3	6.9
	20	1/3	N/A
	30	3/3	N/A

As shown in **Table 9**, free DOX was well tolerated in mice at the dose of 10 mg DOX/kg. However, increasing the DOX dosage to 15 mg/kg caused the death of 2 out of 3 treated mice. Therefore the MTD for free DOX at a single injection was around 10 mg/kg, which was consistent with published work (Xiao, Luo et al. 2011). In DOX-loaded PEG_{5K}-EB_2 micelles-treated mice, average weight loss was only 6.9% and there were no marked changes in the

general activity at a DOX dosage of 15 mg/kg. Increasing the dosage to 20 mg DOX/kg led to the death of one out of 3 treated mice. Based on these data it was estimated that the single i.v. MTD for DOX-loaded PEG_{5K}-EB_2 micelles was 15 mg DOX/kg, which was 1.5-folds of improvement over free DOX. The improved MTD of DOX-loaded PEG_{5K}-EB_2 is likely attributed to multiple mechanisms. First, DOX-loaded PEG_{5K}-EB_2 showed slow and sustained release kinetics (**Figure 28**). Second, the PEG shielding of DOX-loaded PEG_{5K}-EB_2 micelles shall minimize the nonspecific uptake by major organs such as liver, heart and lung. Finally, embelin has hepatoprotective and anti-inflammatory activity which may counteract the adverse effects associated with DOX (Chitra, Sukumar et al. 1994, Bhandari, Jain et al. 2007, Singh, Singh et al. 2009). More studies are needed to better understand the mechanism involved in the reduced toxicity of DOX-loaded PEG_{5K}-EB_2 micelles.

4.3.8 Near infrared fluorescence imaging (NIRI) *in vivo* and *ex vivo*

Previously, tumor-targeting effect of PEG_{5K}-EB_2 was examined in PC-3 xenograft tumor model, in which PEG_{5K}-EB_2 micelles co-loaded with PTX and DiD were able to preferentially accumulate in the tumors. In this study, tumor-targeting ability of PEG_{5K}-EB_2 micelles was further investigated in nude mice bearing subcutaneous CL1 tumors by using DiR as a near infrared fluorescence dye. DiR is a strong lipophilic tricarbocyanine probe and has longer excitation and emission wavelengths in the infrared range than DiD. In addition, it is able to prevent any light absorption by tissues, avoid autofluorescence and scattering commonly associated with the application of visible light dyes (Chen, Corbin et al. 2007). Therefore, DiR is a useful NIRF dye for *in vivo* optical imaging. The mice injected with free DiR showed no

noticeable fluorescence signal in tumors and major organs throughout the 96 h period (**Figure 33A**).

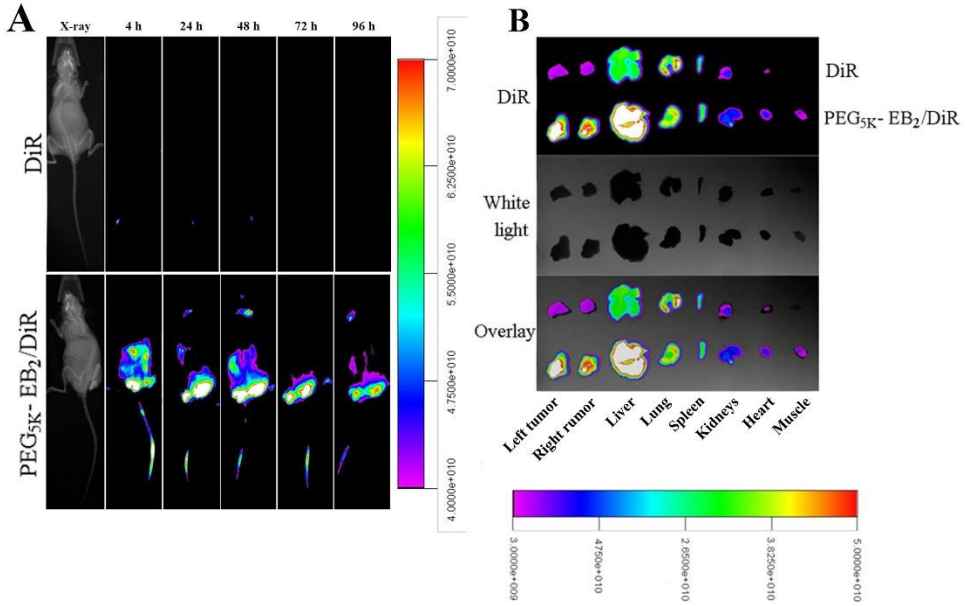

Figure 33 *In vivo* (A) and *ex vivo* (B) NIRF optical images of CL1 tumor-bearing SCID mice injected intravenously with free DiR dye and DiR-loaded PEG_{5K}-EB_2 micelles, respectively. Tumors and major organs were excised for *ex vivo* imaging at 96 h post-injection.

This may be mainly due to the rapid elimination of free DiR by RES and kidney (Hou, Yao et al. 2012). In a sharp contrast, incorporation of DiR into PEG_{5K}-EB_2 micelles led to significantly enhanced accumulation of DiR at tumors. At 4 h post injection, an intense fluorescence signal was discerned in tumor areas, which peaked at 24 h and remained at a substantial level at 96 h, suggesting that PEG_{5K}-EB_2/DiR micelles were able to penetrate leaky tumor vasculature and retained in tumors throughout the 96 h period. This pronounced tumor distribution of DiR/PEG_{5K}-EB_2 micelles could be attributed to the nano-sized particles by taking advantaging of EPR. Moreover, the strong interaction between DiR and embelin molecules may contribute to the excellent stability of the DiR/PEG_{5K}-EB_2 micelles prior to reaching the tumor tissues. More importantly, PEG corona in micelles further prevents the DiR from opsonization.

Following the final imaging at 96 h post-injection, mice were sacrificed and tumors and major organs were excised, imaged and quantified using a Carestream Molecular Imaging System. The intensity of the DiR signal varied in different organs. In free DiR-treated mouse, there was negligible signal of DiR observed in tumors. This is in contrast to the dramatically intense fluorescence signal in tumors for DiR-loaded PEG_{5K}-EB_2 micelles. Not surprisingly, moderate levels of fluorescence signal were observed in liver, spleen and lungs as these are major organs that are accountable for the nonspecific clearance of alien particles by the RES. **Table 10** showed the ratios of DiR signal intensity of tumor to that of liver or spleen.

Table 10 Ratios of DiR signal intensity of tumor to liver or spleen.

	Tumor/liver		Tumor/spleen	
	Left tumor	Right tumor	Left tumor	Right tumor
DiR	0.146	0.139	0.281	0.267
PEG_{5K}-EB_2/DiR	0.940	0.871	2.200	2.038

The ratios of tumor/liver in left and right tumors in PEG_{5K}-EB_2/DiR micelles were 5.44 and 5.27 folds higher than that for free DiR. Similar results were shown for tumor/spleen ratios. These data demonstrated that PEG_{5K}-EB_2 micelles are effective nanocarriers that are able to deliver anticancer therapeutics specifically to tumors.

4.3.9 Pharmacokinetics and biodistribution

In vivo pharmacokinetic profile of DOX was investigated after i.v. bolus in BALB/c mice with the DOX concentration set at 5 mg/kg. **Figure 34A** compared the DOX blood clearance curves among three DOX formulations. As shown in **Figure 34A**, the blood retention times of DOX in both DOX micellar formulations were significantly increased compared to free DOX.

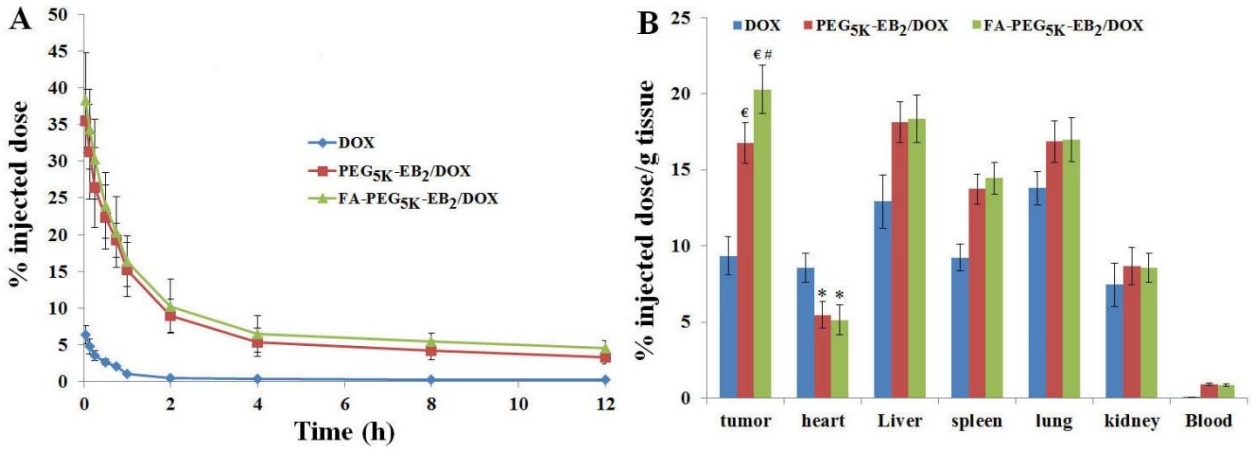

Figure 34 DOX pharmacokinetics (A) and biodistribution profiles (B) after intravenous administration in various DOX formulations at the dose of 5 mg/kg. Values are reported as the means ± SD for triplicate samples *p-value < 0.05 compared to DOX, $^{€}p$-value < 0.005, compared to DOX, $^{\#}p$-value < 0.05 compared to PEG_{5K}-EB_2/DOX.

The pharmacokinetic parameters were obtained by fitting the blood DOX concentration versus time using a non-compartment model and summarized in **Table 11**.

Table 11 Pharmacokinetic parameters of DOX in different formulations.

	$t_{1/2}$ (h)	AUC (μg/mL×h)	CL (mL/h)	C_{max} (μg/mL)	V_d (mL)
DOX	4.41±0.79	5.09±0.31	19.71±1.2	3.23±0.19	26.73±2.12
PEG_{5K}-EB_2/DOX	12.18±1.25	70.54±2.08	1.42±0.042	18.14±1.16	5.16±0.49
FA-PEG_{5K}-EB_2/DOX	15.31±0.94	79.18±5.71	1.17±0.22	20.84±1.55	4.43±0.40

Incorporation of DOX into PEG_{5K}-EB_2 or FA-PEG_{5K}-EB_2 micelles led to substantially greater $t_{1/2}$, AUC, and C_{max} compared to free DOX. The $t_{1/2}$, AUC, and C_{max} of PEG_{5K}-EB_2/FA-PEG_{5K}-EB_2 were 1.76/2.47, 12.86/14.56, and 4.62/5.45-folds higher, respectively, than those of free DOX. However, V_d and CL for both micellar DOX formulations were significantly lower than those for free DOX. These data suggest that DOX formulated in PEG_{5K}-EB_2 or FA-PEG_{5K}-EB_2 micelles was well confined within the blood circulation with significantly increased half-life.

We next went to investigate whether our micellar formulations can improve the biodistribution of DOX. Free DOX, DOX-loaded PEG_{5K}-EB_2, and FA-PEG_{5K}-EB_2 micelles were i.v. administered to 4T1.2 tumor bearing mice at a DOX concentration of 5 mg/kg. Twenty-four h after injection, tumors, blood and major organs were collected for the measurement of DOX.

Compared to free DOX, there were significantly greater amounts of DOX accumulation at tumors for DOX-loaded PEG_{5K}-EB_2 micelles (**Figure 34B**). This likely was attributed to the extended circulation time of DOX-loaded PEG_{5K}-EB_2 micelles and the EPR effect. Coupling of FA to the micellar DOX was associated with further improvement in tumor accumulation of DOX. Both FA-targeted and non-targeted micellar DOX are expected to extravasate into tumors due to their small sizes and the extended half-life in the blood circulation. However, surface decoration with FA shall facilitate the retention of the extravasated micellar DOX at tumor tissues via the FA/folate receptor interaction. FA can further facilitate the subsequent step of intracellular delivery following extravasation.

In addition to enhanced tumor accumulation, relatively high levels of DOX uptake were also noted in liver, spleen and lung, which could be ascribed to the non-specific elimination of nanoparticles by RES. Interestingly, DOX distribution into the heart was significantly reduced in both DOX micellar formulations compared with free DOX. This is significant considering that cardiotoxicity is a major side effect that limits the amount of DOX that can be administered.

4.3.10 *In vivo* antitumor activity

A highly metastatic breast cancer (4T1.2) model was selected in this study to assess the therapeutic efficacy of DOX-loaded micelles in comparison to free DOX and Doxil. An uncontrolled tumor growth was shown in the saline-treated group, which was consistent with the aggressive nature of the 4T1.2 tumor model. Mice treated with free DOX showed modest tumor growth inhibition compared to the saline group with an inhibition rate (IR) of 44.22% (**Table 12**). The PEGylated liposomal formulation of DOX-Doxil exhibited improved antitumor activity over DOX (**Figure 35A**).

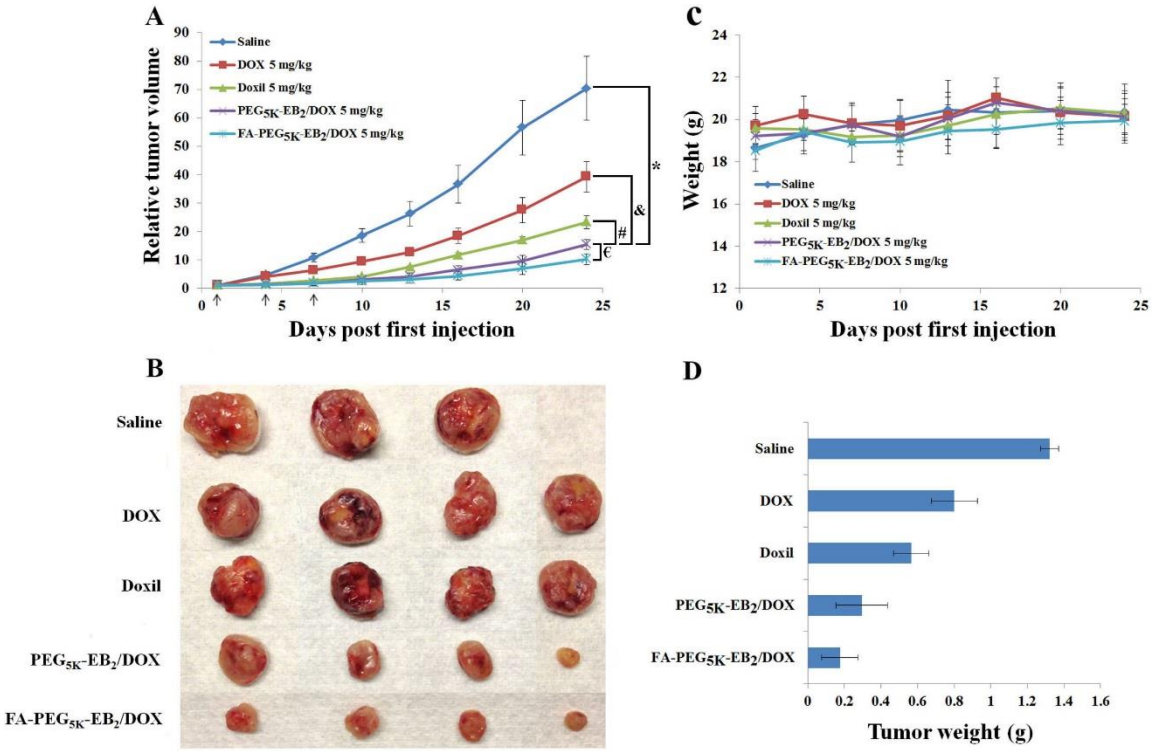

Figure 35 *In vivo* therapeutic study of different DOX formulations in 4T1.2 syngeneic mouse model. Solid arrows mean the i.v. administration A: relative tumor volume. * *p*-value (PEG_{5K}-EB_2/DOX vs Saline) < 0.0001. & *p*-value (PEG_{5K}-EB_2/DOX vs DOX.HCl) < 0.001. # *p*-value (PEG_{5K}-EB_2/DOX vs Doxil) < 0.01. € *p*-value (PEG_{5K}-EB_2/DOX vs FA- PEG_{5K}-EB_2/DOX) < 0.05. B: tumor images. C: mice body weight. D: tumor weight.

The IR in the Doxil group was 66.97% which is an improvement of approximately 1.5-fold over free DOX. The enhanced antitumor activity of Doxil over free DOX is likely attributed to improved DOX accumulation at the tumor site due to the EPR effect (Matsumura and Maeda 1986). Our data also showed that DOX-loaded PEG_{5K}-EB_2 micelles were even more effective than Doxil with an IR of 78.18% (**Figure 35 & Table 12**).

Table 12 Tumor growth inhibition rate (IR) in different treatment groups.

Treatments	IR (%)
DOX	44.22
Doxil	66.97
PEG_{5K}-EB_2:DOX	78.18
FA-PEG_{5K}-EB_2:DOX	85.45

IR (%) = (1-relative tumor volume in the treated group/relative tumor volume in the saline group) × 100%

Furthermore, addition of folic acid to the surface of the PEG_{5K}-EB_2/DOX micelles led to an additional improvement in antitumor activity with an IR of 85.45%. The further improvement of DOX-loaded PEG_{5K}-EB_2 micelles over Doxil is likely due to the very small size of PEG_{5K}-EB_2 micelles (~20 nm). It has been generally known that particles of < 200 nm can effectively extravasate into solid tumors. However, recent studies have suggested that subnano-size (<100 nm) is critical for the particles to minimize the nonspecific uptake by liver and lungs and effectively penetrate the solid tumors including poorly vascularized tumors (Li, Xiao et al. 2010, Luo, Xiao et al. 2010). In addition to facilitating effective tumor accumulation, the inhibitory effect of PEG_{5K}-EB_2 on P-gp function may play a role in the improved antitumor activity of DOX-loaded PEG_{5K}-EB_2 micelles. Finally, the potential synergistic action between the embelin-based carrier and DOX may contribute to the overall antitumor activity. **Figure 35B & 35C** show the images and weights of the tumors collected at the completion of the experiment, which were in agreement with the tumor growth curves (**Figure 35A**). During the entire period of the *in vivo* study, there were no noticeable body weight changes in all treatment groups compared to the saline group (**Figure 35D**). Additionally, serum levels of transaminases (AST and ALT) in the mice from all groups were examined (**Figure 36**).

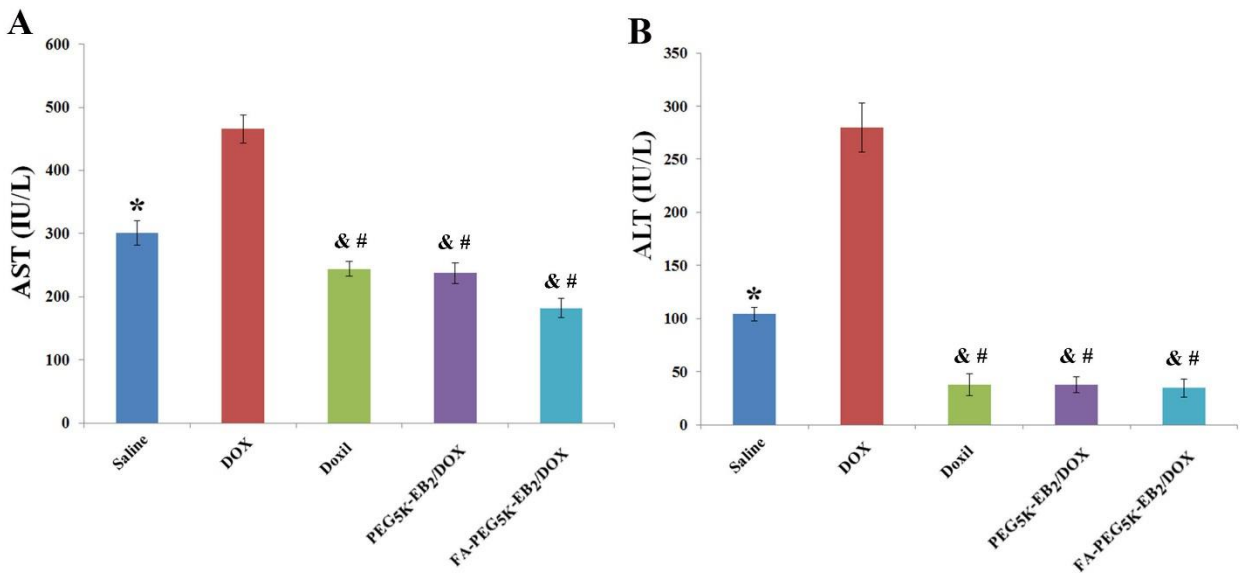

Figure 36 Aspartate aminotransferase (AST) and alanine aminotransferase (ALT) level in different DOX formulations. *p-value < 0.05, compared to DOX, $^{\#}p$-value < 0.01, compared to DOX, $^{\&}p$-value < 0.05, comapared to Saline.

The AST and ALT levels in the DOX-treated group were significantly higher than those in the saline-treated group, suggesting a DOX-related toxicity. No increases in serum levels of AST and ALT were found in the mice treated with Doxil or the DOX-loaded PEG_{5K}-EB_2 micelles. Our data suggest that incorporation of DOX into PEG_{5K}-EB_2 micellar formulation can lead to significantly improved antitumor activity with minimal toxicity.

5.0. DESIGN AND CHARACTERIZATION OF PEG-DERIVATIZED VITAMIN E AS A NANOMICELLAR FORMULATION FOR DELIVERY OF PACLITAXEL

5.1 BACKGROUND

The poor clinical efficacy and the associated severe side effects of conventional chemotherapy in cancer treatment have stimulated the development of novel and effective drug delivery systems. Recently, increasing efforts have been placed on the development of nanotechnology-based drug delivery platforms. Polymeric micelles, liposomes, dendrimers and nanoparticles of biodegradable polymers have been extensively studied as delivery systems to improve cancer treatment (Torchilin 2007). Among the many studied delivery systems, polymeric micelles have drawn considerable attention as a versatile nanotherapeutic platform, owing to ease of preparation, good biocompatibility, and relatively high efficiency in drug delivery (Sutton, Nasongkla et al. 2007, Mi, Liu et al. 2011). It is well known that polymeric micelles can improve the aqueous solubility of poorly water-soluble chemotherapeutic agents by packing them in the hydrophobic core of the micelles. Besides, the blood circulation times of drug-loaded micelles can be significantly prolonged due to the steric hindrance imposed by the presence of the long hydrophilic PEG shell (Sutton, Nasongkla et al. 2007, Mi, Liu et al. 2011). Furthermore, compared to other delivery systems, micelles are highly effective in passive tumor targeting

through the leaky vasculature via enhanced permeability and retention effect (EPR) because of their extremely small sizes ranging from 10 to 100 nm, resulting in favorable biodistribution and improved therapeutic index (Matsumura and Maeda 1986). Nevertheless, most polymeric micellar formulations employ "inert" excipients that not only lack therapeutic activity, but also potentially impose safety concern (Croy and Kwon 2006).

D-alpha-tocopheryl polyethylene glycol succinate 1000 (TPGS) is a hydrophilic derivative of natural Vitamin E, which is generated via coupling of polyethylene glycol (PEG) to Vitamin E succinate via an ester linkage (Sokol, Heubi et al. 1987). Over the last decade, TPGS has been intensively studied in various types of delivery systems: TPGS has been used as an effective emulsifier, solubilizer, additive, permeability enhancer as well as absorption enhancer (Dintaman and Silverman 1999, Yu, Bridgers et al. 1999). As an inhibitor of P-gp, TPGS has also been utilized as an excipient to overcome multidrug resistance (MDR) and improve the bioavailability of anticancer drugs.(Dintaman and Silverman 1999, Varma and Panchagnula 2005, Constantinides, Han et al. 2006, Collnot, Baldes et al. 2007) Examples of TPGS application in nanomedicine platform include TPGS-emulsified PLGA nanoparticles, nanoparticles of TPGS-based copolymers, and TPGS-based micelles, liposomes, and prodrugs (Win and Feng 2006, Cao and Feng 2008, Anbharasi, Cao et al. 2010, Ma, Zheng et al. 2010, Mi, Liu et al. 2011, Muthu, Kulkarni et al. 2011, Mert, Lai et al. 2012, Wang, Sun et al. 2012). In addition, several new derivatives of improved performance have been reported including $TPGS_{5K}$, $TPGS_{2K}$, and PEG_{2K}-Vitamin E_2 conjugate (Mi, Liu et al. 2011, Mert, Lai et al. 2012, Wang, Sun et al. 2012). However, the optimal structure of PEG-Vitamin E conjugates as a micellar delivery system remains incompletely understood.

We have recently developed a PEG-derivatized embelin-based micellar system that is suitable for delivery of poorly water-soluble drugs such as PTX (Huang, Lu et al. 2012). Structurally, PEG-embelin conjugate is very similar to TPGS. Embelin has various biological activities including anti-inflammatory, anti-diabetic, and hepatoprotective effect.(Chitra, Sukumar et al. 1994, Bhandari, Jain et al. 2007, Singh, Singh et al. 2009) Embelin also has antitumor activity and synergizes with other anticancer agents through blocking the activity of X-linked inhibitor of apoptosis protein (XIAP) (Chitra, Sukumar et al. 1994, Sreepriya and Bali 2005, Dai, Qiao et al. 2009, Danquah, Li et al. 2009, Heo, Kim et al. 2011, Huang, Lu et al. 2012). Thus, similar to TPGS, PEG-embelin also functions as a dual functional system for delivery of anticancer agents but with different mechanism of action (Huang, Lu et al. 2012). Optimization of PEG-embelin system has shown that a conjugate with two embelin molecules coupled to PEG is significantly more effective than the conjugate with a 1: 1 molar ratio of PEG and Embelin (Lu, Huang et al. 2013). In addition, the embelin conjugates with PEG_{5K} worked better than the $PEG_{3.5K}$ conjugates (Lu, Huang et al. 2013). This has prompted us to conduct similar study with TPGS micellar system. We have developed four PEG-Vitamin E conjugates that vary in the molecular weight of PEG (PEG_{2K} vs PEG_{5K}) and the molar ratio of PEG/Vitamin E (1/1 vs 1/2) in the conjugates. Our data show that PEG_{5K}-conjugates have lower CMC values and are more effective in PTX loading with respect to both loading capacity and stability. The conjugates with two Vitamin E molecules also worked better than the conjugates with one molecule of Vitamin E, particularly for PEG_{2K}-system. All of the four PEG-Vitamin E conjugates showed the P-gp inhibition activity with their efficiency being comparable to that of TPGS. More importantly, PTX-loaded PEG_{5K}-VE_2 resulted in significantly improved tumor

growth inhibitory effect in comparison to PTX formulated in PEG_{2K}-VE or PEG_{2K}-VE_2, as well as Cremophor EL (Taxol) in a syngeneic mouse model of breast cancer (4T1.2).

5.2 METHODS

5.2.1 Materials

Paclitaxel (98%) was purchased from AK Scientific Inc. (CA, USA). Dulbecco's phosphate buffered saline (DPBS) was purchased from Lonza (MD, USA). Methoxy-$PEG_{2,000}$-OH, Methoxy-$PEG_{5,000}$-OH, dimethyl sulfoxide (DMSO), 3-(4,5-dimethylthiazol-2-yl)-2,5-diphenyl tetrazolium bromide (MTT), Triton X-100, Dulbecco's Modified Eagle's Medium (DMEM) and succinate anhydride were all purchased from Sigma-Aldrich (MO, USA). Fetal bovine serum (FBS) and penicillin-streptomycin solution were from Invitrogen (NY, USA). D-alpha-tocopheryl was purchased from Tokyo Chemical Industry (OR, USA). DCC was purchased from Alfa Aesar (MA, USA). DMAP was purchased from Calbiochem-Novabiochem Corporation (CA, USA). All solvents used in this study were HPLC grade.

5.2.2 Synthesis of PEG_{2K}-VE, PEG_{2K}-VE_2, PEG_{5K}-VE and PEG_{5K}-VE_2

PEG_{5K}-VE_2 was synthesized via solution phase condensation reactions from MeO-PEG-OH with a molecular weight of 5000 Da. (Boc)lysine(Boc)-OH (2 equ.) was coupled onto the terminal-OH of PEG using DCC (2 equ.) and DMAP (0.1 equ.) as coupling reagents in DCM overnight.

Di-Boc lysyl-PEG_{5K} ester was precipitated and washed three times with cold ethanol and ether, respectively. Then, Boc groups were removed via treatment with 50% trifluoroacetic acid in DCM, and the lysyl-PEG_{5K} ester was precipitated and washed three times by cold ethanol and ether, respectively. White powder precipitate was dried under vacuum. Vitamin E succinate was coupled to the deprotected amino groups of lysine with the assistance of DCC (2 equ.) and DMAP (0.1 equ.), resulting in PEG_{5K}-VE_2. This compound was subsequently dialyzed against water and lyophilized to yield a white powder. PEG_{2K}-VE_2 was similarly synthesized as PEG_{5K}-VE_2. PEG_{2K}-VE ($TPGS_{2K}$) and PEG_{5K}-VE ($TPGS_{5K}$) were synthesized following the literature (Mi, Liu et al. 2011).

5.2.3 Preparation and characterization of free or PTX-loaded micelles

PTX-solubilized micelles were prepared by the following method. PTX (10 mM in chloroform) was added to different PEG-Vitamin E conjugates (10 mM in chloroform), respectively, with various carrier/drug molar ratios. The organic solvent was first removed by steady nitrogen flow to form a thin dry film of drug/carrier mixture. The film was further dried under high vacuum for 2 h to remove any traces of remaining solvent. Drug-loaded micelles were formed by suspending the film in DPBS. The drug-free micelles were similarly prepared as described above. The mean diameter of four different micelles with or without loaded drug was assessed by dynamic light scattering (DLS). The morphology and size distribution of PEG_{2K}-VE, PEG_{2K}-VE_2, PEG_{5K}-VE and PEG_{5K}-VE_2 micelles were observed, respectively, using transmission electron microscopy (TEM) after negative staining. The concentration of PTX in PTX-loaded micelles was evaluated by HPLC as described previously (Huang, Lu et al. 2012). The drug loading capacity (DLC) and drug loading efficiency (DLE) were calculated according to the following formula:

DLC (%) = [weight of drug used/(weight of polymer + drug used)] ×100%

DLE (%) = (weight of loaded drug/weight of input drug) ×100%

5.2.4 Stability study of micelles

A series of PTX-loaded micelles with different carrier/PTX molar ratios were prepared as described above and the PTX concentration in all samples was kept at 1 mg/mL. The sizes of samples were measured at different time points following the sample preparation. To examine the effect of serum on the particle stability, the samples were mixed with serum (FBS) at a final serum concentration of 50%. Size changes were monitored by DLS and measurement was terminated when the change of size reached significant difference.

5.2.5 Determination of the critical micelle concentration (CMC)

The CMCs of four different micelles were determined by employing pyrene as a fluorescence probe (La, Okano et al. 1996). A drug-free micelle solution in DPBS (2.5 mg/mL) was prepared via solvent evaporation method. A series of 2-fold dilutions was then made for PEG_{2K}-VE, PEG_{2K}-VE_2, PEG_{5K}-VE and PEG_{5K}-VE_2 micelles, with concentrations ranging from 2×10^{-4} to 0.5mg/mL. At the same time, aliquots of 50 μL of 4.8×10^{-6} M pyrene in chloroform were added into separate vials. The chloroform was first removed by nitrogen flow to form a thin film. The film was further dried under high vacuum for 2 h to remove any traces of remaining solvent. Then, the pre-prepared micelle solutions (400 μL in DPBS) of varying concentrations were added to the pyrene film to obtain a final pyrene concentration of 6×10^{-7} M in each vial. The solutions were kept on a shaker at 37 ℃ for 24 h to reach equilibrium before fluorescence

measurement. The fluorescence intensity of samples was measured at the excitation wavelength of 334 nm and emission wavelength of 390 nm by Synergy H1 Hybrid Multi-Mode Microplate Reader (Winooski, VT). The CMC is determined from the threshold concentration, where the sharp increase in pyrene fluorescence intensity is observed.

5.2.6 *In vitro* drug release study

An *in vitro* drug release study was carried out by dialysis using DPBS (PH = 7.4) containing 0.5% (w/v) Tween 80 as the release medium. Two mL of PTX-loaded micelles (PEG_{2K}-VE, PEG_{2K}-VE_2, PEG_{5K}-VE or PEG_{5K}-VE_2) (1 mg PTX/mL) were sealed in dialysis tubes (MWCO = 12 KDa, Spectrum Laboratories) which were then immersed in 200 mL release medium in a beaker covered with parafilm. The beakers were placed in an incubator shaker at 100 rpm and 37°C. The concentration of PTX remaining in the dialysis tubes at various time points was measured by HPLC with the detector set at 227 nm. Values were reported as the means from triplicate samples.

5.2.7 Cell culture

DU145 and PC-3 are two androgen-independent human prostate cancer cell lines. 4T1.2 is a mouse metastatic breast cancer cell line. MCF-7 and MDA-MB-231 are human breast cancer cell lines. NCI/ADR-RES is Adriamycin (ADR)-resistant cell line. All cell lines were cultured in DMEM containing 10% FBS and 1% penicillin-streptomycin in a humidified environment at 37 ℃ with 5% CO_2.

5.2.8 Hemolytic effect of micelles

Fresh blood samples were collected through cardiac puncture from rats. Heparin was immediately added into 10 mL of blood to prevent coagulation. Red blood cells (RBCs) were separated from plasma by centrifugation at 1500 rpm for 10 min at 4 ℃. RBCs were washed three times with 30 mL ice-cold DPBS. RBCs were then diluted to 2% w/v with ice-cold DPBS and utilized immediately for the hemolysis assay. One mL of diluted RBC suspension was treated with various concentrations (0.0001, 0.001, 0.01, 0.1 and 1.0 mg/mL) of PEG_{2K}-VE, PEG_{2K}-VE_2, PEG_{5K}-VE or PEG_{5K}-VE_2 micelles, and PEI, respectively, and then incubated at 37 ℃ in an incubator shaker for 4 h. The samples were centrifuged at 1500 rpm for 10 min at 4 ℃, and 100 μL of supernatant from each sample was transferred into a 96-well plate. The release of hemoglobin was determined by the absorbance at 540 nm using a microplate reader. RBCs treated with Triton X-100 (2%) and DPBS were considered as the positive and negative controls, respectively. Hemoglobin release was calculated as $(OD_{sample}-OD_{negative\ control})/(OD_{positive\ control}-OD_{negative\ control}) \times 100\%$

5.2.9 *In vitro* cytotoxicity study

The cytotoxicity of PTX formulated in PEG_{2K}-VE, PEG_{2K}-VE_2, PEG_{5K}-VE or PEG_{5K}-VE_2 micelles was assessed with two cancer cell lines (4T1.2 and NCI/ADR-RES) and compared to Taxol formulation. Briefly, 4T1.2 (1000 cells/well) or NCI/ADR-RES (3000 cells/well) cells were seeded in 96-well plates followed by 24 h of incubation in DMEM with 10% FBS and 1% streptomycin-penicillin. Various dilutions of PTX-loaded PEG_{2K}-VE, PEG_{2K}-VE_2, PEG_{5K}-VE or PEG_{5K}-VE_2 micelles, and Taxol (at the equal concentrations of PTX) were added to cells. Cells

were incubated for 72 h and cell viability was assessed by MTT assay as described previously (Huang, Lu et al. 2012). The cytotoxicity of PEG_{2K}-VE, PEG_{2K}-VE_2, PEG_{5K}-VE or PEG_{5K}-VE_2 micelles alone was similarly tested in 4T1.2 (1000 cells/well), NCI/ADR-RES (3000 cells/well), MCF-7 (5000 cells/well), MDA-MB-231 (2000 cells/well) and PC-3 (5000 cells/well) cells as described above.

5.2.10 P-gp ATPase assay

The modulation of P-gp ATPase activity by PEG-derivatized Vitamin E conjugates was conducted by using P-gp-Glo™ assay system (Promega, USA). This assay system provides the necessary reagents for performing luminescent P-gp ATPase assay. Compounds that interact with P-gp can be identified as stimulator or inhibitor of the ATPase activity. The P-gp-Glo™ assay detects the effects of compounds on recombinant human P-gp in a cell membrane fraction. Essentially, the assay relies on an ATP-dependent light-generating reaction of firefly luciferase. The effect of PEG-derivatized Vitamin E conjugates on P-gp ATPase activity was evaluated on a verapamil-stimulated ATPase activity. In this assay, sodium orthovanadate (Na_3VO_4) was employed as a selective inhibitor of P-gp. First, test samples containing verapamil (50μM) and PEG-derivatized Vitamin E conjugates (final concentrations at 10 and 100 μM, respectively) or Na_3VO_4 were added to 96-well plates and incubated with P-gp membrane for 5 min at 37 ℃. Then, the reaction was initiated by the addition of MgATP followed by another 40 minutes' incubation at 37℃. Afterwards, the samples were removed from 37℃ incubator and then ATP detection reagent was added in order to develop the luminescence. Signals were measured 20 minutes later on a plate reading luminometer (Victor^2 1420 multilabel counter). The changes of relative light unit (ΔRLU) were determined as follows:

ΔRLU = (luminescence of Na_3VO_4-treated group) – (luminescence of the samples treated by the mixture of verapamil and PEG-derivatized Vitamin E conjugates).

5.2.11 Animals

Female BALB/c mice, 10-12 weeks were purchased from Charles River (Davis, CA). All animals were housed under pathogen-free conditions according to AAALAC guidelines. All animal-related experiments were performed in full compliance with institutional guidelines and approved by the Animal Use and Care Administrative Advisory Committee at the University of Pittsburgh.

5.2.12 ***In vivo*** **therapeutic study**

A syngeneic murine breast cancer model (4T1.2) was used to examine the therapeutic effect of PTX formulated in PEG_{2K}-VE, PEG_{2K}-VE_2, PEG_{5K}-VE or PEG_{5K}-VE_2 micelles, and Taxol. 2 x 10^5 4T1.2 cells in 200 μL PBS were inoculated s.c. at the right flank of female BALB/c mice. Treatments were initiated when tumors in the mice reached a tumor volume around 50 mm^3 and this day was designated as day 1. On day 1, mice were randomly divided into six groups (n=5) and received i.v. administration of PTX formulated in PEG_{2K}-VE, PEG_{2K}-VE_2, PEG_{5K}-VE or PEG_{5K}-VE_2 micelles, as well as Taxol (10 mg PTX/kg), respectively on days 1, 3, 5, 9, and 12, while control mice received saline. Tumor sizes were measured with digital caliper on days 1, 3, 5, 9, 12, 15 and 18, and calculated according to the following formula: $(L \times W^2)/2$, where L is the longest and W is the shortest in tumor diameters (mm). To compare between groups, relative tumor volume (RTV) was calculated at each measurement time point (where RTV equals the

tumor volume at a given time point divided by the tumor volume prior to first treatment). Mice were sacrificed when tumor reached 2000 mm^3 or developed ulceration. To monitor the potential toxicity, the body weights of all mice from different groups were measured on days 1, 3, 5, 9, 12, 15 and 18.

5.2.13 Statistical analysis

In all statistical analysis, the significance level was set at a probability of $P < 0.05$. All results were reported as the mean ± standard deviation (SD) unless otherwise indicated. Statistical analysis was performed by Student's t-test for two groups, and one-way ANOVA for multiple groups.

5.3 RESULTS

5.3.1 Synthesis of PEG_{2K}-VE, PEG_{2K}-VE_2, PEG_{5K}-VE or PEG_{5K}-VE_2 conjugates

Lysine-linked di-tocopherol polyethylene glycol 5000 succinate was synthesized via solution phase reaction with two Vitamin E succinates attached to mPEG-5000 through the linker of lysine. The synthetic scheme is presented in **Figure 37**.

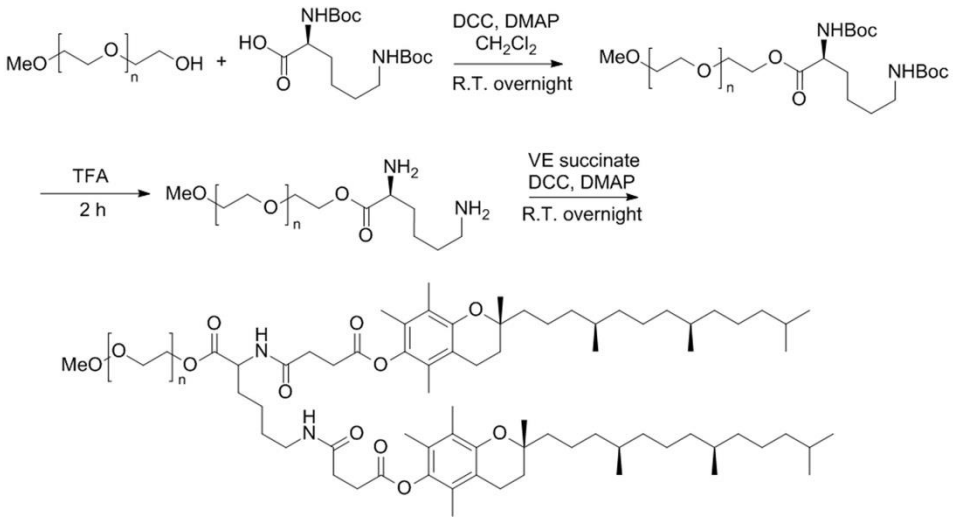

Figure 37 The synthesis scheme of PEG_{5K}-VE_2. First, PEG_{5K} reacted with di-Boc-protected lysine to obtain PEG_{5K}-conjugated di-Boc lysine. Then TFA was employed to remove the Boc groups in order to get free amine. Finally, free amine reacted with Vitamin E succinate to attain PEG_{5K}-VE_2.

Initially, (Boc)lysine(Boc)-OH was coupled onto the terminal –OH of PEG using DCC and DMAP as coupling reagents in DCM. Boc groups were removed by 50% trifluoroacetic acid in DCM. Vitamin E succinate was coupled to the amino groups of lysine, yielding PEG_{5K}-VE_2. The structure of PEG_{5K}-VE_2 was confirmed by ^1H NMR in $CDCl_3$ (**Figure 38**).

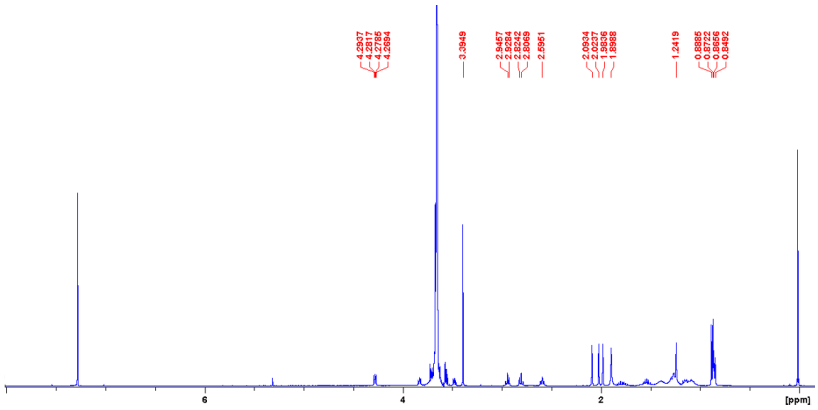

Figure 38 ^1H-NMR spectra (400MHz) of PEG_{5K}-VE_2.

The intense peak at 3.66 ppm was assigned to the methane protons of the polyethylene glycol. The proton peaks below 3.0 ppm were ascribed to the section of Vitamin E succinate. MALDI-

TOF suggested that two Vitamin E succinates were successfully attached to mPEG5000 with the linker of lysine. (**Figure 39**). The HPLC examination of PEG_{5K}-VE_2 was shown in **Figure 40**.

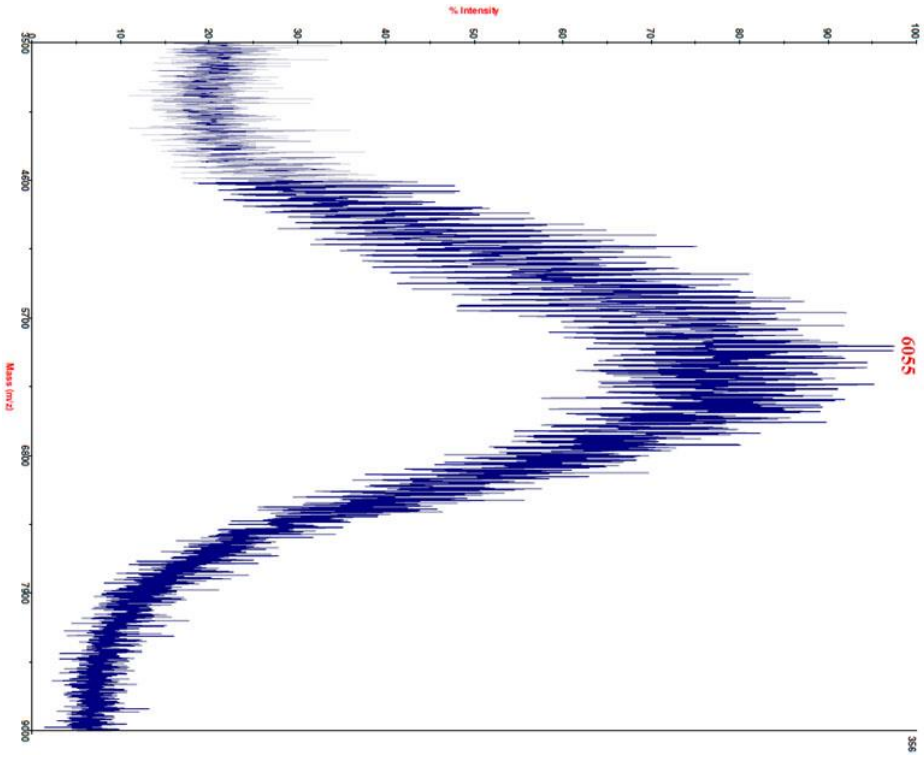

Figure 39 MALDI-TOF of PEG_{5K}-VE_2.

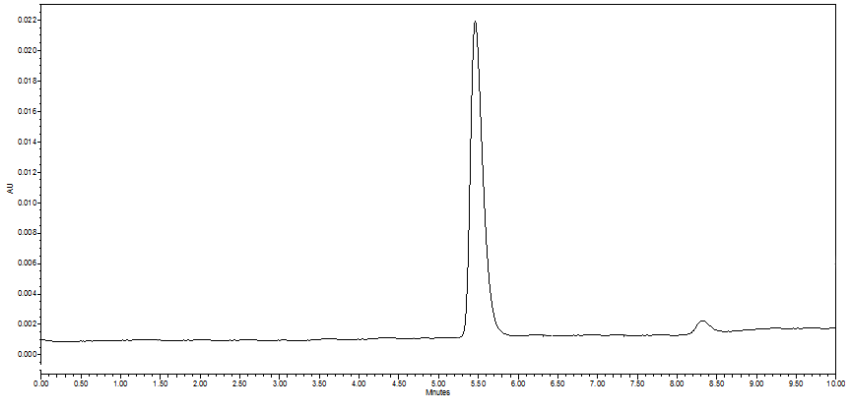

Peak	Retention Time	Area	% Area	Height
1	5.461	227225	96.04	20742
2	8.329	9377	3.96	814

Purity = 96.04%

Figure 40 HPLC trace of PEG_{5K}-VE_2.

PEG_{2K}-VE_2 was synthesized following the same synthesis route of PEG_{5K}-VE_2. PEG_{2K}-VE and PEG_{5K}-VE were synthesized according to the literature (Mi, Liu et al. 2011).

5.3.2 Size & size distribution of micelles

In aqueous solution, the four PEG-derivatized Vitamin E conjugates readily self-assemble to form micellar nanoparticles with the particle sizes of around 20 nm as determined by DLS analysis (**Table 13**).

Table 13 Size of PEG-derivatized Vitamin E micelles.

conjugates	size	PDI
PEG_{2K}-VE	21.5±0.68	0.08
PEG_{2K}-VE_2	18.9±0.08	0.07
PEG_{5K}-VE	19.7±0.09	0.08
PEG_{5K}-VE_2	18.8±0.12	0.09

Figure 41A shows a single peak for PEG_{5K}-VE_2 micelles in size distribution. Negative EM staining revealed spherical particles of uniform size (**Figure 41B**).

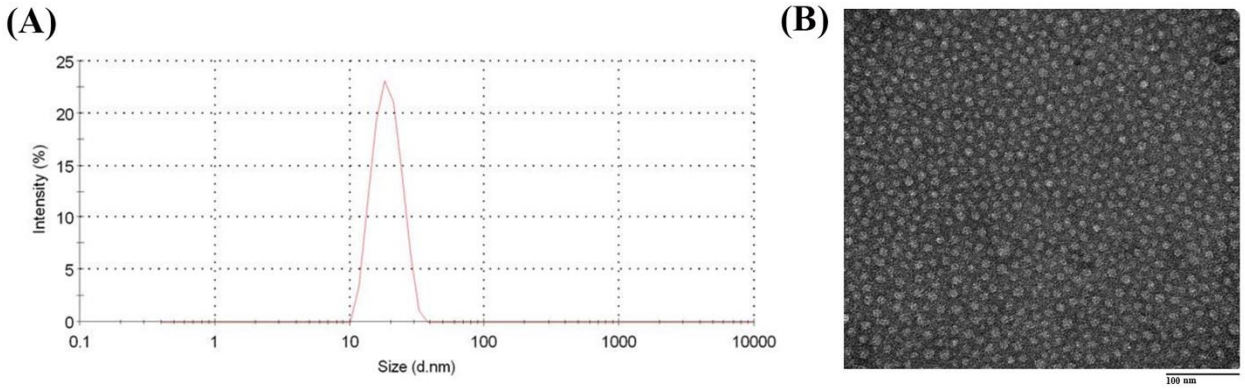

Figure 41 (A) The size distribution of free PEG_{5K}-VE_2 nanoparticles in DPBS and (B) Transmission electron microscopic (TEM) images of PEG_{5K}-VE_2 micelles.

The sizes of the micelles observed under TEM were quite consistent with those measured by DLS. Similar results were shown for the other three micelles (data not shown).

5.3.3 Critical micelle concentration (CMC)

Figure 42 shows the CMC measurements of PEG_{2K}-VE, PEG_{2K}-VE_2, PEG_{5K}-VE, and PEG_{5K}-VE_2 micelles using pyrene as a fluorescence probe.

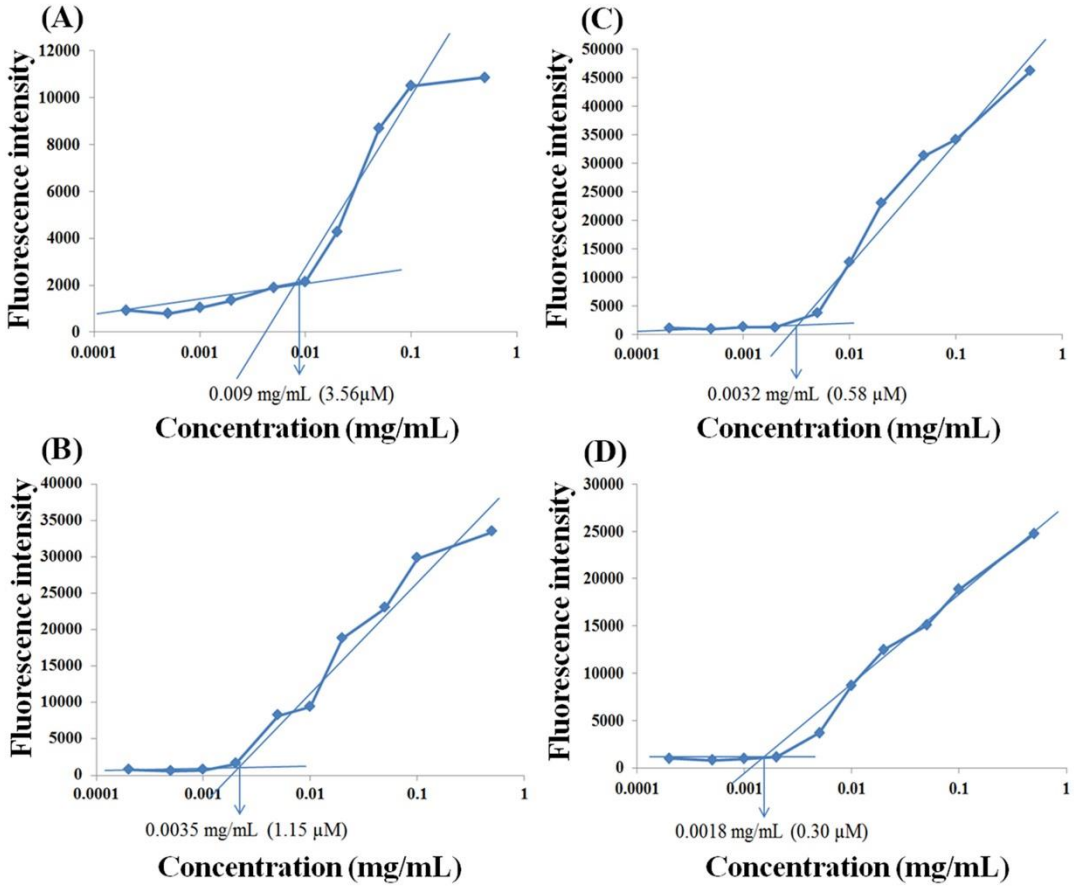

Figure 42 Critical micelle concentration (CMC) measurements of PEG_{2K}-VE (A), PEG_{2K}-VE_2 (B), PEG_{5K}-VE (C) and PEG_{5K}-VE_2 (D) by using pyrene as a hydrophobic fluorescence probe.

Upon incorporation into the micelles, the fluorescence intensity of pyrene increases substantially at the concentration of micelles above the CMC (La, Okano et al. 1996). Based on the partition of the pyrene, the CMC of micelles was obtained by plotting the fluorescence intensity versus logarithm concentration of the polymer. The CMCs of PEG-derivatized micelles were determined from the crossover point at the low concentration range. The CMCs of the

PEG_{5K}-VE and PEG_{5K}-VE_2 conjugates are 0.58 μM and 0.30 μM, respectively, which are lower than those of PEG_{2K}-VE (3.56 μM) and PEG_{2K}-VE_2 (1.15 μM).

5.3.4 Drug loading efficiency (DLE)

DLE is one of the important parameters in drug delivery systems. The PTX loading efficiency of PEG_{2K}-VE, PEG_{2K}-VE_2, PEG_{5K}-VE, and PEG_{5K}-VE_2 micelles with different carrier to drug molar ratios was determined by HPLC (**Table 14**). The sizes of micelles were also examined under corresponding conditions.

Table 14 Physicochemical characterization of PTX-loaded micelles.

carrier/PTX ratio	PTX-loaded micelles[a]	size (nm)[b]	PDI[c]	DLE (%)[d]	stability[e] in DPBS (hour)	stability[e] in 50% FBS (hour)
2.5:1	PEG_{2K}-VE/PTX	34.4±1.22	0.34	42.9	0.1	milky
	PEG_{2K}-VE_2/PTX	26.1±2.42	0.23	64.8	0.2	milky
	PEG_{5K}-VE/PTX	21.3±0.60	0.04	85.4	0.8	0.3
	PEG_{5K}-VE_2/PTX	20.1±0.72	0.05	86.4	1	0.4
5:1	PEG_{2K}-VE/PTX	22.4±0.36	0.14	66.6	0.8	0.5
	PEG_{2K}-VE_2/PTX	23.5±0.35	0.15	69.8	1	0.7
	PEG_{5K}-VE/PTX	20.3±0.59	0.05	86.4	2.3	1.5
	PEG_{5K}-VE_2/PTX	19.7±0.38	0.04	88.4	3	2.1
7.5:1	PEG_{2K}-VE/PTX	23.6±1.31	0.12	71.6	3	0.9
	PEG_{2K}-VE_2/PTX	22.5±0.78	0.11	72.2	3.5	2.1
	PEG_{5K}-VE/PTX	21.1±0.98	0.19	96.4	22	16.5
	PEG_{5K}-VE_2/PTX	20.9±0.56	0.16	98.2	24	19.3
10:1	PEG_{2K}-VE/PTX	21.9±1.34	0.10	86.4	4.2	2.8
	PEG_{2K}-VE_2/PTX	23.6±0.84	0.16	89.7	55.5	30.8
	PEG_{5K}-VE/PTX	19.8±1.23	0.09	96.9	60	39.5
	PEG_{5K}-VE_2/PTX	19.6±1.15	0.12	98.7	68	45.3

[a] The PTX concentration were kept at 1 mg/mL.
[b] Data represents the mean ± standard deviation (n±3) in DPBS.
[c] Polydispersity index.
[d] Drug loading efficiency (%) = (weight of loaded drug/weight of input drug) ×100%.
[e] Data means there was no noticeable size change during the follow-up period.

PEG_{5K}-VE and PEG_{5K}-VE_2 were comparable with respect to DLE at all carrier/drug ratios examined. Both effectively solubilized PTX in aqueous solution in a molar ratio as low as 0.5:1 with particle size remaining around 20 nm. However, these drug-loaded particles were only stable for less than 1 h. At a carrier/drug ratio of 7.5/1, they formed stable mixed micelles with PTX that were stable for about one day in DPBS. Increasing the carrier/drug ratio to 10:1 led to

formation of particles that are stable over 65 h in DPBS. Essentially, all of the added PTX was incorporated into the micelles. In addition, the sizes of the particles remained the same following lyophilization and reconstitution with water (data not shown).

For PEG_{2K}-VE and PEG_{2K}-VE_2 micelles, a minimal carrier/drug ratio of 2.5/1 (m/m) was required to solubilize the drug. PEG_{2K}-VE_2 was more effective than PEG_{2K}-VE in solubilizing PTX with higher DLE at all carrier/drug ratios examined. At a carrier/drug ratio of 10/1, PTX-loaded PEG_{2K}-VE_2 micelles were significantly more stable than PTX formulated in PEG_{2K}-VE micelles (55.5 vs 4.2 h). In addition to evaluating the stability of PTX-loaded micelles in DPBS, their stability in 50% FBS over time was also examined. All of the formulations tested were less stable in serum than in DPBS. Addition of serum to PEG_{5K}-VE_2/PTX (10/1, m/m) mixed micelles resulted in an increase of the particle size from 19.6 nm to 31.7 nm**,** which stayed stable for 45 h. Again, PEG_{5K}-VE_2/PTX shows the best stability in serum among the 4 mixed micelles tested. Overall, the four conjugates were ranked in the order of PEG_{5K}-VE_2 > PEG_{5K}-VE > PEG_{2K}-VE_2 > PEG_{2K}-VE with respect to their efficiency in forming stable mixed micelles with PTX in both DPBS and 50% FBS.

5.3.5 *In vitro* PTX release kinetics

A dialysis method was used to evaluate the release kinetics of PTX from PEG_{2K}-VE, PEG_{2K}-VE_2, PEG_{5K}-VE or PEG_{5K}-VE_2 micelles with DPBS (PH = 7.4) containing 0.5% w/v Tween 80 as the release medium. As shown in **Figure 43**, PTX formulated in PEG_{5K}-VE and PEG_{5K}-VE_2 micelles exhibited significantly better stability than PTX-loaded PEG_{2K}-VE and PEG_{2K}-VE_2 micelles.

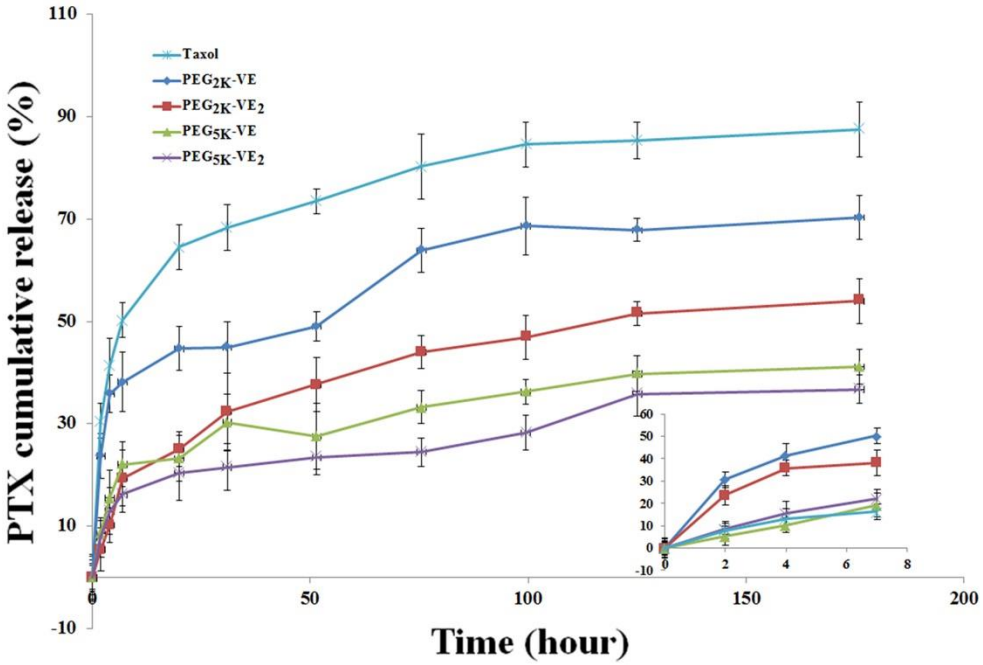

Figure 43 Cumulative PTX release profile from PTX-loaded micelles.

For the first 7 h, there was no significant difference among the 4 micellar systems, during which a burst release due to the relatively high drug concentrations at the very beginning may account for this result. However, significant differences were observed among the 4 formulations during the remaining experimental period. The size of PEG significantly affects the release kinetics: the two conjugates with PEG_{5K} showed significantly slower release kinetics compared to the two conjugates with PEG_{2K}. In addition, the conjugates with two molecules of Vitamin E gave better stability than the PEG-VE conjugates of 1: 1 molar ratio, particularly for PEG_{2K} conjugates. Overall, the four conjugates were ranked in the order of PEG_{5K}-VE_2 > PEG_{5K}-VE > PEG_{2K}-VE_2 > PEG_{2K}-VE with respect to their stability in the release study.

5.3.6 Hemolytic effect of micelles

One concern for micellar systems is whether or not the surface activity of the surfactants affects cell membrane integrity. Therefore, free PEG_{2K}-VE, PEG_{2K}-VE_2, PEG_{5K}-VE and PEG_{5K}-VE_2 micelles were examined for the hemolytic activity and compared to polyethylenimine (PEI), a cationic polymer with potent cell surface activity. As shown in **Figure 44**, treatment with PEI resulted in significant hemolysis in a dose-dependent manner.

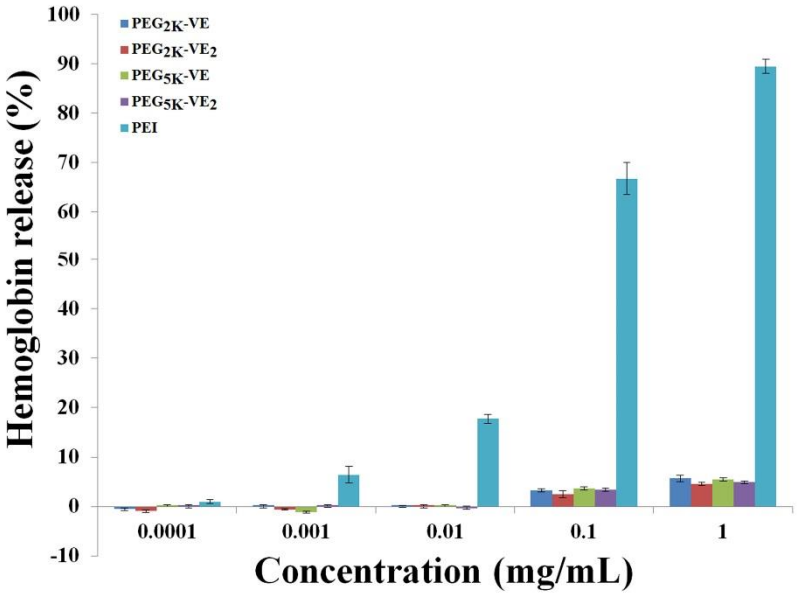

Figure 44 *In vitro* hemolysis assay of PEG-derivatized vitamin E micelles compared with PEI.

In contrast, only a very low level of hemolysis (~5%) was observed for all four blank micelles at the high doses (0.1 and 1 mg/mL) examined. The negligible hemolytic activity suggests that all of the 4 conjugates are mild surfactants that can be suitable for *in vivo* delivery of potent hydrophobic anticancer drugs.

5.3.7 *In vitro* cytotoxicity of free and PTX-loaded micelles

The cytotoxicity of carriers alone was examined in 4T1.2, NCI/ADR-RES, MCF-7, MDA-MB-231, and PC-3 cells, respectively. It was apparent that the single Vitamin E conjugates (PEG_{2K}-VE and PEG_{5K}-VE) showed significantly higher levels of cytotoxicity than those of double Vitamin E conjugates (PEG_{2K}-VE_2 and PEG_{5K}-VE_2) in all five cancer cell lines tested (**Figure 45**).

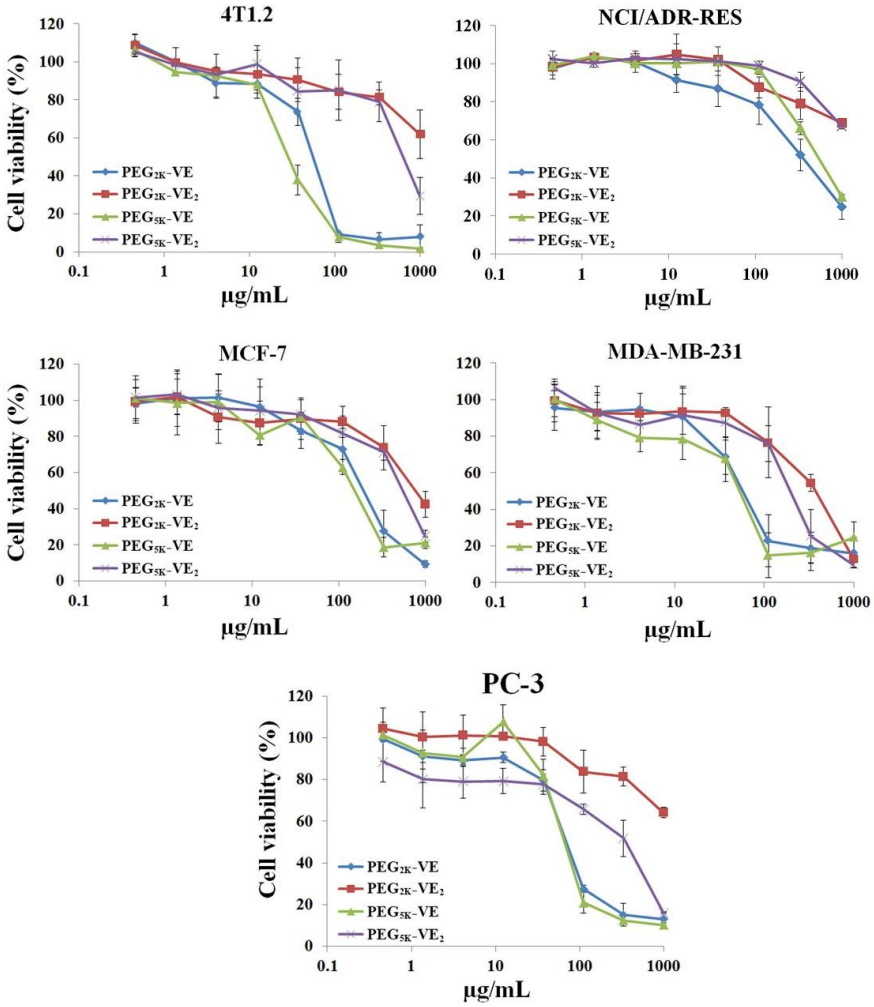

Figure 45 Cell viability after being treated with free PEG_{2K}-VE, PEG_{2K}-VE_2, PEG_{5K}-VE, or PEG_{5K}-VE_2 micelles in the 4T1.2 mouse breast cancer cell line, drug-resistant cell line-NCI/ADR-RES, two human breast cancer cell lines MCF-7 and MDA-MB-231, and an androgen-independent human prostate cancer cell line PC-3

In MDA-MB-231 cells, the IC_{50} for PEG_{2K}-VE_2 and PEG_{5K}-VE_2 is 6 and 4.8 times higher than their single Vitamin E counterparts (**Table 15**). Similar results were shown for the other four cancer cell lines (**Table 15**). It is also apparent that NCI/ADR-RES cells were more sensitive than the other four cancer cell lines to all of the conjugates (**Figure 45 & Table 15**). Again, the single Vitamin E conjugates showed more potent cytotoxicity than the double Vitamin E conjugates in this drug-resistant cell line (**Figure 45 & Table 15**).

Table 15 IC_{50} of free PEG_{2K}-VE, PEG_{2K}-VE_2, PEG_{5K}-VE and PEG_{5K}-VE_2 micelles in tumor cells.

	IC_{50}(μg/mL)			
	PEG_{2K}-VE	PEG_{2K}-VE_2	PEG_{5K}-VE	PEG_{5K}-VE_2
4T1.2	64.30	N/A	30.98	726.44
NCI/ADR-RES	382.75	N/A	630.08	N/A
MCF-7	223.78	839.89	176.29	637.71
MDA-MB-231	66.82	403.93	61.52	224.98
PC-3	79.17	N/A	75.91	366.79

Figure 46A shows the *in vitro* cytotoxicity of PTX formulated in PEG_{2K}-VE, PEG_{2K}-VE_2, PEG_{5K}-VE and PEG_{5K}-VE_2 micelles in comparison with Taxol in 4T1.2 cancer cells. All of the four PTX mixed micelles were less active than Taxol in antitumor activity. Interestingly, different from the study of carriers alone in which single Vitamin E conjugates were more active, PTX-loaded PEG_{5K}-VE_2 micelles were more potent than PTX formulated in the other three micelle formulations. Similar to the study of carriers alone, NCI/ADR-RES tumor cells are also more sensitive than 4T1.2 cancer cells to PTX formulated in either PEG-Vitamin E micelles or Cremophor/ethanol (Taxol) (**Figure 46B**).

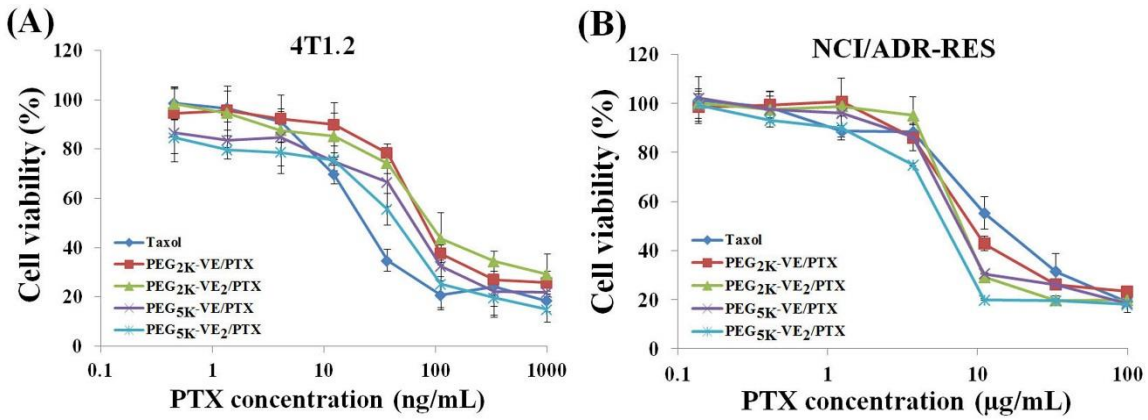

Figure 46 The cytotoxicity of PTX-loaded PEG_{2K}-VE, PEG_{2K}-VE_2, PEG_{5K}-VE, or PEG_{5K}-VE_2 micelles, compared to clinical PTX formulation-Taxol, against the 4T1.2 mouse breast cancer cell line (A) and drug-resistant NCI/ADR-RES cell line (B).

Again, PTX-loaded PEG_{5K}-VE_2 micelles showed the highest level of in vitro cytotoxicity followed by PTX-loaded PEG_{5K}-VE micelles. PTX-PEG_{2K}-VE and PTX-PEG_{2K}-VE_2 are comparable in antitumor activity. However, all of the four PTX micellar formulations were more active than Taxol in NCI/ADR-RES tumor cells, which is quite different from the data in 4T1.2 cells. The IC_{50} of Taxol and several PTX-loaded micelles in the two cancer cell lines were summarized in **Table 16**.

Table 16 IC_{50} of PTX-loaded micelles in 4T1.2 and NCI/ADR-RES cancer cell lines.

	IC_{50}				
	Taxol	PEG_{2K}-VE/PTX	PEG_{2K}-VE_2/PTX	PEG_{5K}-VE/PTX	PEG_{5K}-VE_2/PTX
4T1.2 (ng/mL)	26.16	88.17	95.52	72.75	50.38
NCI/ADR-RES (μg/mL)	15.99	9.88	8.77	8.52	7.10

5.3.8 Inhibition of P-gp ATPase

Figure 47 shows that P-gp ATPase activity was significantly inhibited by TPGS in a concentration-dependent manner.

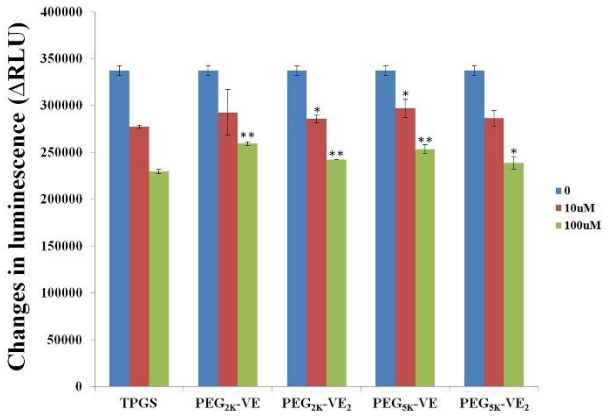

Figure 47 Inhibitory effect of TPGS, PEG_{2K}-VE, PEG_{2K}-VE_2, PEG_{5K}-VE or PEG_{5K}-VE_2 on verapamil-stimulated P-gp ATPase activity. TPGS, PEG_{2K}-VE, PEG_{2K}-VE_2, PEG_{5K}-VE or PEG_{5K}-VE_2 was administered in an amount of 10 or 100 μM along with 50 μM verapamil. Na_3VO_4 was utilized as a selective inhibitor of P-gp in this assay. * indicates $p < 0.05$ and ** indicates $p < 0.001$ compared with TPGS group with equivalent concentration.

Albeit all of the four conjugates were statistically less active than TPGS at 10μM and/or 100μM treatment, they still exhibited significant P-gp inhibitory effect in a Verapamil-induced ATPase assay. What we have found here is quite consistent with the report in the literature (Collnot, Baldes et al. 2007).

5.3.9 *In vivo* therapeutic study

The *in vivo* therapeutic activity of PTX formulated in PEG_{2K}-VE, PEG_{2K}-VE_2, and PEG_{5K}-VE_2 micelles was evaluated in a syngeneic murine breast cancer model (4T1.2), and compared to Taxol. 4T1.2 is a highly metastatic breast cancer cell line and was selected to rigorously assess the *in vivo* therapeutic efficacy of different PTX formulations.

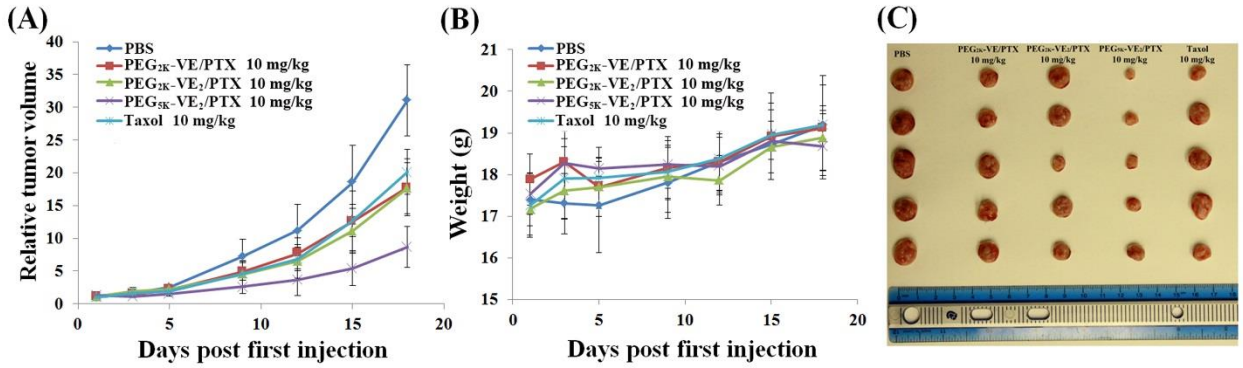

Figure 48 (A) Enhanced antitumor activity of PTX formulated in PEG_{5K}-VE_2 micelles. BABL/c mice were inoculated s.c. with 4T1.2 cells (2 x 10^5 cells/mouse). Five days later, mice received various treatments on days 1, 3, 5, 9, and 12, and tumor growth was monitored and plotted as relative tumor volume. $P < 0.02$ (PEG_{5K}-VE_2/PTX vs. Taxol, PEG_{2K}-VE/PTX or PEG_{2K}-VE_2/PTX), N = 5. (B) Changes of body weight in mice receiving different treatments. (C) Images of tumors removed from the tumor-bearing mice at the completion of the study.

As shown in **Figure 48A**, Taxol formulation showed moderate effect in inhibiting the tumor growth at a dose of 10 mg PTX/kg. Compared to Taxol treatment group, PTX formulated in PEG_{2K}-VE or PEG_{2K}-VE_2 exhibited similar tumor growth inhibitory effect. In contrast, PTX formulated in PEG_{5K}-VE_2 micelles showed a significantly more pronounced antitumor activity at the same dosage. No significant changes in body weight were noticed in all treatment groups compared to PBS control group (**Figure 48B**), suggesting that significant therapeutic effect can be achieved with minimal toxicity.

5.4 DISCUSSION

We have systematically compared the biophysical property and *in vitro* and *in vivo* efficiency of PTX delivery of four PEG-Vitamin E conjugates that differ in the size of PEG motif (PEG_{2K} vs PEG_{5K}) and the molar ratio of PEG/Vitamin E (1/1 vs 1/2) in the conjugates. Our data showed

that PEG_{5K}-conjugates were significantly more effective than PEG_{2K}-conjugates in forming stable mixed micelles with PTX and in mediating delivery of PTX to tumor cells, particularly *in vivo*. In addition, conjugates with two Vitamin E molecules work better than the conjugates with one molecule of Vitamin E.

It is likely that various mechanisms are involved in the carrier/drug interaction for the Vitamin E-based micellar system. Vitamin E has a benzene ring and a long alkyl chain. In addition to hydrophobic interaction with PTX, the hydrogen bonding and the π-π stacking may also contribute to the overall carrier/PTX interaction. The close proximity of two Vitamin E molecules in PEG-VE_2 conjugates is likely to facilitate the formation of a binding pocket that enhances the interaction between the carriers and PTX. This is supported by data from our recent work that inclusion of a drug-interactive motif at the interfacial region of surfactants significantly improves the carrier-drug interaction, leading to improvement in both drug-loading capacity and formulation stability (Gao, Huang et al. 2013). Recently, Wang and colleagues reported a similar work in which they showed that PEG_{2K}-Vitamin E_2 conjugate was more effective than PEG_{2K}-Vitamin E in mediating delivery of doxorubicin to tumors (Wang, Sun et al. 2012). In an independent study with two similar delivery systems based on PEG-embelin and PEG-farnesylthiosalicylic acid (FTS) conjugates, we also showed that conjugates with two embelin or FTS molecules were more effective than conjugates with one embelin or FTS molecule regardless whether $PEG_{3.5K}$ or PEG_{5K} was used (Huang, Lu et al. 2012, Lu, Huang et al. 2013, Zhang, Lu et al. 2013).

As a hydrophilic motif of amphiphilic molecules, the size of PEG also critically affects the performance of the micelles. PEG provides steric hindrance, which is critical for ensuring long circulation property of the micelles. PEG decoration has also been shown to facilitate the

penetration of nanoparticles through the mucus layer (Lai, Wang et al. 2009, Mert, Lai et al. 2012). In this regard, PEGs of higher MW are expected to be more effective than those of lower MW. However, the size of PEG also affects the CMC which in turn significantly affects the performance of the micelles, particularly *in vivo*. Different micellar systems appear to be differentially affected by the size of PEG (Luo, Xiao et al. 2010, Mi, Liu et al. 2011, Huang, Lu et al. 2012, Lu, Huang et al. 2013). In a systematic study on the SAR of PEG-cholic acid cluster-based micellar system, PEG_{2K} was shown to be the optimal hydrophilic motif (Luo, Xiao et al. 2010). Our data clearly showed that PEG_{5K}-conjugates (with either one or two Vitamin E molecules) were more active than PEG_{2K}-conjugates in forming stable mixed micelles with PTX. PEG_{5K}-conjugates formed stable complexes with PTX at lower carrier/PTX molar ratios compared to PEG_{2K}-conjugates. In addition, PTX formulated in PEG_{5K}-micelles displayed much slower release kinetics. We have similarly demonstrated the advantages of PEG_{5K} over $PEG_{3.5K}$ in PEG-embelin and PEG-FTS micellar systems (Huang, Lu et al. 2012, Lu, Huang et al. 2013, Zhang, Lu et al. 2013). In the study by Hanes and colleagues, PLGA particles coated with $TPGS_{5K}$ were more effective than the particles decorated with $TPGS_{1K}$ in penetrating human cervicovaginal mucus (Mert, Lai et al. 2012).

The four different PEG-Vitamin E conjugates showed varied levels of activity by themselves in four cancer cell lines. Overall, the single Vitamin E conjugates were more potent than the conjugates with two Vitamin E molecules in all cell lines tested. The more potent activity of single Vitamin E conjugates is unlikely due to the more active surface activity of the single chain conjugates as all of the four conjugates showed minimal hemolytic activity at much higher concentrations tested. It is possible that active Vitamin E is more readily released from the single Vitamin E conjugates than the ones with two Vitamin E molecules due to less steric

hindrance to intracellular esterases. More studies are needed in the future to examine if the single Vitamin E conjugates indeed yield greater amounts of active free Vitamin E intracellularly.

Different from the cytotoxicity profiles of the conjugates alone, PTX formulated in PEG_{5K}-VE_2 micelles showed higher levels of cytotoxicity than PTX formulated in other three micellar systems in both 4T1.2 and NCI/ADR-RES tumor cell lines. This might be attributed to a more efficient intracellular delivery of PTX via PEG_{5K}-VE_2 micelles as PEG_{5K}-VE_2 formed the most stable mixed micelles with PTX among the four micellar systems tested. Despite the difference in the levels of cytotoxicity among the four types of micellar PTX, all of them were less active than Taxol formulation in 4T1.2 tumor cells. Interestingly we saw a reversal of the pattern in NCI/ADR-RES tumor cells: all of the four micellar PTX were more active than Taxol in this drug resistant cell line. The improved *in vitro* cytotoxicity of the PTX micellar formulations in this drug resistant cell line can be ascribed to the well-known inhibitory effect of P-gp efflux pump by Vitamin E derivatives and thus an improved bioavailability of PTX inside the tumor cells (Dintaman and Silverman 1999, Varma and Panchagnula 2005, Constantinides, Han et al. 2006, Collnot, Baldes et al. 2007). This hypothesis was supported by the P-gp ATPase activity assay in this work (**Figure 47**). Our results were consistent with previous studies with various types of delivery system that involve the use of TPGS (Dintaman and Silverman 1999, Varma and Panchagnula 2005, Constantinides, Han et al. 2006, Collnot, Baldes et al. 2007).

In vivo therapy study clearly showed a significantly higher level of antitumor activity for PTX formulated in PEG_{5K}-VE_2 micelles compared to either Taxol or other two micellar formulations. This is likely due to the significantly improved loading capacity and stability for PEG_{5K}-VE_2 micelles, which shall lead to more effective delivery of PTX to tumor tissue *in vivo*. No significant difference was noticed between PEG_{2K}-Vitamin E_2 and PEG_{2K}-Vitamin E in

antitumor activity despite the demonstrated advantages of PEG_{2K}-Vitamin E_2 over PEG_{2K}-Vitamin E in biophysical property. This might be due to the aggressive nature of 4T1.2 tumor model, which requires significant improvement of the formulation to achieve a significant gain in the therapeutic benefit.

6.0. AN IMPROVED D-A-TOCOPHEROL-BASED NANOCARRIER FOR TARGETED DELIVERY OF DOXORUBICIN WITH REVERSAL OF MULTIDRUG RESISTANCE

6.1 BACKGROUND

Doxorubicin (DOX), one of the most potent anticancer agents, has been widely used for the treatment of ovarian, breast, prostate, cervix, brain, and lung cancers. It functions by intercalating between base pairs of the DNA helix, resulting in the suppression of DNA synthesis (Momparler, Karon et al. 1976, Fornari, Randolph et al. 1994, Tacar, Sriamornsak et al. 2013). In addition, doxorubicin stabilizes the topoisomerase II-DNA complex after it has broken the DNA chain for replication, which prevents the DNA double helix from being resealed and thereby arrests the process of replication (Pommier, Leo et al. 2010, Tacar, Sriamornsak et al. 2013). However, its clinical application has been compromised by its limited efficacy *in vivo* and systemic side effects (Minotti, Menna et al. 2004, Takemura and Fujiwara 2007). Hence, there is a need to develop an effective drug carrier to specifically deliver DOX to tumors.

In the last two decades, D-α-tocopheryl polyethylene glycol succinate (TPGS) has gained increasing attention as an ideal biomaterial in developing various drug delivery systems such as micelles, liposomes, and other nanoparticles (Win and Feng 2006, Cao and Feng 2008, Anbharasi, Cao et al. 2010, Ma, Zheng et al. 2010, Mi, Liu et al. 2011, Muthu, Kulkarni et al. 2011, Wang, Sun et al. 2012). TPGS is able to function as a solubilizer, emulsifier, additive,

permeability enhancer as well as absorption enhancer (Dintaman and Silverman 1999, Yu, Bridgers et al. 1999). Additionally, TPGS is capable of overcoming multidrug resistance mediated by P-gp efflux pump (Dintaman and Silverman 1999, Varma and Panchagnula 2005, Constantinides, Han et al. 2006, Collnot, Baldes et al. 2007). As a stand-alone micellar formulation, the performance of TPGSs is affected by the molecular weight of PEG and the molar ratio of Vitamin E/PEG in the conjugates (Lu, Huang et al. 2013). Previously, our lab developed PEG_{5K}-VE_2 nanomicelles comprising one molecule of polyethylene glycol 5000 and two molecules of Vitamin E succinate, which demonstrated improved performance in formulating and delivering paclitaxel (PTX) over other TPGS micellar formulations ($TPGS_{5K}$, $TPGS_{2K}$ and PEG_{2K}-Vitamin E_2) (Lu, Huang et al. 2013). Nonetheless, this improved system still has limited drug loading capacity. This is likely due to the fact that loading of drugs into these micellar formulations is largely driven by hydrophobic interaction. Such mechanism of carrier/drug interaction, while working well for highly hydrophobic drugs, may show limited effectiveness for many moderately hydrophobic drugs. This limitation is also shared by many other existing micellar systems (Lu, Huang et al. 2013, Lu, Huang et al. 2013, Zhang, Lu et al. 2013, Chen, Zhang et al. 2014).

Recently, Park's group has demonstrated that inclusion of a hydrotropic molecule into the hydrophobic part of a block copolymer was able to improve the accommodation of drugs that are not entirely hydrophobic or lipophilic (Kim, Kim et al. 2010, Kim, Kim et al. 2011). This was mainly due to the additional mechanism of carrier/drug interaction rendered by the hydrotropic molecules introduced. Hydrotropes, small amphiphilic molecules, are capable of solubilizing hydrophobic compounds in aqueous solutions through hydrogen bonding. Incorporation of the

hydrotropic molecule into polymeric micelles led to improvement in both drug loading capacity and the colloidal stability of drug-formulated micelles.

We have recently shown that incorporation of a drug-interactive domain at the interfacial region of PEGylated lipopeptides resulted in a significant improvement in loading of hydrophobic drugs (Gao, Huang et al. 2013, Zhang, Lu et al. 2014). Among a number of functional motifs examined, fluorenylmethyloxycarbonyl (Fmoc), a commonly used amine protecting group in peptide chemistry, was found to be the most effective drug-interactive group in facilitating carrier/drug interaction (Gao, Huang et al. 2013). A PEGylated lipopeptide with a built-in Fmoc at the interfacial region was effective in formulating various types of therapeutic agents of diverse structures (Zhang, Lu et al. 2014). Delivery of PTX via this formulation led to significant inhibition of tumor growth in a murine breast cancer model (4T1.2) (Zhang, Lu et al. 2014).

This study is focused on the development of a new TPGS-based nanomicellar system with a built-in drug interactive motif, PEG_{5K}-Fmoc-VE_2. We hypothesized that incorporation of Fmoc at the interfacial region of PEG_{5K}-VE_2 shall greatly improve its performance in formulating and delivering hydrophobic anticancer agents. DOX was used as a model hydrophobic drug. Systematic comparison between PEG_{5K}-VE_2 and PEG_{5K}-Fmoc-VE_2 micelles was conducted with respect to the drug loading capacity and efficiency, stability, intracellular uptake, maximum tolerated dose, as well as *in vitro* and *in vivo* antitumor efficacy. Our data showed that PEG_{5K}-Fmoc-VE_2 was more effective than PEG_{5K}-VE_2 in forming stable mixed micelles with DOX. More importantly, DOX-loaded PEG_{5K}-Fmoc-VE_2 micelles exhibited significantly improved antitumor activity *in vivo*.

6.2 METHODS

6.2.1 Materials

Doxorubicin hydrochloride (98%) (DOX.HCl) was purchased from AK Scientific Inc. (CA, USA). Doxil was purchased from Avanti® Polar Lipids (AL, USA). Methoxy-$PEG_{5,000}$-OH, succinate anhydride, Boc-lys-(Boc)-OH, Fmoc-lys-(Boc)-OH, 3-(4,5-dimethylthiazol-2-yl)-2,5-diphenyl tetrazolium bromide (MTT), aspartic acid, trypsin-EDTA solution, Triton X-100, and Dulbecco's Modified Eagle's Medium (DMEM) were all purchased from Sigma-Aldrich (MO, USA). D-alpha-tocopherol was purchased from Tokyo Chemical Industry (OR, USA). N,N'-dicyclohexylcarbodiimide (DCC) was purchased from Alfa Aesar (MA, USA). 4-Dimethylaminopyridine (DMAP) was purchased from Calbiochem-Novabiochem Corporation (CA, USA). Fetal bovine serum (FBS) and penicillin-streptomycin solution were from Invitrogen (NY, USA). All solvents used in this study were HPLC grade.

6.2.2 Synthesis of PEG_{5K}-Fmoc-VE_2 and PEG_{5K}-VE_2

PEG_{5K}-VE_2 was synthesized as reported previously (Lu, Huang et al. 2013). PEG_{5K}-Fmoc-VE_2 was synthesized as follows: First, Fmoc-lys(Boc)-OH (4 eq.) was coupled to the terminal -OH of MeO-PEG_{5K}-OH with the assistance of DCC (4 eq.) and DMAP (0.2 eq.) in DCM overnight. The resulting PEG_{5K}-Fmoc-lys-(Boc) was washed and precipitated thrice by cold ethanol and ether, respectively. Boc group was then removed with 50% trifluoroacetic (TFA) acid in DCM for 2 h, and the resulting (PEG_{5K}-Fmoc-lys-NH_2) was precipitated by cold ethanol and ether thrice, respectively. Boc-lys(Boc)-OH (2 eq.) was then conjugated to the terminal -NH_2 of

PEG_{5K}-Fmoc-lys via DCC (2 eq.) and DMAP (0.1 eq.) as coupling reagents in DCM overnight. The PEG_{5K}-Fmoc-di-Boc obtained was precipitated and washed thrice with cold ethanol and ether, respectively. Boc groups in PEG_{5K}-Fmoc-di-Boc were removed by 50% TFA in DCM for 2 h, and the resulting (PEG_{5K}-Fmoc-di-NH_2) was purified via precipitation in cold ethanol and ether, respectively. Finally, Vitamin E succinate (4 eq.) was coupled onto the deprotected amino groups of PEG_{5K}-Fmoc-di-NH_2 with DCC (4 eq.) and DMAP (0.2 eq.) as coupling reagents in DCM overnight to produce PEG_{5K}-Fmoc-VE_2. The resulting PEG_{5K}-Fmoc-VE_2 was further purified via precipitation in cold ethanol and ether, respectively. The purified PEG_{5K}-Fmoc-VE_2 was dried under vacuum prior to use. The identity and purity of PEG_{5K}-Fmoc-VE_2 were confirmed by ^{1}NMR, MALDI-TOF and HPLC.

6.2.3 Preparation and characterization of DOX-loaded micelles

DOX·HCl was first neutralized by 3 molar eq. triethylamine in $CHCl_3$/MeOH (1:1. v:v) to eliminate HCl. PEG_{5K}-Fmoc-VE_2/DOX mixed micelles were prepared as described before (Lu, Huang et al. 2013). Briefly, PEG_{5K}-Fmoc-VE_2 (10 mM in $CHCl_3$) was mixed with DOX (10 mM in $CHCl_3$/MeOH) under different carrier/drug molar ratios. The mixture was first dried by nitrogen flow to form a thin dry film. The dry film was further dried under vacuum for 4 h to remove any traces of remaining solvent. The film was then reconstituted in saline without sonication. The micellar formulations were filtered through a 0.22 μm filter prior to characterization. The DOX-loaded PEG_{5K}-VE_2 micelles were similarly prepared as mentioned above. The mean diameter and size distribution of micelles with or without loaded drug were evaluated by dynamic light scattering (DLS). The morphology of DOX-free or DOX-loaded micelles was evaluated under TEM. The concentration of DOX in micelles was assessed by

HPLC-Fluorescence detection (Excitation: 490 nm; Emission: 590 nm). The drug loading capacity (DLC) and drug loading efficiency (DLE) were calculated according to the following formula:

DLC (%) = [weight of drug loaded/(weight of polymer in the nanomicelles without free DOX + weight of drug loaded)]

DLE (%) = (weight of loaded drug/weight of input drug) ×100%

6.2.4 DOX release kinetics

The cumulative release kinetics of DOX *in vitro* was conducted by dialysis technique using DPBS (PH = 7.4) containing 0.5% (w/v) Tween 80 as the release medium. Free DOX was utilized as a control. Two mL of DOX-loaded PEG_{5K}-VE_2 or PEG_{5K}-Fmoc-VE_2 micelles (1 mg DOX/mL) were sealed in dialysis tubes (MWCO = 12 KDa, Spectrum Laboratories). The dialysis tubes were immersed in 500 mL release medium in a beaker capped with parafilm. The beakers were kept in an incubator shaker at 100 rpm and 37°C. At predetermined time points, aliquots of samples were collected, diluted, and filtered through a 0.22 μm filter prior to analysis by HPLC with the detector set at 490 nm. Values were reported as the means from triplicate samples.

6.2.5 Fluorescence quenching studies

PEG_{5K}-VE_2/DOX and PEG_{5K}-Fmoc-VE_2/DOX were prepared at varying carrier to drug molar ratio as mentioned above. To examine fluorescence quenching of the carriers, the molar concentrations of carriers were kept constant for comparison. In another set of experiment, DOX

concentration was kept constant to examine the fluorescence quenching of DOX. The samples were placed into a 96-well plate, and the fluorescence intensity of carriers was recorded on a Synergy H1 Hybrid reader (BioTek), using an excitation wavelength of 270 nm and emission wavelength from 300-500 nm. The fluorescence intensity of DOX was examined using an excitation wavelength of 480 nm and emission wavelength from 510-650 nm.

6.2.6 UV absorbance spectroscopy of DOX

The absorption spectra were collected using Varian Cary 50 Bio UV-Visible Spectrophotometer over a wavelength ranging from 300 to 800 nm. PEG_{5K}-VE_2/DOX and PEG_{5K}-Fmoc-VE_2/DOX were prepared at a molar ratio of 2.5/1. All samples in distilled water were loaded into a quartz cell and measured against distilled water as the reference.

6.2.7 Fourier transform infrared spectroscopy (FT-IR)

FT-IR of DOX, DOX-loaded PEG_{5K}-VE_2, and DOX-loaded PEG_{5K}-Fmoc-VE_2 was evaluated using a VERTEX 70/70v FT-IR spectrometer (Bruker) to determine the hydrogen bonding of carrier/carrier and carrier/drug in the frequency of 4997-500 cm^{-1} (KBr pellet).

6.2.8 Hemolytic effect of PEG_{5K}-Fmoc-VE_2

The hemolytic activity of PEG_{5K}-Fmoc-VE_2 was examined using rat red blood cells (RBCs) following our published method (Lu, Huang et al. 2013).

6.2.9 Cell culture

Mouse breast cancer cell line, 4T1.2, human prostate cancer cell line, PC-3, and adriamycin (ADR)-resistant cell line, NCI/ADR-RES, were used in this work. All cell lines were cultured in DMEM containing 10% FBS and 1% penicillin-streptomycin in a humidified environment at 37 ℃ with 5% CO_2.

6.2.10 Animals

Male and female and nude mice of 6-8 weeks of age were purchased from Harlan (Livermore, CA). Female BALB/c mice of 10-12 weeks of age were purchased from Charles River (Davis, CA). All animals were housed under pathogen-free conditions according to AAALAC (Association for Assessment and Accreditation of Laboratory Animal Care) guidelines. All animal-related experiments were performed in full compliance with institutional guidelines and approved by the Animal Use and Care Administrative Advisory Committee at the University of Pittsburgh.

6.2.11 *In vitro* cytotoxicity

The cytotoxicity of DOX formulated in PEG_{5K}-VE_2 or PEG_{5K}-Fmoc-VE_2 was evaluated in 4T1.2, PC-3, and NCI/ADR-RES cell lines, in comparison to free DOX and Doxil. Briefly, cells were seeded in 96-well plates followed by overnight attachment. Then cells were treated by different DOX formulations of varied concentrations. Free PEG_{5K}-VE_2 or PEG_{5K}-Fmoc-VE_2, at concentrations equivalent to those of carriers in the corresponding DOX formulation groups, was

also added into cells. Cells were incubated for 72 h and cell viability was determined by MTT assay (Huang, Lu et al. 2012).

6.2.12 Intracellular uptake

3×10^5 NCI/ADR-RES cells/well were seeded into 6-well plates and incubated overnight prior to any treatment. Then cells were treated with free DOX, Doxil, and DOX-loaded PEG_{5K}-VE_2 and PEG_{5K}-Fmoc-VE_2, respectively at a DOX concentration of 6 μg/mL. Cells were then incubated for 1 h or 3 h at 37 ℃. After that, cells were washed three times with cold PBS and fixed with 4% paraformaldehyde for 30 min. The nuclei were then stained by Hoechst33342 for 5 min. Subsequently, cells were washed thrice with cold PBS. The intracellular uptake of DOX in various formulations was observed under confocal laser scanning microscopy (CLSM, FluoView 1000, Olympus, Japan).

Quantitative cellular uptake of various DOX formulations was evaluated by flow cytometry. Briefly, NCI/ADR-RES cells were prepared as described above. Following treatment with various DOX formulations at 37 ℃ for 1 h or 3 h, cells were washed with cold PBS thrice, and resuspended in 500 μL PBS prior to the flow cytometry analysis with CyAn™ ADP Analyzer (Beckman Coulter, Inc.). Cell-associated DOX was excited with an argon laser (480 nm), and fluorescence was detected at 570 nm. Twenty-thousand events were collected for each sample.

6.2.13 P-gp ATPase assay

The effect of PEG_{5K}-Fmoc-VE_2 conjugate on P-gp was investigated through examining its impact on a verapamil-stimulated ATPase activity as reported previously (Lu, Huang et al. 2013).

6.2.14 Near infrared fluorescence (NIRF) imaging

The tumor-targeting efficiency and biodistribution of PEG_{5K}-Fmoc-VE_2 *in vivo* was examined using a near infrared fluorescence dye, DiD. Nude mice bearing PC-3 xenograft were employed in this study. Two hundred μL of DiD-loaded PEG_{5K}-Fmoc-VE_2 (DiD concentration in the formulation was 0.4 mg/mL) was i.v. injected into each mouse. At different time points (0.5 h, 6 h, 24 h, 48 h, 72 h and 96 h) post-injection, mice were imaged under Carestream Molecular Imaging System (Carestream Health, Inc.) with the excitation at 630 nm and the emission at 700 nm using an exposure time of 60 s. After 96 h, mice were euthanized and tumors and major organs were excised and imaged with Carestream Molecular Imaging System. The tissue distribution of DiD in tumors and other organs was quantified by measuring the signal intensity at the region of interest.

6.2.15 Pharmacokinetics and biodistribution

PEG_{5K}-VE_2/DOX, PEG_{5K}-Fmoc-VE_2/DOX, and free DOX were administered i.v. at a dose of 5 mg DOX/kg in 200 μL saline (n = 3). At predetermined time points (3 min, 8 min, 15 min, 30 min, 45 min, 1 h, 2 h, 4 h, 8 h and 12 h), blood was obtained from mice using a heparinized

capillary tube. Plasma samples were isolated from the blood by centrifuging at 3000 rpm for 10 min. DOX in plasma was extracted via an extraction buffer (10% Triton X-100, deionized water, and isopropanol at a volumetric ratio of 1:2:15). The concentration of DOX at various time points was measured by HPLC with the detector set at 490 nm (Waters Alliance 2695 Separations Module combined with Waters 2998 Photodiode Array Detector, Waters Symmetry C18 5 μm 4.6*250 mm column, mobile phase: 80% MeOH:20% H_2O isocrate, flow rate: 0.6 mL/min). Pharmacokinetic parameters such as $t_{1/2}$, volume of distribution (V_d), area under the curve (AUC), and clearance (CL) were calculated by fitting the blood DOX concentrations to a non-compartment model using Phoenix WinNonlin.

For biodistribution study, free DOX and DOX-loaded micelles were i.v. injected into 4T1.2 tumor-bearing mice at a dose of 5 mg DOX/kg, respectively (n = 3). At 24 h post-injection, major organs (liver, spleen, lung, heart, and kidney), tumors, and blood were collected from the mice. Tissues were then homogenized utilizing a Power Gen 500 homogenizer (Fisher Scientific), in which 100 mg tissues were mixed with 900 μL extraction buffer, and DOX was extracted overnight at -20 °C. The samples were centrifuged at 3,000 rpm for 10 min, and the supernatant was then dried and dissolved in 400 μL 75% MeOH. Subsequently, the samples were further centrifuged at 14,500 rpm for 5 min to remove undissolved materials prior to HPLC measurement as mentioned above. The % injected dose and the % injected dose per gram (tissue) were calculated using the following equations:

% injected dose = (dose in blood or in tissue samples)/injected dose × 100%

% injected dose/g tissue = % injected dose/weight of tissue (g)

6.2.16 Maximum tolerated dose (MTD)

Groups of 3 female BALB/c mice were treated intravenously with free DOX (5, 10, and 15 mg DOX/kg), DOX-loaded PEG_{5K}-VE_2 (5, 10, 15, 20, and 30 mg DOX/kg) or DOX-loaded PEG_{5K}-Fmoc-VE_2 (10, 15, 20, 25, 30, and 35 mg DOX/kg), respectively. Changes in body weight and general signs, and survival of mice were followed daily for two weeks. The MTD was determined as the maximal dose that causes neither mouse mortality nor greater than 15% loss in body weight and other significant changes in the general movement and signs within the entire period of the experiment.

6.2.17 *In vivo* antitumor efficacy

Both drug-sensitive (4T1.2 and PC-3) and drug-resistant (KB 8-5) tumor models were used to evaluate the therapeutic effect of DOX formulated in PEG_{5K}-VE_2 and PEG_{5K}-Fmoc-VE_2 micelles. 4T1.2 is an aggressive syngeneic murine breast cancer model and PC-3 and KB 8-5 are human prostate and cervical cancer xenograft model, respectively.

In the breast cancer model, 1 x 10^5 4T1.2 cells in 200 μL PBS were inoculated s.c. at the right flank of female BALB/c mice. Various treatments were started when tumors reached a tumor volume around 50 mm^3 and this day was named as day 1. On day 1, mice were randomly divided into six groups (n = 5) and received i.v. administration of free DOX (10 mg DOX/kg), Doxil (10 mg DOX/kg), DOX-loaded PEG_{5K}-VE_2 (10 mg DOX/kg), DOX-loaded PEG_{5K}-Fmoc-VE_2 (10 mg DOX/kg), DOX-loaded PEG_{5K}-Fmoc-VE_2 (20 mg DOX/kg) and saline, respectively on days 1, 4, and 7. Tumor sizes were monitored with a digital caliper on days 1, 4, 7, 10, 12,15, 18, 21, and 25 and calculated based on the formula: $(L \times W^2)/2$, where L and W are length and

width of each tumor. To compare between groups, relative tumor volume (RTV) was calculated at each measurement time point (where RTV equals the tumor volume at a given time point divided by the tumor volume prior to first treatment). Mice were sacrificed if tumors reached 2000 mm^3 or developed ulceration. Tumor growth inhibition rate (IR) was also calculated and defined as following:

IR (%) = (1 – relative tumor volume in the treated group/relative tumor volume in the saline group) × 100%.

Furthermore, to monitor the systemic toxicity, the body weights of mice were measured at the time of tumor size measurement.

In PC-3 xenograft tumor model, 2×10^6 PC-3 cells in 200 μL PBS were inoculated s.c. at the right flank in male nude mice. Treatments were initiated when tumors in the mice reached a volume around 50 mm^3 and different groups (n = 6) were similarly treated as mentioned above on days 1, 4, and 7. Tumor size and body weight were monitored as described above.

In KB 8-5 xenograft tumor model, 5×10^6 cells were inoculated s.c at the right flank of female nude mice. When the tumor volume reached approximately 50 mm^3, 6 groups of mice (n = 5) were treated with saline, DOX (5 mg/kg), DOX (7.5 mg/kg), PEG_{5K}-VE_2/DOX (5 mg/kg), PEG_{5K}-Fmoc-VE_2/DOX (5 mg/kg), and PEG_{5K}-Fmoc-VE_2/DOX (7.5 mg/kg), respectively, on days 1, 4, and 7. Tumor size and body weight were monitored very three days.

6.2.18 Statistical analysis

In all statistical analyses, the significance level was set at a probability of $P < 0.05$. All results were reported as the mean ± standard deviation (SD) unless otherwise indicated. Statistical

analysis was performed by using the Student's t-test for two groups, and one-way ANOVA for multiple groups, followed by Newman-Keuls test if $P < 0.05$.

6.3 RESULTS AND DISCUSSION

6.3.1 Coupling of Fmoc motif to PEG_{5K}-VE_2 at the interfacial region

In an effort to improve the TPGS-based micellar formulation, we have previously synthesized and characterized four PEG- Vitamin E conjugates that vary in the molecular weight of PEG (2 vs 5K) and the molar ratio of PEG/Vitamin E (1/1 vs 1/2) (Lu, Huang et al. 2013). Our results showed that the conjugate with one molecule of PEG_{5K} and two molecules of Vitamin E (PEG_{5K}-VE_2) was most effective in formulating and delivering PTX to tumor cells *in vitro* and *in vivo*. In this study, Fmoc was incorporated into PEG_{5K}-VE_2 at the interfacial region to further improve the performance of this carrier. Our recent study has shown that Fmoc is a highly effective drug-interactive motif and that incorporation of this motif into lipid-core micelles greatly facilitates the carrier/drug interaction. The synthesis route of PEG_{5K}-Fmoc-VE_2 was presented in **Figure 49**.

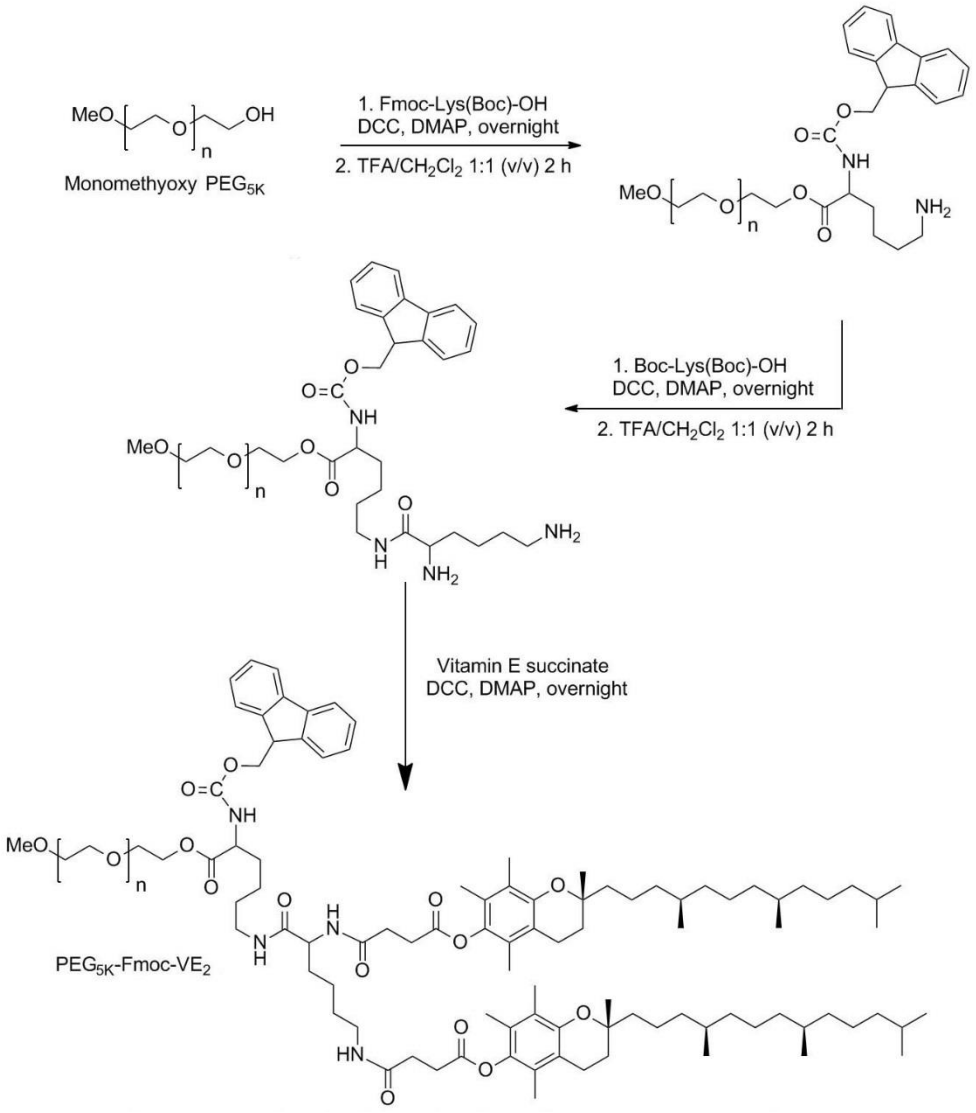

Figure 49 Synthetic route of PEG_{5K}-Fmoc-VE_2 conjugate.

Briefly, MeO-PEG_{5K}-OH was first reacted with Fmoc-lys-(Boc)-OH to yield PEG_{5K}-Fmoc-lys-(Boc) followed by the removal of Boc to expose the terminal NH_2. PEG_{5K}-Fmoc-lys-NH_2 was then coupled to Boc-lys-(Boc) to generate PEG_{5K}-Fmoc-di-Boc followed by the removal of Boc groups. Finally, Vitamin E succinate was conjugated to PEG_{5K}-Fmoc-di-NH_2 to produce PEG_{5K}-Fmoc-VE_2. The chemical identity of the final product was verified by ^{1}NMR (**Figure 50**) and MALDI-TOF (**Figure 51**). HPLC showed that the purity of the conjugate was 97.8% (**Figure 52**).

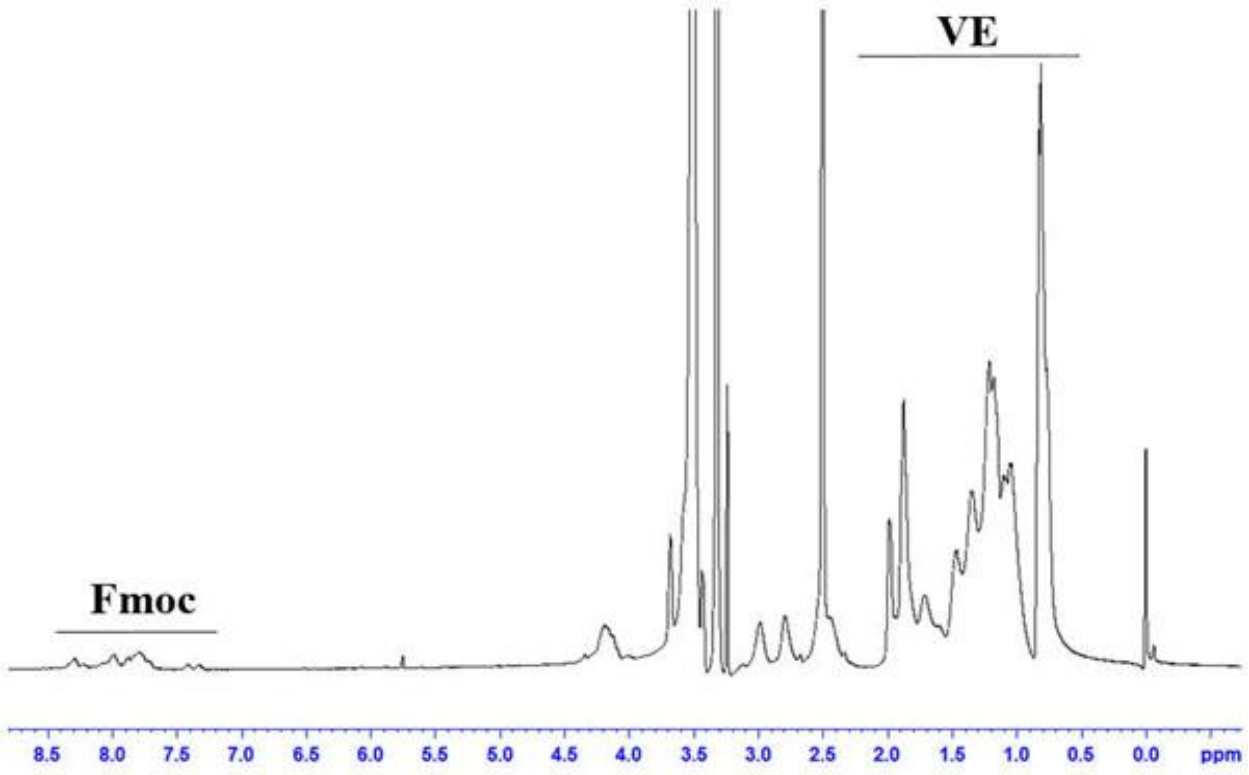

Figure 50 ^{1}H-NMR spectrum (400 MHz) of PEG_{5K}-Fmoc-VE_2 in DMSO.

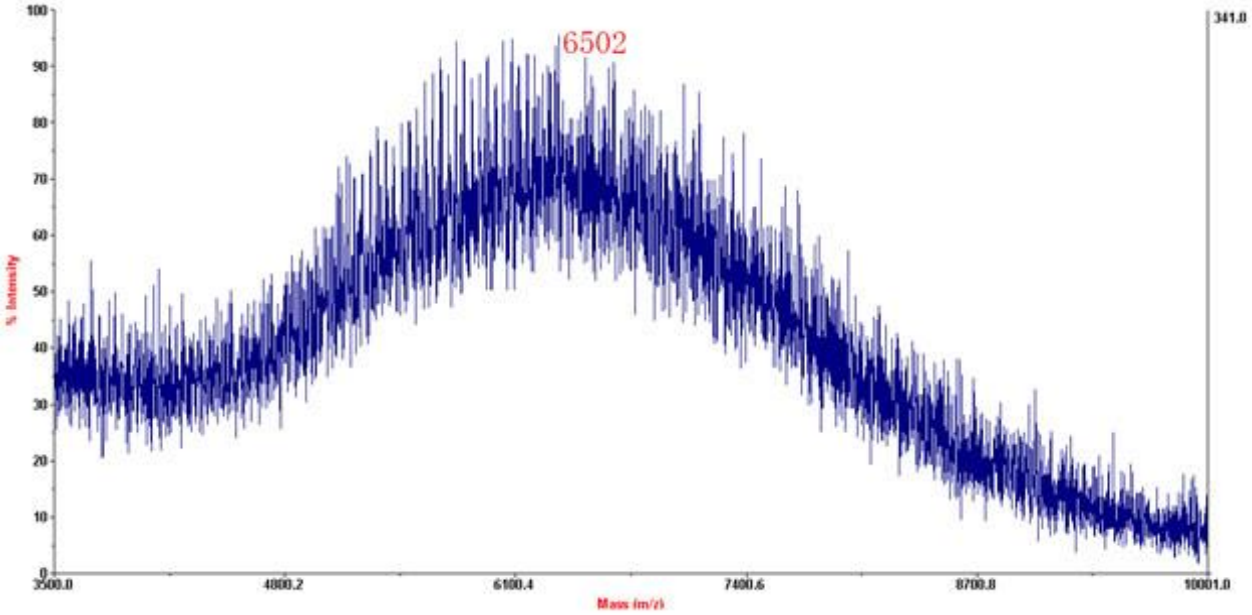

Figure 51 MALDI-TOF of PEG_{5K}-Fmoc-VE_2.

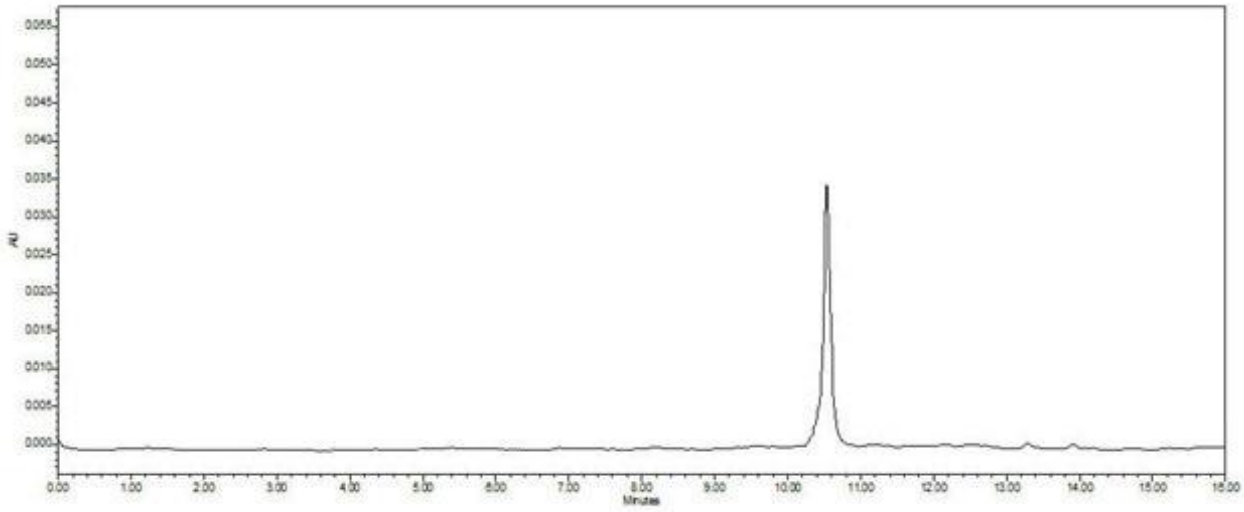

Peak	Migration Time	Area	% Area	Height
1	10.535	294912	97.8	34804
2	13.278	3070	1.02	491
3	13.916	3557	1.18	561

Purity = 97.8 %

System: Waters Alliance 2695 Separations Module combined with Waters 2475 Fluorescence detector
Column: Hibar 250-4 LiChrosorb RP-8 (5 micron) Sorbent Lot no. L59040432
HPLC Method: HPLC-Fluorescence detection (Excitation: 490 nm and Emission: 590 nm, Gain: 3, Sensitivity (FUFS): 10000)
Solvent: A: 5% Acetonitrile: 95% H_2O, containing 5 mM CH_3COONH_4, 0.1% (V/V) CH_3COOH, pH=3.55
B: Acetonitrile
A:B=1:1
Flow rate: 1.0 mL/min

Figure 52 HPLC trace of PEG_{5K}-Fmoc-VE_2.

6.3.2 Physicochemical characterizations of DOX-free and DOX-loaded PEG_{5K}-Fmoc-VE_2

In aqueous solution, PEG_{5K}-Fmoc-VE_2 readily self-assembled into elongated worm-like nanoassemblies with a particle size around 55 nm as determined by DLS analysis (**Figure 53**, **Table 17**).

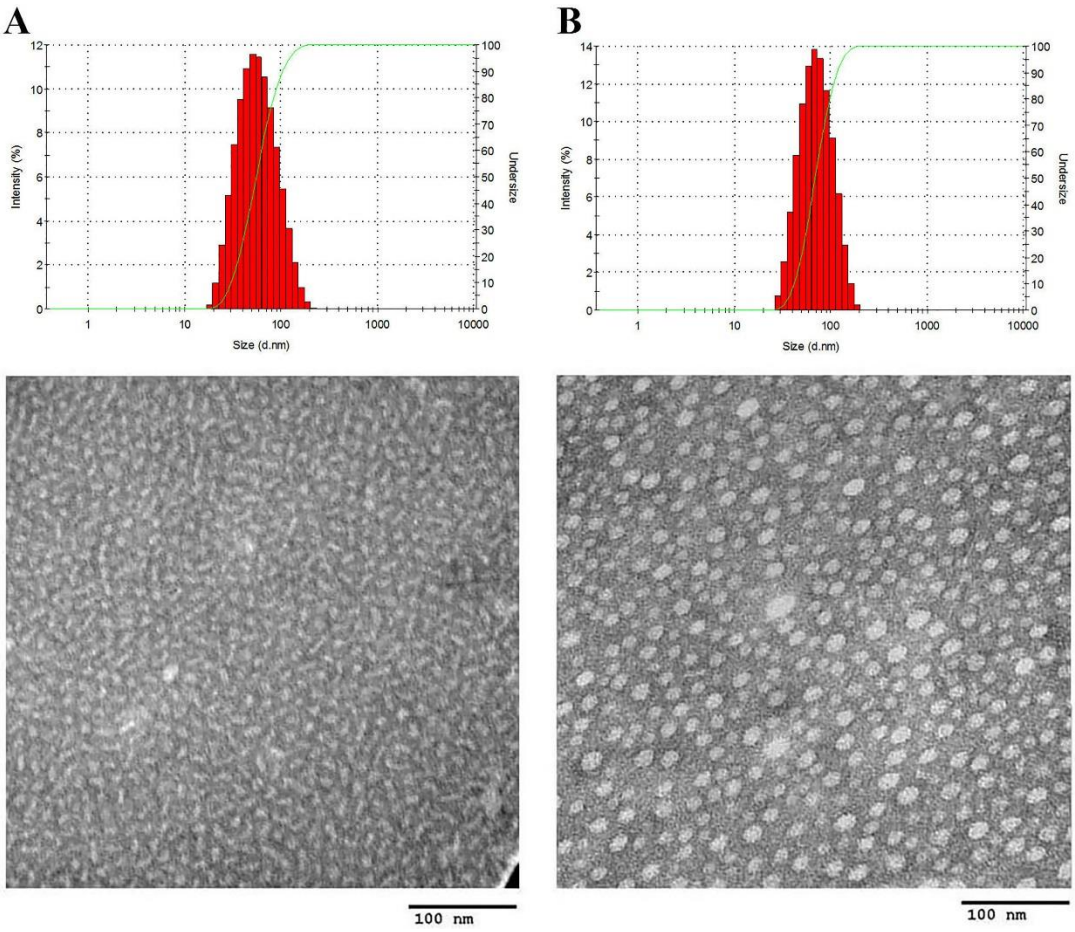

Figure 53 Size distribution and TEM of PEG_{5K}-Fmoc-VE_2 (A), and PEG_{5K}-Fmoc-VE_2/DOX (0.1:1 m/m) (B).

Table 17 Biophysical characterization of DOX-loaded PEG_{5K}-VE_2 or PEG_{5K}-Fmoc-VE_2.

	Molar ratios	Size	PDI	DLC (%)	DLE (%)
PEG_{5K}-VE_2	N/A	18.8±0.12	0.09	N/A	N/A
PEG_{5K}-VE_2:DOX	2.5:1	23.2±0.91	0.15	2.9	84.3
		24.5±0.17 (89 h later)	0.24		
PEG_{5K}-Fmoc-VE_2	N/A	55.0±0.84	0.12		
		50.5±1.42 (One month later)	0.23		
PEG_{5K}-Fmoc-VE_2:DOX	0.1:1	61.4±2.36	0.21	39.9	79.5
		62.4±1.83 (42 h later)	0.25		
	0.2:1	53.6±1.54	0.18	26.5	86.4
		56.8±1.87 (96 h later)	0.24		
	0.5:1	51.1±2.12	0.12	13.9	96.3
		52.7±1.89 (290 h later)	0.23		

This is in contrast to PEG_{5K}-VE_2 without Fmoc motif that formed typical spherical particles (**Figure 54**).

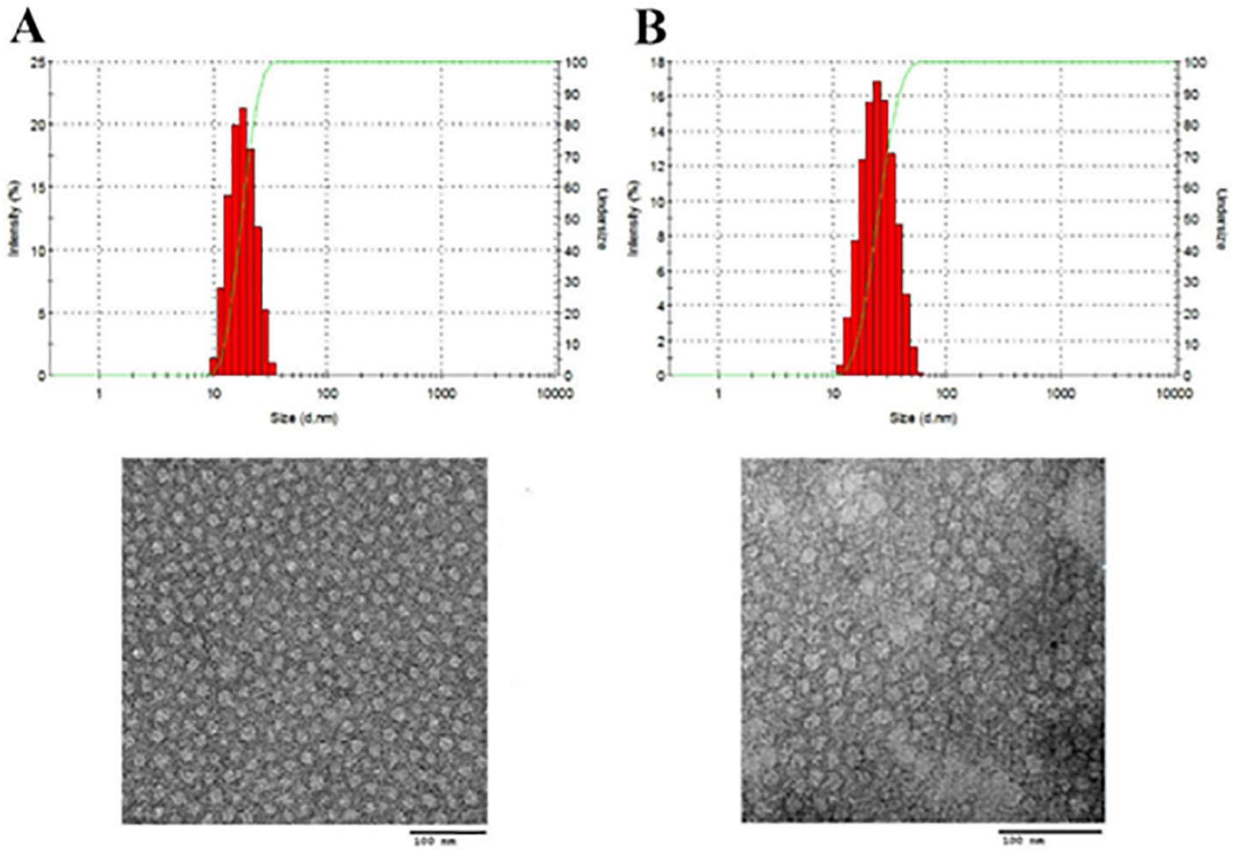

Figure 54 Size distribution and TEM of PEG_{5K}-VE_2 (A), and PEG_{5K}-VE_2/DOX (2.5:1 m/m) (B).

A similar result was found in a recent study with an Fmoc-containing PEG-lipopeptide (Zhang, Lu et al. 2014). The formation of the filamentous structure is likely attributed to the Fmoc-mediated strong interaction among the carrier molecules since Fmoc-containing peptides are known to self-assemble into nanofibers or nanotubues (Zhang, Gu et al. 2003, Jayawarna, Smith et al. 2007). However, in the case of Fmoc-containing PEG-lipopeptide, both lipid and Fmoc contributed to the formation of filamentous structure as the counterpart without lipid formed spherical structure (Zhang, Lu et al. 2014). It is likely that both the benzene ring and the alkane chain of Vitamin E are involved in the formation of filamentous structure.

Interestingly, following the incorporation of DOX into PEG_{5K}-Fmoc-VE_2, the morphology of the nanoparticles started to change drastically from filamentous (**Figure 53**) to spherical structure (**Figure 53**). This is likely due to the fact that the carrier/drug interaction impacted the interaction among the carrier molecules themselves following the incorporation of DOX, leading to the structural rearrangement. Both PEG_{5K}-VE_2 and DOX-loaded PEG_{5K}-VE_2 micelles were found to be spherical with a diameter around 20 nm (**Figure 54**).

Table 17 compares the DOX loading capacity (DLC) and efficiency (DLE) of PEG_{5K}-VE_2 and PEG_{5K}-Fmoc-VE_2. For PEG_{5K}-VE_2, a minimal carrier/drug molar ratio of 2.5/1 was needed to form stable mixed micelles with DOX. In contrast, only a carrier/drug ratio of 0.1/1 was needed for PEG_{5K}-Fmoc-VE_2 to form stable mixed micelles with DOX. At this ratio, the DLC for PEG_{5K}-Fmoc-VE_2 was 39.9% which is about 13-fold higher than that (2.9%) for PEG_{5K}-VE_2. Increasing the carrier/drug ratio was associated with a further increase in both DLE and the colloidal stability of the DOX-loaded micelles.

To confirm whether DOX was indeed incorporated into the PEG_{5K}-Fmoc-VE_2 nanoassemblies, ^{1}H-NMR studies were conducted for a number of samples including free DOX in D_2O, PEG_{5K}-Fmoc-VE_2 in D_2O or DMSO, and DOX formulated in PEG_{5K}-Fmoc-VE_2 in D_2O. The concentration of DOX was kept at 1 mg/mL. As shown in **Figure 55**, free DOX showed a ^{1}H NMR spectrum in D_2O that was consistent with data from literature (Wang, Wang et al. 2010).

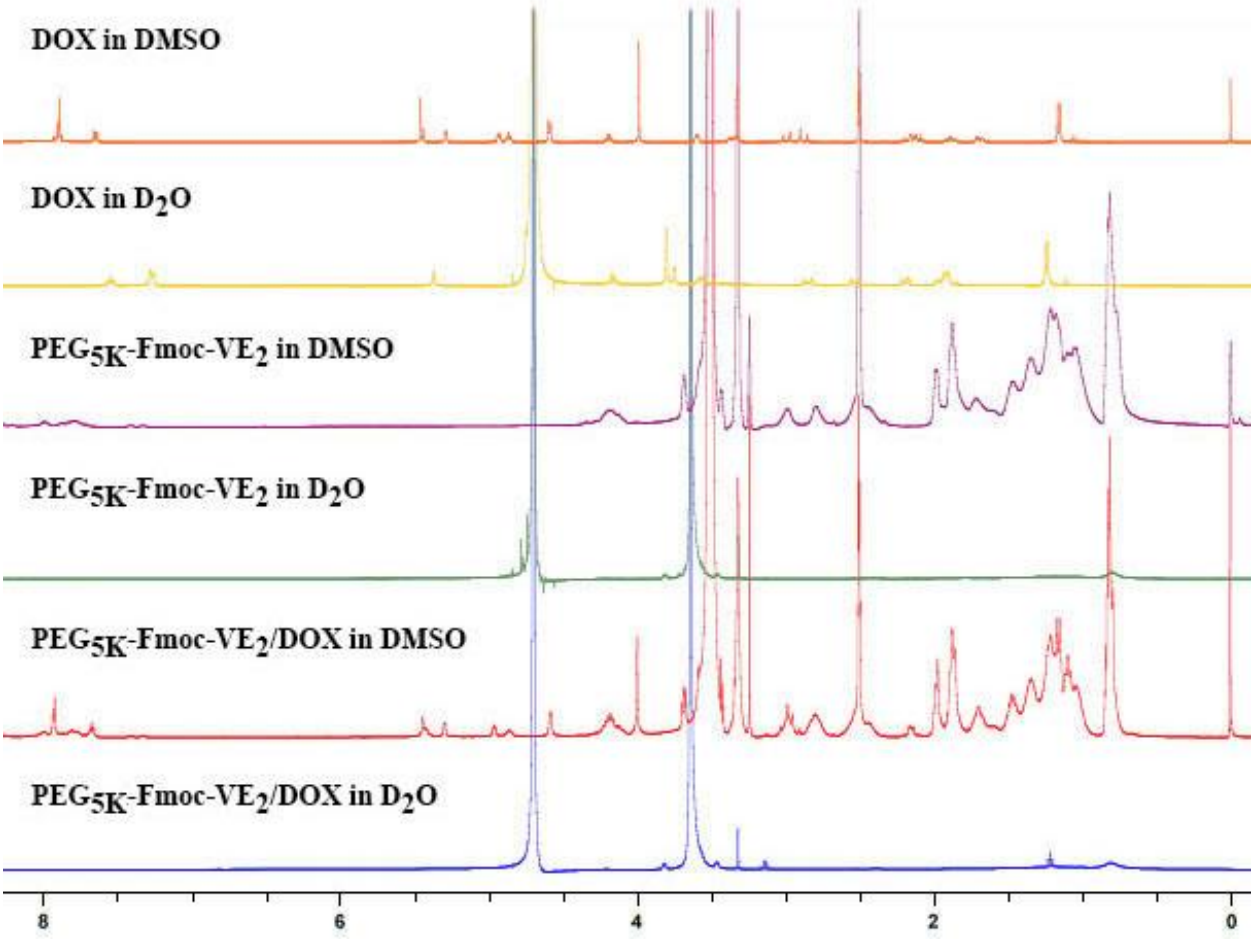

Figure 55 ^{1}H-NMR spectra of free DOX in D_2O, PEG_{5K}-Fmoc-VE_2 in D_2O or DMSO and DOX formulated in PEG_{5K}-Fmoc-VE_2 in D_2O or DMSO. Concentration of DOX was 1 mg/mL.

A ^{1}H-NMR spectrum was discerned for PEG_{5K}-Fmoc-VE_2 in DMSO that matched to its structure (**Figure 55**). However, when the ^{1}H NMR spectrum of PEG_{5K}-Fmoc-VE_2 was collected in D_2O, the VE signals (0.5-3 ppm) and Fmoc signals (7-8.5 ppm) were substantially suppressed (**Figure 55**). This could be ascribed to the self-assembling process of PEG_{5K}-Fmoc-VE_2, as VE and Fmoc are hydrophobic and aggregated inward, while the highly hydrophilic PEG is oriented outward into the water phase, resulting in the shielding of the signals of VE and Fmoc by PEG. Similarly, a shielding of VE and Fmoc signals was observed when PEG_{5K}-Fmoc-VE_2/DOX was examined in D_2O (**Figure 55**). In addition, the typical spectrum of DOX was barely visible, indicating that DOX was effectively encapsulated into the interior core of PEG_{5K}-Fmoc-VE_2 micelles.

6.3.3 DOX release kinetics *in vitro*

To further understand the stability of DOX-loaded nanomicelles, the *in vitro* release kinetics of DOX was evaluated with dialysis method using DPBS (PH = 7.4) containing 0.5% (w/v) Tween 80 as the release medium. Free DOX was employed as a control. As shown in **Figure 56**, PEG_{5K}-VE_2/DOX micelles exhibited significantly slower release kinetics over free DOX.

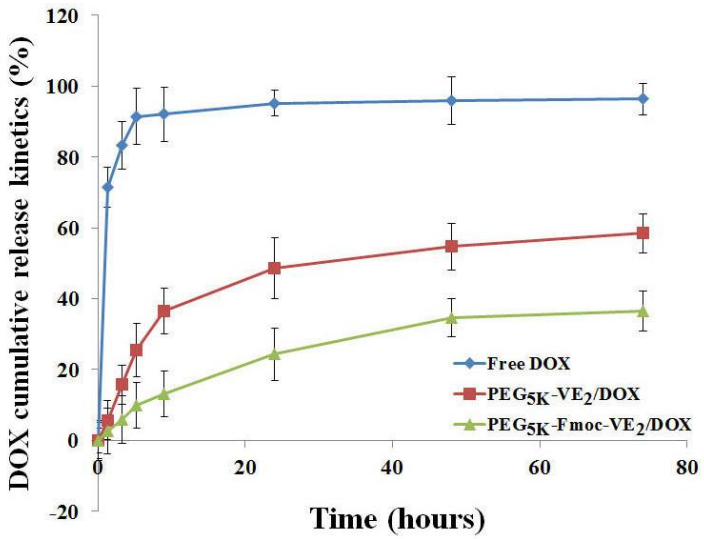

Figure 56 DOX cumulative release kinetics from free DOX, DOX-loaded PEG_{5K}-VE_2 and DOX-loaded PEG_{5K}-Fmoc-VE_2 micelles.

During the first 9 h, 92.14% of DOX was released in the free DOX group, which was substantially higher than that in PEG_{5K}-VE_2 micelles (36.57%). Notably, after introducing Fmoc group into PEG_{5K}-VE_2, the release rate of DOX was further reduced. In addition, there was essentially no initial burst release for DOX-loaded PEG_{5K}-Fmoc-VE_2 nanoassemblies. Furthermore, DOX formulated in PEG_{5K}-Fmoc-VE_2 exhibited significantly slower DOX release over PEG_{5K}-VE_2/DOX during the entire period. The amount of released DOX after 74 h was only 36.45% for PEG_{5K}-Fmoc-VE_2/DOX mixed micelles, which is significantly less than that for free DOX (96.35%) and PEG_{5K}-VE_2/DOX (58.44%). The significantly slower and controlled

release of DOX in DOX-loaded PEG_{5K}-Fmoc-VE_2 formulation may be attributed to the strong interactions between the carrier and DOX as well as among the carrier molecules themselves.

6.3.4 Mechanism of interacrions between carrier and payload

The significantly improved DLC of PEG_{5K}-Fmoc-VE_2 over PEG_{5K}-VE_2 suggests a role of Fmoc/DOX interaction in the formation of PEG_{5K}-Fmoc-VE_2/DOX mixed micelles. To test this hypothesis, we examined the Fmoc/DOX interaction via fluorescence quenching assay. As shown in **Figure 57**, there is a distinct fluorescence peak at 310 nm, which is consistent with the fluorescence spectrum of Fmoc (Mao, Zhang et al. 2006). Incorporation of DOX into PEG_{5K}-Fmoc-VE_2 led to a significant quenching of the fluorescence in a dose-dependent manner. **Figure 57B** shows the DOX fluorescence intensity at 595 nm before and after incorporation into PEG_{5K}-Fmoc-VE_2. Likewise, PEG_{5K}-Fmoc-VE_2 caused the quenching of DOX fluorescence in a dose-dependent manner. The quenching of either Fmoc or DOX fluorescence is likely due to the energy transfer triggered by the intermolecular π-π stacking interaction between the Fmoc motif and the aromatic rings of DOX.

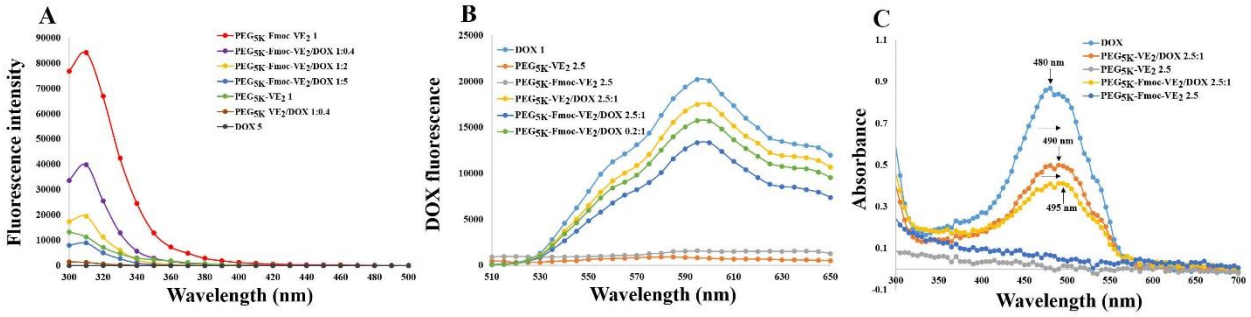

Figure 57 A: fluorescence intensity of the carriers. B: Fluorescence change of DOX. C: UV-absorbance of DOX.

We also noticed a fluorescence emission at 300 nm from PEG_{5K}-VE_2 (**Figure 57A**). This is likely attributed to the benzene ring in Vitamin E as no fluorescence emission was detected at this wavelength from a similar conjugate of PEG with two molecules of oleic acid (data not shown). Similarly, PEG_{5K}-VE_2 and DOX caused the quenching of the other's fluorescence in a dose-dependent manner (**Figure 57A& B**), suggesting that the benzene ring in Vitamin E is also involved in the carrier/DOX π-π stacking interaction, albeit to a lesser extent.

Figure 57C shows the UV-absorbance of free DOX and DOX formulated in PEG_{5K}-VE_2 or PEG_{5K}-Fmoc-VE_2 micelles. A clear red shift of DOX UV-absorbance was detected in both micellar formulations, particularly in PEG_{5K}-Fmoc-VE_2/DOX mixed micelles, further supporting the notion that π-π stacking contributed to the carrier/DOX interactions.

In addition to hydrophobic interaction and π-π stacking, hydrogen bonding is likely to be involved in the carrier (PEG_{5K}-VE_2 or PEG_{5K}-Fmoc-VE_2)/DOX interaction. The carbamate group in Fmoc, the amide bond in lysine, as well as the ester linkage in between Vitamin E and lysine could interact with the hydroxyl groups in DOX through hydrogen bonding. To test this hypothesis, FT-IR was employed to compare the hydrogen bonding in DOX-loaded micelles and that in carrier alone. As shown in **Figure 58B**, after subtracting the IR of PEG_{5K}-Fmoc-VE_2 from that of PEG_{5K}-Fmoc-VE_2/DOX, two peaks at 1637.1 cm^{-1} and 1754.3 cm^{-1} were detected. The reduction of absorbance at 1754.3 cm^{-1} and a simultaneous increase of absorbance at 1637.1 cm^{-1} suggest that incorporation of DOX led to disruption of the hydrogen bonding among carrier molecules themselves and, at the same time, the formation of new hydrogen bonding between carrier and DOX molecules. Similar results were found for PEG_{5K}-VE_2 micellar system (**Figure 58D**).

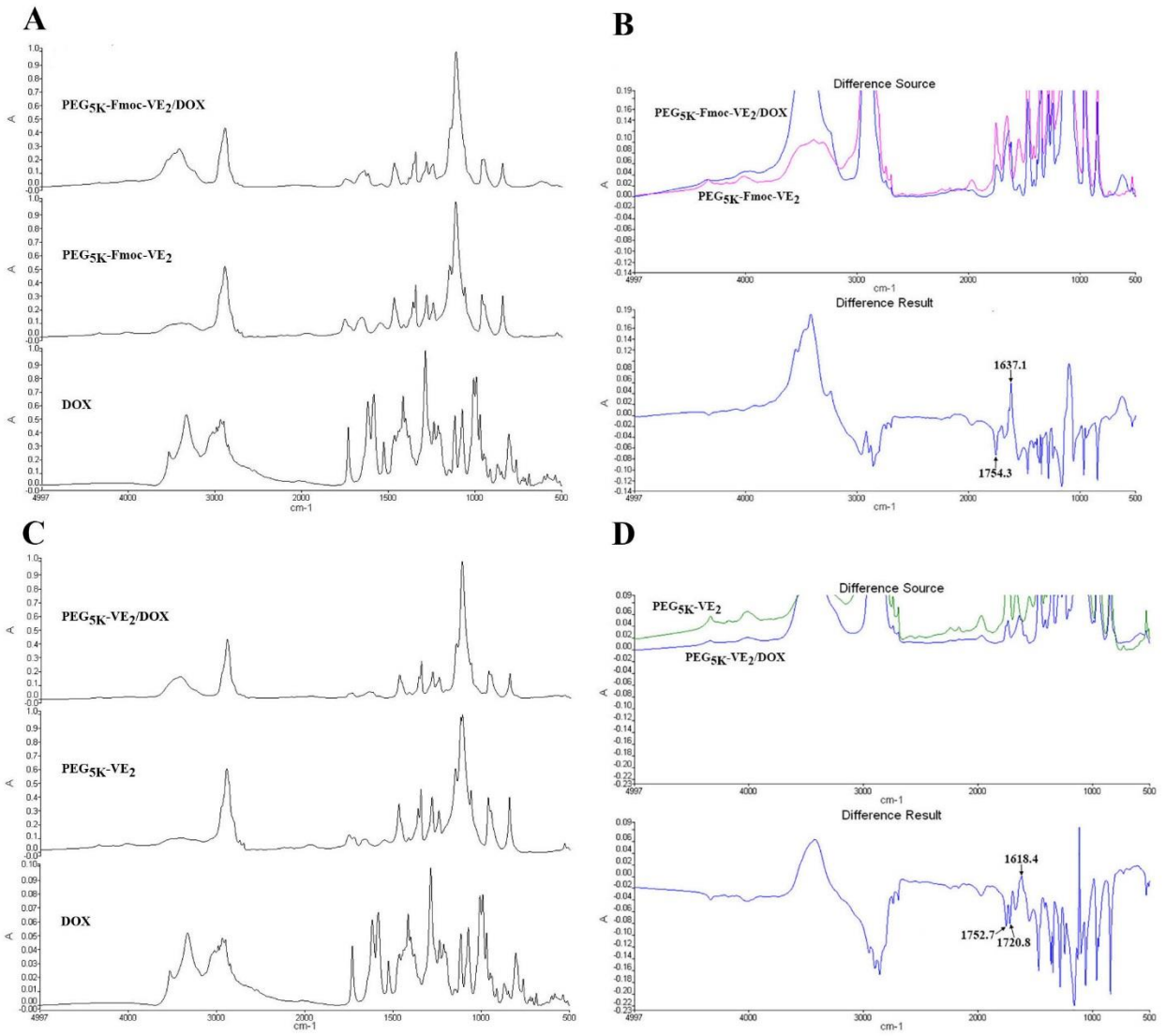

Figure 58 A: FT-IR of DOX, PEG_{5K}-Fmoc-VE_2, and PEG_{5K}-Fmoc-VE_2/DOX. B: Difference of FT-IR between PEG_{5K}-Fmoc-VE_2 and PEG_{5K}-Fmoc-VE_2/DOX. C: FT-IR of DOX, PEG_{5K}-VE_2, and PEG_{5K}-VE_2/DOX. D: Difference of FT-IR between PEG_{5K}-VE_2 and PEG_{5K}-VE_2/DOX.

6.3.5 Evaluation of the hemolytic activity of PEG_{5K}-Fmoc-VE_2

As an intravenous formulation, the potential hemolytic activity of PEG_{5K}-Fmoc-VE_2 micellar formulation needs to be addressed. **Figure 59** shows the result of a hemolysis assay.

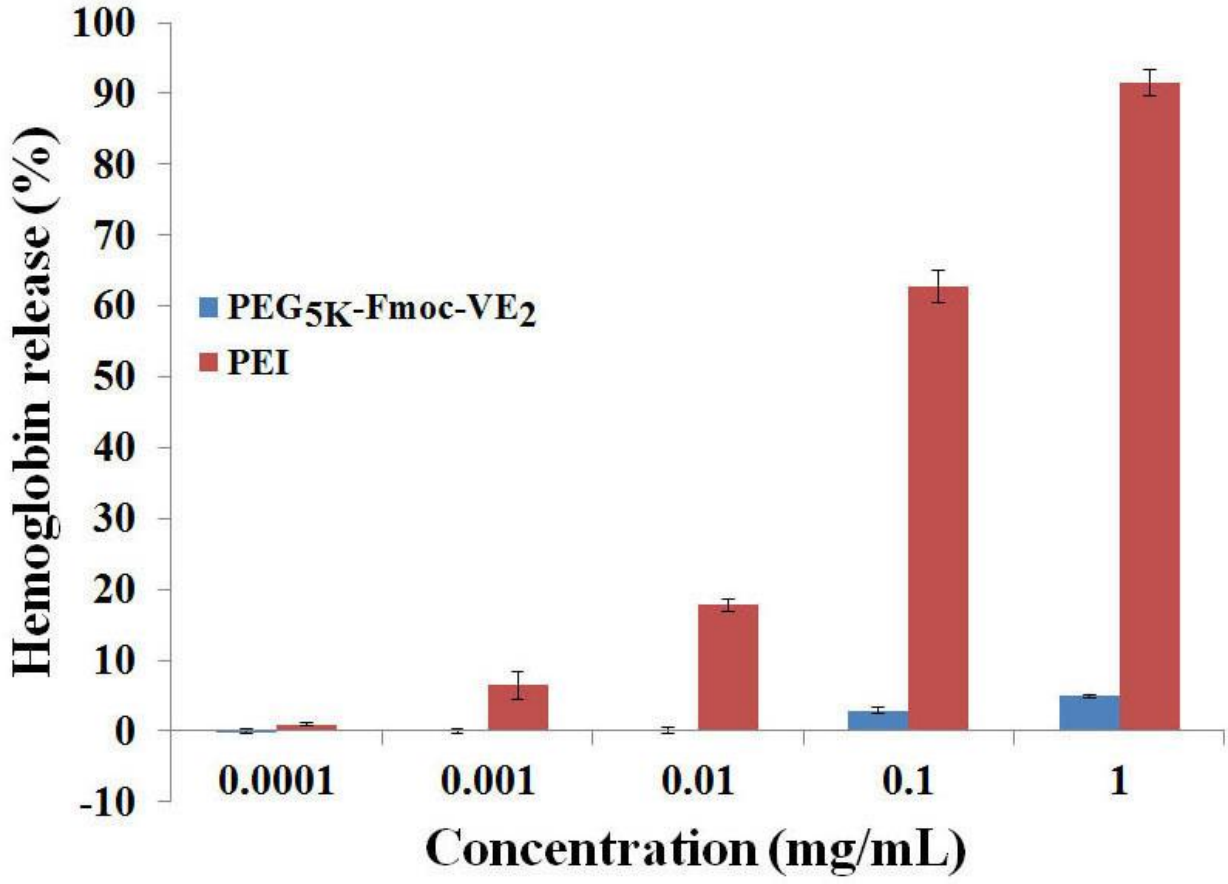

Figure 59 *In vitro* hemolysis assay of PEG_{5K}-Fmoc-VE_2 in comparison to PEI.

PEI, a cationic polymer with potent cell surface activity, was included as a positive control. Treatment with PEI led to significant hemolysis in a dose-dependent manner. At a concentration of 1 mg/mL, almost all of the red blood cells were lysed by PEI. In contrast, only negligible level of hemolysis was observed for PEG_{5K}-Fmoc-VE_2 even at the concentration of 1 mg/mL. The very low level of hemolytic effect of PEG_{5K}-Fmoc-VE_2 indicates that PEG_{5K}-Fmoc-VE_2 is a mild surfactant that can be safely administered intravenously.

6.3.6 *In vitro* cytotoxicity

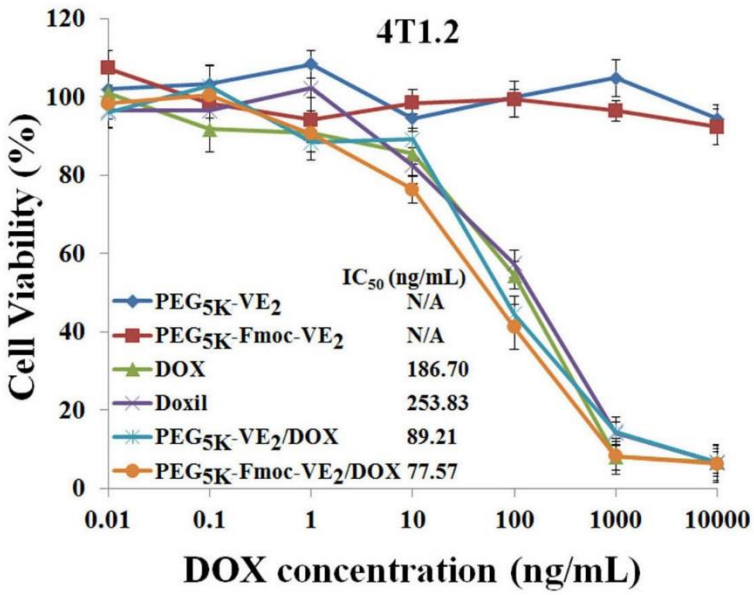

Figure 60 The cytotoxicity of PEG_{5K}-VE_2/DOX and PEG_{5K}-Fmoc-VE_2/DOX against mouse breast cancer cell line, 4T1.2, compared to DOX and Doxil.

Figure 60 shows the cytotoxic effect of different DOX formulations on murine breast cancer cells, 4T1.2. Cells were challenged by DOX, Doxil, PEG_{5K}-VE_2/DOX and PEG_{5K}-Fmoc-VE_2/DOX at various concentrations of DOX, and the cytotoxicity was determined by MTT assay 72 h later. A time- and concentration-dependent cell-killing effect was shown for all DOX formulations in 4T1.2 cells. The IC_{50} was 186.70, 253.83, 89.21, and 77.57 ng/mL for DOX, Doxil, PEG_{5K}-VE_2/DOX, and PEG_{5K}-Fmoc-VE_2/DOX, respectively. The higher levels of cytotoxicity for the two micellar DOX formulations were likely due to an increased cellular uptake of DOX and effective release following intracellular delivery (**Figure 60**). Doxil was slightly less active than free DOX, which is likely due to the ineffective release of DOX from the liposomes following intracellular delivery (Zhao, Alakhova et al. 2013).

6.3.7 Reversal of multidrug resistance

Drug resistance is one of the major factors involved in the failure of chemotherapy (Hu and Zhang 2009). Various mechanisms have been identified that are involved in the different types and/or stages of cancers (Gottesman 2002, Yuan, Li et al. 2008). One major mechanism involves the overexpression of P-glycoprotein (P-gp), which plays an important role in developing multiple drug resistance (MDR) (Tijerina, Fowers et al. 2000). P-gp, a member of ATP-binding cassette transporter, is one of the major drug efflux transporters and increased expression of P-gp leads to decreased drug accumulation in multidrug-resistant cells, and the development of resistance to anticancer drugs (Desai, Sawada et al. 2013). NCI/ADR-RES is a drug-resistant cell line that involves the overexpression of P-gp (Xu, Kang et al. 2004). Thus, following the evaluation of cytotoxicity of the different DOX formulations in 4T1.2 cells, their cytotoxicity was further examined in NCI/ADR-RES cells. As shown in **Figure 61**, the overall anti-proliferative effects of all DOX formulations were significantly reduced in NCI/ADR-RES cells compared to drug-sensitive cell line, 4T1.2 cells.

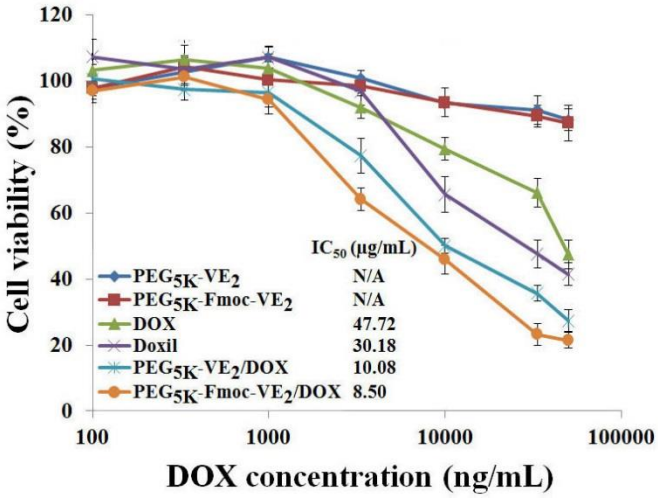

Figure 61 The anti-proliferative effect of PEG_{5K}-VE_2/DOX and PEG_{5K}-Fmoc-VE_2/DOX in a drug resistant cell line, NCI/ADR-RES, in comparison to DOX and Doxil.

This is somewhat expected considering the drug resistant nature of NCI/ADR-RES cells. It is also apparent that PEG_{5K}-Fmoc-VE_2/DOX exhibited a higher level of cytotoxicity than the

remaining DOX formulations in NCI/ADR-RES cells (**Figure 61**). More importantly, PEG_{5K}-Fmoc-VE_2/DOX was 5.6-times as effective as free DOX in NCI/ADR-RES cells, which represents a more dramatic improvement of cytotoxicity over free DOX compared to that (2.4-times) in 4T1.2 cells. It is also worth noting that Doxil was more active than free DOX in NCI/ADR-RES cells, which is in contrast to what was shown in 4T1.2 cells. These data suggested that both PEG_{5K}-Fmoc-VE_2 and Doxil formulations were capable of partially reversing the drug resistance in NCI/ADR-RES cells.

To examine whether the improved cytotoxicity of DOX-loaded PEG_{5K}-Fmoc-VE_2 was due to the enhanced intracellular delivery of DOX, DOX uptake was evaluated in NCI/ADR-RES cells following treatment of different DOX formulations. **Figure 62A** shows the fluorescence images of cells 1 h following the different treatments.

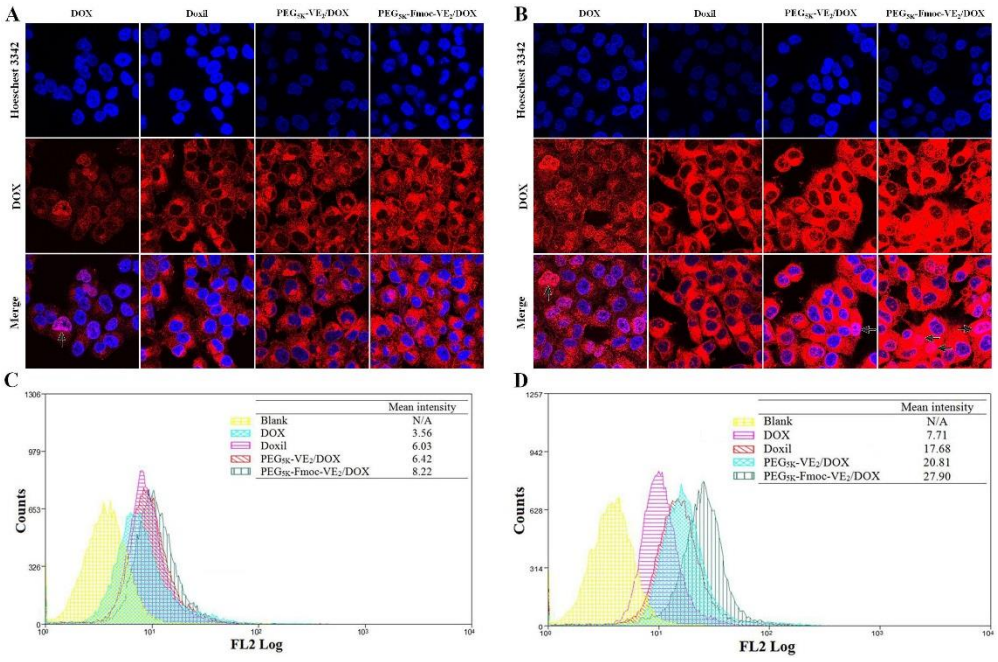

Figure 62 Confocal laser scanning microscopy (CLSM) images of NCI/ADR-RES cells incubated with free DOX, Doxil, PEG_{5K}-VE_2/DOX and PEG_{5K}-Fmoc-VE_2/DOX for 1 h (A) and 3 h (B); Quantitative analysis of uptake of different DOX formulations in NCI/ADR-RES cells after 1 h (C) and 3 h (D) treatment using flow cytometry. Arrows indicated the area that was co-localized by DOX.

Least amounts of fluorescence signals were observed in the cells treated with free DOX, which could be attributed to the free accessibility of DOX by P-gp efflux transporter that is overexpressed in NCI/ADR-RES cells. Cells treated with Doxil showed increased fluorescence signals compared to free DOX group. This was consistent with the report that liposomal DOX was able to bypass the drug transport in MDR cells (Ogawara, Un et al. 2009). It is also apparent that cells treated with PEG_{5K}-Fmoc-VE_2/DOX showed the strongest fluorescence signals. Similar results were shown in cells treated with different DOX formulation for 3 h (**Figure 62B**). The DOX uptake efficiency was further quantified by flow cytometry (**Figure 62C & D**). The data were consistent with what was found in confocal imaging. Cells treated with PEG_{5K}-Fmoc-VE_2/DOX provided the highest level of cell-associated fluorescence signals. Endocytosis is likely to be involved in the cellular uptake of micellar DOX as punctuated distribution was visualized for both micellar formulations. More studies will be conducted in the future to further elucidate the mechanism of cellular uptake of PEG_{5K}-Fmoc-VE_2/DOX.

The more effective DOX accumulation in cells treated with PEG_{5K}-Fmoc-VE_2/DOX is likely attributed to the stable mixed micelles as a result of strong carrier/DOX interaction as discussed earlier. This will minimize the release of DOX from the micelles before they are taken up by the tumor cells. On the other hand, PEG_{5K}-Fmoc-VE_2 may facilitate the intracellular accumulation of DOX via inhibiting the function of P-gp. $TPGS_{1K}$ is a well-known inhibitor of P-gp via directly inhibiting the activity of P-gp ATPase. We hypothesized that PEG_{5K}-Fmoc-VE_2 shall possess a similar biological activity considering the structural similarity between TPGS and PEG_{5K}-Fmoc-VE_2. To test this hypothesis, the effect of PEG_{5K}-Fmoc-VE_2 on P-gp activity was evaluated via examining its impact on verapamil-stimulated P-gp ATPase activity (**Figure 63**).

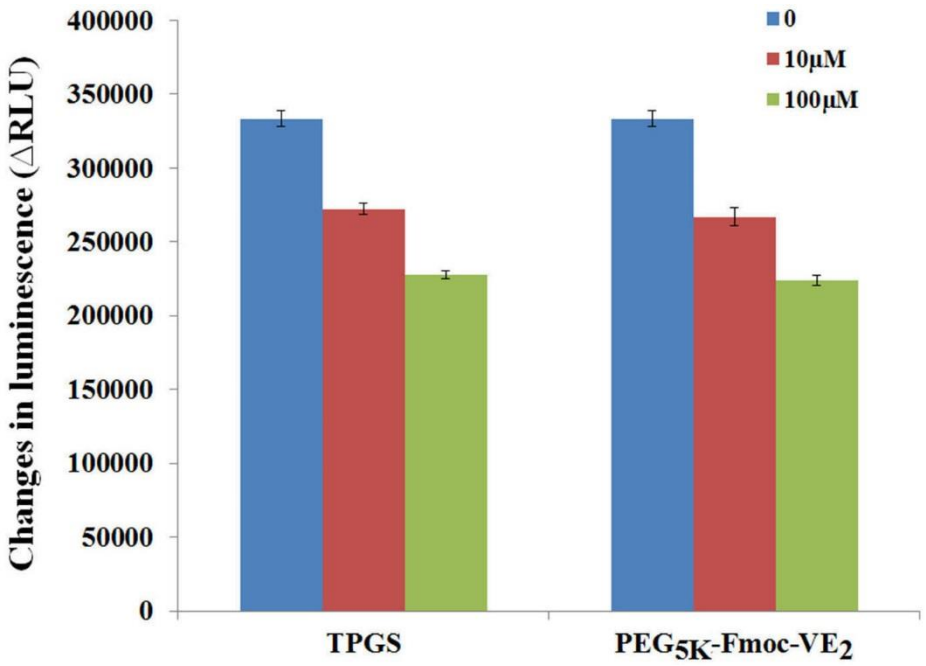

Figure 63 Inhibitory effect of TPGS and PEG_{5K}-Fmoc-VE_2 on verapamil-stimulated P-gp ATPase activity.

$TPGS_{1k}$ was utilized as a positive control. ΔRLU represents the consumption of ATP in the system. As expected, $TPGS_{1k}$ treatment led to a decrease of ΔRLU in a dose-dependent fashion. Importantly, PEG_{5K}-Fmoc-VE_2 showed a level of inhibition on P-gp ATPase activity that was comparable to that of $TPGS_{1K}$. The mechanism for the inhibition of P-gp ATPase by PEG_{5K}-Fmoc-VE_2 is not clearly understood at present. PEG_{5K}-Fmoc-VE_2 may be a substrate for ATPase and compete directly with other substrates for the binding to ATPase. In addition, PEG_{5K}-Fmoc-VE_2 may bind to the ATPase-substrate complex, limiting the effectiveness of ATPase to hydrolyze ATP. More studies are underway to fully unveil the details on how PEG_{5K}-Fmoc-VE_2 inhibits P-gp ATPase activity. It should be noted that, in addition to DOX, there are many other potent chemotherapeutics that are the substrates of P-gp, such as camptothecin and paclitaxel. Therefore, PEG_{5K}-Fmoc-VE_2 may hold a promise to improve the effectiveness of these therapeutic agents as well.

6.3.8 Near infrared fluorescence imaging

The ability of PEG_{5K}-Fmoc-VE_2 for targeting tumors was investigated in nude mice bearing PC-3 xenograft, using a hydrophobic near infrared fluorescence (NIRF) dye, DiD. Two hundred µL of PEG_{5K}-Fmoc-VE_2 nanoparticles containing DiD was intravenously injected into a mouse bearing bilateral PC-3 tumors. Fluorescence signals were observed in tumor areas as early as 6 h post-injection, which peaked around 24 h and retained at a significant level for 96 h (**Figure 64A**).

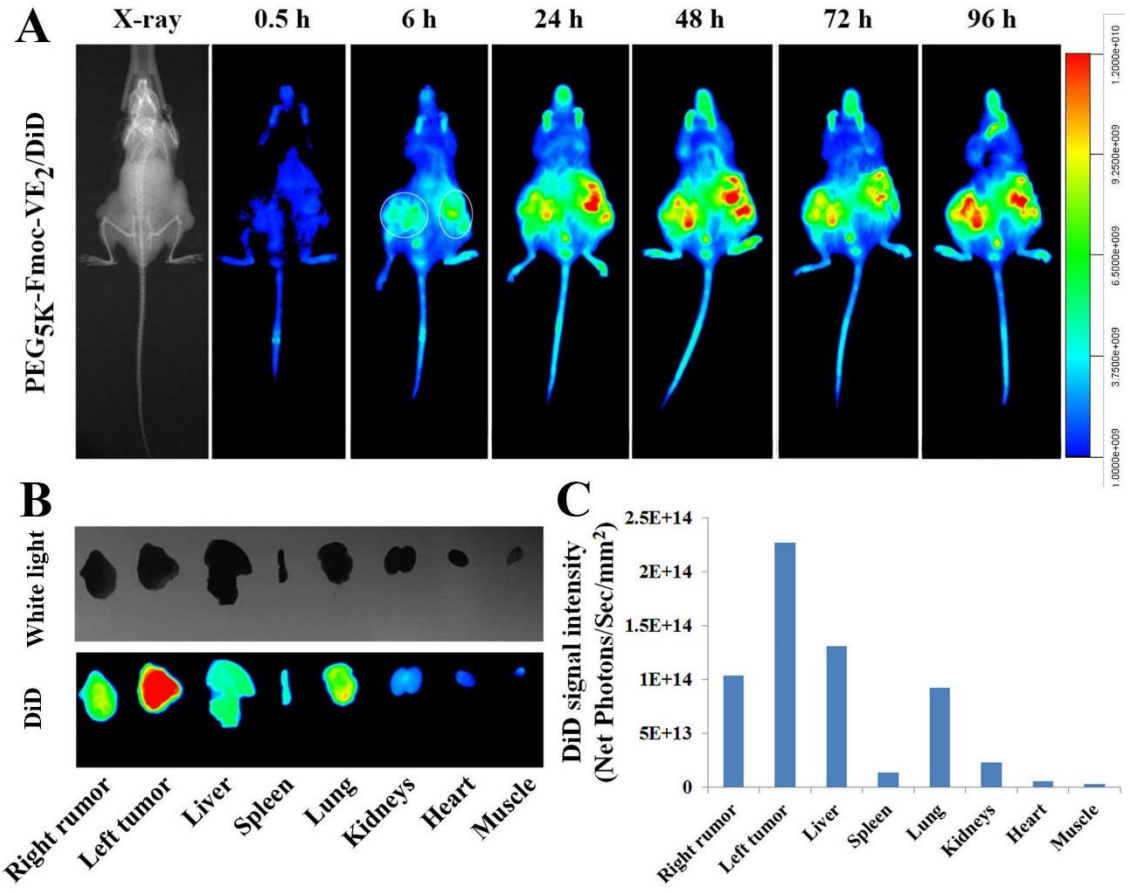

Figure 64 *In vivo* (A) and *ex vivo* (B) NIRF optical images of PC-3 tumor-bearing nude mice administered intravenously with DiD-loaded PEG_{5K}-Fmoc-VE_2 nanoparticles. Tumors and major organs were excised for *ex vivo* imaging at 96 h post-injection and the quantitated DiD fluorescence intensity from different organs were presented (C).

Following the last imaging at 96 h post-injection, mice were sacrificed and tumors and major organs were excised, imaged and quantified using a Carestream Molecular Imaging System (**Figure 64B**). Intense fluorescence signals were observed in tumors for DiD-loaded PEG_{5K}-Fmoc-VE_2. Moderate levels of fluorescence signals were also discerned in liver and lungs, which was due to the nonspecific clearance of foreign particles via the RES. **Figure 64C** showed the quantified fluorescence intensity for different organs, which was consistent with the observation in **Figure 64B**. The effective tumor accumulation of PEG_{5K}-Fmoc-VE_2/DiD could be ascribed to its excellent stability endowed by the strong carrier/DiD and carrier/carrier interactions. PEG on the surface of the carrier can also provide shielding effect against opsonins. Furthermore, the very small sizes of PEG_{5K}-Fmoc-VE_2/DiD nanoparticles shall facilitate the extravasation and deep penetration into the tumor tissues (Li, Xiao et al. 2010, Luo, Xiao et al. 2010).

6.3.9 *In vivo* DOX pharmacokinetics and biodistribution

The DOX blood kinetics as a function of time following i.v. bolus administration of DOX, DOX-loaded PEG_{5K}-VE_2 and DOX-loaded PEG_{5K}-Fmoc-VE_2 was illustrated in **Figure 65A.** It is apparent that the DOX-loaded PEG_{5K}-Fmoc-VE_2 showed the highest level of DOX retention in circulation in comparison to free DOX and DOX-loaded PEG_{5K}-VE_2. Meanwhile, the pharmacokinetic parameters, obtained by fitting the data to a non-compartment model, were outlined in **Table 18**. Incorporation of DOX into PEG_{5K}-VE_2 micelles resulted in a significantly greater $t_{1/2}$, AUC, and C_{max} over free DOX. However, these parameters were further improved in DOX-loaded PEG_{5K}-Fmoc-VE_2 nanomicelles.

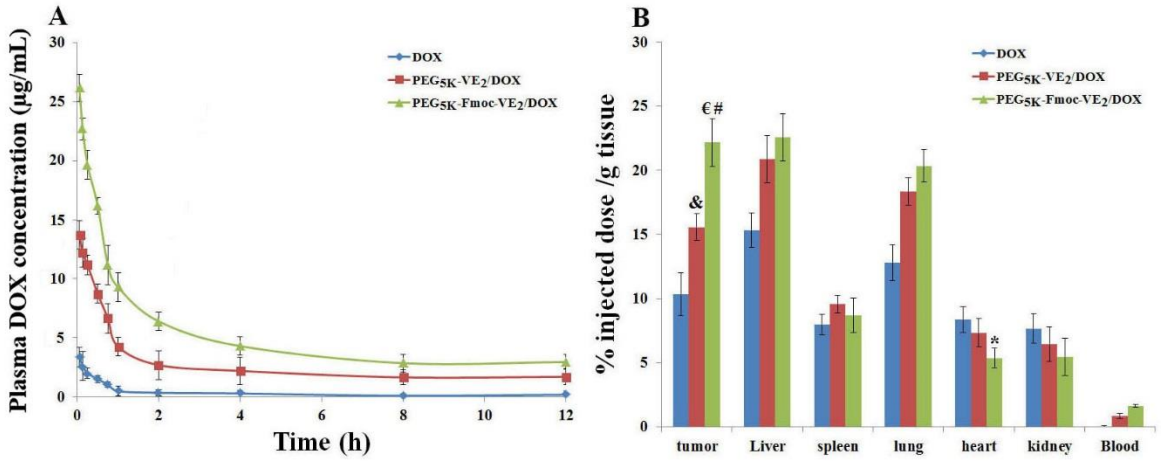

Figure 65 DOX pharmacokinetics (A) and biodistribution profiles (B) in 4T1.2-tumor bearing mice receiving intravenous administration of different DOX formulations at the dose of 5mg/kg. *p < 0.05, compared to DOX and PEG_{5K}-VE_2/DOX; $^{€}p$ < 0.005, compared to DOX; $^{\#}p$ < 0.01, compared to PEG_{5K}-VE_2/DOX; $^{\&}p$ < 0.01, compared to DOX.

Table 18 Pharmacokinetics of DOX in different formulations.

	$t_{1/2}$ (h)	AUC (μg/mL×h)	CL (mL/h)	C_{max} (μg/mL)	V_d (mL)
DOX	4.20±0.35	5.43±0.11	18.40±2.39	3.64 ±0.30	25.32±2.15
PEG_{5K}-VE_2/DOX	14.89±2.08	70.58±6.68	1.47±0.15	14.51±1.39	6.26±0.43
PEG_{5K}-Fmoc-VE_2/DOX	19.41±1.76	104.36±11.52	0.72±0.055	27.62±2.60	3.29±0.24

The $t_{1/2}$, AUC, and C_{max} of DOX in PEG_{5K}-Fmoc-VE_2/DOX were 3.62, 18.22, and 6.59-folds higher, respectively, than those of free DOX. In contrast, V_d and CL for PEG_{5K}-Fmoc-VE_2/DOX were significantly lower than those for free DOX and PEG_{5K}-VE_2/DOX. Taken together, these data demonstrated that DOX formulated in PEG_{5K}-Fmoc-VE_2 micelles was able to circulate for a significantly longer period of time in blood.

Next we went on to investigate whether our PEG_{5K}-Fmoc-VE_2/DOX formulation can improve the DOX biodistribution profile in tumor-bearing mice. Different DOX formulations were i.v. administered to 4T1.2 tumor-bearing mice at a DOX dosage of 5 mg/kg. Twenty-four h following the injection, blood, tumors, and major organs were collected for the quantification of DOX. Compared to free DOX, there were significantly greater amounts of DOX accumulated in tumors for both types of DOX nanomicelles (**Figure 65B**), which was attributed to the EPR effect of micellar formulations. We also noticed that DOX formulated in PEG_{5K}-Fmoc-VE_2

micelles was more effective in tumor accumulation compared to the counterpart without Fmoc motif (**Figure 65B**). This is likely attributed to a better stability of PEG_{5K}-Fmoc-VE_2/DOX mixed micelles in the blood due to the enhanced carrier/drug interaction as discussed before. In addition, the presence of Fmoc may help improve the carrier stability via imposing steric hindrance against the degrading enzymes in the blood. Indeed, PEG_{5K}-Fmoc-VE_2 is less sensitive to esterase-mediated cleavage than the counterpart without an Fmoc motif (**Figure 66**) in an *in vitro* study.

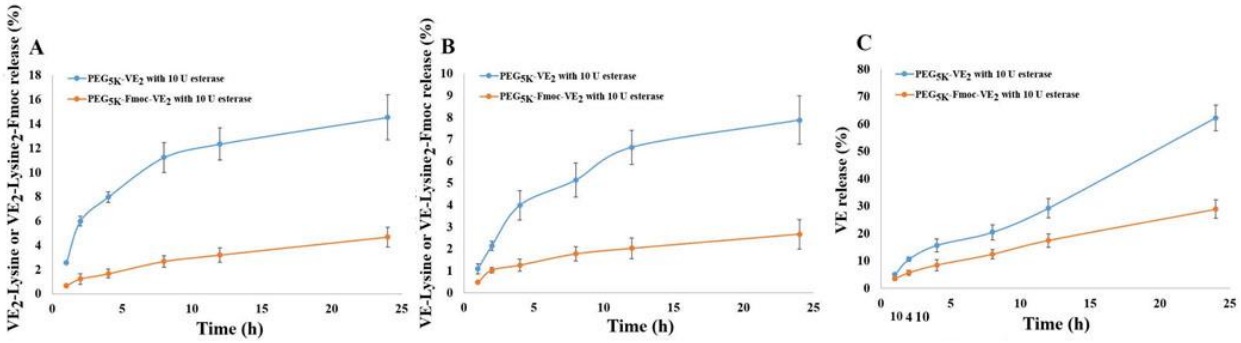

Figure 66 Stability test of PEG_{5K}-VE_2 and PEG_{5K}-Fmoc-VE_2 in the presence of esterase.

The improved stability of PEG_{5K}-Fmoc-VE_2/DOX mixed micelles may contribute significantly to a longer $t_{1/2}$ in the blood (**Table 18**) and thus increased chance for passive accumulation at tumor tissues via EPR effect.

Relatively high levels of DOX uptake were also observed in liver and lung, which was due to the nonspecific uptake of particles by these tissues. Importantly, heart distribution of DOX was significantly reduced in PEG_{5K}-Fmoc-VE_2/DOX compared with free DOX and PEG_{5K}-VE_2/DOX. This is significant considering that cardiotoxicity is a major adverse effect associated with the application of DOX in clinic. This will allow higher dose of DOX to be used to maximize the therapeutic effect.

6.3.10 Maximum tolerated dose (MTD)

To examine whether the significantly improved stability of PEG_{5K}-Fmoc-VE_2/DOX will lead to reduced systemic toxicity *in vivo*, MTD of various DOX formulations was assessed in tumor-free mice (**Table 19**).

Table 19 MTD of DOX and DOX-loaded nanomicellar formulations.

Formulations	Does (mg/kg)	Animal death	Weight loss (%)
DOX	5	0/3	2.2
	10	0/3	7.8
	15	2/3	N/A
DOX-loaded PEG_{5K}-VE_2	5	0/3	0.9
	10	0/3	-1.8
	15	0/3	3.9
	20	0/3	6.2
	30	3/3	N/A
DOX-loaded PEG_{5K}-Fmoc-VE_2	10	0/3	-2.2
	15	0/3	0.2
	20	0/3	-1.3
	25	0/3	3.5
	30	0/3	7.4
	35	2/3	N/A

Mice were treated with i.v. bolus injection of different doses of free DOX, PEG_{5K}-VE_2/DOX and PEG_{5K}-Fmoc-VE_2/DOX followed by observation of changes in body weight and other general signs of toxicity. As shown in Table 19, no significant toxicity was noticed for free DOX group at a dosage of 10 mg DOX/kg. Increasing the dosage to 15 mg/kg led to the death of 2 out of 3 treated mice. Therefore, the MTD for free DOX at a single injection was around 10 mg/kg, which was consistent with the literature (Xiao, Luo et al. 2011). PEG_{5K}-VE_2/DOX was well tolerated at a dosage of 20 mg/kg: no significant changes were observed in the general appearance or activity other than 6.2% weight loss. Increasing the DOX dose to 30 mg/kg resulted in the death of all 3 treated mice, suggesting that the single i.v. MTD for DOX-loaded PEG_{5K}-VE_2 micelles was around 20 mg DOX/kg, which was a 2-fold increase over free DOX. PEG_{5K}-Fmoc-VE_2/DOX showed a lowest level of toxicity with a MTD around 30 mg/kg, which was 3-fold and 1.5-fold increase over free DOX and PEG_{5K}-VE_2/DOX, respectively. The improved MTD of DOX-loaded PEG_{5K}-Fmoc-VE_2 is likely attributed to a slower and sustained

DOX release kinetics (**Figure 56**) due to the enhanced stability, which will liberate its payload gradually instead of a bursting release; as such, the toxicity will be better tolerated. In addition, it has been shown that Vitamin E and Fmoc both have anti-inflammatory activities which may also contribute to the reduced toxicity of PEG_{5K}-Fmoc-VE_2/DOX (Yen, Hwang et al. 2009, Buse and El-Aneed 2010, Shirpoor, Norouzi et al. 2013). More studies are still needed to fully elucidate the underlying mechanisms for the reduced toxicity of PEG_{5K}-Fmoc-VE_2/DOX.

6.3.11 *In vivo* anti-tumor efficacy

Both drug-sensitive (4T1.2 and PC-3) and drug-resistant (KB 8-5) tumor models were employed to evaluate the *in vivo* anti-tumor activity of DOX-loaded PEG_{5K}-Fmoc-VE_2. 4T1.2 is an aggressive syngeneic murine breast cancer model. As depicted in **Figure 67A**, a rapid and unrestrained growth of tumors was observed in mice treated with saline and mice had to be sacrificed early due to the development of severe ulceration.

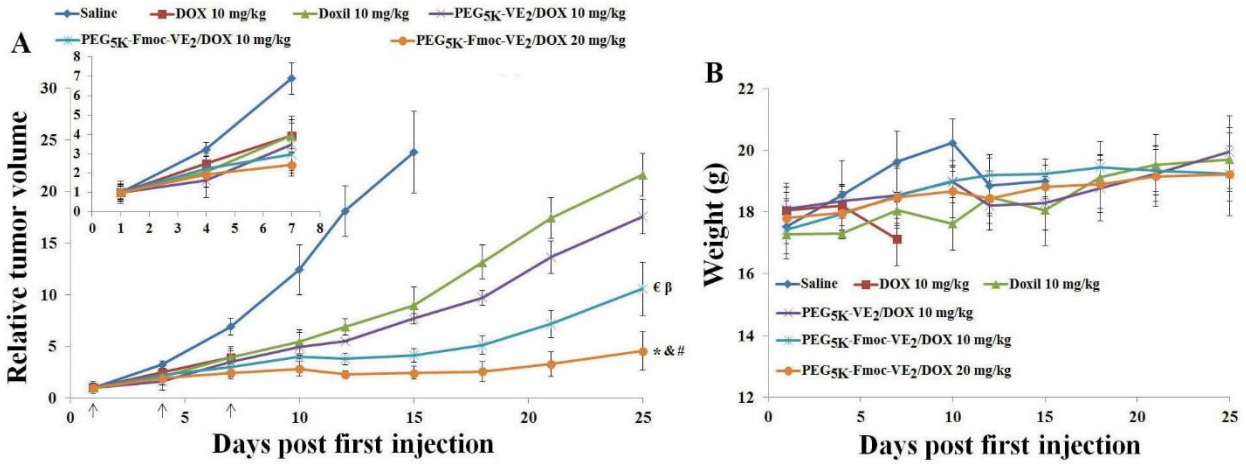

Figure 67 *In vivo* antitumor activity of different DOX formulations in 4T1.2 syngeneic mouse model. Solid arrows indicate the i.v. administration. A: relative tumor volume. B: body weight. *p < 0.0005, compared to Doxil. $^{\&}p$ < 0.001, compared to PEG_{5K}-VE_2/DOX; $^{\#}p$ < 0.05, compared to PEG_{5K}-Fmoc-VE_2/DOX (10 mg/kg); $^{€}p$ < 0.05, compared to PEG_{5K}-VE_2/DOX; $^{\beta}p$ < 0.005, compared to Doxil.

After three consecutive injections, all of the mice treated with free DOX died from systemic toxicity on day 7. PEGylated liposomal DOX (Doxil) was well tolerated and showed a moderate level of activity in delaying the tumor growth, which is consistent with previous reports (Schiffelers, Koning et al. 2003, Ishida, Shiraga et al. 2009, Ogawara, Un et al. 2009, Chen, Wang et al. 2010, Maeng, Lee et al. 2010). It is also apparent that incorporation of Fmoc motif into PEG_{5K}-VE_2/DOX led to a significant improvement in antitumor activity. The IRs were 82.63, 67.73, and 62.24% for PEG_{5K}-Fmoc-VE_2/DOX, PEG_{5K}-VE_2/DOX, and Doxil, respectively (**Table 20**). In addition, increasing DOX dosage to 20 mg/kg resulted in further enhancement in the antitumor activity of DOX-loaded PEG_{5K}-Fmoc-VE_2 micelles. No obvious toxicity was noticed at both dosages (**Figure 67B**).

Table 20 Tumor growth inhibition rate (IR) in 4T1.2 tumor bearing mice.

Different DOX formulations	IR (%)
Doxil 10 mg/kg	62.24
PEG_{5K}-VE_2/DOX 10 mg/kg	67.73
PEG_{5K}-Fmoc-VE_2/DOX 10 mg/kg	82.63
PEG_{5K}-Fmoc-VE_2/DOX 20 mg/kg	89.77

$$IR\ (\%) = (1 - relative\ tumor\ volume\ in\ the\ treated\ group \div relative\ tumor\ volume\ in\ the\ saline\ group) \times 100\%$$

IR (%) was calculated based on the RTV on day 15 (Mice in saline group died after day 15. Mice in DOX group died after third injection due to severe toxicity)

The improved performance of the two micellar formulations (PEG_{5K}-VE_2 and PEG_{5K}-Fmoc-VE_2) over Doxil in inhibiting the tumor growth may be attributed to their more effective accumulation at tumors based on their relatively small size (~20 nm and ~60 nm for PEG_{5K}-VE_2/DOX and PEG_{5K}-Fmoc-VE_2/DOX, respectively). It has been generally regarded that a drug carrier needs to have a size range of ~200 nm in order to capitalize on the EPR effect. However, recent studies have shown that sub-100 nm is required for particles to effectively penetrate the tumor tissues, particularly poorly vascularized tumors (Li, Xiao et al. 2010, Luo, Xiao et al.

2010). The size advantage of the two micellar DOX formulations over Doxil (~100 nm) may contribute to their enhanced antitumor activity. In addition, the carriers may contribute to the overall antitumor activity via delaying or reversing the drug resistance through inhibiting the activity of P-gp. The further improved performance of PEG_{5K}-Fmoc-VE_2 over PEG_{5K}-VE_2 is likely due to the more effective drug/carrier interaction as well as the interaction among the carrier molecules themselves, leading to improved formulation stability and more effective DOX delivery to tumors (**Figure 65**).

After demonstrating effective inhibition of tumor growth in the syngeneic murine breast cancer model, the therapeutic effect of DOX-loaded PEG_{5K}-Fmoc-VE_2 micelles was further examined in nude mice bearing human prostate cancer xenograft (PC-3) (**Figure 68)**. In this study, a lower DOX dosage (5 mg/kg) was used to avoid the death of animals in free DOX group, which allowed the comparison of all treatment groups over a relatively long period of time. Similarly, PEG_{5K}-Fmoc-VE_2/DOX gave the highest level of tumor growth inhibition among all DOX formulations examined. Doubling the DOX dosage to 10 mg/kg led to a further improvement of the antitumor efficacy (**Figure 68A**).

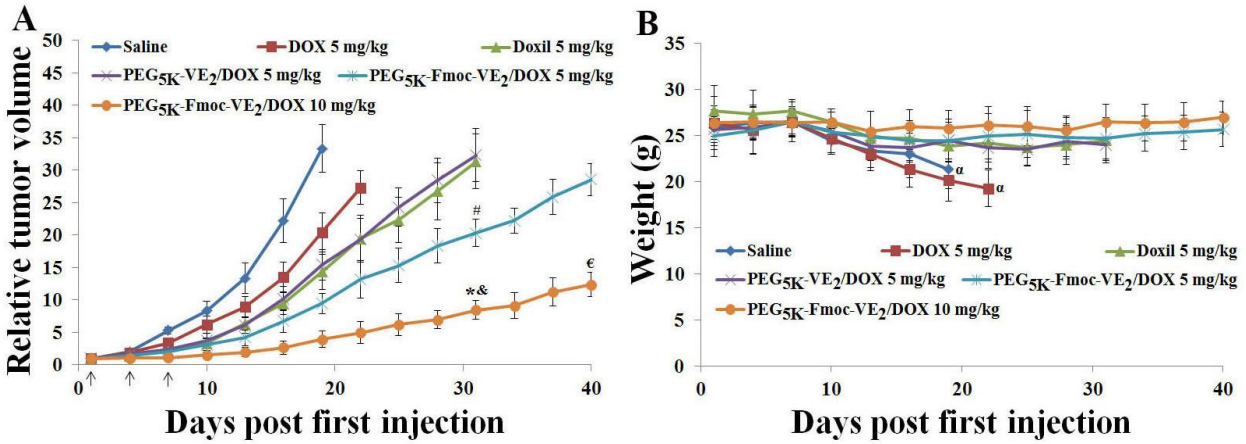

Figure 68 *In vivo* antitumor activity of various DOX formulations in PC-3 tumor-bearing mice. Solid arrows indicate the i.v. administration. A: relative tumor volume. B: body weight. *$p < 0.001$, compared to PEG_{5K}-VE_2/DOX or Doxil on day 31; $^{\&}p < 0.01$, compared to PEG_{5K}-Fmoc-VE_2/DOX (5 mg/kg) on day 31; $^{\#}p < 0.01$, compared to PEG_{5K}-VE_2/DOX or Doxil on day 31; $^{€}p < 0.001$, compared to PEG_{5K}-Fmoc-VE_2/DOX (5 mg/kg) on day 40; $^{\alpha}p < 0.05$, compared to day 1.

Table 21 Tumor growth inhibition rate (IR) in PC-3 tumor bearing mice.

Different DOX formulations	IR (%)
DOX 5 mg/kg	38.72
Doxil 5 mg/kg	56.98
PEG_{5K}-VE_2/DOX 5 mg/kg	53.71
PEG_{5K}-Fmoc-VE_2/DOX 5 mg/kg	71.64
PEG_{5K}-Fmoc-VE_2/DOX 10 mg/kg	88.10

$$IR\ (\%) = (1 - relative\ tumor\ volume\ in\ the\ treated\ group \div relative\ tumor\ volume\ in\ the\ saline\ group) \times 100\%$$

IR (%) was calculated based on the RTV on day 19 (Mice in saline group died after day 19)

Table 21 shows the IR of different DOX formulations on day 19. Mice in both saline and free DOX groups showed significant loss of body weight after day 19 (**Figure 68B**), which was likely attributed to the cachexia that is caused by the overgrowth of tumor. No significant changes were noticed in other treatment groups in either body weight (**Figure 68B**) or the general appearance.

Figure 69 shows the *in vivo* antitumor activity of DOX-loaded PEG_{5K}-Fmoc-VE_2 micelles in a drug-resistant tumor model, KB 8-5.

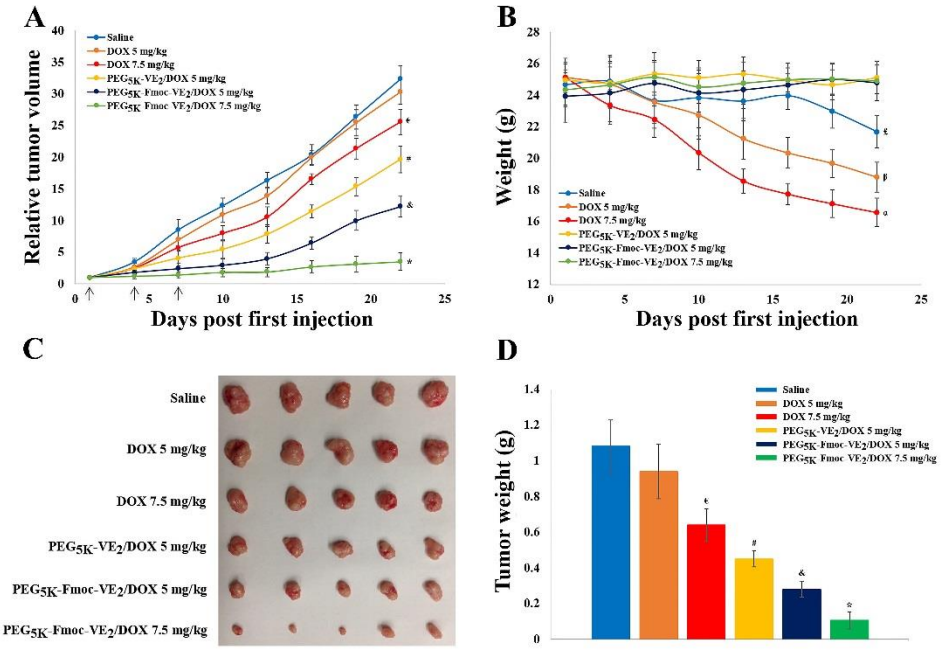

Figure 69 *In vivo* antitumor activity of varying DOX formulations in a drug-resistant xenograft tumor model, KB 8-5. Solid arrows indicate the i.v. injection. A: relative tumor volume. *$p < 0.002$, compared to PEG_{5K}-Fmoc-VE_2/DOX (5 mg/kg); $^{\&}p < 0.01$, compared to PEG_{5K}-VE_2/DOX (5 mg/kg); $^{\#}p < 0.05$, compared to DOX (7.5 mg/kg); $^{\epsilon}p < 0.05$, compared to DOX (5 mg/kg) or saline. B: body weight, $^{\alpha}p < 0.0005$, compared to day 1; $^{\beta}p < 0.005$, compared to day 1; $^{£}p < 0.05$, compared to day 1. C: tumor images. D: tumor weight, *$p < 0.005$, compared to PEG_{5K}-Fmoc-VE_2/DOX (5 mg/kg); $^{\&}p < 0.01$, compared to PEG_{5K}-VE_2/DOX (5 mg/kg); $^{\#}p < 0.001$, compared to DOX (7.5 mg/kg); $^{\epsilon}p < 0.05$, compared to DOX (5 mg/kg).

At a dosage of 5 mg/kg, free DOX barely showed any effect in inhibiting the tumor growth. Increasing the dose to 7.5 mg/kg only led to a slight improvement in antitumor activity. These are in consistence with the drug-resistant nature of this tumor model (Ma, Liu et al. 2014). In contrast, incorporation of DOX into PEG_{5K}-VE_2 led to a significant improvement in antitumor activity: PEG_{5K}-VE_2/DOX at 5 mg/kg was even more effective than free DOX at 7.5 mg/kg. In agreement with studies in other tumor models (**Figure 67 & 68**), PEG_{5K}-Fmoc-VE_2/DOX was even more effective than PEG_{5K}-VE_2/DOX in inhibiting the tumor growth at a same dosage (5 mg/kg). Increasing the dose to 7.5 mg/kg led to almost complete inhibition of tumor growth with an IR of 89.21% (**Figure 69 & Table 22**).

Table 22 Tumor growth inhibition rate (IR) in KB 8-5 tumor bearing mice.

Different DOX formulations	IR (%)
DOX 5 mg/kg	6.13
DOX 7.5 mg/kg	20.91
PEG_{5K}-VE_2/DOX 5 mg/kg	39.15
PEG_{5K}-Fmoc-VE_2/DOX 5 mg/kg	62.15
PEG_{5K}-Fmoc-VE_2/DOX 7.5 mg/kg	89.21

$$IR\ (\%) = (1 - relative\ tumor\ volume\ in\ the\ treated\ group \div relative\ tumor\ volume\ in\ the\ saline\ group) \times 100\%$$

$IR\ (\%)$ was calculated based on the RTV on day 22

Both micellar formulations were well tolerated. In contrast, significant weight loss was observed in free DOX-treated mice at both dosages (**Figure 69B**). Data from **Figure 69** strongly suggest that our improved formulation is capable of reversing the drug-resistance, at least partially, although more studies are needed to better understand the underlying mechanism.

7.0 THE SELF-ASSEMBLING CAMPTOTHECIN-TOCOPHEROL PRODRUG: AN EFFECTIVE APPROACH OF FORMULATING CAMPTOTHECIN

7.1 BACKGROUND

Owing to the sparingly water solubility, many chemotherapeutics have encountered difficulties in efficient dose delivery and untoward side effects. Camptothecin (CPT), a potent anticancer agent targeting a wide spectrum of cancers, is such an example (Hatefi and Amsden 2002, Mu, Elbayoumi et al. 2005). It functions by inhibiting the activity of topoisomerase I during DNA replication in the S-phase of the cell cycle, leading to cell death eventually (Hsiang and Liu 1988). In physiological condition, the terminal ring of CPT can be readily converted from active lactone form (pH<5) into carboxylate form (pH>8) (Fassberg and Stella 1992, Mu, Elbayoumi et al. 2005). In order to be active, CPT has to maintain its lactone form *in vivo*. However, the active form of CPT is highly lipophilic and hard to be formulated in conventional surfactants such as Tween 80 or other lipid (Mu, Elbayoumi et al. 2005, Natesan, Sugumaran et al. 2014). Hence, attempts to formulate CPT and efficiently deliver CPT to the pathological sites have attracted numerous efforts across the drug delivery field.

In the past a few decades, nanomedicine has rapidly become the powerful therapeutic platform in combatting against a variety of diseases including cancer (Shoshani, Darszon et al.

1994, Liaw, Aoyagi et al. 1999, Bawarski, Chidlowsky et al. 2008). Different nanotechnology-based approaches were utilized to help dissolve and stabilize CPT, such as encapsulation of CPT in polymeric micelles or liposomal CPT formulation (Daoud, Fetouh et al. 1995, Barreiro-Iglesias, Bromberg et al. 2004). However, most of them were neither with adequate stability nor sufficient drug loading to reach the optimal therapeutic dose. Recently, polymer-drug conjugates have been heavily paid attention and achieved considerable improvement regarding the formulation stability and *in vivo* efficacy of the coupled therapeutic agents due to the prolonged circulation time and enhanced tumor accumulation (Cabral and Kataoka 2014). Caiolfa et al found that poly(HPMA)-CPT conjugates with proteinase sensitive linker showed dramatically improved antitumor activity in HT29 human colon carcinoma xenografts (Caiolfa, Zamai et al. 2000). McRae Page et al reported that Poly(MPC-DHLA)-CPT conjugates with disulfide linkage had promise in killing MCF-7 and COLO-205 (McRae Page, Martorella et al. 2013). However, the steric hindrance imposed in polymer-CPT conjugates is postulated to be a huge burden to fully liberate the parental CPT. Therefore, it is necessary to develop CPT-derivatized prodrugs with less steric hindrance and more accessibility for redox agents or enzymes targeting to the linker.

Vitamin E (VE), a nontoxic, nonimmunogenic, and biocompatible lipid, acts by hindering the production of reactive oxygen species (ROS) generated when fat undergoes oxidation (Brigelius-Flohe and Traber 1999). Also, synergistic effects were achieved in a number of VE-based nanocarrier-delivered chemotherapeutics (Mi, Liu et al. 2011, Wang, Sun et al. 2012, Lu, Huang et al. 2013). Further, it has been found that VE was capable of overcoming the multidrug resistance (MDR) through inhibiting the p-gp efflux pump (Tang, Fu et al. 2013).

The focus of this report is to develop a CPT prodrug that can be effectively and readily loaded into nanocarriers with improved solubility, enhanced in *vivo* stability and diminished unwanted adverse effects of the parental CPT. It was claimed that the introduction of additional steric hindrance onto the hydroxyl moiety on CPT was able to greatly decrease the hydrolysis of lactone ring to the carboxylate form, resulting in the strengthened stability of parental CPT (Zhao, Lee et al. 2000, Li, Lv et al. 2009). To this end, in the present study, CPT was covalently linked to α-tocopherol (VE) through disulfide bond (CPT-S-S-VE) at the hydroxyl group. Disulfide linkage has been intensely employed as a reduction-sensitive spacer to facilitate the release of the conjugated anticancer drugs in a variety of polymer-drug conjugates (van der Vlies, Hasegawa et al. 2012, Kostkova, Etrych et al. 2013, McRae Page, Martorella et al. 2013). Glutathione (GSH), a reducing agent with high concentration in cells especially in tumor cells (~10 mM), was able to selectively break the disulfide bond to liberate the bundled active agents (Wu, Fang et al. 2004). In order to better evaluate the efficiency of CPT-S-S-VE in releasing CPT, VE-based CPT prodrug with carbonate ester bond (CPT-VE) was synthesized simultaneously. It is expected that the CPT-VE and CPT-S-S-VE will have significantly less lactone hydrolysis *in vivo* compared to free CPT. Not long ago, PEG-derivatized VE (PEG_{5K}-VE_2) and PEG_{5K}-VE_2 conjugates containing drug-interactive motif-Fmoc (PEG_{5K}-Fmoc-VE_2) were developed by our group and found to be quite efficient in delivering the Paclitaxel or Doxorubicin to tumors with improved antitumor efficacy. Given the VE chain in CPT produgs, PEG_{5K}-VE_2 and PEG_{5K}-Fmoc-VE_2 were used as solubilizer and stabilizer for the CPT-VE or CPT-S-S-VE during their self-assembling process. Surprisingly, the PEG_{5K}-Fmoc-VE_2/CPT-VE and PEG_{5K}-Fmoc-VE_2/CPT-S-S-VE both self-aggregated to nanofibers observed under cryoEM. The interactions between the carrier and prodrugs were investigated by NMR, fluorescence, UV-

absorbance, and FT-IR studies. Besides, the CPT release from prodrugs was determined both *in vitro* and in tumor-bearing mice. The mechanism of uptake of the prodrugs nanofibers were also investigated. Furthermore, the antitumor activity of CPT prodrugs' nanoassemblies were evaluated both *in vitro* and *in vivo*.

7.2 METHODS

7.2.1 Materials

D-α-Tocopherol succinate, Triphosgene, 3-(4,5-dimethylthiazol-2-yl)-2,5-diphenyl tetrazolium bromide (MTT), trypsin-EDTA solution, Triton X-100, and Dulbecco's Modified Eagle's Medium (DMEM) were all purchased from Sigma-Aldrich (MO, USA). D-alpha-tocopherol was purchased from Tokyo Chemical Industry (OR, USA). Camptothecin, Bis (2-hydroxyethyl) disulfide, and N,N'-dicyclohexylcarbodiimide (DCC) was purchased from Alfa Aesar (MA, USA). 4-Dimethylaminopyridine (DMAP) was purchased from Calbiochem-Novabiochem Corporation (CA, USA). Fetal bovine serum (FBS) and penicillin-streptomycin solution were from Invitrogen (NY, USA). LysoTracker was purchased from Life Technologies (Carlsbad, CA). All solvents used in this study were HPLC grade.

7.2.2 Synthesis of Camptothecin-Vitamin E conjugate with carbonate ester bond (CPT-VE)

First, CPT (1 eq. molar) and DMAP (2 eq. molar) were dissolved in 20 mL DCM with stirring, then triphosgene (0.35 eq. molar) was added dropwise into the yellowish solution. The reaction

was allowed for 20 min at room temperature. Afterwards, Vitamin E (2 eq. molar) was added into the solution and reacted overnight. The resultant CPT-VE was purified via column. Mobile phase: MeOH/DCM (2:98). Yield = 68%. ^{1}H-NMR (CDCl3-d_6, ppm) (**Figure 70**).

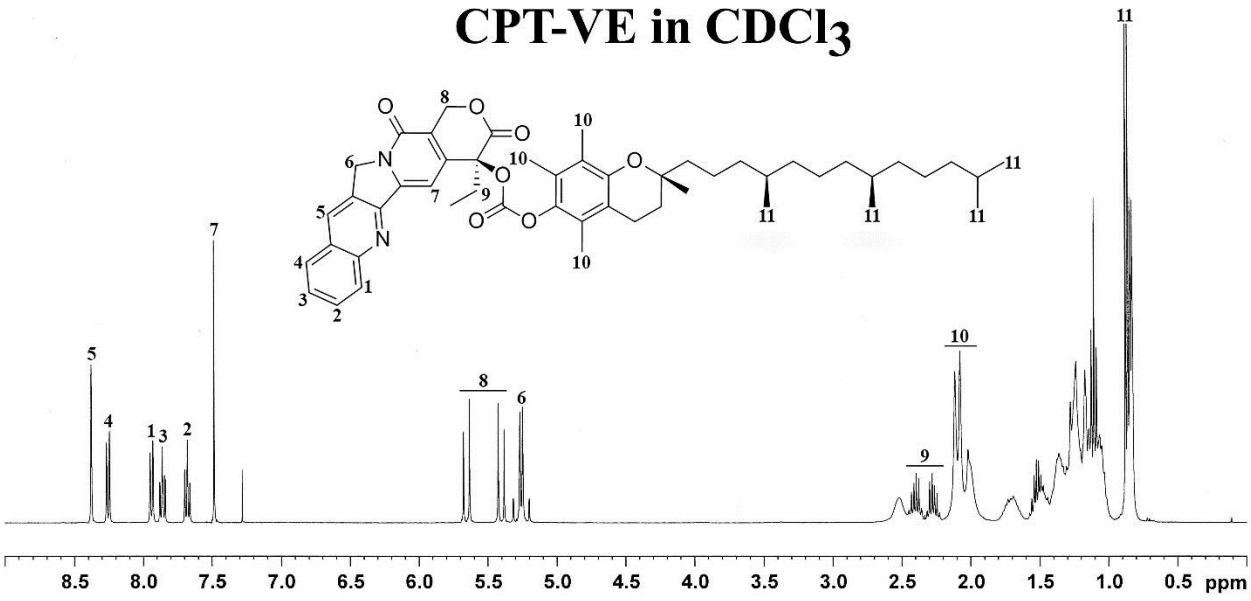

Figure 70 ^{1}H-NMR spectrum (400 MHz) of CPT-VE in $CDCl_3$.

^{13}C-NMR (CDCl3-d_6, ppm) 167.12, 157.30, 152.90, 152.26, 149.69, 148.99, 146.57, 145.77, 140.96, 131.11, 130.63, 129.80, 128.43, 128.21, 128.02, 120.20, 95.65, 78.23, 75.09, 67.06, 50.00, 39.36, 37.42, 37.37, 37.27, 32.75, 32.67, 31.74, 31.02, 27.96, 24.80, 24.78, 24.41, 22.73, 22.64, 21.00, 20.48, 19.75, 19.69, 19.63, 19.61, 12.72, 11.87, 11.71, 7.72. ESI-MS: $C_{50}H_{64}N_2O_7$ ($M+1^+$) 805.4714, found at 805.4721.

7.2.3 Synthesis of Camptothecin-Vitamin E conjugate with disulfide bond (CPT-S-S-VE)

First, Vitamin E succinate (1 eq. molar) reacted with Bis (2-hydroxyethyl) disulfide (2 eq. molar) with the assistance of DCC (2 eq. molar) and DMAP (0.2 eq. molar) overnight. The resultant

VE-S-S-OH was purified through column. Mobile phase: ethyl acetate/ petroleum ether (2:3). Yield = 75%. ^{1}H-NMR (CDCl3-d_6, ppm) (**Figure 71**).

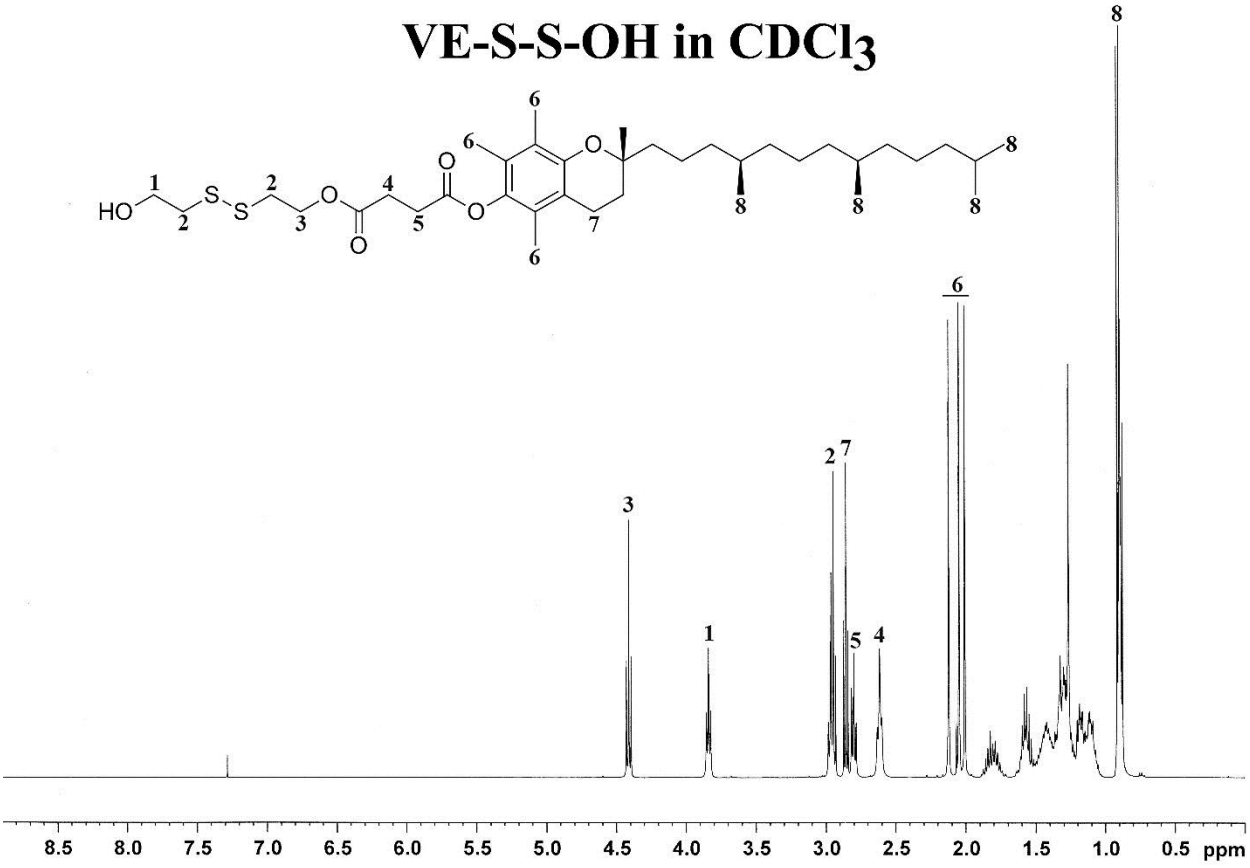

Figure 71 ^{1}H-NMR spectrum (400 MHz) of VE-S-S-OH in $CDCl_3$.

^{13}C-NMR (CDCl3-d_6, ppm) 172.12, 171.07, 149.46, 140.46, 126.65, 124.92, 123.03, 117.42, 75.07, 62.73, 60.36, 41.51, 39.40, 37.47, 37.44, 37.31, 36.95, 32.80, 32.71, 31.16, 29.05, 28.76, 28.00, 24.83, 24.46, 22.78, 22.69, 21.04, 20.62, 19.81, 19.71, 12.98, 12.12, 11.85. ESI-MS: $C_{37}H_{62}O_6S_2$ ($M+Na^+$) 689.3885, found at 689.3882.

Second, CPT (1 eq. molar) and DMAP (2 eq. molar) were dissolved in 20 mL DCM with stirring, then triphosgene (0.35 eq. molar) was added dropwise into the yellowish solution. The reaction was allowed for 20 min at room temperature. Then, VE-S-S-OH (2 eq. molar) was added into the solution in second step for overnight. The final product (CPT-S-S-VE) was

purified via column. Mobile phase: ethyl acetate/petroleum ether (7:4). Yield = 58%. ^{1}H-NMR (CDCl3-d_6, ppm) (**Figure 72**).

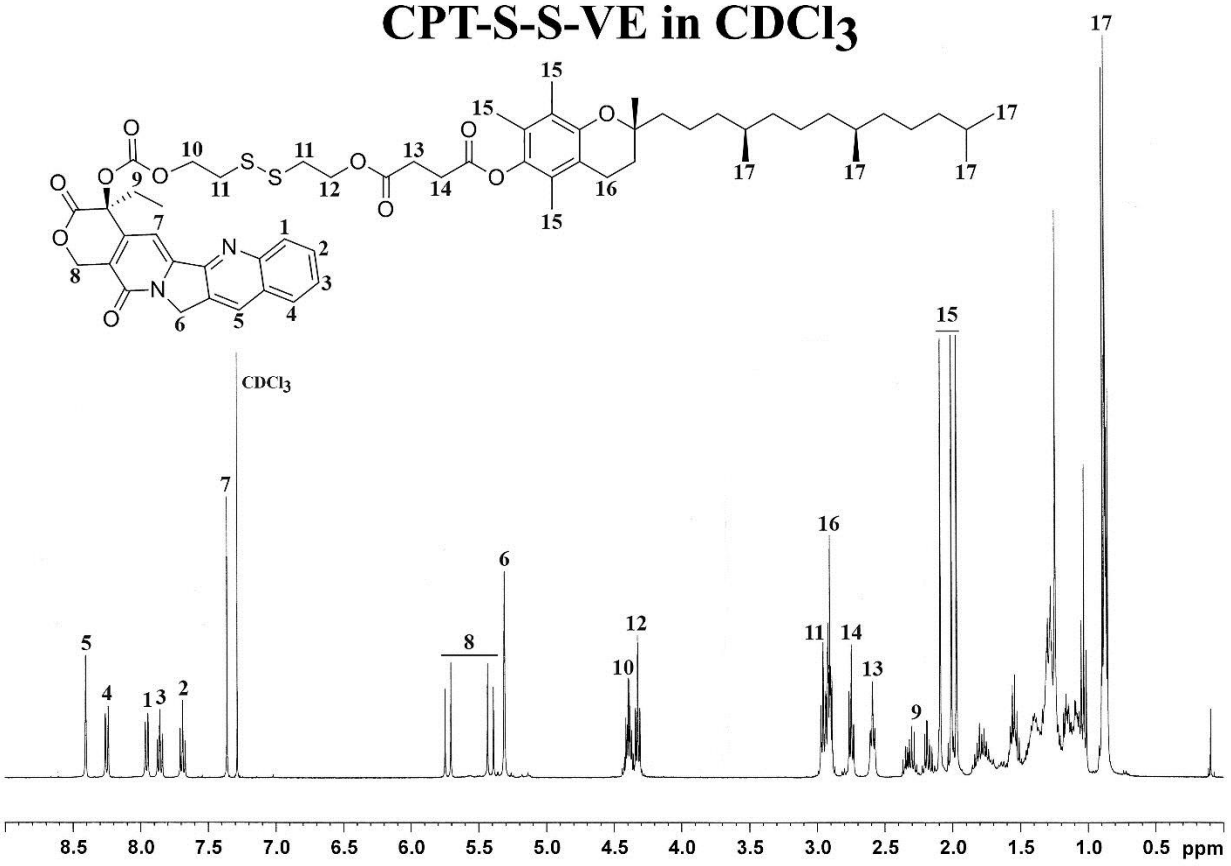

Figure 72 ^{1}H-NMR spectrum (400 MHz) of CPT-S-S-VE in $CDCl_3$.

^{13}C-NMR (CDCl3-d_6, ppm) 171.90, 170.86, 167.25, 157.30, 153.45, 152.31, 149.43, 148.91, 146.52, 145.61, 140.43, 131.17, 130.73, 129.70, 128.49, 128.19, 128.09, 126.66, 124.92, 123.01, 120.27, 117.38, 95.96, 78.05, 77.35, 77.03, 76.71, 75.05, 70.57, 69.27, 67.08, 66.53, 62.50, 50.01, 39.37, 37.45, 37.43, 37.29, 37.12, 36.56, 32.80, 32.71, 31.90, 29.00, 28.75, 27.98, 24.80, 24.45, 22.72, 22.63, 21.02, 20.58, 19.76, 19.66. ESI-MS: $C_{58}H_{76}N_2O_{11}S_2$ ($M+H^+$) 1041.4891, found at 1041.4887.

7.2.4 Biophysical characterization of CPT, CPT-VE, and CPT-S-S-VE nanoparticles

CPT-VE or CPT-S-S-VE dissolved in DCM was mixed with predetermined amount of PEG_{5K}-Fmoc-VE_2 (PEG_{5K}-VE_2). The solution was blown out by nitrogen flow and further vacuumed for four hours. The resultant formulations were filtered through a 0.22 μm filter prior to characterization. PEG_{5K}-VE_2/CPT and PEG_{5K}-Fmoc-VE_2/CPT were prepared through dialysis method. First, both CPT and PEG_{5K}-Fmoc-VE_2 (PEG_{5K}-VE_2) were dissolved in DMSO and mixed well. Then the DMSO solution was transferred into a dialysis bag (MWCO 12,000) and dialyzed against 200 mL deionized water for 4 days with stirring at room temperature, during which the water was replaced with fresh one every day. The diameter and size distribution of the nanoformulations were evaluated by dynamic light scattering (DLS). The morphology was determined by cryoEM. The concentrations of CPT, CPT-VE, and CPT-S-S-VE in nanoparticles were measured by UPLC-QTOFMS Analysis. The drug loading capacity (DLC) and drug loading efficiency (DLE) were calculated according to the literature.

7.2.5 Fluorescence quenching

PEG_{5K}-Fmoc-VE_2/CPT-VE and PEG_{5K}-Fmoc-VE2/CPT-S-S-VE were prepared as the method described above. The samples were put into a 96-well plate, and the fluorescence intensity of PEG_{5K}-Fmoc-VE_2 was recorded on a Synergy H1 Hybrid reader (BioTek), employing an excitation wavelength of 270 nm and emission wavelength from 300-500 nm. The fluorescence intensity of prodrugs was examined using an excitation wavelength of 370 nm and emission wavelength from 400-700 nm.

7.2.6 UV absorbance spectroscopy

The absorption spectra of CPT (DMSO), CPT-VE (DMSO), CPT-S-S-VE (DMSO), PEG5K-Fmoc-VE2/CPT-VE (water) and PEG5K-Fmoc-VE2/CPT-S-S-VE (water) were collected using Varian Cary 50 Bio UV-Visible Spectrophotometer over a wavelength ranging from 310 to 420 nm. All samples were loaded into a quartz cell and measured against distilled water or DMSO as the reference.

7.2.7 Fourier transform infrared spectroscopy (FT-IR)

FT-IR of CPT-VE, CPT-S-S-VE, PEG5K-Fmoc-VE2/CPT-VE, PEG5K-Fmoc-VE2/CPT-S-S-VE and PEG5K-Fmoc-VE2 was determined using a VERTEX 70/70v FT-IR spectrometer (Bruker) to determine the potential hydrogen bonding of carrier/drug in the frequency of 4997-500 cm-1 (KBr pellet).

7.2.8 Cell culture

4T1.2, mouse breast cancer cell line, was used in this work and cultured in DMEM containing 10% FBS and 1% penicillin-streptomycin in a humidified environment at 37 ℃ with 5% CO_2.

7.2.9 Animals

Female BALB/c mice of 10-12 weeks of age were purchased from Charles River (Davis, CA). Animals were housed under pathogen-free conditions according to AAALAC (Association for

Assessment and Accreditation of Laboratory Animal Care) guidelines. All animal-related experiments were performed in full compliance with institutional guidelines and approved by the Animal Use and Care Administrative Advisory Committee at the University of Pittsburgh.

7.2.10 *In vitro* cytotoxicity

The anti-proliferation of CPT-VE, CPT-S-S-VE, PEG_{5K}-Fmoc-VE_2/CPT-VE and PEG_{5K}-Fmoc-VE_2/CPT-S-S-VE with or without 10 mM GSH was evaluated in 4T1.2 in comparison to free CPT. Briefly, 2000 cells/well were seeded into 96-well plates following overnight attachment. Next day, cells were challenged by CPT-VE, CPT-S-S-VE, PEG_{5K}-Fmoc-VE_2/CPT-VE and PEG_{5K}-Fmoc-VE_2/CPT-S-S-VE with or without 10 mM GSH and CPT of various concentrations (equivalent CPT concentration). Free PEG_{5K}-Fmoc-VE_2, at concentrations equivalent to the amount of carriers in formulating CPT-VE and CPT-S-S-VE, was also added into cells. Cells were incubated for 72 h and cell viability was examined by MTT assay (Huang, Lu et al. 2012, Lu, Huang et al. 2013, Lu, Huang et al. 2013, Lu, Zhao et al. 2014).

7.2.11 CPT release inside cells

1×10^6 4T1.2 cells were grown into 6-well plates and allowed overnight attachment. Afterwards, cells were treated by CPT-VE and CPT-S-S-VE (100 ng/mL in terms of CPT) for 24 h. Then, the cells were washed with ice-cold PBS three times and extracted in MeOH. The extraction was dried under gentle stream of clean dry air, then redissolved in a mixture of MeOH:H_2O (1:1, v/v). The lysates were vortexed and then centrifuged at 14,000 rpm for 10 min at 4°C. Finally, supernatants were transferred to another set of 1.5 mL microtubes and stored at -80°C for MS

analysis. UPLC-QTOFMS Analysis: Chromatographic separation of CPT was performed on an Acquity UPLC BEH C18 column (2.1 × 50 mm, 1.7 μm; Waters, Milford, MA). The flow rate of the mobile phase was 0.5 ml/min using a gradient ranging from 2% to 98% acetonitrile/water containing 0.1% formic acid in 6 minutes. The column temperature was maintained at 50°C. Waters SYNAPT G2S TOF-MS (Waters, Milford, MA) was operated in positive mode with electrospray ionization. The source and desolvation temperatures were set at 150°C and 500°C, respectively. Nitrogen was applied as the cone gas (50 L/h) and desolvation gas (800 L/h). Data were processed using QuanLynx (v 4.1, Waters). Extracted ion chromatograms (EICs) were extracted using a 20 mDa window centered on the expected m/z 349.11 for CPT.

7.2.12 Uptake study

2,000 4T1.2 cells/well were seeded into 96-well plates and incubated overnight prior to treatment. Then cells were treated with PEG_{5K}-Fmoc-VE_2/CPT-VE and PEG_{5K}-Fmoc-VE_2/CPT-S-S-VE for 2 h at 4 or 37 ℃, followed by 24 h incubation at a CPT concentration of 6 μg/mL.

Mechanistic investigation of the uptake pathway was further performed by using confocal laser scanning microscopy (CLSM, FluoView 1000, Olympus, Japan). Briefly, 3×10^5 4T1.2 cells/well were seeded into 6-well plates and incubated overnight. Then cells were challenged with PEG_{5K}-Fmoc-VE_2/CPT-VE and PEG_{5K}-Fmoc-VE_2/CPT-S-S-VE for 30 min at 37 ℃ at a CPT concentration of 6 μg/mL. After that, cells were washed three times with cold PBS and fixed with 4% paraformaldehyde for 30 min. Then, the lysotracker was applied to cells for 5 min. Subsequently, cells were washed thrice with cold PBS prior to the observation under CLSM.

7.2.13 Biodistribution

PEG_{5K}-Fmoc-VE_2/CPT-VE and PEG_{5K}-Fmoc-VE_2/CPT-S-S-VE (carrier/drug: 0.75:1) were intravenously injected into 4T1.2 tumor bearing mice at the dose of 5 mg CPT/kg, respectively (n=3). At 24 h post-injection, tumors, liver, spleen, lung, heart, kidneys and blood were harvested from the mice. Tissues were homogenized using Power Gen 500 homogenizer (Fisher Scientific) with 100 mg tissues mixed with 900 μL methanol, and the CPT was extracted overnight at -20 °C. The samples were then centrifuged at 14,000 rpm for 10 min at 4°C and the supernatant was measured by UPLC-QTOFMS as described above.

7.2.14 *In vivo* antitumor therapeutic study

Antitumor efficacy of PEG_{5K}-Fmoc-VE_2/CPT-VE and PEG_{5K}-Fmoc-VE_2/CPT-S-S-VE was investigated in 4T1.2 tumor bearing mice. 2 x 10^5 4T1.2 cells in 200 μL saline were inoculated subcutaneously at the right flank of female BALB/c mice. Mice were randomly distributed to five groups (n = 5), when tumors in the mice arrived at a volume of 50-100 mm^3, and this day was designated as day 1. From day 1, mice were i.v. administered, saline, free CPT (5 mg/kg) (i.p. injection because of its low solubility) (Zhen Gu et al), PEG_{5K}-Fmoc-VE_2/CPT-VE (5 mg CPT/kg), PEG_{5K}-Fmoc-VE_2/CPT-S-S-VE (5 mg CPT/kg), and PEG_{5K}-Fmoc-VE_2/CPT-S-S-VE (10 mg CPT/kg) on days 1, 4, and 7, respectively. Tumor sizes were measured with a digital caliper on days 1, 4, 7, 9, 12, 15, 18, 21 and calculated according to the following formula: $(L \times W^2)/2$, where L and W are length and width of each tumor. Meanwhile, the tumor growth inhibition rate (IR) was assessed and defined as: IR % = (1 – tumor volume in the treated group/ tumor volume in the saline group) × 100%. Mice body weight was also monitored as an

indication of toxicity. Tumors from all groups were weighted and imaged at the termination of the study. In the meantime, the tumors were also subject to the H&E staining.

7.2.15 Statistical analysis

In all statistical analyses, the significance level was set at a probability of $P < 0.05$. All results were reported as the mean ± standard deviation (SD) unless otherwise indicated. Statistical analysis was performed by using the Student's t-test for two groups, and one-way ANOVA for multiple groups, followed by Newman-Keuls test if $P < 0.05$.

7.3 RESUTLS

7.3.1 Synthesis of VE-derivatized CPT prodrugs

CPT, a highly lipophilic anticancer agent, was hard to be physically entrapped in polymeric delivery systems. In an attempt to ameliorate the compatibility of CPT, one VE molecule was coupled to CPT at its hydroxyl group through either carbonate ester bond (CPT-VE) or disulfide linkage (CPT-S-S-VE). Complete synthetic route was illustrated in **Figure 73** (CPT-VE) and **Figure 74** (CPT-S-S-VE).

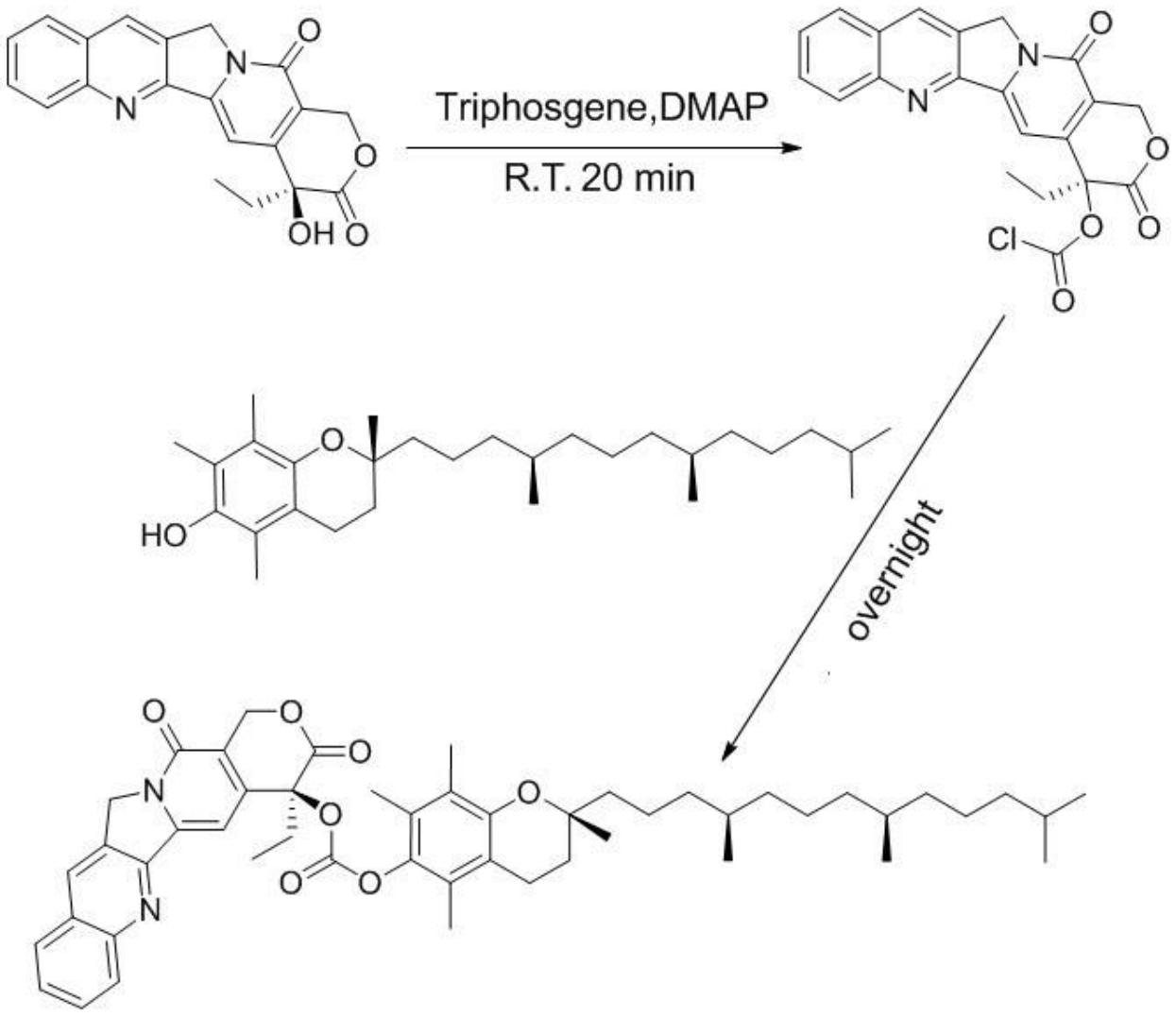

Figure 73 Synthetic route of CPT-VE.

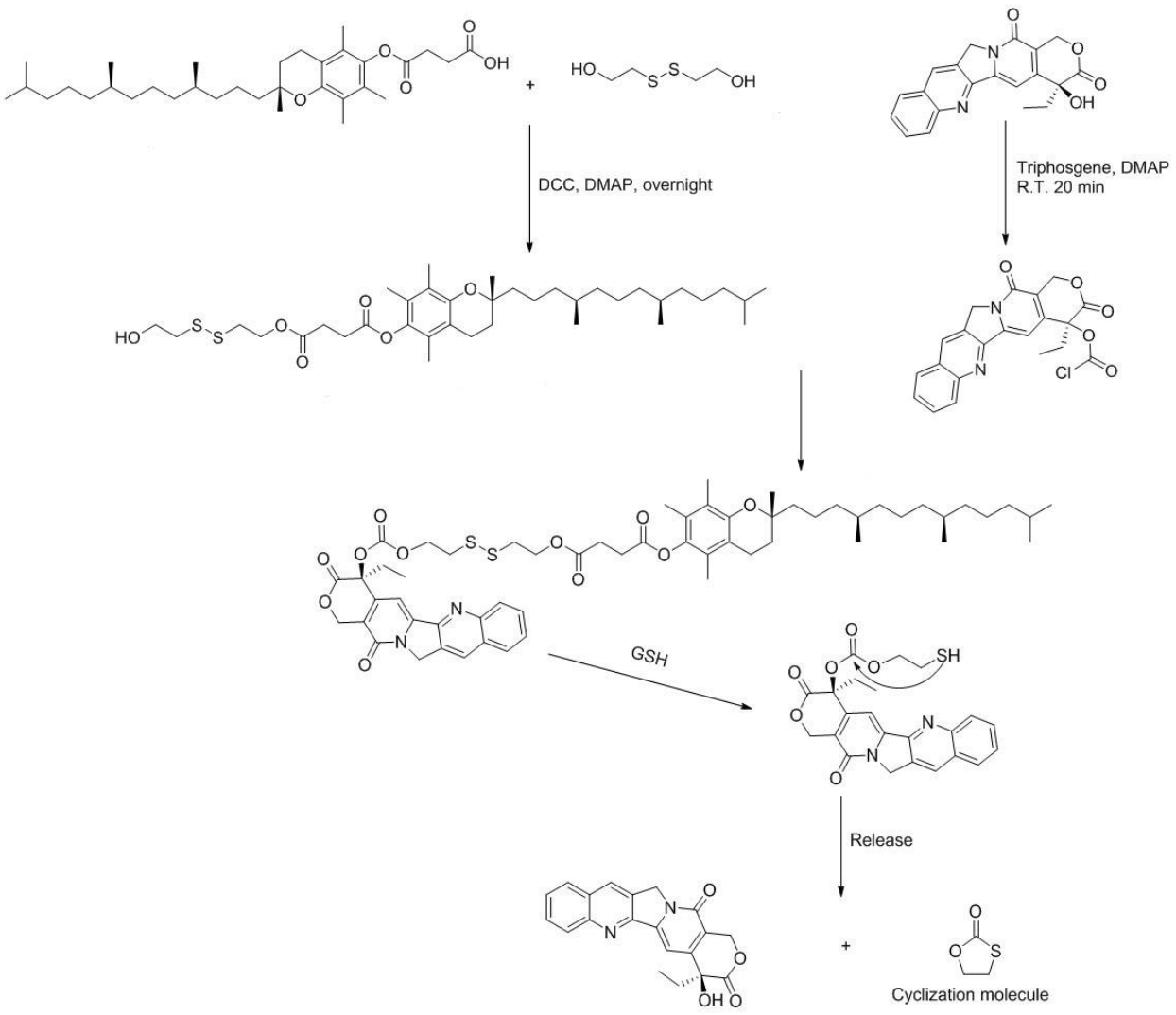

Figure 74 Synthetic route of CPT-S-S-VE.

For the synthesis of CPT-VE, first CPT was reacted with triphosgene for 20 min with the assistance of DMAP to generate CPT-COCl, which was further conjugated by VE overnight to yield CPT-VE. In the synthesis of CPT-S-S-VE, initially, tocopherol-succinate was coupled with Bis (2-hydroxyethyl) disulfide to obtain VE-S-S-OH. Meanwhile, CPT-COCl was acquired by reacting CPT with triphosgene. Then, VE-S-S-OH and CPT-COCl were conjugated together to yield CPT-S-S-VE.

7.3.2 Biophysical characterization of CPT, CPT-VE, and CPT-S-S-VE nanoassemblies

After the synthesis of CPT-VE and CPT-S-S-VE, we found that both of them can be readily dissolved in DCM (>100 mg/mL in terms of CPT). However, less than 2 mg of free CPT can be dissolved in 1 mL DCM (data not shown). In aqueous solution, PEG_{5K}-Fmoc-VE_2/CPT-VE and PEG_{5K}-Fmoc-VE_2/CPT-S-S-VE were able to readily self-assemble into nanofibers. Surprisingly, the nanofibers in PEG_{5K}-Fmoc-VE_2/CPT-S-S-VE was entangled together. In a sharp contrast, spherical nanomicelles were identified in PEG_{5K}-VE_2/CPT-VE, PEG_{5K}-VE_2/CPT-S-S-VE, PEG_{5K}-VE_2/CPT, and PEG_{5K}-Fmoc-VE_2/CPT (**Figure 75**).

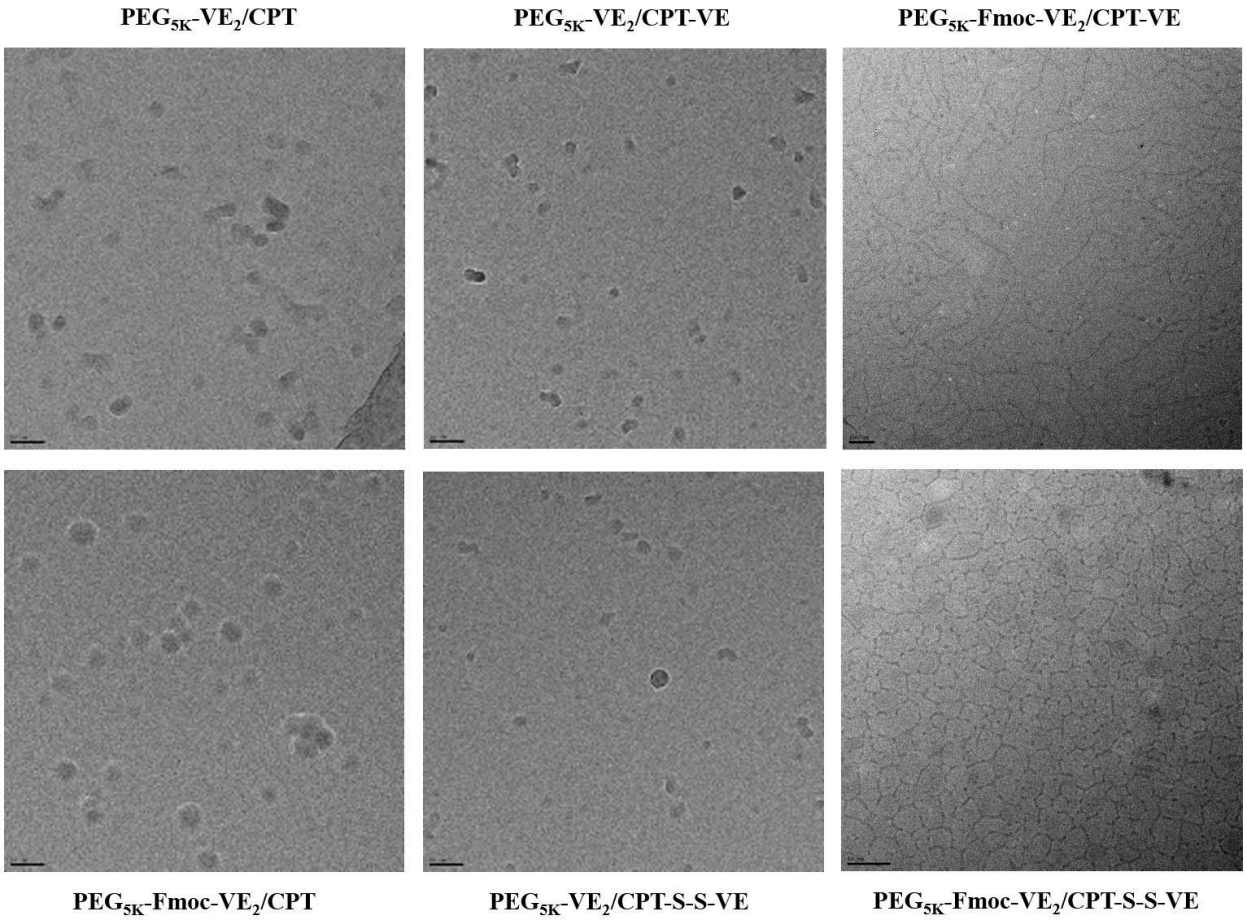

Figure 75 CryoEM imaging of PEG_{5K}-VE_2/CPT, PEG_{5K}-Fmoc-VE_2/CPT, PEG_{5K}-VE_2/CPT-VE, PEG_{5K}-VE_2/CPT-S-S-VE, PEG_{5K}-Fmoc-VE_2/CPT-VE, and PEG_{5K}-Fmoc-VE_2/CPT-S-S-VE.

As shown in **Table 23**, DLCs of CPT were only 0.30% and 0.65% in PEG_{5K}-VE_2 and PEG_{5K}-Fmoc-VE_2 nanomicelles, respectively.

Table 23 Biophysical characterization of CPT, CPT-VE, and CPT-S-S-VE nanoformulations

	Molar ratio	DLC (%)	DLE (%)	Size (nm)	PDI	Stability	Zeta potential (mv)
PEG_{5K}-VE_2/CPT	15:1	0.30	79.6	52.3±2.8	0.24	4 days	1.35±0.02
PEG_{5K}-Fmoc-VE_2/CPT	7.5:1	0.65	85.3	76.4±3.6	0.25	8 days	0.87±0.06
PEG_{5K}-VE_2/CPT-VE	0.75:1	4.7	72.5	85.4±3.5	0.23	5 days	-1.22±0.32
	1:1	4.3	83.8	52.3±2.2	0.21	7 days	-1.03±0.13
PEG_{5K}-VE_2/CPT-S-S-VE	0.5:1	6.2	71.7	62.2±2.4	0.24	7 days	-0.66± 0.08
	0.75:1	5.3	85.4	48.6±1.8	0.22	12 days	0.16±0.03
PEG_{5K}-Fmoc-VE_2/CPT-VE	0.5:1	6.6	76.2	93.2±4.5	0.26	21 days	-1.29±0.18
	0.75:1	5.4	89.1	87.4±4.6	0.22	30 days	-0.95±0.21
PEG_{5K}-Fmoc-VE_2/CPT-S-S-VE	0.25:1	9.2	70.6	81.5±3.9	0.20	31 days	-1.03±0.25
	0.5:1	6.8	83.5	57.6±2.1	0.17	62 days	-0.78±0.14
	0.75:1	5.7	96.3	49.7±1.8	0.15	75 days	0.64±0.12

PDI: polydispersity index

Stability: no significant size change was observed during the time period tested

$$DLC\ (\%) = [weight\ of\ CPT\ loaded \div (weight\ of\ carrier + weight\ of\ CPT\ or\ CPT\ prodrugs\ loaded)]$$

$$DLE\ (\%) = (weight\ of\ loaded\ drug \div weight\ of\ input\ drug) \times 100\%$$

Nonetheless, the DLCs of CPT were improved drastically in PEG_{5K}-VE_2/CPT-VE (4.7%) and PEG_{5K}-VE_2/CPT-S-S-VE (6.2%), or in PEG_{5K}-Fmoc-VE_2/CPT-VE (6.6%) and PEG_{5K}-Fmoc-VE_2/CPT-S-S-VE (9.2%). In addition, the stability of CPT nanoformulations was also enhanced significantly when CPT prodrugs instead of free CPT were formulated in carriers, in which PEG_{5K}-Fmoc-VE_2 offered markedly better formulation stability compared to that of PEG_{5K}-VE_2. Size distributions of CPT, CPT-VE, and CPT-S-S-VE nanoassemblies exhibited homogenously distributed nanoparticles (**Figure 76)**, which was consistent with the cryoEM results (**Figure 75)**.

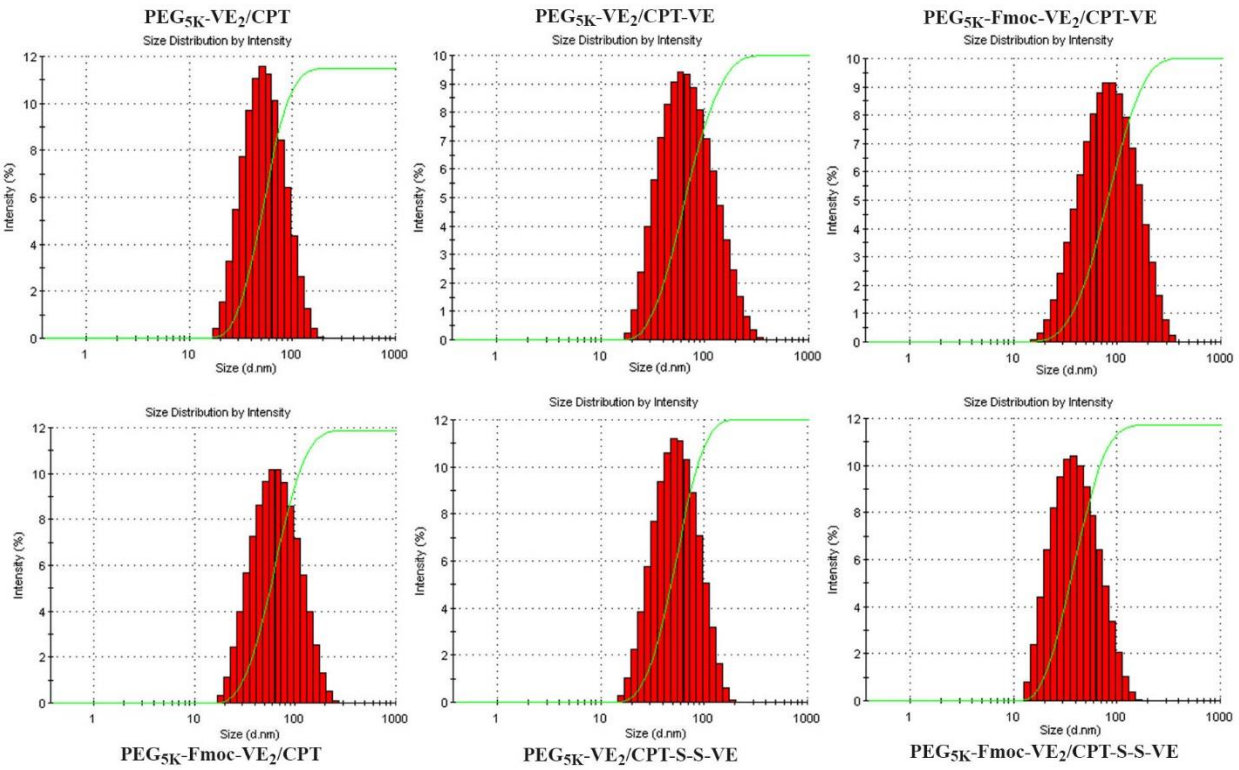

Figure 76 Size distribution of PEG_{5K}-VE_2/CPT, PEG_{5K}-Fmoc-VE_2/CPT, PEG_{5K}-VE_2/CPT-VE, PEG_{5K}-VE_2/CPT-S-S-VE, PEG_{5K}-Fmoc-VE_2/CPT-VE, and PEG_{5K}-Fmoc-VE_2/CPT-S-S-VE.

7.3.3 Confirmation of CPT prodrugs loading by NMR investigation

To confirm whether CPT-VE or CPT-S-S-VE was indeed encapsulated into the PEG_{5K}-Fmoc-VE_2. A series of ^{1}NMR studies were conducted, including CPT-VE in $CDCl_3$, CPT-S-S-VE in $CDCl_3$,

PEG_{5K}-Fmoc-VE_2 in $CDCl_3$ or D_2O, PEG_{5K}-Fmoc-VE_2/CPT-VE in $CDCl_3$ or D_2O, and PEG_{5K}-Fmoc-VE_2/CPT-S-S-VE in $CDCl_3$ or D_2O. CPT-VE and PEG_{5K}-Fmoc-VE_2 exhibited their authentic peaks in $CDCl_3$ in **Figure 77A,** respectively. Mixed PEG_{5K}-Fmoc-VE_2/CPT-VE in $CDCl_3$ also clearly showed the typical peaks for PEG_{5K}-Fmoc-VE_2 and CPT-VE, respectively (**Figure 77A**).

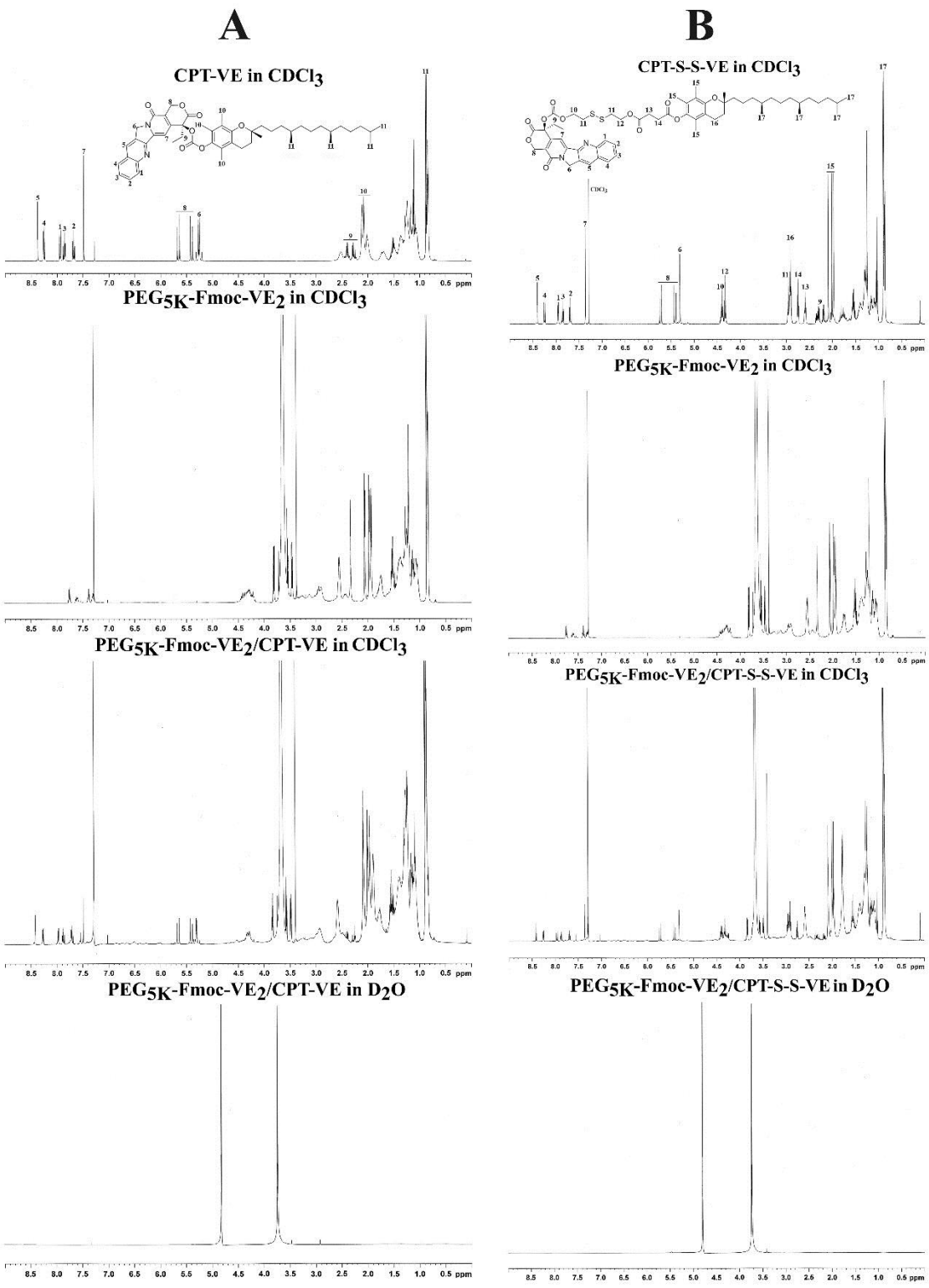

Figure 77 A: NMR spectra of CPT-VE in $CDCl_3$, PEG_{5K}-Fmoc-VE_2 in $CDCl_3$, PEG_{5K}-Fmoc-VE_2/CPT-VE in $CDCl_3$, and PEG_{5K}-Fmoc-VE_2/CPT-S-S-VE in D_2O; B: NMR spectra of CPT-S-S-VE in $CDCl_3$, PEG_{5K}-Fmoc-VE_2 in $CDCl_3$, PEG_{5K}-Fmoc-VE_2/CPT-S-S-VE in $CDCl_3$, and PEG_{5K}-Fmoc-VE_2/CPT-S-S-VE in D_2O.

However, when PEG_{5K}-Fmoc-VE_2/CPT-VE was measured in D_2O, the peaks for PEG_{5K}-Fmoc-VE_2 and CPT-VE were completely gone, except the PEG and solvent peaks. Similar data was obtained in CPT-S-S-VE system (**Figure 77B**). All of the NMR samples were subject to overnight scanning in order to rule out the possibility that the disappearances of the peaks were due to the lack of scanning.

7.3.4 Fluorescence study

In order to better understand the driving force of forming the CPT or CPT prodrugs nanoparticles, fluorescence quenching assay was performed. In **Figure 78A,** CPT, CPT-VE, and CPT-S-S-VE, showed similar fluorescence patterns when excited at 370 nm.

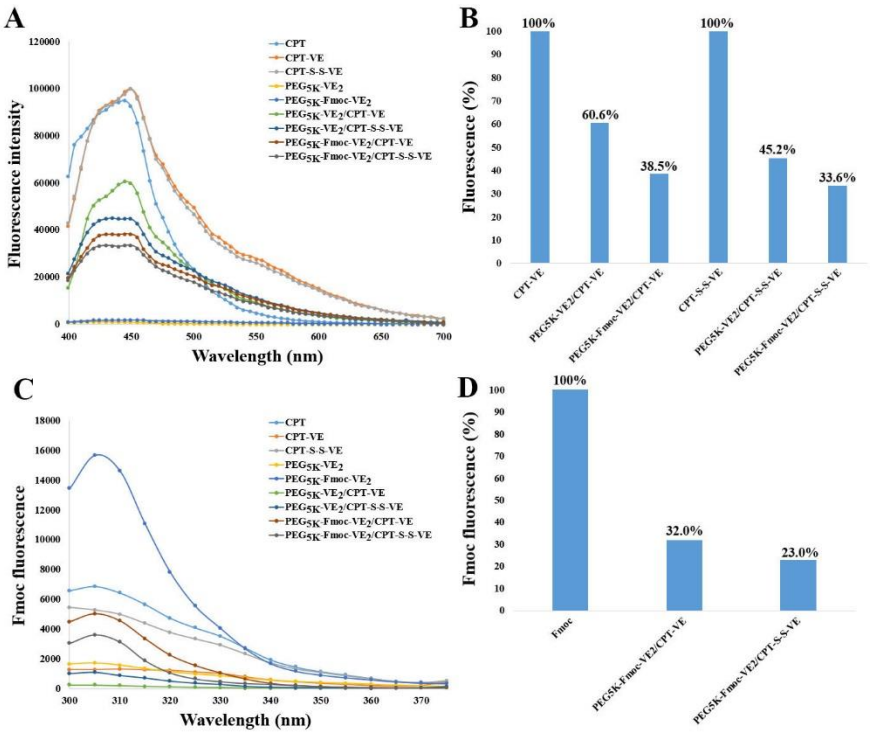

Figure 78 A: fluorescence quenching study of CPT-VE or CPT-S-S-VE nanoformulations. B: quantitation of the fluorescence decrease in CPT-VE or CPT-S-S-VE nanoassemblies compared to the free CPT-VE or CPT-S-S-VE. C: Fmoc Fluorescence. D: reduction of Fmoc fluorescence intensity after incorporating CPT-VE or CPT-S-S-VE into PEG_{5K}-Fmoc-VE_2.

Two carriers, PEG_{5K}-VE_2 and PEG_{5K}-Fmoc-VE_2, did not have any fluorescence signals under the same condition. However, the fluorescence intensity of CPT-VE, and CPT-S-S-VE, was decreased dramatically when loaded into carriers. As illustrated in **Figure 78B**, there was significantly more fluorescence reduction when CPT-VE or CPT-S-S-VE, was incorporated into PEG_{5K}-Fmoc-VE_2 in comparison to PEG_{5K}-VE_2.

Meanwhile, Fmoc fluorescence was also investigated. In **Figure 78C**, typical Fmoc signal was observed in PEG_{5K}-Fmoc-VE_2, the intensity of which was diminished remarkably when CPT prodrugs were loaded inside, particularly for CPT-S-S-VE. Our data suggested that the strong carrier/payload interactions were achieved including hydrophobic interaction and π-π stacking effect.

7.3.5 UV absorbance evaluation

Figure 79 shows the UV-absorbance of free CPT, CPT-VE, and CPT-S-S-VE, and CPT-VE or CPT-S-S-VE formulated in PEG_{5K}-Fmoc-VE_2. A significant decrease of UV-absorbance was discerned in both CPT prodrugs formulated in PEG_{5K}-Fmoc-VE_2, especially for CPT-S-S-VE system. Further, a clear red shift of UV-absorbance was detected in both CPT-VE and CPT-S-S-VE nanoassemblies, suggesting that the π-π stacking contributed significantly to the overall carrier/drug interactions

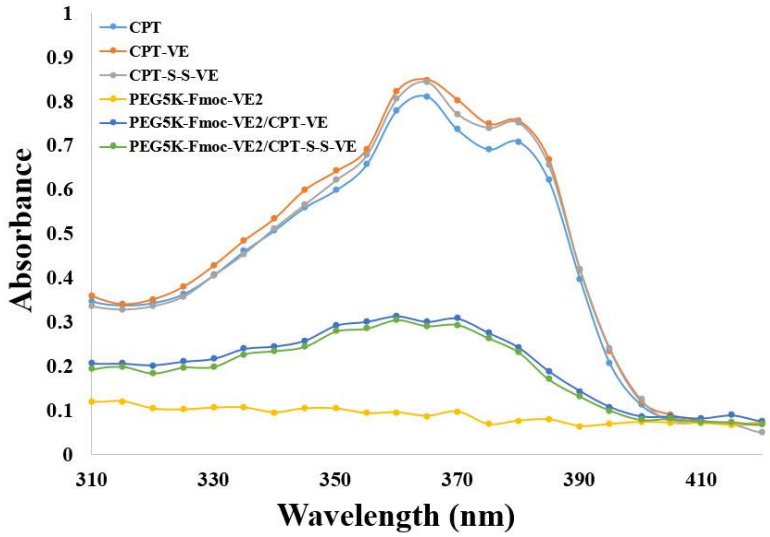

Figure 79 UV-absorbance of CPT-VE, CPT-S-S-VE, PEG_{5K}-Fmoc-VE_2/CPT-VE, and PEG_{5K}-Fmoc-VE_2/CPT-S-S-VE.

7.3.6 FT-IR measurement

Fourier transform infrared spectroscopy (FT-IR) is a good measure for the hydrogen bonding. Therefore, PEG_{5K}-Fmoc-VE_2/CPT-VE and PEG_{5K}-Fmoc-VE_2/CPT-S-S-VE, were further subject to FT-IR determination. As depicted in **Figure 80A**, after subtracting the IR of PEG_{5K}-Fmoc-VE_2 from that of PEG_{5K}-Fmoc-VE_2/CPT-VE, two new peaks at 1463.11 cm^{-1} and 1472.51 cm^{-1} were identified.

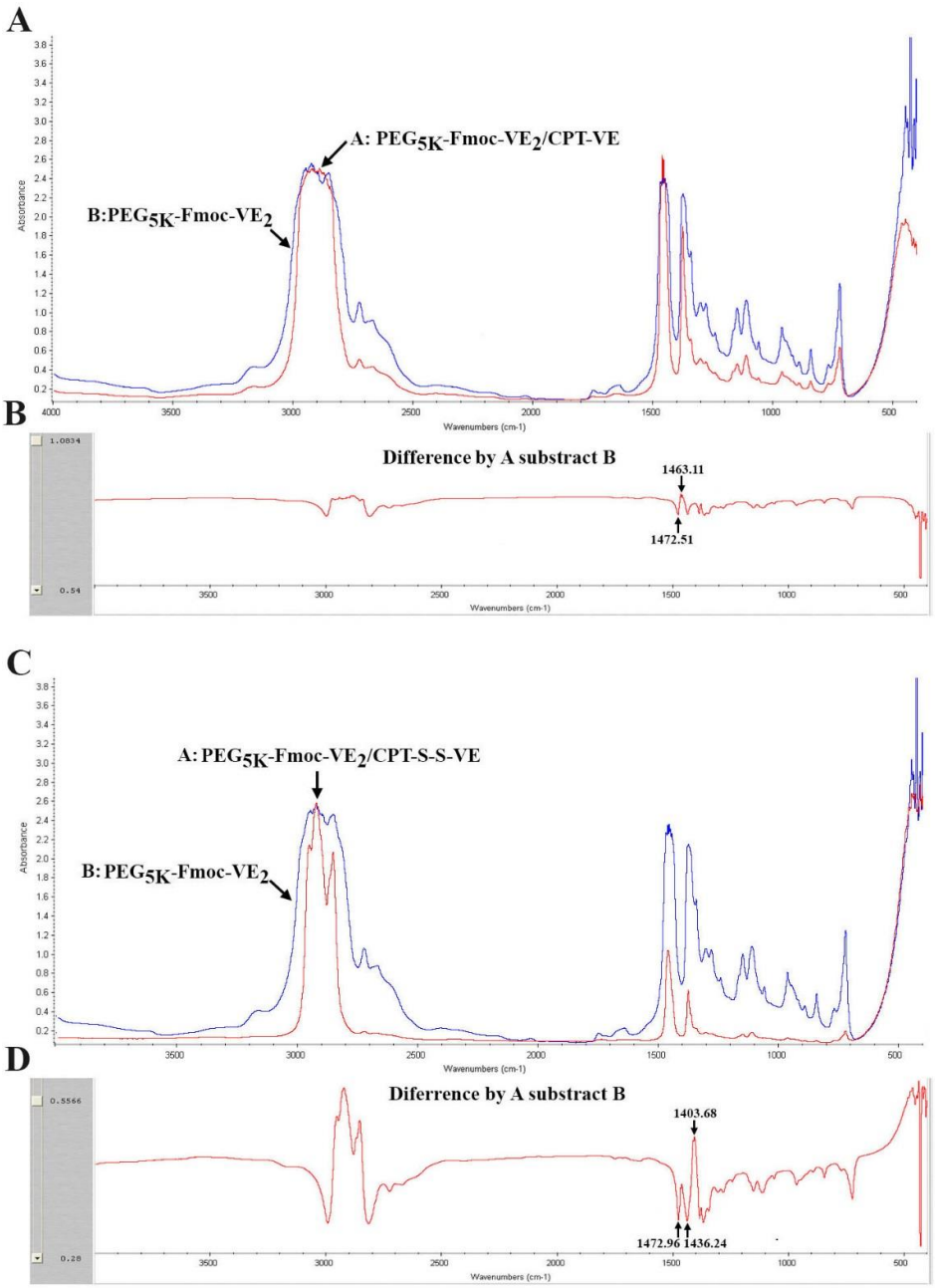

Figure 80 A: FT-IR of PEG_{5K}-Fmoc-VE_2, and PEG_{5K}-Fmoc-VE_2/CPT-VE. B: Difference of FT-IR between PEG_{5K}-Fmoc-VE_2 and PEG_{5K}-Fmoc-VE_2/CPT-VE. C: FT-IR of PEG_{5K}-Fmoc-VE_2, and PEG_{5K}-Fmoc-VE_2/CPT-S-S-VE. D: Difference of FT-IR between PEG_{5K}-Fmoc-VE_2, and PEG_{5K}-Fmoc-VE_2/CPT-S-S-VE.

The decrease of absorbance at 1472.51 cm^{-1} and a concurrent increase of absorbance at 1463.11 cm^{-1} demonstrated that incorporation of CPT-VE resulted in the disruption of the hydrogen bonding among carrier molecules and the formation of new hydrogen bonding between carrier

and CPT-VE molecules simultaneously (Lu, Zhao et al, 2014). Similar findings were garnered in PEG_{5K}-Fmoc-VE_2/CPT-S-S-VE system (**Figure 80B**).

7.3.7 *In vitro* cell-killing activity

In an attempt to see whether VE-derivatized CPTs still retain the biological function of its parental CPT, cytotoxicity of free CPT, CPT-VE, CPT-S-S-VE, PEG_{5K}-Fmoc-VE_2/CPT-VE and PEG_{5K}-Fmoc-VE_2/CPT-S-S-VE was assessed in 4T1.2 cells (**Figure 81**).

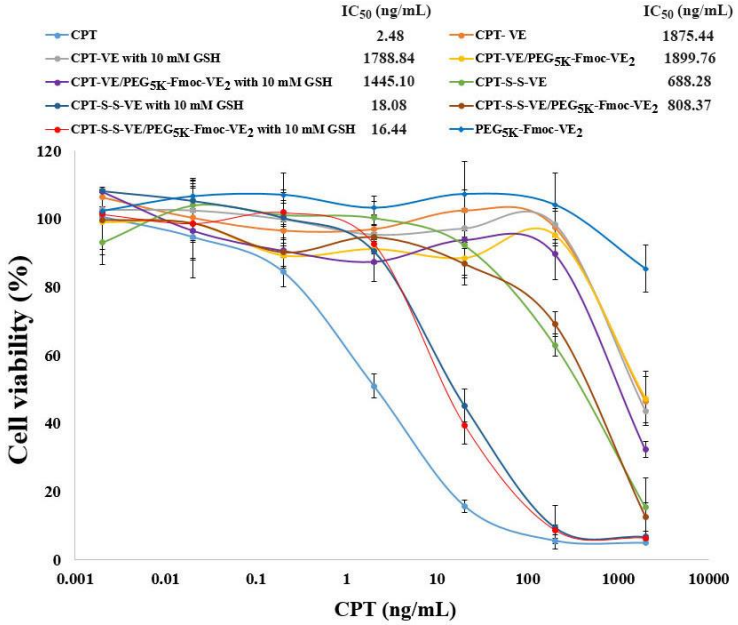

Figure 81 The cell-killing effect of CPT-VE, CPT-S-S-VE, PEG_{5K}-Fmoc-VE_2/CPT-VE, and PEG_{5K}-Fmoc-VE_2/CPT-S-S-VE with or without GSH (10 mM), comparing to free CPT in 4T1.2 cancer cell.

Aiming to examine disulfide bond-responsive release of CPT, GSH, a disulfide bond reducer, was added. Both CPT-VE and CPT-S-S-VE presented a dose-dependent antiproliferative effect at the higher concentration range, with CPT-S-S-VE more effective. Addition of GSH led to a dramatically enhanced cell-killing effect in CPT-S-S-VE system, while not much difference was observed in CPT-VE, indicating the merit of CPT-S-S-VE over CPT-VE in releasing CPT.

7.3.8 CPT intracellular release

To confirm that the enhanced cytotoxicity in CPT-S-S-VE was indeed ascribed to the more CPT release, CPT concentration inside cells was measured after treating cells at 100 ng/mL in terms of CPT for 24 h. Apparently, from the data shown in **Figure 82**, CPT-S-S-VE excelled CPT-VE in releasing CPT, as which provided almost 2-fold more CPT release than did CPT-VE.

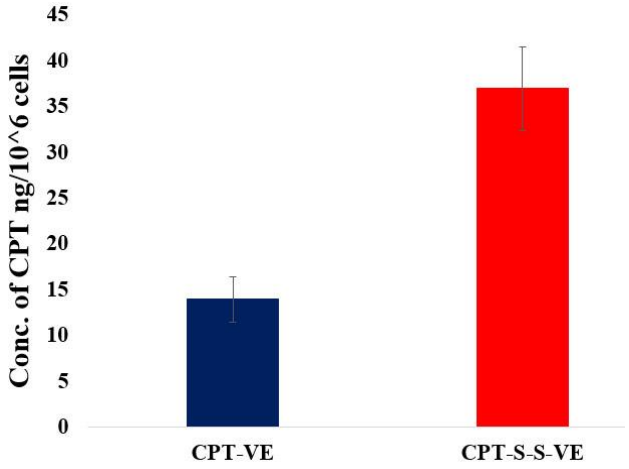

Figure 82 Intracellular release of CPT in 4T1.2 cells treated by CPT-VE and CPT-S-S-VE (100 ng/mL in terms of CPT) for 24 h.

7.3.9 Uptake of CPT-VE and CPT-S-S-VE nanoassemblies

Herein, mechanism of intracellular uptake of CPT-VE and CPT-S-S-VE formulated PEG_{5K}-Fmoc-VE_2 nanofibers was investigated. First, temperature dependence of uptake was evaluated by comparing the cytotoxicity of PEG_{5K}-Fmoc-VE_2/CPT-VE and PEG_{5K}-Fmoc-VE_2/CPT-S-S-VE after incubation at 4 and 37 °C, respectively (**Figure 83**).

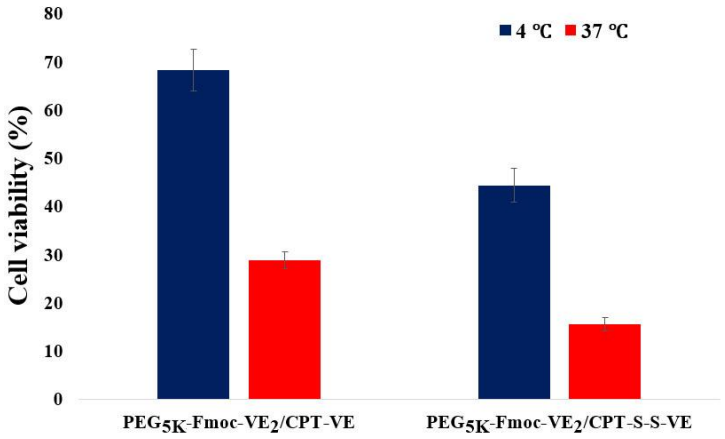

Figure 83 The cell viability in 4T1.2 cells after being treated with PEG_{5K}-Fmoc-VE_2/CPT-VE and PEG_{5K}-Fmoc-VE_2/CPT-S-S-VE for 2 h at 4 or 37 ℃, followed by 24 h incubation at a CPT concentration of 6 μg/mL.

The cell viability was significantly improved in cells incubated at 4 °C in both CPT prodrugs formulations, implying a much lower intracellular uptake and the involvement of active transportation under this circumstance. This finding is in concert with the literature, in which pinocytic/endocytic uptake was deactivated at 4 °C. Further, confocal laser scanning microscope was conducted (**Figure 84**). As shown in **Figure 84**, the fluorescence from CPT prodrugs nanofibers were well colocolized with that from LysoTracter, indicating that endocytotic pathway was employed during the uptake. Moreover, significantly enhanced fluorescence signal was detected in PEG_{5K}-Fmoc-VE_2/CPT-S-S-VE compared to that in PEG_{5K}-Fmoc-VE_2/CPT-VE. This was consistent with the studies performed in **Figure 81-83**, in which more release of CPT from CPT-S-S-VE was correlated.

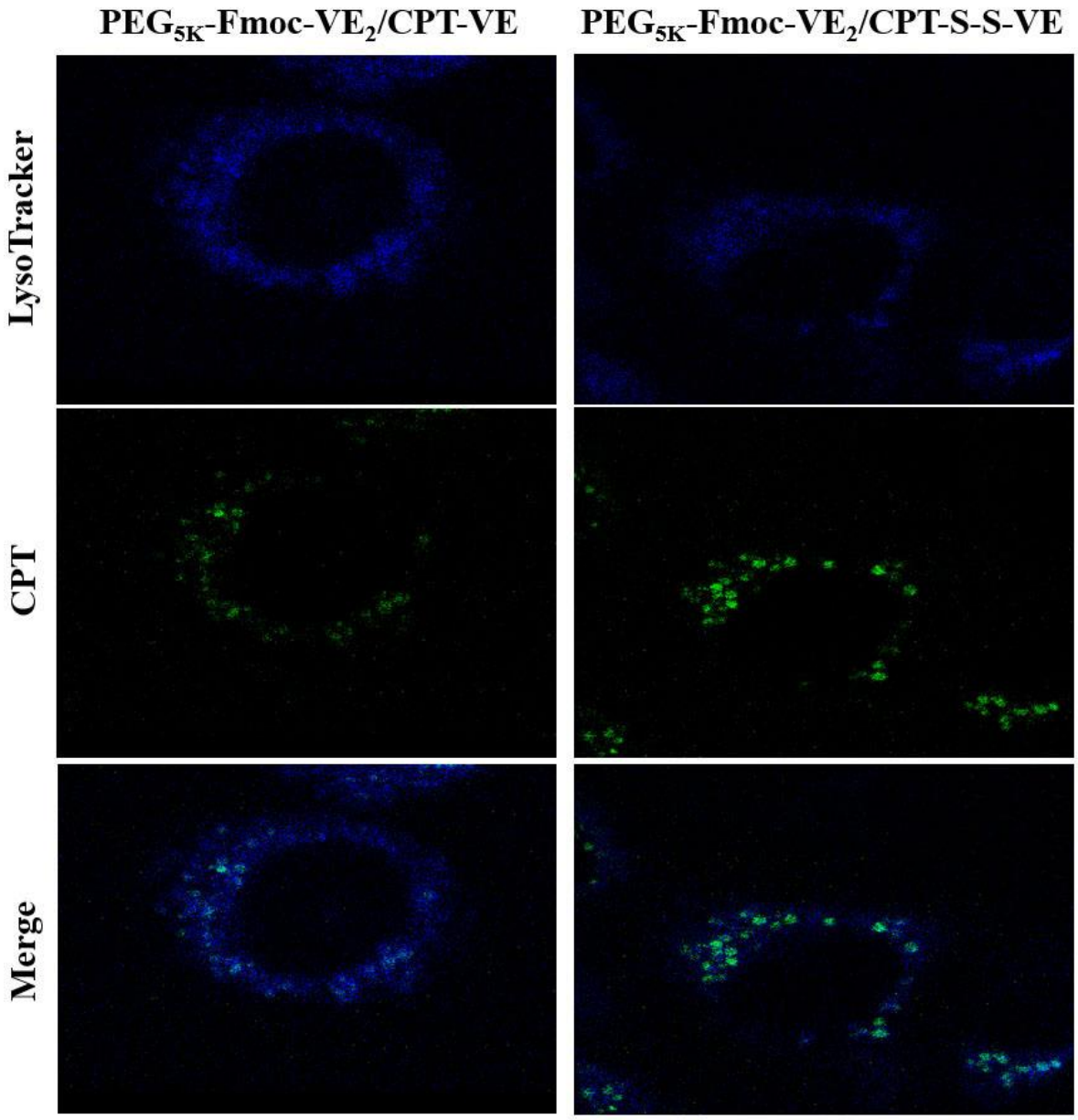

Figure 84 Confocal laser scanning microscopy (CLSM) images of 4T1.2 cells incubated with free PEG_{5K}-Fmoc-VE_2/CPT-VE and PEG_{5K}-Fmoc-VE_2/CPT-S-S-VE for 30 min at 37 ℃ at a CPT concentration of 6 μg/mL.

7.3.10 *In vivo* biodistribution

Efforts were also made to figure out the *in vivo* tissue distribution of CPT in both PEG_{5K}-Fmoc-VE_2/CPT-VE and PEG_{5K}-Fmoc-VE_2/CPT-S-S-VE in tumor-bearing mice. Twenty-four h post

the injection of PEG_{5K}-Fmoc-VE_2/CPT-VE and PEG_{5K}-Fmoc-VE_2/CPT-S-S-VE, at the 5 mg CPT/kg, blood, tumor, heart, liver, lung, spleen, and kidneys were collected for the measurement of CPT. Compared to PEG_{5K}-Fmoc-VE_2/CPT-VE, significantly greater amount of CPT was accumulated in tumor from PEG_{5K}-Fmoc-VE_2/CPT-S-S-VE nanofibers (**Figure 85**).

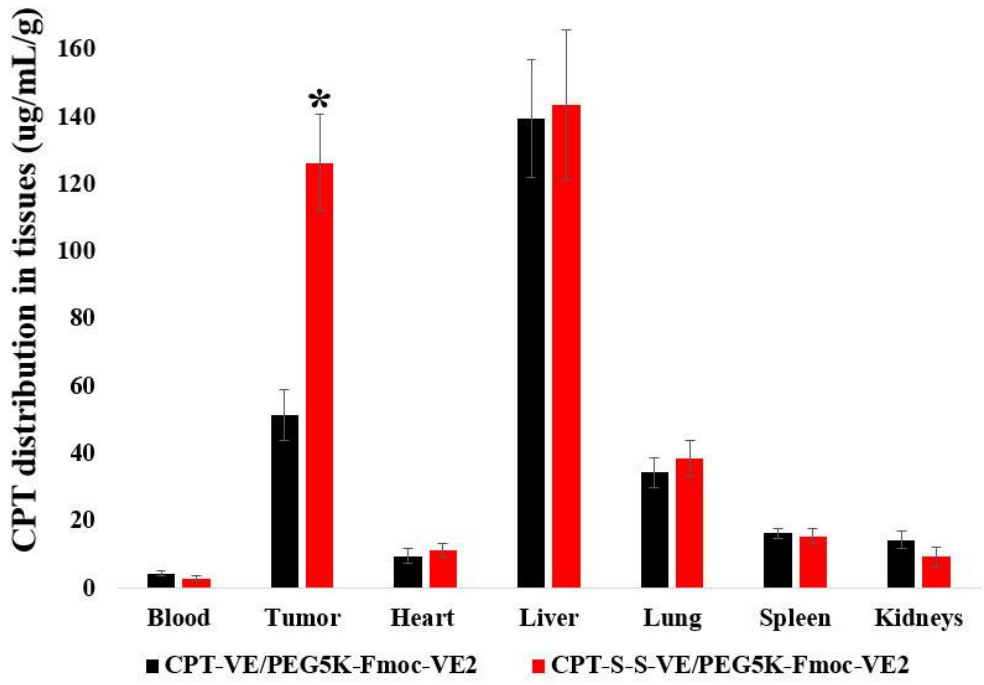

Figure 85 Tissue biodistribution of PEG_{5K}-Fmoc-VE_2/CPT-VE and PEG_{5K}-Fmoc-VE_2/CPT-S-S-VE (5mg CPT/kg) in 4T1.2-tumor bearing mice. *$p < 0.001$, compared to PEG_{5K}-Fmoc-VE_2/CPT-VE.

7.3.11 Antitumor activity.

In vivo antitumor effect of CPT prodrugs nanoassemblies was examined in 4T1.2 breast tumor bearing mice (**Figure 86**). As expected, mice quickly developed tumors in an uncontrolled manner after being injected by saline (**Figure 86A**). In free CPT treated group, the tumor growth was moderately suppressed. Greatly improved antitumor activity was achieved in PEG_{5K}-Fmoc-VE_2/CPT-VE-challenged group over that of free CPT. Strikingly, when mice was injected by PEG_{5K}-Fmoc-VE_2/CPT-S-S-VE, a drastically enhanced tumor growth inhibition was observed

with an IR at 81.90%. Furthermore, doubling the dose to 10 mg CPT/kg led to almost complete remission in mice bearing tumors (IR=93.48%) (**Table 24**). All of the treatments were well tolerated by mice evidenced by no significant weight changes of mice during the experimental period (**Figure 86B**).Tumors across the groups were also imaged and weighted after terminating the study (**Figure 86C & D**).

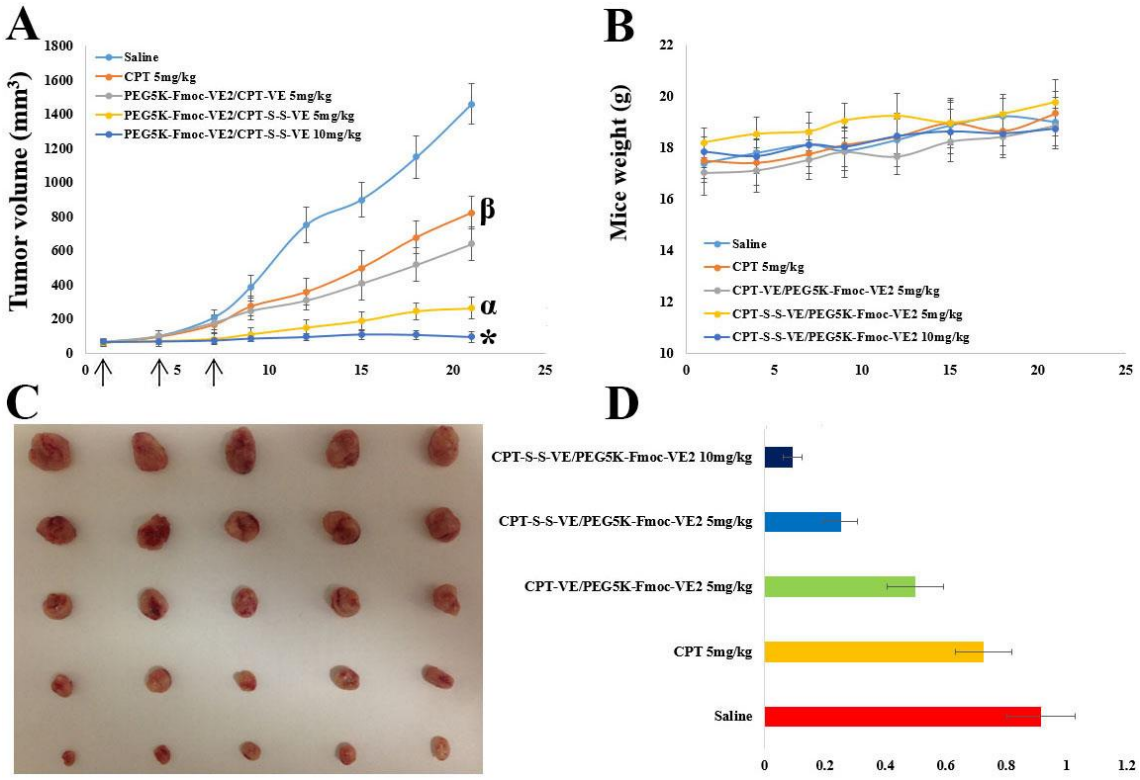

Figure 86 Antitumor efficacy of varying CPT or CPT prodrugs nanoformulations in 4T1.2 breast tumor model. Solid arrows indicate the i.v. injection. A: tumor volume. *p < 0.01, compared to PEG_{5K}-Fmoc-VE_2/CPT-S-S-VE (5 mg/kg); $^{\alpha}p$ < 0.001, compared to PEG_{5K}-Fmoc-VE_2/CPT-VE (5 mg/kg) and CPT (5 mg/kg); $^{\beta}p$ < 0.001, compared to saline; B: mouse body weight, C: tumor images. D: tumor weight.

Table 24 Tumor growth inhibition rate (IR) in 4T1.2 tumor bearing mice.

Treatments	IR (%)
CPT 5 mg/kg	43.69
PEG_{5K}-Fmoc-VE_2/CPT-VE 5 mg/kg	56.06
PEG_{5K}-Fmoc-VE_2/CPT-S-S-VE 5 mg/kg	81.90
PEG_{5K}-Fmoc-VE_2/CPT-S-S-VE 10 mg/kg	93.48

IR % = (1 – tumor volume in the treated group/ tumor volume in the saline group) × 100%
IR % was calculated based on the tumor volume on day 21

Further, tumors were also subject to H&E staining. As depicted in **Figure 87**, tumors from the mice treated with PEG_{5K}-Fmoc-VE_2/CPT-S-S-VE exhibited a significantly greater wealth of apoptotic cells, particularly in 10 mg/kg group, in comparison to the tumors from saline, free CPT, and PEG_{5K}-Fmoc-VE_2/CPT-VE-treated groups, which is aligned with the observation in the study of suppressing tumor growth (**Figure 86**).

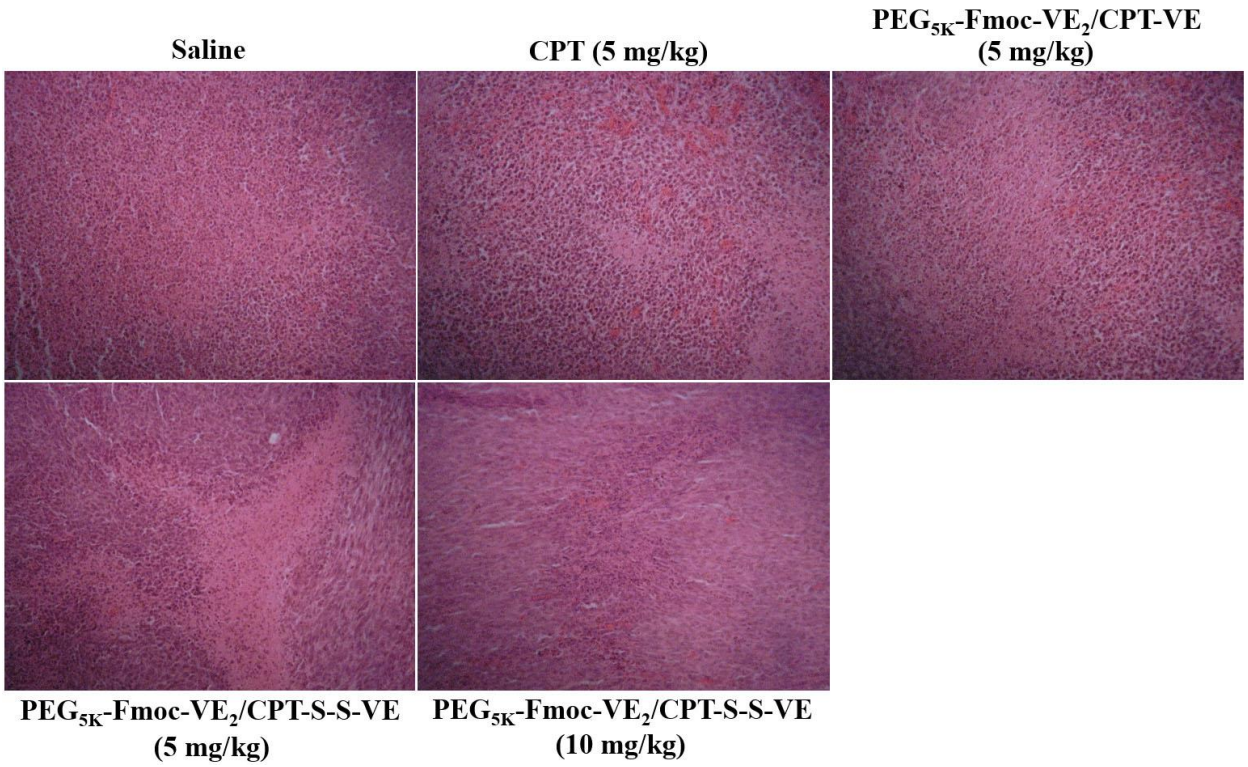

Figure 87 H&E staining of tumor tissues.

7.4 DISCUSSION

The emphasis of the current work was placed on improving the compatibility of CPT with the nanocarriers developed recently in our laboratory and the stability of CPT (Lu, Huang et al. 2013) (Lu, Zhao et al. 2014). To this end, CPT prodrugs were constructed through conjugating CPT to VE at its hydroxyl group via either disulfide bond (CPT-S-S-VE) or carbonate ester linkage (CPT-VE).

CPT is not stable in blood stream, as where the basic medium can convert its active lactone ring form to inactive carboxylate form, leading to the reduced biological activity of CPT (Fassberg and Stella 1992, Mu, Elbayoumi et al. 2005). It has been well established that introduction of steric hindrance to the hydroxyl group of the CPT will greatly enhance the stability of the lactone ring (Zhao, Lee et al. 2000, Li, Lv et al. 2009). Also, CPT prodrugs that are formulated in nanoparticles can not only be prevented from being converted to carboxylate form due to the isolation from the mildly basic environment, but also be protected from opsonization (Yen, Cabral et al. 2014). Moreover, the neutralized nanoparticles (**Table 23**) could reduce the possibility of being bound by blood proteins and transverse the cell membrane more efficiently (Ukawa, Akita et al. 2014). Therefore, formulating CPT-VE or CPT-S-S-VE in nanoparticles will inevitably strengthen the integrity of active CPT.

For the synthesis of CPT-VE, first, direct conjugation of CPT to VE-succinate was undertaken. It was anticipated that the carboxylate group in VE-succinate can be coupled with the hydroxyl moiety in CPT readily with the catalysis of DCC and DMAP. However, several attempts were in vain, which may be due to the inadequate accessibility at the hydroxyl group in CPT and the insufficient conjugation between –OH and –COOH. Afterwards, triphosgene was applied to further activate the –OH of CPT to –COCl, which is much easier to react with other

nucleophiles, including –OH (ref), and also led to increased accessibility of the reacting moiety. Therefore, VE (-OH) was linked to CPT-COCl to successfully yield CPT-VE with carbonate ester bond. For the synthesis of CPT-S-S-VE, in order to minimize the generation of VE-S-S-VE in the first step, 1 eq. molar of VE-succinate was conjugated to 2 eq. molar of $HOCH_2CH_2$-S-S-CH_2CH_2OH, under which products were mostly comprised of VE-S-S-OH. Then, VE-S-S-OH was coupled to CPT-COCl (as mentioned above) to yield CPT-S-S-VE with disulfide bond. Reduction-sensitive prodrugs have been intensively studied and posed great potential in effectively releasing the active parental drugs (Xiao, Qi et al. 2011, van der Vlies, Hasegawa et al. 2012, Xing, Mao et al. 2012).

It was noted that CPT-VE and CPT-S-S-VE can both self-assemble into nanofibers upon stabilization by PEG_{5K}-Fmoc-VE_2 in aqueous solution. Previously, we found that PEG_{5K}-Fmoc-VE_2 can self-assemble into nanotubular or worm-like micelles, in which Fmoc motif played a crucial role in forming the unique elongated micelles (Lu, Zhao et al. 2014). Herein, in order to elucidate the contribution of Fmoc in the formation of nanofibers in PEG_{5K}-Fmoc-VE_2/CPT-VE and PEG_{5K}-Fmoc-VE_2/CPT-S-S-VE, PEG_{5K}-VE_2/CPT-VE and PEG_{5K}-VE_2/CPT-S-S-VE were prepared and scoped under cryoEM, interestingly, both of which were found to be spherical micelles, suggesting the indispensable role of Fmoc in producing nanofibers. Furthermore, efforts have also been taken to investigate the function of VE in nanofiber development. Again, nanospheres were identified in both PEG_{5K}-VE_2/CPT and PEG_{5K}-Fmoc-VE_2/CPT formulations, which implied that introduction of VE to CPT contribute considerably to the formation of the nanofibers as well. Notably, the inter-connected nanofibers formed in PEG_{5K}-Fmoc-VE_2/CPT-S-S-VE system were different from that in PEG_{5K}-Fmoc-VE_2/CPT-VE, which could be arisen from the crosslinking nature of the disulfide group (Herlambang, Kumagai et al. 2011).

In **Table 23**, the CPT DLCs were dramatically improved in CPT prodrugs nanoassemblies, especially in PEG_{5K}-Fmoc-VE_2/CPT-S-S-VE system, compared to CPT nanoformulations. This is highly likely due to the addition of VE molecule to CPT so that the compatibility of CPT-VE or CPT-S-S-VE to carriers (PEG_{5K}-Fmoc-VE_2 and PEG_{5K}-VE_2) was significantly ameliorated, in which the hydrophobic interaction between VE molecules from payloads and carriers could act as the driving force to form nanoparticles during self-assembly process of the carriers, leading to both increased DLC and enhanced stability. Besides, the additional hydrogen bonding (**Figure 80**) could also contribute greatly to the formation of the stable nanofibers in PEG_{5K}-Fmoc-VE_2/CPT-S-S-VE and PEG_{5K}-Fmoc-VE_2/CPT-VE. Futhermore, the flexible CPT-S-S-VE could offer the increased degree of freedom of rotation, in contrast to relatively rigid CPT-VE, which could adjust the spatial arrangement of CPT-S-S-VE to the optimal position so as to be anchored into carriers in a more stabilized fashion. This was reflected in **Figure 78 & 79**, in which significantly more fluorescence quenching and decrease of UV absorbance were yielded in CPT-S-S-VE formulations over that in CPT-VE system. Furthermore, the higher levels of CPT loading in PEG_{5K}-Fmoc-VE_2 over PEG_{5K}-VE_2 could be attributed to the introduction of the Fmoc, which as a drug-interactive motif can provide additional drug/carrier π-π stacking interaction to further enhance the drug loading and formulation stability as unveiled in the fluorescence study in **Figure 78** (Gao, Huang et al. 2013, Zhang, Lu et al. 2014) (Lu, Zhao et al. 2014).

In vivo biodistribution assay demonstrated that both PEG_{5K}-Fmoc-VE_2/CPT-S-S-VE and PEG_{5K}-Fmoc-VE_2/CPT-VE can accumulate at tumor areas and release CPT. As discussed above, the significantly enhanced drug/carrier interactions equipped PEG_{5K}-Fmoc-VE_2/CPT-S-S-VE and PEG_{5K}-Fmoc-VE_2/CPT-VE nanoassemblies with superior stability *in vivo*, leading to the

prolonged blood circulation. It has also been established that the elongated nanoparticles tend to circulate longer period of time compared to the spherical counterparts (Geng, Dalhaimer et al. 2007). Both of these will result in the increased chance of nanofibers to get to tumurol sites. However, significantly improved CPT accumulation was noticed in PEG_{5K}-Fmoc-VE_2/CPT-S-S-VE over PEG_{5K}-Fmoc-VE_2/CPT-VE. This could be attributed to the following facts. First, Luo et al reported that size of nanoparticles smaller than 64 nm was prerequisite in order to effectively and deeply penetrate solid tumor tissue, especially in refractory tumor (Luo, Xiao et al. 2010). Therefore, smaller sized PEG_{5K}-Fmoc-VE_2/CPT-S-S-VE (49.7 nm) is more efficient in penetrating the tumor tissue compared to the relatively larger sized PEG_{5K}-Fmoc-VE_2/CPT-VE (87.4 nm). Moreover, the disulfide bond linked VE-derivatized CPT is more likely to readily release CPT, considering the relatively high GSH concentration in tumor cells (Wu, Fang et al. 2004). The enhanced tumor distribution of CPT in PEG_{5K}-Fmoc-VE_2/CPT-S-S-VE can contribute significantly to the dramatically higher level of delaying the tumor growth, compared to saline, free CPT, and PEG_{5K}-Fmoc-VE_2/CPT-VE (**Figure 86**). Furthermore, the internalization of PEG_{5K}-Fmoc-VE_2/CPT-S-S-VE was modulated via endocytosis, which allows them to escape the P-gp-mediated efflux pump (Lu, Huang et al. 2013), leading to the enhanced intracellular accumulation of active CPT, consequently, resulting in the superior antitumor efficacy.

Hence, VE-derivatized CPT can serve as a proof-of-concept model to solve the issues facing the drug delivery field when highly hydrophobic drugs are hard to be formulated directly. However, modification to the parent drug oftentimes can lead to the reduction or absence of the biological activity of the parental drug, thereby, effective liberation of the parental drug via

trigger-responsive release should be taken into account, such as, pH, redox, protonation-stimulated release.

8.0 SUMMARY AND PERSPECTIVES

Chemotherapeutics have played a pivotal role in the battle of combatting against notorious cancer. Administration of anticancer agents to patients can greatly hinder the growth of tumor, but the therapeutic index remains unsatisfactory and oftentimes leads to the severe side effects due to the poor bioavailability and lack of tumor specific targetability. To address this issue, during the last couple of decades, nanotechnology-based medicine has emerged and attracted considerable attention, among which polymeric micellar drug formulations have been investigated extensively because of the technical ease, the ability to solubilize poorly water soluble drugs as well as the superior tumor targeting capability due to the extremely small size (10-100 nm) based on EPR effect (Matsumura and Maeda 1986, Torchilin 2007).

In my graduate work, I worked on several cohesive strategies to develop dual functional nanomicellar carriers for the targeted delivery of chemotherapeutics to cancer aiming to resolve the challenges facing in the drug delivery. First, dual functional carrier derived from the PEG-conjugated Embelin (PEG-EB) was developed. Being a long aliphatic hydrophobic molecule, Embelin has antitumor activity through suppressing the activity of XIAP (X-chromosome-linked apoptosis protein) (Nikolovska-Coleska, Xu et al. 2004). However, its utility is greatly restrained by its poor solubility and limited oral bioavailability (Singh, Guru et al. 2014). Coupling of PEG to EB can significantly increase its solubility, and surprisingly the PEG-EB conjugates can self-

assemble into nanomicelles which can effectively solubilize and formulate other hydrophobic antineoplastic agents (Huang, Lu et al. 2012, Lu, Huang et al. 2013). Distinct from most of existing drug delivery system, our carrier itself has antitumor activity and can further synergize with co-delivered therapeutics. After systemic investigations, we found that PTX-loaded PEG-derivatized Embelin micellar formulation exerted significantly enhanced antitumor efficacy and less systemic toxicity compared to Taxol. Moreover, the system was further improved by attaching a tumor-specific ligand-folate onto the surface of the PEG_{5K}-EB_2 micelles (FA-PEG_{5K}-EB_2), which led to a dramatically augmented tumor cell growth inhibition in both drug sensitive and resistant cancers when delivering DOX (Lu, Zhao et al. 2014).

Besides, efforts were also made on the systemic study of SAR on a PEG-Vitamin E (PEG-VE)-based dual functional carrier. Our data suggested that the molecular weight of PEG and the molar ratio of PEG/VE significantly impacted the overall performance of the conjugates. A conjugate of PEG (5K) with two VE molecules (PEG_{5K}-VE_2) was the most efficient formulation in delivering PTX (Lu, Huang et al. 2013). Additionally, the conjugates well retained the intrinsic function of VE in inhibiting the activity of P-gp. Finally, the PEG_{5K}-VE_2/PTX nanomicelles exhibited the highest level of delaying tumor development compared to PEG_{2K}-VE/PTX, PEG_{2K}-VE_2/PTX, and Taxol (Lu, Huang et al. 2013).

As an independent approach to improve the performance of the current micellar formulations including our dual functional carriers, it was demonstrated that incorporation of a drug-interactive motif (Fmoc) into the interfacial region of PEG_{5K}-VE_2 (PEG_{5K}-Fmoc-VE_2) led to a significant improvement in both drug loading and formulation stability (Lu, Zhao et al. 2014). The nanoformulations with interfacial Fmoc motif showed markedly elevated

antineoplastic efficacy than the counterpart without Fmoc in several animal models including drug resistant tumor model (Lu, Zhao et al. 2014).

Our improved vectors worked well for most of the hydrophobic chemotherapeutics, but cannot effectively accommodate camptothecin (CPT), a potent anticancer agent. Herein, I have shown that this problem can be resolved via derivatizing CPT with VE via either carbonate ester bond (CPT-VE) or disulfide linkage (CPT-S-S-VE) (Lu, Liu et al. submitted). Our results indicated that the antitumor activity was remarkably impacted by the type of carrier (with or without interfacial Fmoc) and the chemical linkage between CPT and VE. When CPT-VE or CPT-S-S-VE was formulated in PEG_{5K}-Fmoc-VE_2, the CPT loading and formulation stability were predominantly higher than in PEG_{5K}-VE_2. Furthermore, reduction-sensitive linked CPT-S-S-VE showed the significantly enhanced anticancer therapeutic index in comparison to CPT-VE when formulated in PEG_{5K}-Fmoc-VE_2 micelles, or free CPT (Lu, Liu et al. submitted).

The two biggest concerns facing the polymeric micellar drug delivery system are the insufficient stability *in vivo* upon dilution and the limited drug loading. Several novel approaches have been developed to enhance the formulation stability and drug loading by improving the drug/carrier interactions, such as the hydrotrope or Fmoc-containing polymers, incorporation of the same anticancer agent into the hydrophobic portion in polymeric micelles (Huh, Lee et al. 2005, Kim, Kim et al. 2010, Kim, Kim et al. 2011, Gao, Huang et al. 2013, Cabral and Kataoka 2014, Zhang, Lu et al. 2014). There is still a long way to go so as to eradicate cancer, albeit advancement in drug delivery has been achieved. In addition, dual functional carrier based on PEG-derivatized bioactive molecules could represent a novel platform in chemotherapy. In such a system, synergistic effect will be easily obtained between the carrier and loaded drug to maximize the antitumor efficacy, meanwhile, the side effects arisen from the loaded anticancer

agents could also be potentially offset by the contribution from the biofunctional carrier. Furthermore, in addition to the passive targeting to tumor, active targeting by attaching ligand into micelles should also be employed in order to further improve the efficiency of intercellular uptake, and minimize the off-target untoward effects.

Besides, conjugation of a second molecule such as a lipid (VE), to originally hard-to-be formulated hydrophobic drugs may be deemed as a promising approach to effectively solubilize drugs, in which VE-derivatized CPT can serve as a proof-of-concept model that holds great potential in drug delivery field. The underlying mechanism of this phenomenon could be attributed to the spatial rearrangement of the loaded drug so that they can better fit to the hydrophobic pocket in the micelles, leading to the enhanced carrier/drug interactions. Conventional polymeric micelle has a hydrophobic core where the hydrophobic anticancer agents (PTX, CPT) can be solubilized. Whereas, for the hydrophilic drugs such as platinum drugs, gemcitabine, and Fluorouracil, micellar system is of no use. Although hydrophilic drugs are soluble *in vivo*, the non-specific absorption by epithelium cells may impose severe safety concern. Therefore, nanoformulations for them are indispensably needed. Conjugation of a lipid, such as VE, may address this issue. First, after derivatizing hydrophilic drugs with a lipid, the hydrophobicity will be increased significantly, which could allow originally hydrophilic drugs to be formulated inside the hydrophobic core of the micelles. The antineoplastic activity of those hydrophilic agents could be markedly enhanced via the tumor targeted delivery by polymeric micelle with significantly decreased possibility of poisoning the normal tissues. However, modification to the parent drug oftentimes can lead to the reduction or absence of the biological activity of the parental drug, thereby, effective liberation of the parental drug via stimuli-

responsive release should be taken into consideration, such as, pH, redox, protonation-triggered release.

BIBLIOGRAPHY

Adak, T., J. Kumar, N. A. Shakil and S. Walia (2012). "Development of controlled release formulations of imidacloprid employing novel nano-ranged amphiphilic polymers." Journal of Environmental Science and Health Part B-Pesticides Food Contaminants and Agricultural Wastes **47**(3): 217-225.

Aggarwal, N., S. Goindi and S. D. Mehta (2012). "Preparation and evaluation of dermal delivery system of griseofulvin containing vitamin E-TPGS as penetration enhancer." AAPS PharmSciTech **13**(1): 67-74.

Ahn, K. S., G. Sethi and B. B. Aggarwal (2007). "Embelin, an inhibitor of X chromosome-linked inhibitor-of-apoptosis protein, blocks nuclear factor-kappaB (NF-kappaB) signaling pathway leading to suppression of NF-kappaB-regulated antiapoptotic and metastatic gene products." Mol Pharmacol **71**(1): 209-219.

Akhtar, M. J., M. Ahamed, H. A. Alhadlaq, S. A. Alrokayan and S. Kumar (2014). "Targeted anticancer therapy: Overexpressed receptors and nanotechnology." Clinica Chimica Acta **436**: 78-92.

Al-Batran, S. E., H. G. Meerpohl, G. von Minckwitz, A. Atmaca, U. Kleeberg, N. Harbeck, W. Lerbs, D. Hecker, J. Sehouli, A. Knuth and E. Jager (2006). "Reduced incidence of severe palmar-plantar erythrodysesthesia and mucositis in a prospective multicenter phase II trial with pegylated liposomal doxorubicin at 40 mg/m2 every 4 weeks in previously treated patients with metastatic breast cancer." Oncology **70**(2): 141-146.

Al-Jamal, K. T., T. Sakthivel and A. T. Florence (2003). "Dendrisomes: cationic lipidic dendron vesicular assemblies." Int J Pharm **254**(1): 33-36.

Anbharasi, V., N. Cao and S. S. Feng (2010). "Doxorubicin conjugated to D-alpha-tocopheryl polyethylene glycol succinate and folic acid as a prodrug for targeted chemotherapy." J Biomed Mater Res A **94**(3): 730-743.

Bae, Y., S. Fukushima, A. Harada and K. Kataoka (2003). "Design of environment-sensitive supramolecular assemblies for intracellular drug delivery: polymeric micelles that are responsive to intracellular pH change." Angew Chem Int Ed Engl **42**(38): 4640-4643.

Barreiro-Iglesias, R., L. Bromberg, M. Temchenko, T. A. Hatton, A. Concheiro and C. Alvarez-Lorenzo (2004). "Solubilization and stabilization of camptothecin in micellar solutions of pluronic-g-poly(acrylic acid) copolymers." J Control Release **97**(3): 537-549.

Bawarski, W. E., E. Chidlowsky, D. J. Bharali and S. A. Mousa (2008). "Emerging nanopharmaceuticals." Nanomedicine **4**(4): 273-282.

Baylin, S. B. and J. E. Ohm (2006). "Epigenetic gene silencing in cancer - a mechanism for early oncogenic pathway addiction?" Nat Rev Cancer **6**(2): 107-116.

Bedi, D., J. W. Gillespie, V. A. Petrenko, Jr., A. Ebner, M. Leitner, P. Hinterdorfer and V. A. Petrenko (2013). "Targeted delivery of siRNA into breast cancer cells via phage fusion proteins." Mol Pharm **10**(2): 551-559.

Berezovskaya, O., A. D. Schimmer, A. B. Glinskii, C. Pinilla, R. M. Hoffman, J. C. Reed and G. V. Glinsky (2005). "Increased expression of apoptosis inhibitor protein XIAP contributes to anoikis resistance of circulating human prostate cancer metastasis precursor cells." Cancer Res **65**(6): 2378-2386.

Bhandari, U., N. Jain and K. K. Pillai (2007). "Further studies on antioxidant potential and protection of pancreatic beta-cells by Embelia ribes in experimental diabetes." Exp Diabetes Res **2007**: 15803.

Bieri, J. G. and R. P. Evarts (1974). "Gamma tocopherol: metabolism, biological activity and significance in human vitamin E nutrition." Am J Clin Nutr **27**(9): 980-986.

Brigelius-Flohe, R. and M. G. Traber (1999). "Vitamin E: function and metabolism." FASEB J **13**(10): 1145-1155.

Burns, F. J., A. N. Uddin, F. Wu, A. Nadas and T. G. Rossman (2004). "Arsenic-induced enhancement of ultraviolet radiation carcinogenesis in mouse skin: a dose-response study." Environ Health Perspect **112**(5): 599-603.

Buse, J. and A. El-Aneed (2010). "Properties, engineering and applications of lipid-based nanoparticle drug-delivery systems: current research and advances." Nanomedicine (Lond) **5**(8): 1237-1260.

Cabral, H. and K. Kataoka (2014). "Progress of drug-loaded polymeric micelles into clinical studies." J Control Release **190**: 465-476.

Cabral, H., Y. Matsumoto, K. Mizuno, Q. Chen, M. Murakami, M. Kimura, Y. Terada, M. R. Kano, K. Miyazono, M. Uesaka, N. Nishiyama and K. Kataoka (2011). "Accumulation of

sub-100 nm polymeric micelles in poorly permeable tumours depends on size." Nat Nanotechnol **6**(12): 815-823.

Caiolfa, V. R., M. Zamai, A. Fiorino, E. Frigerio, C. Pellizzoni, R. d'Argy, A. Ghiglieri, M. G. Castelli, M. Farao, E. Pesenti, M. Gigli, F. Angelucci and A. Suarato (2000). "Polymer-bound camptothecin: initial biodistribution and antitumour activity studies." J Control Release **65**(1-2): 105-119.

Cao, N. and S. S. Feng (2008). "Doxorubicin conjugated to D-alpha-tocopheryl polyethylene glycol 1000 succinate (TPGS): conjugation chemistry, characterization, in vitro and in vivo evaluation." Biomaterials **29**(28): 3856-3865.

Chavanpatil, M. D., A. Khdair, B. Gerard, C. Bachmeier, D. W. Miller, M. P. Shekhar and J. Panyam (2007). "Surfactant-polymer nanoparticles overcome P-glycoprotein-mediated drug efflux." Mol Pharm **4**(5): 730-738.

Chen, J., I. R. Corbin, H. Li, W. Cao, J. D. Glickson and G. Zheng (2007). "Ligand conjugated low-density lipoprotein nanoparticles for enhanced optical cancer imaging in vivo." J Am Chem Soc **129**(18): 5798-5799.

Chen, J., Z. Nikolovska-Coleska, G. Wang, S. Qiu and S. Wang (2006). "Design, synthesis, and characterization of new embelin derivatives as potent inhibitors of X-linked inhibitor of apoptosis protein." Bioorg Med Chem Lett **16**(22): 5805-5808.

Chen, X., X. Wang, Y. Wang, L. Yang, J. Hu, W. Xiao, A. Fu, L. Cai, X. Li, X. Ye, Y. Liu, W. Wu, X. Shao, Y. Mao, Y. Wei and L. Chen (2010). "Improved tumor-targeting drug delivery and therapeutic efficacy by cationic liposome modified with truncated bFGF peptide." J Control Release **145**(1): 17-25.

Chen, Y., X. Zhang, J. Lu, Y. Huang, J. Li and S. Li (2014). "Targeted delivery of curcumin to tumors via PEG-derivatized FTS-based micellar system." AAPS J **16**(3): 600-608.

Cheng, C., H. Wei, J. L. Zhu, C. Chang, H. Cheng, C. Li, S. X. Cheng, X. Z. Zhang and R. X. Zhuo (2008). "Functionalized thermoresponsive micelles self-assembled from biotin-PEG-b-P(NIPAAm-co-HMAAm)-b-PMMA for tumor cell target." Bioconjug Chem **19**(6): 1194-1201.

Cheng, G., J. Zielonka, D. M. McAllister, A. C. Mackinnon, Jr., J. Joseph, M. B. Dwinell and B. Kalyanaraman (2013). "Mitochondria-targeted vitamin E analogs inhibit breast cancer cell energy metabolism and promote cell death." BMC Cancer **13**: 285.

Cheng, L. S. and D. P. Cao (2009). "Effect of Tail Architecture on Self-Assembly of Amphiphiles for Polymeric Micelles." Langmuir **25**(5): 2749-2756.

Cheon Lee, S., C. Kim, I. Chan Kwon, H. Chung and S. Young Jeong (2003). "Polymeric micelles of poly(2-ethyl-2-oxazoline)-block-poly(epsilon-caprolactone) copolymer as a carrier for paclitaxel." J Control Release **89**(3): 437-446.

Chitra, M., E. Sukumar, V. Suja and C. S. Devi (1994). "Antitumor, anti-inflammatory and analgesic property of embelin, a plant product." Chemotherapy **40**(2): 109-113.

Choucair, A. and A. Eisenberg (2003). "Control of amphiphilic block copolymer morphologies using solution conditions." European Physical Journal E **10**(1): 37-44.

Cloninger, M. J. (2002). "Biological applications of dendrimers." Curr Opin Chem Biol **6**(6): 742-748.

Collnot, E. M., C. Baldes, M. F. Wempe, R. Kappl, J. Huttermann, J. A. Hyatt, K. J. Edgar, U. F. Schaefer and C. M. Lehr (2007). "Mechanism of inhibition of P-glycoprotein mediated efflux by vitamin E TPGS: influence on ATPase activity and membrane fluidity." Mol Pharm **4**(3): 465-474.

Constantinides, P. P., J. Han and S. S. Davis (2006). "Advances in the use of tocols as drug delivery vehicles." Pharm Res **23**(2): 243-255.

Croce, C. M. (2008). "Oncogenes and cancer." N Engl J Med **358**(5): 502-511.

Croy, S. R. and G. S. Kwon (2006). "Polymeric micelles for drug delivery." Curr Pharm Des **12**(36): 4669-4684.

Cui, C., Y. N. Xue, M. Wu, Y. Zhang, P. Yu, L. Liu, R. X. Zhuo and S. W. Huang (2013). "Cellular uptake, intracellular trafficking, and antitumor efficacy of doxorubicin-loaded reduction-sensitive micelles." Biomaterials **34**(15): 3858-3869.

Dai, Y., L. Qiao, K. W. Chan, M. Yang, J. Ye, J. Ma, B. Zou, Q. Gu, J. Wang, R. Pang, H. Y. Lan and B. C. Wong (2009). "Peroxisome proliferator-activated receptor-gamma contributes to the inhibitory effects of Embelin on colon carcinogenesis." Cancer Res **69**(11): 4776-4783.

Danhier, F., T. T. Kouhe, N. Duhem, B. Ucakar, A. Staub, N. Draoui, O. Feron and V. Preat (2014). "Vitamin E-based micelles enhance the anticancer activity of doxorubicin." Int J Pharm **476**(1-2): 9-15.

Danhier, F., N. Magotteaux, B. Ucakar, N. Lecouturier, M. Brewster and V. Preat (2009). "Novel self-assembling PEG-p-(CL-co-TMC) polymeric micelles as safe and effective delivery system for paclitaxel." Eur J Pharm Biopharm **73**(2): 230-238.

Danquah, M., C. B. Duke, 3rd, R. Patil, D. D. Miller and R. I. Mahato (2012). "Combination therapy of antiandrogen and XIAP inhibitor for treating advanced prostate cancer." Pharm Res **29**(8): 2079-2091.

Danquah, M., F. Li, C. B. Duke, 3rd, D. D. Miller and R. I. Mahato (2009). "Micellar delivery of bicalutamide and embelin for treating prostate cancer." Pharm Res **26**(9): 2081-2092.

Daoud, S. S., M. I. Fetouh and B. C. Giovanella (1995). "Antitumor effect of liposome-incorporated camptothecin in human malignant xenografts." Anticancer Drugs **6**(1): 83-93.

Desai, P. V., G. A. Sawada, I. A. Watson and T. J. Raub (2013). "Integration of in silico and in vitro tools for scaffold optimization during drug discovery: predicting P-glycoprotein efflux." Mol Pharm **10**(4): 1249-1261.

Dharap, S. S., B. Qiu, G. C. Williams, P. Sinko, S. Stein and T. Minko (2003). "Molecular targeting of drug delivery systems to ovarian cancer by BH3 and LHRH peptides." J Control Release **91**(1-2): 61-73.

Dintaman, J. M. and J. A. Silverman (1999). "Inhibition of P-glycoprotein by D-alpha-tocopheryl polyethylene glycol 1000 succinate (TPGS)." Pharm Res **16**(10): 1550-1556.

Dong, Y. and S. S. Feng (2005). "Poly(d,l-lactide-co-glycolide)/montmorillonite nanoparticles for oral delivery of anticancer drugs." Biomaterials **26**(30): 6068-6076.

Duhem, N., F. Danhier, V. Pourcelle, J. M. Schumers, O. Bertrand, C. S. Leduff, S. Hoeppener, U. S. Schubert, J. F. Gohy, J. Marchand-Brynaert and V. Preat (2014). "Self-assembling doxorubicin-tocopherol succinate prodrug as a new drug delivery system: synthesis, characterization, and in vitro and in vivo anticancer activity." Bioconjug Chem **25**(1): 72-81.

Duhem, N., F. Danhier and V. Preat (2014). "Vitamin E-based nanomedicines for anti-cancer drug delivery." J Control Release **182**: 33-44.

Dysken, M. W., M. Sano, S. Asthana, J. E. Vertrees, M. Pallaki, M. Llorente, S. Love, G. D. Schellenberg, J. R. McCarten, J. Malphurs, S. Prieto, P. Chen, D. J. Loreck, G. Trapp, R. S. Bakshi, J. E. Mintzer, J. L. Heidebrink, A. Vidal-Cardona, L. M. Arroyo, A. R. Cruz, S. Zachariah, N. W. Kowall, M. P. Chopra, S. Craft, S. Thielke, C. L. Turvey, C. Woodman, K. A. Monnell, K. Gordon, J. Tomaska, Y. Segal, P. N. Peduzzi and P. D. Guarino (2014). "Effect of vitamin E and memantine on functional decline in Alzheimer disease: the TEAM-AD VA cooperative randomized trial." JAMA **311**(1): 33-44.

Elliott, R. L., M. C. Elliott, F. Wang and J. F. Head (1993). "Breast carcinoma and the role of iron metabolism. A cytochemical, tissue culture, and ultrastructural study." Ann N Y Acad Sci **698**: 159-166.

Fassberg, J. and V. J. Stella (1992). "A kinetic and mechanistic study of the hydrolysis of camptothecin and some analogues." J Pharm Sci **81**(7): 676-684.

Fornari, F. A., J. K. Randolph, J. C. Yalowich, M. K. Ritke and D. A. Gewirtz (1994). "Interference by doxorubicin with DNA unwinding in MCF-7 breast tumor cells." Mol Pharmacol **45**(4): 649-656.

Francisco, K. R., M. A. da Silva, E. Sabadini, G. Karlsson and C. A. Dreiss (2010). "Effect of monomeric and polymeric co-solutes on cetyltrimethylammonium bromide wormlike micelles: rheology, Cryo-TEM and small-angle neutron scattering." J Colloid Interface Sci **345**(2): 351-359.

Gana-Weisz, M., J. Halaschek-Wiener, B. Jansen, G. Elad, R. Haklai and Y. Kloog (2002). "The Ras inhibitor S-trans,trans-farnesylthiosalicylic acid chemosensitizes human tumor cells without causing resistance." Clin Cancer Res **8**(2): 555-565.

Gao, X., Y. Huang, A. M. Makhov, M. Epperly, J. Lu, S. Grab, P. Zhang, L. Rohan, X. Q. Xie, P. Wipf, J. Greenberger and S. Li (2013). "Nanoassembly of surfactants with interfacial drug-interactive motifs as tailor-designed drug carriers." Mol Pharm **10**(1): 187-198.

Gao, Y., L. B. Li and G. Zhai (2008). "Preparation and characterization of Pluronic/TPGS mixed micelles for solubilization of camptothecin." Colloids Surf B Biointerfaces **64**(2): 194-199.

Gaucher, G., M. H. Dufresne, V. P. Sant, N. Kang, D. Maysinger and J. C. Leroux (2005). "Block copolymer micelles: preparation, characterization and application in drug delivery." J Control Release **109**(1-3): 169-188.

Geng, Y., P. Dalhaimer, S. S. Cai, R. Tsai, M. Tewari, T. Minko and D. E. Discher (2007). "Shape effects of filaments versus spherical particles in flow and drug delivery." Nature Nanotechnology **2**(4): 249-255.

Giovannucci, E., Y. Liu, E. B. Rimm, B. W. Hollis, C. S. Fuchs, M. J. Stampfer and W. C. Willett (2006). "Prospective study of predictors of vitamin D status and cancer incidence and mortality in men." J Natl Cancer Inst **98**(7): 451-459.

Gottesman, M. M. (2002). "Mechanisms of cancer drug resistance." Annu Rev Med **53**: 615-627.

Greenspan, P., E. P. Mayer and S. D. Fowler (1985). "Nile red: a selective fluorescent stain for intracellular lipid droplets." J Cell Biol **100**(3): 965-973.

Ha, J. C., S. Y. Kim and Y. M. Lee (1999). "Poly(ethylene oxide)-poly(propylene oxide)-poly(ethylene oxide) (Pluronic)/poly(epsilon-caprolactone) (PCL) amphiphilic block copolymeric nanospheres. I. Preparation and characterization." J Control Release **62**(3): 381-392.

Haklai, R., M. G. Weisz, G. Elad, A. Paz, D. Marciano, Y. Egozi, G. Ben-Baruch and Y. Kloog (1998). "Dislodgment and accelerated degradation of Ras." Biochemistry **37**(5): 1306-1314.

Hamaguchi, T., T. Doi, T. Eguchi-Nakajima, K. Kato, Y. Yamada, Y. Shimada, N. Fuse, A. Ohtsu, S. Matsumoto, M. Takanashi and Y. Matsumura (2010). "Phase I study of NK012, a novel SN-38-incorporating micellar nanoparticle, in adult patients with solid tumors." Clin Cancer Res **16**(20): 5058-5066.

Han, Y., Y. Feng, H. Sun, Z. Li, Y. Han and H. Wang (2011). "Wormlike micelles formed by sodium erucate in the presence of a tetraalkylammonium hydrotrope." J Phys Chem B **115**(21): 6893-6902.

Hanahan, D. and R. A. Weinberg (2000). "The hallmarks of cancer." Cell **100**(1): 57-70.

Hanahan, D. and R. A. Weinberg (2011). "Hallmarks of cancer: the next generation." Cell **144**(5): 646-674.

Hatefi, A. and B. Amsden (2002). "Camptothecin delivery methods." Pharm Res **19**(10): 1389-1399.

Heo, J. Y., H. J. Kim, S. M. Kim, K. R. Park, S. Y. Park, S. W. Kim, D. Nam, H. J. Jang, S. G. Lee, K. S. Ahn, S. H. Kim, B. S. Shim, S. H. Choi and K. S. Ahn (2011). "Embelin suppresses STAT3 signaling, proliferation, and survival of multiple myeloma via the protein tyrosine phosphatase PTEN." Cancer Lett **308**(1): 71-80.

Herlambang, S., M. Kumagai, T. Nomoto, S. Horie, S. Fukushima, M. Oba, K. Miyazaki, Y. Morimoto, N. Nishiyama and K. Kataoka (2011). "Disulfide crosslinked polyion complex micelles encapsulating dendrimer phthalocyanine directed to improved efficiency of photodynamic therapy." J Control Release **155**(3): 449-457.

Hodul, P. J., Y. Dong, K. Husain, J. M. Pimiento, J. Chen, A. Zhang, R. Francois, W. J. Pledger, D. Coppola, S. M. Sebti, D. T. Chen and M. P. Malafa (2013). "Vitamin E delta-tocotrienol induces p27(Kip1)-dependent cell-cycle arrest in pancreatic cancer cells via an E2F-1-dependent mechanism." PLoS One **8**(2): e52526.

Holcik, M., H. Gibson and R. G. Korneluk (2001). "XIAP: apoptotic brake and promising therapeutic target." Apoptosis **6**(4): 253-261.

Hou, L., J. Yao, J. Zhou and Q. Zhang (2012). "Pharmacokinetics of a paclitaxel-loaded low molecular weight heparin-all-trans-retinoid acid conjugate ternary nanoparticulate drug delivery system." Biomaterials **33**(21): 5431-5440.

Hsiang, Y. H. and L. F. Liu (1988). "Identification of mammalian DNA topoisomerase I as an intracellular target of the anticancer drug camptothecin." Cancer Res **48**(7): 1722-1726.

Hu, C. M. and L. Zhang (2009). "Therapeutic nanoparticles to combat cancer drug resistance." Curr Drug Metab **10**(8): 836-841.

Huang, Y., J. Lu, X. Gao, J. Li, W. Zhao, M. Sun, D. B. Stolz, R. Venkataramanan, L. C. Rohan and S. Li (2012). "PEG-derivatized embelin as a dual functional carrier for the delivery of paclitaxel." Bioconjug Chem **23**(7): 1443-1451.

Huh, K. M., S. C. Lee, Y. W. Cho, J. Lee, J. H. Jeong and K. Park (2005). "Hydrotropic polymer micelle system for delivery of paclitaxel." J Control Release **101**(1-3): 59-68.

Husain, K., R. A. Francois, T. Yamauchi, M. Perez, S. M. Sebti and M. P. Malafa (2011). "Vitamin E delta-tocotrienol augments the antitumor activity of gemcitabine and suppresses constitutive NF-kappaB activation in pancreatic cancer." Mol Cancer Ther **10**(12): 2363-2372.

Ishida, T., E. Shiraga and H. Kiwada (2009). "Synergistic antitumor activity of metronomic dosing of cyclophosphamide in combination with doxorubicin-containing PEGylated liposomes in a murine solid tumor model." J Control Release **134**(3): 194-200.

Jayawarna, V., A. Smith, J. E. Gough and R. V. Ulijn (2007). "Three-dimensional cell culture of chondrocytes on modified di-phenylalanine scaffolds." Biochem Soc Trans **35**(Pt 3): 535-537.

Ji, X., Z. Wang, A. Geamanu, F. H. Sarkar and S. V. Gupta (2011). "Inhibition of cell growth and induction of apoptosis in non-small cell lung cancer cells by delta-tocotrienol is associated with notch-1 down-regulation." J Cell Biochem **112**(10): 2773-2783.

Kakizawa, Y. and K. Kataoka (2002). "Block copolymer micelles for delivery of gene and related compounds." Advanced Drug Delivery Reviews **54**(2): 203-222.

Kim, J. Y., S. Kim, M. Papp, K. Park and R. Pinal (2010). "Hydrotropic solubilization of poorly water-soluble drugs." J Pharm Sci **99**(9): 3953-3965.

Kim, J. Y., S. Kim, R. Pinal and K. Park (2011). "Hydrotropic polymer micelles as versatile vehicles for delivery of poorly water-soluble drugs." J Control Release **152**(1): 13-20.

Klaassen, C. D. and L. M. Aleksunes (2010). "Xenobiotic, bile acid, and cholesterol transporters: function and regulation." Pharmacol Rev **62**(1): 1-96.

Kostkova, H., T. Etrych, B. Rihova, L. Kostka, L. Starovoytova, M. Kovar and K. Ulbrich (2013). "HPMA copolymer conjugates of DOX and mitomycin C for combination therapy: physicochemical characterization, cytotoxic effects, combination index analysis, and anti-tumor efficacy." Macromol Biosci **13**(12): 1648-1660.

Kraitzer, A., Y. Kloog, R. Haklai and M. Zilberman (2011). "Composite fiber structures with antiproliferative agents exhibit advantageous drug delivery and cell growth inhibition in vitro." J Pharm Sci **100**(1): 133-149.

Kumar, G. K., R. Dhamotharan, N. M. Kulkarni, S. Honnegowda and S. Murugesan (2011). "Embelin ameliorates dextran sodium sulfate-induced colitis in mice." Int Immunopharmacol **11**(6): 724-731.

Kuper, H., P. Boffetta and H. O. Adami (2002). "Tobacco use and cancer causation: association by tumour type." Journal of Internal Medicine **252**(3): 206-224.

La, S. B., T. Okano and K. Kataoka (1996). "Preparation and characterization of the micelle-forming polymeric drug indomethacin-incorporated poly(ethylene oxide)-poly(beta-benzyl L-aspartate) block copolymer micelles." J Pharm Sci **85**(1): 85-90.

Lachelt, U., V. Wittmann, K. Muller, D. Edinger, P. Kos, M. Hohn and E. Wagner (2014). "Synthetic polyglutamylation of dual-functional MTX ligands for enhanced combined cytotoxicity of poly(I:C) nanoplexes." Mol Pharm **11**(8): 2631-2639.

Lai, S. K., Y. Y. Wang and J. Hanes (2009). "Mucus-penetrating nanoparticles for drug and gene delivery to mucosal tissues." Adv Drug Deliv Rev **61**(2): 158-171.

Lang-Lazdunski, L. (2014). "Surgery for malignant pleural mesothelioma: Why, when and what?" Lung Cancer **84**(2): 103-109.

Laouini, A., V. Andrieu, L. Vecellio, H. Fessi and C. Charcosset (2014). "Characterization of different vitamin E carriers intended for pulmonary drug delivery." Int J Pharm **471**(1-2): 385-390.

Lee, B. J., Y. F. Tseng, C. H. Yen and P. T. Lin (2013). "Effects of coenzyme Q10 supplementation (300 mg/day) on antioxidation and anti-inflammation in coronary artery

disease patients during statins therapy: a randomized, placebo-controlled trial." Nutr J **12**(1): 142.

Lee, E. S., K. Na and Y. H. Bae (2005). "Doxorubicin loaded pH-sensitive polymeric micelles for reversal of resistant MCF-7 tumor." J Control Release **103**(2): 405-418.

Li, F., M. Danquah and R. I. Mahato (2010). "Synthesis and characterization of amphiphilic lipopolymers for micellar drug delivery." Biomacromolecules **11**(10): 2610-2620.

Li, G., J. Liu, Y. Pang, R. Wang, L. Mao, D. Yan, X. Zhu and J. Sun (2011). "Polymeric micelles with water-insoluble drug as hydrophobic moiety for drug delivery." Biomacromolecules **12**(6): 2016-2026.

Li, H., L. Piao, B. Yu, B. C. Yung, W. Zhang, P. G. Wang, J. L. Lee and R. J. Lee (2011). "Delivery of calf thymus DNA to tumor by folate receptor targeted cationic liposomes." Biomaterials **32**(27): 6614-6620.

Li, Q., H. Lv, Y. Zu, Z. Qu, L. Yao, L. Su, C. Liu and L. Wang (2009). "Synthesis and antitumor activity of novel 20s-camptothecin analogues." Bioorg Med Chem Lett **19**(2): 513-515.

Li, S. D. and L. Huang (2009). "Nanoparticles evading the reticuloendothelial system: role of the supported bilayer." Biochim Biophys Acta **1788**(10): 2259-2266.

Li, Y., A. Sen, J. Ren, L. M. Askew, E. Sidahmed, D. E. Brenner, M. T. t. Ruffin, D. K. Turgeon and Z. Djuric (2014). "Effects of Vitamin E From Supplements and Diet on Colonic alpha- and gamma-tocopherol Concentrations in Persons at Increased Colon Cancer Risk." Nutr Cancer: 1-9.

Li, Y., K. Xiao, J. Luo, J. Lee, S. Pan and K. S. Lam (2010). "A novel size-tunable nanocarrier system for targeted anticancer drug delivery." J Control Release **144**(3): 314-323.

Li, Y., K. Xiao, J. Luo, W. Xiao, J. S. Lee, A. M. Gonik, J. Kato, T. A. Dong and K. S. Lam (2011). "Well-defined, reversible disulfide cross-linked micelles for on-demand paclitaxel delivery." Biomaterials **32**(27): 6633-6645.

Liaw, J., T. Aoyagi, K. Kataoka, Y. Sakurai and T. Okano (1999). "Permeation of PEO-PBLA-FITC polymeric micelles in aortic endothelial cells." Pharm Res **16**(2): 213-220.

Liu, S. Q., N. Wiradharma, S. J. Gao, Y. W. Tong and Y. Y. Yang (2007). "Bio-functional micelles self-assembled from a folate-conjugated block copolymer for targeted intracellular delivery of anticancer drugs." Biomaterials **28**(7): 1423-1433.

Liu, Y., L. Huang and F. Liu (2010). "Paclitaxel nanocrystals for overcoming multidrug resistance in cancer." Mol Pharm **7**(3): 863-869.

Loo, T. W., M. C. Bartlett and D. M. Clarke (2004). "Disulfiram metabolites permanently inactivate the human multidrug resistance P-glycoprotein." Mol Pharm **1**(6): 426-433.

Lorusso, D., A. Di Stefano, V. Carone, A. Fagotti, S. Pisconti and G. Scambia (2007). "Pegylated liposomal doxorubicin-related palmar-plantar erythrodysesthesia ('hand-foot' syndrome)." Ann Oncol **18**(7): 1159-1164.

Lu, J., Y. Huang, W. Zhao, Y. Chen, J. Li, X. Gao, R. Venkataramanan and S. Li (2013). "Design and characterization of PEG-derivatized vitamin E as a nanomicellar formulation for delivery of paclitaxel." Mol Pharm **10**(8): 2880-2890.

Lu, J., Y. Huang, W. Zhao, R. T. Marquez, X. Meng, J. Li, X. Gao, R. Venkataramanan, Z. Wang and S. Li (2013). "PEG-derivatized embelin as a nanomicellar carrier for delivery of paclitaxel to breast and prostate cancers." Biomaterials **34**(5): 1591-1600.

Lu, J., W. Zhao, Y. Huang, H. Liu, R. Marquez, R. B. Gibbs, J. Li, R. Venkataramanan, L. Xu, S. Li and S. Li (2014). "Targeted delivery of Doxorubicin by folic Acid-decorated dual functional nanocarrier." Mol Pharm **11**(11): 4164-4178.

Lu, J., W. Zhao, H. Liu, R. Marquez, Y. Huang, Y. Zhang, J. Li, W. Xie, R. Venkataramanan, L. Xu and S. Li (2014). "An improved d-alpha-tocopherol-based nanocarrier for targeted delivery of doxorubicin with reversal of multidrug resistance." J Control Release **196C**: 272-286.

Lu, Z. R., P. Kopeckova, Z. Wu and J. Kopecek (1998). "Functionalized semitelechelic poly[N-(2-hydroxypropyl)methacrylamide] for protein modification." Bioconjug Chem **9**(6): 793-804.

Lukyanov, A. N. and V. P. Torchilin (2004). "Micelles from lipid derivatives of water-soluble polymers as delivery systems for poorly soluble drugs." Adv Drug Deliv Rev **56**(9): 1273-1289.

Luo, J., K. Xiao, Y. Li, J. S. Lee, L. Shi, Y. H. Tan, L. Xing, R. Holland Cheng, G. Y. Liu and K. S. Lam (2010). "Well-defined, size-tunable, multifunctional micelles for efficient paclitaxel delivery for cancer treatment." Bioconjug Chem **21**(7): 1216-1224.

Luo, W., H. Morrison, M. de Groh, C. Waters, M. DesMeules, E. Jones-McLean, A. M. Ugnat, S. Desjardins, M. Lim and Y. Mao (2007). "The burden of adult obesity in Canada." Chronic Dis Can **27**(4): 135-144.

Ma, Y., D. Liu, D. Wang, Y. Wang, Q. Fu, J. K. Fallon, X. Yang, Z. He and F. Liu (2014). "Combinational delivery of hydrophobic and hydrophilic anticancer drugs in single nanoemulsions to treat MDR in cancer." Mol Pharm **11**(8): 2623-2630.

Ma, Y., Y. Zheng, K. Liu, G. Tian, Y. Tian, L. Xu, F. Yan, L. Huang and L. Mei (2010). "Nanoparticles of Poly(Lactide-Co-Glycolide)-d-a-Tocopheryl Polyethylene Glycol 1000 Succinate Random Copolymer for Cancer Treatment." Nanoscale Res Lett **5**(7): 1161-1169.

Maeng, J. H., D. H. Lee, K. H. Jung, Y. H. Bae, I. S. Park, S. Jeong, Y. S. Jeon, C. K. Shim, W. Kim, J. Kim, J. Lee, Y. M. Lee, J. H. Kim, W. H. Kim and S. S. Hong (2010). "Multifunctional doxorubicin loaded superparamagnetic iron oxide nanoparticles for chemotherapy and magnetic resonance imaging in liver cancer." Biomaterials **31**(18): 4995-5006.

Mao, J., H. Zhang, J. Luo, L. Li, R. Zhao, R. Zhang and G. Liu (2006). "New method for HPLC separation and fluorescence detection of malonaldehyde in normal human plasma." J Chromatogr B Analyt Technol Biomed Life Sci **832**(1): 103-108.

Marom, M., R. Haklai, G. Ben-Baruch, D. Marciano, Y. Egozi and Y. Kloog (1995). "Selective inhibition of Ras-dependent cell growth by farnesylthiosalisylic acid." J Biol Chem **270**(38): 22263-22270.

Matsumura, Y. and K. Kataoka (2009). "Preclinical and clinical studies of anticancer agent-incorporating polymer micelles." Cancer Sci **100**(4): 572-579.

Matsumura, Y. and H. Maeda (1986). "A new concept for macromolecular therapeutics in cancer chemotherapy: mechanism of tumoritropic accumulation of proteins and the antitumor agent smancs." Cancer Res **46**(12 Pt 1): 6387-6392.

McRae Page, S., M. Martorella, S. Parelkar, I. Kosif and T. Emrick (2013). "Disulfide cross-linked phosphorylcholine micelles for triggered release of camptothecin." Mol Pharm **10**(7): 2684-2692.

Mei, L., Z. P. Zhang, L. Y. Zhao, L. Q. Huang, X. L. Yang, J. T. Tang and S. S. Feng (2013). "Pharmaceutical nanotechnology for oral delivery of anticancer drugs." Advanced Drug Delivery Reviews **65**(6): 880-890.

Mert, O., S. K. Lai, L. Ensign, M. Yang, Y. Y. Wang, J. Wood and J. Hanes (2012). "A poly(ethylene glycol)-based surfactant for formulation of drug-loaded mucus penetrating particles." J Control Release **157**(3): 455-460.

Mi, Y., Y. Liu and S. S. Feng (2011). "Formulation of Docetaxel by folic acid-conjugated d-alpha-tocopheryl polyethylene glycol succinate 2000 (Vitamin E TPGS(2k)) micelles for targeted and synergistic chemotherapy." Biomaterials **32**(16): 4058-4066.

Miller, T., A. Hill, S. Uezguen, M. Weigandt and A. Goepferich (2012). "Analysis of Immediate Stress Mechanisms upon Injection of Polymeric Micelles and Related Colloidal Drug Carriers: Implications on Drug Targeting." Biomacromolecules **13**(6): 1707-1718.

Minotti, G., P. Menna, E. Salvatorelli, G. Cairo and L. Gianni (2004). "Anthracyclines: molecular advances and pharmacologic developments in antitumor activity and cardiotoxicity." Pharmacol Rev **56**(2): 185-229.

Momparler, R. L., M. Karon, S. E. Siegel and F. Avila (1976). "Effect of adriamycin on DNA, RNA, and protein synthesis in cell-free systems and intact cells." Cancer Res **36**(8): 2891-2895.

Mu, L., T. A. Elbayoumi and V. P. Torchilin (2005). "Mixed micelles made of poly(ethylene glycol)-phosphatidylethanolamine conjugate and d-alpha-tocopheryl polyethylene glycol 1000 succinate as pharmaceutical nanocarriers for camptothecin." Int J Pharm **306**(1-2): 142-149.

Mu, L. and S. S. Feng (2002). "Vitamin E TPGS used as emulsifier in the solvent evaporation/extraction technique for fabrication of polymeric nanospheres for controlled release of paclitaxel (Taxol)." J Control Release **80**(1-3): 129-144.

Musacchio, T., V. Laquintana, A. Latrofa, G. Trapani and V. P. Torchilin (2009). "PEG-PE micelles loaded with paclitaxel and surface-modified by a PBR-ligand: synergistic anticancer effect." Mol Pharm **6**(2): 468-479.

Muthu, M. S., S. A. Kulkarni, J. Xiong and S. S. Feng (2011). "Vitamin E TPGS coated liposomes enhanced cellular uptake and cytotoxicity of docetaxel in brain cancer cells." Int J Pharm **421**(2): 332-340.

Nakanishi, T., S. Fukushima, K. Okamoto, M. Suzuki, Y. Matsumura, M. Yokoyama, T. Okano, Y. Sakurai and K. Kataoka (2001). "Development of the polymer micelle carrier system for doxorubicin." J Control Release **74**(1-3): 295-302.

Natesan, S., A. Sugumaran, C. Ponnusamy, V. Jeevanesan, G. Girija and R. Palanichamy (2014). "Development and evaluation of magnetic microemulsion: tool for targeted delivery of camptothecin to BALB/c mice-bearing breast cancer." J Drug Target **22**(10): 913-926.

Nehate, C., S. Jain, A. Saneja, V. Khare, N. Alam, R. Dubey and P. N. Gupta (2014). "Paclitaxel Formulations: Challenges and Novel Delivery Options." Curr Drug Deliv.

Nikolovska-Coleska, Z., L. Xu, Z. Hu, Y. Tomita, P. Li, P. P. Roller, R. Wang, X. Fang, R. Guo, M. Zhang, M. E. Lippman, D. Yang and S. Wang (2004). "Discovery of embelin as a cell-permeable, small-molecular weight inhibitor of XIAP through structure-based computational screening of a traditional herbal medicine three-dimensional structure database." J Med Chem **47**(10): 2430-2440.

O'Brien, M. E., N. Wigler, M. Inbar, R. Rosso, E. Grischke, A. Santoro, R. Catane, D. G. Kieback, P. Tomczak, S. P. Ackland, F. Orlandi, L. Mellars, L. Alland, C. Tendler and C. B. C. S. Group (2004). "Reduced cardiotoxicity and comparable efficacy in a phase III trial of pegylated liposomal doxorubicin HCl (CAELYX/Doxil) versus conventional doxorubicin for first-line treatment of metastatic breast cancer." Ann Oncol **15**(3): 440-449.

O'Hagan, H. M., H. P. Mohammad and S. B. Baylin (2008). "Double Strand Breaks Can Initiate Gene Silencing and SIRT1-Dependent Onset of DNA Methylation in an Exogenous Promoter CpG Island." Plos Genetics **4**(8).

Ogawara, K., K. Un, K. Tanaka, K. Higaki and T. Kimura (2009). "In vivo anti-tumor effect of PEG liposomal doxorubicin (DOX) in DOX-resistant tumor-bearing mice: Involvement of cytotoxic effect on vascular endothelial cells." J Control Release **133**(1): 4-10.

Paal, K., J. Muller and L. Hegedus (2001). "High affinity binding of paclitaxel to human serum albumin." Eur J Biochem **268**(7): 2187-2191.

Patil, V., K. Gada, R. Panwar, S. Majewski, Y. Tekabe, A. Varvarigou and B. A. Khaw (2013). "In vitro demonstration of enhanced prostate cancer toxicity: pretargeting with Bombesin bispecific complexes and targeting with polymer-drug-conjugates." Journal of Drug Targeting **21**(10): 1012-1021.

Paulos, C. M., J. A. Reddy, C. P. Leamon, M. J. Turk and P. S. Low (2004). "Ligand binding and kinetics of folate receptor recycling in vivo: impact on receptor-mediated drug delivery." Mol Pharmacol **66**(6): 1406-1414.

Paz, A., R. Haklai, G. Elad-Sfadia, E. Ballan and Y. Kloog (2001). "Galectin-1 binds oncogenic H-Ras to mediate Ras membrane anchorage and cell transformation." Oncogene **20**(51): 7486-7493.

Pommier, Y., E. Leo, H. Zhang and C. Marchand (2010). "DNA topoisomerases and their poisoning by anticancer and antibacterial drugs." Chem Biol **17**(5): 421-433.

Portales, F., S. Thezenas, E. Samalin, E. Assenat, P. Senesse and M. Ychou (2011). "Incidence and Management of Bone Metastases in Gastrointestinal Cancer." Annals of Oncology **22**: v87-v87.

Prashant, C., M. Dipak, C. T. Yang, K. H. Chuang, D. Jun and S. S. Feng (2010). "Superparamagnetic iron oxide--loaded poly(lactic acid)-D-alpha-tocopherol polyethylene glycol 1000 succinate copolymer nanoparticles as MRI contrast agent." Biomaterials **31**(21): 5588-5597.

Rekers, N. H., E. G. C. Troost, C. M. L. Zegers, W. T. V. Germeraad, L. J. Dubois and P. Lambin (2014). "Stereotactic ablative body radiotherapy combined with immunotherapy: Present status and future perspectives." Cancer Radiotherapie **18**(5-6): 391-395.

Reul, R., J. Nguyen and T. Kissel (2009). "Amine-modified hyperbranched polyesters as non-toxic, biodegradable gene delivery systems." Biomaterials **30**(29): 5815-5824.

Rotblat, B., M. Ehrlich, R. Haklai and Y. Kloog (2008). "The Ras inhibitor farnesylthiosalicylic acid (Salirasib) disrupts the spatiotemporal localization of active Ras: a potential treatment for cancer." Methods Enzymol **439**: 467-489.

Schiffelers, R. M., G. A. Koning, T. L. ten Hagen, M. H. Fens, A. J. Schraa, A. P. Janssen, R. J. Kok, G. Molema and G. Storm (2003). "Anti-tumor efficacy of tumor vasculature-targeted liposomal doxorubicin." J Control Release **91**(1-2): 115-122.

Shaha, M., V. Pandian, M. A. Choti, E. Stotsky, J. M. Herman, Y. Khan, C. Libonati, T. M. Pawlik, R. D. Schulick and A. E. Belcher (2011). "Transitoriness in cancer patients: a cross-sectional survey of lung and gastrointestinal cancer patients." Supportive Care in Cancer **19**(2): 271-279.

Sharma, A. K., L. Zhang, S. Li, D. L. Kelly, V. Y. Alakhov, E. V. Batrakova and A. V. Kabanov (2008). "Prevention of MDR development in leukemia cells by micelle-forming polymeric surfactant." J Control Release **131**(3): 220-227.

Shen, H. W., L. F. Zhang and A. Eisenberg (1999). "Multiple pH-induced morphological changes in aggregates of polystyrene-block-poly(4-vinylpyridine) in DMF/H2O mixtures." Journal of the American Chemical Society **121**(12): 2728-2740.

Shen, J., G. S. Song, M. An, X. Q. Li, N. Wu, K. C. Ruan, J. Q. Hu and R. G. Hu (2014). "The use of hollow mesoporous silica nanospheres to encapsulate bortezomib and improve efficacy for non-small cell lung cancer therapy." Biomaterials **35**(1): 316-326.

Shen, J. M., T. Yin, X. Z. Tian, F. Y. Gao and S. Xu (2013). "Surface Charge-Switchable Polymeric Magnetic Nanoparticles for the Controlled Release of Anticancer Drug." Acs Applied Materials & Interfaces **5**(15): 7014-7024.

Shirpoor, A., L. Norouzi, M. H. Khadem Ansari, B. Ilkhanizadeh and R. Gharaaghaji (2013). "Vasoprotective effect of vitamin E: rescue of ethanol-induced atherosclerosis and inflammatory stress in rat vascular wall." Int Immunopharmacol **16**(4): 498-504.

Shoshani, L., A. Darszon, M. Tuena de Gomez-Puyou and A. Gomez-Puyou (1994). "Activity and fluorescence changes of lactate dehydrogenase induced by guanidine hydrochloride in reverse micelles." Eur J Biochem **221**(3): 1027-1032.

Shuai, X., H. Ai, N. Nasongkla, S. Kim and J. Gao (2004). "Micellar carriers based on block copolymers of poly(epsilon-caprolactone) and poly(ethylene glycol) for doxorubicin delivery." J Control Release **98**(3): 415-426.

Singh, B., S. K. Guru, R. Sharma, S. S. Bharate, I. A. Khan, S. Bhushan, S. B. Bharate and R. A. Vishwakarma (2014). "Synthesis and anti-proliferative activities of new derivatives of embelin." Bioorg Med Chem Lett **24**(20): 4865-4870.

Singh, D., R. Singh, P. Singh and R. S. Gupta (2009). "Effects of embelin on lipid peroxidation and free radical scavenging activity against liver damage in rats." Basic Clin Pharmacol Toxicol **105**(4): 243-248.

Sokol, R. J., J. E. Heubi, N. Butler-Simon, H. J. McClung, J. R. Lilly and A. Silverman (1987). "Treatment of vitamin E deficiency during chronic childhood cholestasis with oral d-alpha-tocopheryl polyethylene glycol-1000 succinate." Gastroenterology **93**(5): 975-985.

Song, N., M. Ding, Z. Pan, J. Li, L. Zhou, H. Tan and Q. Fu (2013). "Construction of targeting-clickable and tumor-cleavable polyurethane nanomicelles for multifunctional intracellular drug delivery." Biomacromolecules **14**(12): 4407-4419.

Sreepriya, M. and G. Bali (2005). "Chemopreventive effects of embelin and curcumin against N-nitrosodiethylamine/phenobarbital-induced hepatocarcinogenesis in Wistar rats." Fitoterapia **76**(6): 549-555.

Sutton, D., N. Nasongkla, E. Blanco and J. Gao (2007). "Functionalized micellar systems for cancer targeted drug delivery." Pharm Res **24**(6): 1029-1046.

Tacar, O., P. Sriamornsak and C. R. Dass (2013). "Doxorubicin: an update on anticancer molecular action, toxicity and novel drug delivery systems." J Pharm Pharmacol **65**(2): 157-170.

Takemura, G. and H. Fujiwara (2007). "Doxorubicin-induced cardiomyopathy from the cardiotoxic mechanisms to management." Prog Cardiovasc Dis **49**(5): 330-352.

Tamm, I., S. M. Kornblau, H. Segall, S. Krajewski, K. Welsh, S. Kitada, D. A. Scudiero, G. Tudor, Y. H. Qui, A. Monks, M. Andreeff and J. C. Reed (2000). "Expression and prognostic significance of IAP-family genes in human cancers and myeloid leukemias." Clin Cancer Res **6**(5): 1796-1803.

Tang, J., Q. Fu, Y. Wang, K. Racette, D. Wang and F. Liu (2013). "Vitamin E reverses multidrug resistance in vitro and in vivo." Cancer Lett **336**(1): 149-157.

Tang, N., G. Du, N. Wang, C. Liu, H. Hang and W. Liang (2007). "Improving penetration in tumors with nanoassemblies of phospholipids and doxorubicin." J Natl Cancer Inst **99**(13): 1004-1015.

Tijerina, M., K. D. Fowers, P. Kopeckova and J. Kopecek (2000). "Chronic exposure of human ovarian carcinoma cells to free or HPMA copolymer-bound mesochlorin e6 does not induce P-glycoprotein-mediated multidrug resistance." Biomaterials **21**(21): 2203-2210.

Toncheva, V., E. Schacht, S. Y. Ng, J. Barr and J. Heller (2003). "Use of block copolymers of poly(ortho esters) and poly (ethylene glycol) micellar carriers as potential tumour targeting systems." J Drug Target **11**(6): 345-353.

Torchilin, V. (2009). "Multifunctional and stimuli-sensitive pharmaceutical nanocarriers." Eur J Pharm Biopharm **71**(3): 431-444.

Torchilin, V. P. (2007). "Micellar nanocarriers: pharmaceutical perspectives." Pharm Res **24**(1): 1-16.

Ukawa, M., H. Akita, Y. Hayashi, R. Ishiba, K. Tange, M. Arai, K. Kubo, Y. Higuchi, K. Shimizu, S. Konishi, M. Hashida and H. Harashima (2014). "Neutralized nanoparticle composed of SS-cleavable and pH-activated lipid-like material as a long-lasting and liver-specific gene delivery system." Adv Healthc Mater **3**(8): 1222-1229.

van der Vlies, A. J., U. Hasegawa and J. A. Hubbell (2012). "Reduction-sensitive tioguanine prodrug micelles." Mol Pharm **9**(10): 2812-2818.

van Dongen, M. A., J. E. Silpe, C. A. Dougherty, A. K. Kanduluru, S. K. Choi, B. G. Orr, P. S. Low and M. M. Banaszak Holl (2014). "Avidity mechanism of dendrimer-folic acid conjugates." Mol Pharm **11**(5): 1696-1706.

Varma, M. V. and R. Panchagnula (2005). "Enhanced oral paclitaxel absorption with vitamin E-TPGS: effect on solubility and permeability in vitro, in situ and in vivo." Eur J Pharm Sci **25**(4-5): 445-453.

Verma, G., V. K. Aswal, G. Fritz-Popovski, C. P. Shah, M. Kumar and P. A. Hassan (2011). "Dilution induced thickening in hydrotrope-rich rod-like micelles." J Colloid Interface Sci **359**(1): 163-170.

Vijayakumar, M. R., M. S. Muthu and S. Singh (2013). "Copolymers of poly(lactic acid) and D-alpha-tocopheryl polyethylene glycol 1000 succinate-based nanomedicines: versatile multifunctional platforms for cancer diagnosis and therapy." Expert Opin Drug Deliv **10**(4): 529-543.

Vinogradov, S., E. Batrakova, S. Li and A. Kabanov (1999). "Polyion complex micelles with protein-modified corona for receptor-mediated delivery of oligonucleotides into cells." Bioconjug Chem **10**(5): 851-860.

von Gruenigen, V., H. Frasure, N. Fusco, R. DeBernardo, E. Eldermire, S. Eaton and S. Waggoner (2010). "A double-blind, randomized trial of pyridoxine versus placebo for the prevention of pegylated liposomal doxorubicin-related hand-foot syndrome in gynecologic oncology patients." Cancer **116**(20): 4735-4743.

Wang, C., Y. Wang, Y. Wang, M. Fan, F. Luo and Z. Qian (2011). "Characterization, pharmacokinetics and disposition of novel nanoscale preparations of paclitaxel." Int J Pharm **414**(1-2): 251-259.

Wang, J., D. A. Mongayt, A. N. Lukyanov, T. S. Levchenko and V. P. Torchilin (2004). "Preparation and in vitro synergistic anticancer effect of vitamin K3 and 1,8-diazabicyclo[5,4,0]undec-7-ene in poly(ethylene glycol)-diacyllipid micelles." Int J Pharm **272**(1-2): 129-135.

Wang, J., J. Sun, Q. Chen, Y. Gao, L. Li, H. Li, D. Leng, Y. Wang, Y. Sun, Y. Jing, S. Wang and Z. He (2012). "Star-shape copolymer of lysine-linked di-tocopherol polyethylene glycol 2000 succinate for doxorubicin delivery with reversal of multidrug resistance." Biomaterials **33**(28): 6877-6888.

Wang, J. B., Y. Jiang, H. Liang, P. Li, H. J. Xiao, J. Ji, W. Xiang, J. F. Shi, Y. G. Fan, L. Li, D. Wang, S. S. Deng, W. Q. Chen, W. Q. Wei, Y. L. Qiao and P. Boffetta (2012). "Attributable causes of cancer in China." Ann Oncol **23**(11): 2983-2989.

Wang, Y., D. Liu, Q. Zheng, Q. Zhao, H. Zhang, Y. Ma, J. K. Fallon, Q. Fu, M. T. Haynes, G. Lin, R. Zhang, D. Wang, X. Yang, L. Zhao, Z. He and F. Liu (2014). "Disulfide bond bridge insertion turns hydrophobic anticancer prodrugs into self-assembled nanomedicines." Nano Lett **14**(10): 5577-5583.

Wang, Y., R. Wang, X. Lu, W. Lu, C. Zhang and W. Liang (2010). "Pegylated phospholipids-based self-assembly with water-soluble drugs." Pharm Res **27**(2): 361-370.

Win, K. Y. and S. S. Feng (2006). "In vitro and in vivo studies on vitamin E TPGS-emulsified poly(D,L-lactic-co-glycolic acid) nanoparticles for paclitaxel formulation." Biomaterials **27**(10): 2285-2291.

Woodle, M. C., C. M. Engbers and S. Zalipsky (1994). "New amphipatic polymer-lipid conjugates forming long-circulating reticuloendothelial system-evading liposomes." Bioconjug Chem **5**(6): 493-496.

Wu, G., Y. Z. Fang, S. Yang, J. R. Lupton and N. D. Turner (2004). "Glutathione metabolism and its implications for health." J Nutr **134**(3): 489-492.

Xiao, H., R. Qi, S. Liu, X. Hu, T. Duan, Y. Zheng, Y. Huang and X. Jing (2011). "Biodegradable polymer - cisplatin(IV) conjugate as a pro-drug of cisplatin(II)." Biomaterials **32**(30): 7732-7739.

Xiao, K., Y. Li, J. Luo, J. S. Lee, W. Xiao, A. M. Gonik, R. G. Agarwal and K. S. Lam (2011). "The effect of surface charge on in vivo biodistribution of PEG-oligocholic acid based micellar nanoparticles." Biomaterials **32**(13): 3435-3446.

Xiao, K., J. Luo, W. L. Fowler, Y. Li, J. S. Lee, L. Xing, R. H. Cheng, L. Wang and K. S. Lam (2009). "A self-assembling nanoparticle for paclitaxel delivery in ovarian cancer." Biomaterials **30**(30): 6006-6016.

Xiao, K., J. Luo, Y. Li, J. S. Lee, G. Fung and K. S. Lam (2011). "PEG-oligocholic acid telodendrimer micelles for the targeted delivery of doxorubicin to B-cell lymphoma." J Control Release **155**(2): 272-281.

Xie, Z., H. Guan, X. Chen, C. Lu, L. Chen, X. Hu, Q. Shi and X. Jing (2007). "A novel polymer-paclitaxel conjugate based on amphiphilic triblock copolymer." J Control Release **117**(2): 210-216.

Xing, T., C. Mao, B. Lai and L. Yan (2012). "Synthesis of disulfide-cross-linked polypeptide nanogel conjugated with a near-infrared fluorescence probe for direct imaging of reduction-induced drug release." ACS Appl Mater Interfaces **4**(10): 5662-5672.

Xu, D., H. Kang, M. Fisher and R. L. Juliano (2004). "Strategies for inhibition of MDR1 gene expression." Mol Pharmacol **66**(2): 268-275.

Yan, L., W. Chen, X. Zhu, L. Huang, Z. Wang, G. Zhu, V. A. Roy, K. N. Yu and X. Chen (2013). "Folic acid conjugated self-assembled layered double hydroxide nanoparticles for high-efficacy-targeted drug delivery." Chem Commun (Camb) **49**(93): 10938-10940.

Yao, J., Y. Zhang, S. Ramishetti, Y. H. Wang and L. Huang (2013). "Turning an antiviral into an anticancer drug: Nanoparticle delivery of acyclovir monophosphate." Journal of Controlled Release **170**(3): 414-420.

Yen, C. T., T. L. Hwang, Y. C. Wu and P. W. Hsieh (2009). "Design and synthesis of new N-(fluorenyl-9-methoxycarbonyl) (Fmoc)-dipeptides as anti-inflammatory agents." Eur J Med Chem **44**(5): 1933-1940.

Yen, H. C., H. Cabral, P. Mi, K. Toh, Y. Matsumoto, X. Liu, H. Koori, A. Kim, K. Miyazaki, Y. Miura, N. Nishiyama and K. Kataoka (2014). "Light-Induced Cytosolic Activation of Reduction-Sensitive Camptothecin-Loaded Polymeric Micelles for Spatiotemporally Controlled In Vivo Chemotherapy." ACS Nano.

Yin, H., R. I. Litvinov, G. Vilaire, H. Zhu, W. Li, G. A. Caputo, D. T. Moore, J. D. Lear, J. W. Weisel, W. F. Degrado and J. S. Bennett (2006). "Activation of platelet alphaIIbbeta3 by an exogenous peptide corresponding to the transmembrane domain of alphaIIb." J Biol Chem **281**(48): 36732-36741.

Yoo, H. S. and T. G. Park (2004). "Folate receptor targeted biodegradable polymeric doxorubicin micelles." J Control Release **96**(2): 273-283.

Yu, L., A. Bridgers, J. Polli, A. Vickers, S. Long, A. Roy, R. Winnike and M. Coffin (1999). "Vitamin E-TPGS increases absorption flux of an HIV protease inhibitor by enhancing its solubility and permeability." Pharm Res **16**(12): 1812-1817.

Yu, Y. S., L. F. Zhang and A. Eisenberg (1998). "Morphogenic effect of solvent on crew-cut aggregates of apmphiphilic diblock copolymers." Macromolecules **31**(4): 1144-1154.

Yuan, H., X. Li, J. Wu, J. Li, X. Qu, W. Xu and W. Tang (2008). "Strategies to overcome or circumvent P-glycoprotein mediated multidrug resistance." Curr Med Chem **15**(5): 470-476.

Zeng, F., H. Lee and C. Allen (2006). "Epidermal growth factor-conjugated poly(ethylene glycol)-block- poly(delta-valerolactone) copolymer micelles for targeted delivery of chemotherapeutics." Bioconjug Chem **17**(2): 399-409.

Zhang, L., Y. He, G. Ma, C. Song and H. Sun (2012). "Paclitaxel-loaded polymeric micelles based on poly(varepsilon-caprolactone)-poly(ethylene glycol)-poly(varepsilon-caprolactone) triblock copolymers: in vitro and in vivo evaluation." Nanomedicine **8**(6): 925-934.

Zhang, P., J. Lu, Y. Huang, W. Zhao, Y. Zhang, X. Zhang, J. Li, R. Venkataramanan, X. Gao and S. Li (2014). "Design and evaluation of a PEGylated lipopeptide equipped with drug-interactive motifs as an improved drug carrier." AAPS J **16**(1): 114-124.

Zhang, X., Y. Huang, W. Zhao, Y. Chen, P. Zhang, J. Li, R. Venkataramanan and S. Li (2014). "PEG-farnesyl thiosalicylic acid telodendrimer micelles as an improved formulation for targeted delivery of paclitaxel." Mol Pharm **11**(8): 2807-2814.

Zhang, X., Y. Huang, W. Zhao, H. Liu, R. Marquez, J. Lu, P. Zhang, Y. Zhang, J. Li, X. Gao, R. Venkataramanan, L. Xu and S. Li (2014). "Targeted Delivery of Anticancer Agents via a Dual Function Nanocarrier with an Interfacial Drug-Interactive Motif." Biomacromolecules **15**(11): 4326-4335.

Zhang, X., K. Liu, Y. Huang, J. Xu, J. Li, X. Ma and S. Li (2014). "Reduction-sensitive dual functional nanomicelles for improved delivery of paclitaxel." Bioconjug Chem **25**(9): 1689-1696.

Zhang, X., J. Lu, Y. Huang, W. Zhao, Y. Chen, J. Li, X. Gao, R. Venkataramanan, M. Sun, D. B. Stolz, L. Zhang and S. Li (2013). "PEG-farnesylthiosalicylate conjugate as a nanomicellar carrier for delivery of paclitaxel." Bioconjug Chem **24**(3): 464-472.

Zhang, Y., H. Gu, Z. Yang and B. Xu (2003). "Supramolecular hydrogels respond to ligand-receptor interaction." J Am Chem Soc **125**(45): 13680-13681.

Zhang, Y., Y. Huang, P. Zhang, X. Gao, R. B. Gibbs and S. Li (2012). "Incorporation of a selective sigma-2 receptor ligand enhances uptake of liposomes by multiple cancer cells." Int J Nanomedicine **7**: 4473-4485.

Zhang, Y., Y. Huang, W. Zhao, J. Lu, P. Zhang, X. Zhang, J. Li, X. Gao, R. Venkataramanan and S. Li (2014). "Fmoc-Conjugated PEG-Vitamin E2 Micelles for Tumor-Targeted Delivery of Paclitaxel: Enhanced Drug-Carrier Interaction and Loading Capacity." AAPS J **16**(6): 1282-1291.

Zhang, Y. F., Y. X. Huang and S. Li (2014). "Polymeric Micelles: Nanocarriers for Cancer-Targeted Drug Delivery." Aaps Pharmscitech **15**(4): 862-871.

Zhang, Z. and S. S. Feng (2006). "Nanoparticles of poly(lactide)/vitamin E TPGS copolymer for cancer chemotherapy: synthesis, formulation, characterization and in vitro drug release." Biomaterials **27**(2): 262-270.

Zhang, Z., S. H. Lee, C. W. Gan and S. S. Feng (2008). "In vitro and in vivo investigation on PLA-TPGS nanoparticles for controlled and sustained small molecule chemotherapy." Pharm Res **25**(8): 1925-1935.

Zhang, Z., Z. Liu, L. Ma, S. Jiang, Y. Wang, H. Yu, Q. Yin, J. Cui and Y. Li (2013). "Reversal of multidrug resistance by mitochondrial targeted self-assembled nanocarrier based on stearylamine." Mol Pharm **10**(6): 2426-2434.

Zhao, H., C. Lee, P. Sai, Y. H. Choe, M. Boro, A. Pendri, S. Guan and R. B. Greenwald (2000). "20-O-acylcamptothecin derivatives: evidence for lactone stabilization." J Org Chem **65**(15): 4601-4606.

Zhao, L., Y. Shi, S. Zou, M. Sun, L. Lil and G. Zhail (2011). "Formulation and in vitro evaluation of quercetin loaded polymeric micelles composed of pluronic P123 and D-a-tocopheryl polyethylene glycol succinate." J Biomed Nanotechnol **7**(3): 358-365.

Zhao, X., H. Li and R. J. Lee (2008). "Targeted drug delivery via folate receptors." Expert Opin Drug Deliv **5**(3): 309-319.

Zhao, Y., D. Y. Alakhova, J. O. Kim, T. K. Bronich and A. V. Kabanov (2013). "A simple way to enhance Doxil(R) therapy: drug release from liposomes at the tumor site by amphiphilic block copolymer." J Control Release **168**(1): 61-69.

Zheng, N., W. Dai, W. Du, H. Zhang, L. Lei, H. Zhang, X. Wang, J. Wang, X. Zhang, J. Gao and Q. Zhang (2012). "A novel lanreotide-encoded micelle system targets paclitaxel to the tumors with overexpression of somatostatin receptors." Mol Pharm **9**(5): 1175-1188.

Zhu, W., M. M. Cromie, Q. Cai, T. Lv, K. Singh and W. Gao (2014). "Curcumin and vitamin E protect against adverse effects of benzo[a]pyrene in lung epithelial cells." PLoS One **9**(3): e92992.